

Testing and Diagnosis of High Voltage and Extra High Voltage Power Cables with Damped AC Voltages

Cichecki, P

DOI

[10.4233/uuid:f50c2129-6771-468b-aa3c-7c1fdac4e425](https://doi.org/10.4233/uuid:f50c2129-6771-468b-aa3c-7c1fdac4e425)

Publication date

2018

Document Version

Final published version

Citation (APA)

Cichecki, P. (2018). *Testing and Diagnosis of High Voltage and Extra High Voltage Power Cables with Damped AC Voltages*. [Dissertation (TU Delft), Delft University of Technology].
<https://doi.org/10.4233/uuid:f50c2129-6771-468b-aa3c-7c1fdac4e425>

Important note

To cite this publication, please use the final published version (if applicable).
Please check the document version above.

Copyright

Other than for strictly personal use, it is not permitted to download, forward or distribute the text or part of it, without the consent of the author(s) and/or copyright holder(s), unless the work is under an open content license such as Creative Commons.

Takedown policy

Please contact us and provide details if you believe this document breaches copyrights.
We will remove access to the work immediately and investigate your claim.

**Testing and Diagnosis of High Voltage and
Extra High Voltage Power Cables with
Damped AC Voltages**

Testing and Diagnosis of High Voltage and Extra High Voltage Power Cables with Damped AC Voltages

Proefschrift

ter verkrijging van de graad van doctor
aan de Technische Universiteit Delft,
op gezag van de Rector Magnificus prof. dr. Ir. T.H.J.J. van der Hagen,
voorzitter van het College voor Promoties,
in het openbaar te verdedigen op maandag 10 december om 15:00 uur

door

Piotr Cichecki

elektrotechnisch ingenieur
geboren te Garwolin, Polen

This dissertation has been approved by the:
Promotor: Prof. dr. J.J. Smit

Composition of the doctoral committee:

Rector Magnificus	chairman
Prof. dr. J.J. Smit	Delft University of Technology

Independent members:

Prof.dr. R. Ross	Delft University of Technology
Prof.dr.ir. P. Bauer	Delft University of Technology
Prof.dr.ing. S. Tenbohlen	Universität Stuttgart
Prof.dr.ing. R. Plath	Technische Universität Berlin
Prof.dr.hab.ir. E. Gulski	Poznan University of Technology
Dr. A. Rodrigo Mor	Delft University of Technology



This research was financially and technically supported by the KSANDR foundation (The Netherlands) and the ONSITE HV Group (Switzerland)

*The cover page was designed by: Print Point S.C.
Warsaw, Poland*

Printed by: Print Point S.C.

Copyright © 2018 by Piotr Cichecki

All rights reserved

ISBN: 978-83-952726-0-8

An electronic version of this dissertation is available at
<http://repository.tudelft.nl/>

“To my wife Edyta and my children Adrianna and Alexander”

SUMMARY

The thesis focuses on on-site testing and diagnosis of transmission power cables circuits. Based on the application of methods for on-site voltage generation and its use for advanced diagnosis, comprehensive testing and diagnostic procedures have been investigated in this thesis.

The described method utilises damped AC voltages (DAC) for testing purposes and sensitive partial discharge (PD) as well as dielectric loss measurements. As the application of this technique is gaining more and more popularity, the practical issues related to test procedures, diagnostic parameter limits and the general usage experience can be evaluated. Practical applications of the damped AC method including insulation diagnosis are based on investigations of HV cables in the laboratory as well as in the field on-site. Transmission cables in the range of 50 kV up to 230 kV were tested with the DAC method. With regard to cross-linked polyethylene (XLPE) and impregnated paper cable insulation, a comparison of results of laboratory and field experiments has been performed. Failure related defects which are traceable and detectable through PD are described in order to understand the feasibility of the on-site application of DAC voltages for condition assessment of HV/EHV power cables. The thesis shows that DAC test voltages provide a suitable and effective method to detect and localise PD related ageing or installation defects.

Due to the fact that cable joints in newly installed circuits are the weakest links, modern slip-on joints with defects were investigated with continuous AC and damped AC (DAC) energising. Differences in PD amplitude, PD intensity, phase resolved PD patterns (PRPD) characteristics between AC and DAC energising voltages were analysed. The effectiveness of DAC systems in detection of PDs in field conditions was analysed in acceptance (after-lying) tests of newly installed XLPE cables. Practical aspects of DAC voltage level selection, number of DAC voltage excitations and complete test procedures were verified on 110 kV up to 230 kV cables circuits. Issues regarding background noise and disturbance filtering are explained. The interpretation of test results and examples of TDR (Time Domain Reflectometry) analysis are discussed.

To find out a relation between ageing status and dielectric loss values, samples of impregnated paper insulation have been artificially aged in laboratory conditions. Accelerated ageing took almost 8 months at a temperature of 100°C. During this process dielectric loss was measured at different voltages to find the connection with insulation thermal degradation at the various electrical field stressing.

Finally, to support asset management decisions about aged paper insulated cable circuits, life consumption and future life models for paper insulated power cables have been developed. These models combine input data from operational conditions, e.g. ground temperature, cable temperature with dissipation factor measurements using the DAC method. Our developed algorithm may help in selecting the optimum cable load in order to extend insulation life time and avoid accelerated ageing which may improve cable reliability.

The DAC method investigated in this thesis can be used for fast and reliable PD diagnosis of HV and EHV cables according to voltage levels as described in the IEC standard. The compact size of DAC systems and short time necessary to set up the system and to execute the test is a huge benefit during on-site testing. Information provided by the DAC method allows avoidance of new cable failures and shows the actual insulation condition of in-service cables.

SAMENVATTING

Dit proefschrift heeft de focus op on-site testen en diagnosticeren van hoogspanningskabel verbindingen. In deze thesis zijn geavanceerde test en diagnostische procedures voor hoogspanningskabels onderzocht met behulp van een methode, waarbij op locatie hoogspanning wordt opgewekt en tevens diagnostiek kan worden toegepast.

De beschreven methode past gedempte AC spanning (DAC) toe voor test doeleinden met gevoelige deelontladingsmetingen alsmede diëlektrische verliesmetingen. Doordat de populariteit van deze testtechniek steeds meer toeneemt, kunnen de praktische zaken met betrekking tot de test procedures, diagnostische parameter limieten en algemene gebruikerservaring worden geëvalueerd. Praktische toepassingen met de DAC methode inclusief isolatiediagnose zijn gebaseerd op metingen aan hoogspanningskabels, zowel in het laboratorium als op locatie in het net. Transmissiekabels in de spanningsklasse van 50 kV tot en met 230 kV zijn getest met de DAC methode.

Met betrekking tot vernet polyethylene (XLPE) en geïmpregneerd papier/olie kabelisolatie is een vergelijking van laboratorium en veldmetingen gemaakt. Fout gerelateerde defecten, die traceerbaar en detecteerbaar zijn met deelontladingen (PD), zijn beschreven om de haalbaarheid vast te stellen van de testmethode met DAC spanningen voor conditiebepaling van HV/EHV hoogspanningskabels in veldapplicaties. Deze thesis concludeert dat een DAC test spanning een bruikbare en effectieve methode oplevert om deelontladingen te detecteren en te lokaliseren, die gerelateerd zijn aan veroudering of installatie defecten.

Omdat kabelmoffen in nieuw geïnstalleerde verbindingen de zwakke schakels zijn, zijn moderne opschuifmoffen met defecten onderzocht met zowel continue als gedempte AC spanning. Verschillen in PD amplitude, PD intensiteit, fase resulterende PD patroon karakteristieken tussen AC en DAC (PRPD) spanning zijn geanalyseerd. The effectiviteit van DAC systemen in het detecteren van deelontladingen in veldcondities zijn geanalyseerd in acceptatie (na-installatie) testen van nieuw geïnstalleerde XLPE kabels. Praktische aspecten, zoals DAC spanningskeuze, aantal DAC spanningspulsen en complete testprocedures zijn geverifieerd aan 110 kV tot en met 230 kV kabelverbindingen. Problemen met achtergrondruis en ruisfiltering zijn toegelicht. De interpretatie van test resultaten en voorbeelden van time domain reflectometry analyses zijn behandeld.

Om een relatie te vinden tussen de verouderingsconditie en de waarde van de diëlektrisch verliezen, zijn samples van geïmpregneerd papierisolatie kunstmatig verouderd onder laboratorium condities. Versnelde veroudering duurde bijna 8 maanden op een temperatuur van 100°C. Gedurende dit proces zijn diëlektrische verliezen voor verschillende spanningen gemeten om een relatie te vinden met thermisch veroudering van de isolatie onder de verschillende elektrische belastingen.

Tenslotte, om de asset management beslissingen te ondersteunen bij verouderde kabels met papierisolatie, zijn levensduurconsumptie en levensduurvoorspellingsmodellen voor papiergeïsoleerde kabels ontwikkeld. Deze modellen combineren gegevens van operationele condities, zoals bijvoorbeeld, grondtemperatuur, kabeltemperatuur, met de dissipatiefactor metingen met behulp van de DAC methode. Ons ontwikkelde algoritme kan helpen in het selecteren van de optimale kabel belasting om zo de isolatielevensduur te verlengen en om versnelde veroudering tegen te gaan, hetgeen de kabel betrouwbaarheid mogelijk zal vergroten.

De onderzochte DAC methode in deze thesis kan worden gebruikt voor snelle en betrouwbare PD diagnoses aan HV en EHV kabels op spanningsniveaus overeenkomstig de IEC standaard. De compacte grootte van het DAC systeem, de benodigde tijd om het systeem op te stellen en de tijd om de test uit te voeren zijn een groot voordeel gedurende netwerktesten. Informatie verkregen met de DAC methode maakt het mogelijk om nieuwe kabelfouten te voorkomen en om de actuele kabelconditie van in bedrijf zijnde kabels weer te geven.

TABLE OF CONTENTS

- Summaryvii
- Samenvattingviii
- Table of Contentsix
- 1. Introduction 1
 - 1.1 (E) HV Power Cables-underground transmission network..... 2
 - 1.2 After-laying testing and condition assessment of transmission cables 4
 - 1.2.1 New cable systems..... 6
 - 1.2.2 Service aged cable systems..... 7
 - 1.3 On-site testing methodology 10
 - 1.4 Asset management for transmission cables 16
 - 1.5 Objectives of present study 18
 - 1.6 Structure of the thesis 19
- 2. Transmission power cable accessory installation and assembling related defects 20
 - 2.1 Accessory assembly 20
 - 2.1.1 Assembling process..... 21
 - 2.1.2 Electric field distribution in cable system 22
 - 2.1.3 Electric field enhancement 26
 - 2.2 Typical installation and assembly defects..... 28
 - 2.2.1 Voids, contaminations on the dielectric surface 29
 - 2.2.2 Dielectric surface mechanical damage..... 30
 - 2.2.3 Remaining semi-conductive screen 31
 - 2.2.4 Missing semi-conductive screen 31
 - 2.2.5 Damages to the slip-on stress cone 32
 - 2.2.6 Incorrect joint connector assembly 33
 - 2.2.7 Imperfect sealing of joints and terminations 33
 - 2.3 Installation and assembly defects symptoms 34
 - 2.4 Conclusions 35
- 3. Transmission cables ageing related defects 37
 - 3.1 Ageing of oil impregnated cable insulation 38
 - 3.1.1 Cellulose chains breaking (de-polymerization/scission) 38
 - 3.1.2 Water content (hydrolysis) 39
 - 3.1.3 Gas content (gasification) 40
 - 3.1.4 Electrical treeing/tracking 41
 - 3.1.5 Oil contamination 42

3.2	Ageing of XLPE cable insulation	43
3.2.1	Chemical decomposition	44
3.2.2	Physical decomposition	45
3.2.3	Electrical erosion/treeing	45
3.3	Mechanically induced defects (all types of insulation)	47
3.3.1	Mechanical defects due to soil/ground movements	47
3.3.2	Thermo-mechanical related defects	48
3.4	Defects symptoms.....	50
3.5	Conclusions	51
4.	Damped AC.....	52
4.1	Damped AC resonance.....	53
4.1.1	Mathematical model	55
4.2	DAC testing voltage.....	57
4.2.1	DAC voltage test procedure	58
4.2.2	Voltage withstand test	61
4.3	Partial discharge measurements using DAC.....	64
4.3.1	IEC 60270 PD detection with DAC	64
4.3.2	DAC circuit calibration.....	67
4.3.3	PD parameters measured with DAC (according to IEE400.4)	70
4.4	Dielectric loss estimation using DAC	78
4.5	Conclusions	80
5.	Comparison of AC and DAC voltages for defects detection by PD.....	81
5.1	Defects for the laboratory investigation	82
5.1.1	Electric field distribution for defects 1, 2, 3	85
5.1.2	Effect of the voltage frequency on the electric field and inception voltage in the bounded cavity	89
5.2	Description of the test setup.....	91
5.2.1	AC energizing method and IEC60270 PD detection.....	92
5.2.2	DAC energizing and IEC60270 PD detection.....	92
5.3	Voltage withstand tests after cable installation in the lab.....	95
5.4	Missing outer semi-conductive screen (Defect type 1): 50 Hz AC vs. DAC.....	96
5.4.1	PDIV delay time at 50 Hz AC.....	96
5.4.2	PD magnitude at 50 Hz AC.....	97
5.4.3	PRPD patterns at 50 Hz AC	98
5.4.4	PDIV delay time at DAC	98
5.4.5	PD magnitude at DAC	101

5.4.6	PRPD patterns at DAC	103
5.5	Extra semi-conductive screen in the joint (Defect type 2): 50 Hz AC vs. DAC.....	105
5.5.1	PDIV delay time at 50 Hz AC.....	105
5.5.2	PD magnitude at 50 Hz AC	106
5.5.3	PRPD patterns at 50 Hz AC.....	107
5.5.4	PDIV delay time at DAC.....	108
5.5.5	PD magnitude at DAC.....	110
5.5.6	PRPD patterns at DAC	111
5.6	Investigation: Electrode-bound cavity (Defect type 3): 50 Hz AC vs. DAC	114
5.6.1	PDIV delay time at 50 Hz AC.....	114
5.6.2	PD magnitude at 50 Hz AC	115
5.6.3	PRPD patterns at 50 Hz AC.....	117
5.6.4	PDIV delay time at DAC.....	118
5.6.5	PD magnitude at DAC.....	119
5.6.6	PRPD patterns at DAC	120
5.7	Conclusions.....	123
6.	On-site testing and diagnosis of transmission cables with DAC voltages.....	125
6.1	Case study 1: Diagnosis of a newly installed 150 kV XLPE cable after breakdown	127
6.1.1	PD vs. Test voltage characteristics	128
6.1.2	PRPD patterns analysis.....	129
6.1.3	TDR traces	130
6.1.4	PD mappings	131
6.2	Case study 2: Testing and diagnosis of a newly installed 220 kV XLPE cable.....	132
6.2.1	PD vs. Test voltage characteristics	132
6.2.2	PRPD patterns analysis.....	133
6.2.3	TDR traces.....	133
6.2.4	PD mapping.....	136
6.2.5	Voltage Withstand Diagnosis	137
6.3	Case Study 3: Diagnosis of the service-aged transmission cables.....	137
6.3.1	Procedures for onsite diagnosis of service aged cables with DAC	140
6.3.2	PD vs. Test voltage (50 kV Circuit no. 4).....	143
6.3.3	PRPD patterns (50 kV Circuit no. 4).....	144
6.3.4	TDR traces (50 kV Circuit no. 4).....	146
6.3.5	PD mapping (50 kV Circuit no. 4)	146
6.3.6	Dielectric loss (50 kV Circuit no. 4).....	147
6.3.7	Voltage Withstand Diagnosis (50 kV Circuit no. 4).....	148

6.4	Overview of the diagnostic results of 13x50 kV oil-filled cables	150
6.5	Overview of the diagnostic results of 9x150 kV external gas-pressurised cables	153
6.6	Conclusions	156
7.	Life time estimation of service aged paper-oil insulated cables	159
7.1	Laboratory investigation on ageing phenomena of oil-impregnated paper cable insulation	160
7.2	Insulation life consumption (ILC) calculation	168
7.3	Operational life consumption (OLC) calculation	169
7.4	Total Life Consumption (TLC) calculation	170
7.5	Future life profile calculation	171
7.6	The further cable lifetime estimation-model application on service aged 150 kV cables....	172
7.7	Conclusions	178
8.	Conclusions and future work.....	179
	Appendixes.....	182
	List	198
	List of publications.....	206
	Acknowledgment	211
	Curriculum vitae	212

1. Introduction

Transmission underground power cable circuits represent an important asset of the high voltage power infrastructure in most countries around the world. Due to the economic development and global population increase, power networks are expanding and therefore growth of the number of the installed kilometres is observed. Furthermore, transmission networks constructed as overhead lines are extended or reconstructed by new links. When overhead line installations cannot be used because of social or technical reasons, the underground transmission cables are an alternative solution. This ongoing process of continuous installation of the cable circuits is accompanied by the increased expectation on the quality assurance of the installation processes. Due to the fact that the existing procedures for after-laying testing reflects only the minimum requirements on safe operation, the after-laying procedures should be revised and updated with the newest best-practice applications including users' experience.

The availability of energy transmission paths is related to system redundancy and failure rates of the particular cable link in the network. Failures can be of different origin, e.g. external (due to mechanical damage by third parties, installation related defects) or internal (due to cable system insulation defects or design problems). Recognition of failure symptoms is related to study of factors which may induce failure related defects in the transmission cable system. Knowledge about service conditions, e.g. load, ground temperature or cable construction is necessary to understand the relationship completely, e.g. between a particular cable type and a degradation process. Threat of functionality loss, outages, penalties for the delays in energy delivery paid to customer and repair costs are major consequences in case of unexpected failure of transmission systems. Environmental pollution, e.g. oil leakages from oil filled cables in case of external damage to the cable lead cover, also generates costs as a consequence of cable damage. Thus, to prevent asset failures, network operators are forced to implement, as a part of preventive maintenance, reliable assessment "tools" to check the condition of the most strategic transmission links and make the prioritisation of the assets that are in the worst condition and therefore are unreliable [1, 2, 3].

Besides visual inspections of, e.g. oil pressure/leakages or loss of continuity of external sheaths performed as a part of periodical maintenance of transmission cable circuits, technical data concerning transmission systems have to be collected by on-site testing and diagnosis. Such methods are used for verification of the cable insulation quality in different life stages. It is achieved through on-site tests and diagnosis where different cable insulation problems, e.g. partial discharge activity due to an internal insulation defect or increased dielectric losses can be detected, recognised and localised. Respectively, the service situation of cable circuits and tasks set for the particular situation can be divided as presented in Figure 1.1.



Figure 1.1: Approaches to maintaining power cable reliability.

1.1 (E) HV Power Cables-underground transmission network

Underground transmission power cables are insulated systems designed to transport large amounts of energy in the range of hundreds of MVA (Mega-Volt-Ampere) at different voltage levels (Figure 1.2) having low losses and high reliability level. Cables represent 30 percent lower power losses than overhead lines at high circuit loads [4]. Typical European underground transmission networks operate with three-phase alternating current (AC) at different voltage levels. The standard power frequency in, e.g. USA/Canada and some countries of the Middle East is 60 Hz, while in Europe it is 50 Hz. Nowadays two types of transmission cables are mostly utilised for HV and EHV: cables with laminated insulation, e.g. Self-Contained Fluid Filled (SCFF), High Pressure Fluid Filled (HPFF) and cables with extruded polymeric insulation, e.g. cross-linked polyethylene (XLPE). A survey [2, 3] shows that more than 90% of the cables installed worldwide between 2000 and 2005 were XLPE cables at voltages below 220 kV. For operating voltages above 220 kV, SCFF cables represented 40% of the installed cables. The prevailing trend is an increased application of XLPE cables in particular for EHV voltages [2]. Another survey presented for example by Polish TSO-PGE Dystrybucja shows that since 2010 newly installed HV transmission power cables in the range of 110 kV in Poland consist of XLPE cables only [5].

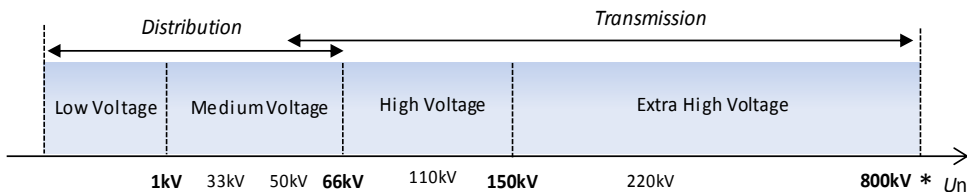


Figure 1.2: Power Cable network voltage ratings e.g. in The Netherlands. Rating borders for some of countries can differ and in many countries HV transmission range starts at 30 kV, 50 kV or 66 kV. [*]- Highest voltage rating for transmission cables so far (2015).

A transmission power infrastructure represents major capital investments. In 2006 almost 33000 kilometres of underground transmission cables circuits were reported to be in service by the European TSOs [2]. Trend shows further growth of lengths of underground

transmission networks in the future (Figure 1.3). This fast growth in cable lengths is also visible for the submarine cables where more and more extruded cables are used as presented in Figure 1.4.

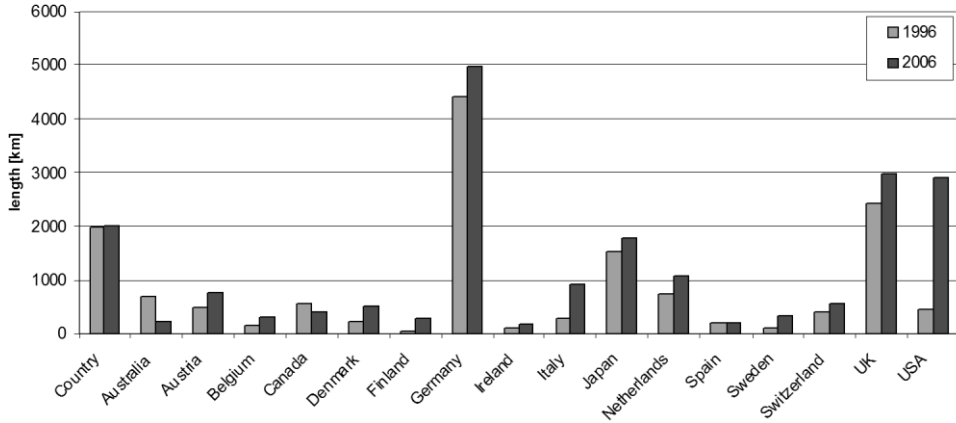


Figure 1.3: Increase (per km) of installed underground power cable in the range from 110 kV to 219 kV between years 1996-2006 [2].

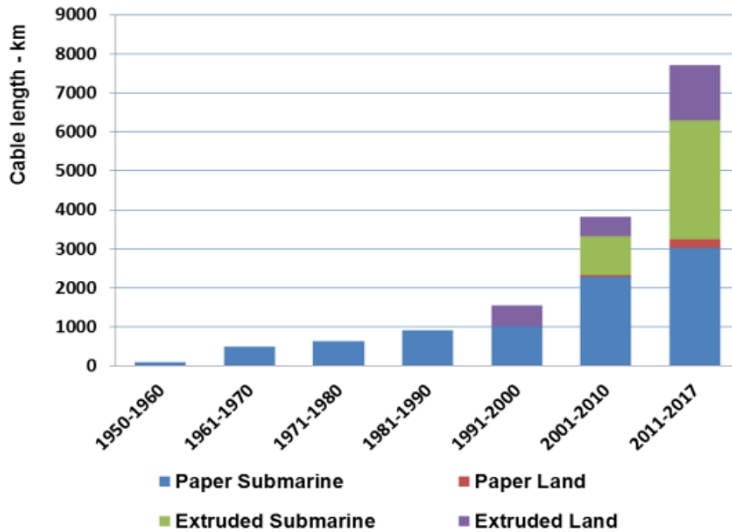


Figure 1.4: Installed kilometres of underground and submarine EHV power cables (AC and DC) in the world (transmission range 220kV-800kV) [6].

According to the 2016 year global market research report regarding HV cables entitled “High Voltage Cables & Accessories Market by Type (Overhead, Underground, & Submarine), by Overhead Products (Conductors, Fittings & Fixtures), by Underground and Submarine Products (XLPE Cables, MI Cables, Cable Joints, & Cable Terminations), and by Region-Global Trends & Forecasts to 2020”. The HV cable market is supposed to grow from \$29 billion in

2015 to \$39 billion by 2020. Continuous growth of the underground transmission networks is triggered by three major factors of influence:

- Increase in human population and as a direct result, growing energy demands in densely populated areas.
- Development of polymeric insulating materials and technologically advanced HV cable system constructions and in future e.g. superconducting cables which allow upgrading the capacity and reliability of the energy transport.
- High reliability e.g. 99.96% of service availability is claimed by international statistics regarding 380 kV underground cable circuits (discussed in the next paragraph) [3].

The transition from laminated to extruded power cables since the end of 60s' has resulted in continuously growing number of installed extruded transmission cables systems. As a result, production of laminated cables has gradually decreased. Extruded systems are cheaper and faster to produce (no impregnated medium). Quick installation and lower maintenance costs of extruded cables make transmission cables more and more affordable in terms of costs than overhead lines. In 2014, the ratio of the installation costs (per 1 km) between underground cables (HV range) and overhead lines was 10 to 3 (more than 3x higher cable costs) depending on the urbanisation level of the installation area [6].

Furthermore, the continuous development of technology-advanced transmission cables, e.g. HTS (High Temperature Superconductive Cables) allows for energy transmission with lower total losses than in case of traditional power cables and overhead lines. Application of extremely low loss insulating systems for regular high and extra high voltages is still being tested, however the results obtained in HV laboratories seem to put forward this trend in upcoming years for power cable applications [4].

Lastly, part of the overhead transmission lines, which were installed in the so called "country side" 40-50 years ago, are nowadays part of the populated towns and urban areas. In most of the cases, safety and public concerns forced the conversion to the underground transmission cables. The liberalisation of energy trading between the countries is also one of the factors leading to bulk power transmission over large distances. In case of highly industrialised heavy populated countries, e.g. Germany, The Netherlands, UK, Sweden, and Denmark, it is feasible only with the application of underground transmission cables.

1.2 After-laying testing and condition assessment of transmission cables

The survey on transmission cables reliability presented in CIGRE TB 379 [3] shows that in the circuit length of 40 km, the number of cable failures during the nominal 40 year of service life would be approximately 4 for HV/EHV SCFF cables, which would mean 1 failure every 10 years. For HV/EHV XLPE cables the expected failure rate would be 1 failure every 20 years. Expected failure rates over 40 years for a typical transmission cable configuration consisting of six terminations are low for both SCFF and XLPE cable systems. However, for the cable joints, expected failures during the nominal life would be 1 and 2 failures for SCFF and XLPE cable systems, respectively. On the other hand, if a failure of transmission cable system

occurs, depending on the type of insulation, a repair can take up to several days or weeks. Duration of the outages varies widely, depending on the circumstances of the failure, availability of parts and skill level of an available repair personnel. A typical duration of e.g. gas-pressurised cable outage is 8 to 12 days [4]. The duration of HV/EHV XLPE outages is 5 to 9 days. A repair of a fault in SCFF/HPFF system is estimated to be from 2 to 9 months, depending on the extent of the damage [3, 4].

The reliability can be lower at the beginning of service life influenced by failures due to e.g. installation errors, which represent so called “infant mortality” period. At the end of service life, failures are related to ageing which represent a “wear-out” period. The “bath tube curve” reflects the average failure behaviour of a cable population (Figure 1.5). Changes over lifetime are showing that the failure rate of transmission cable is not constant over the life cycle.

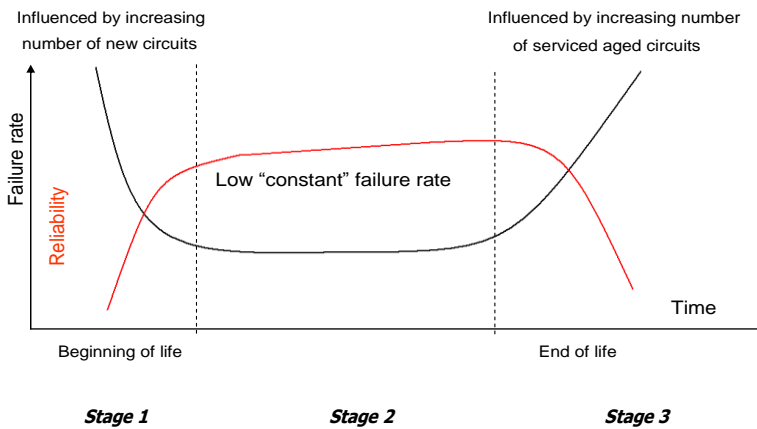


Figure 1.5: Bath-tube curve describing HV/EHV equipment reliability and failure rate during service life [2, 3].

The transition from stage 1 to stage 2 depends greatly on the quality of cable manufacturing and the quality of the installation and service conditions, e.g. over-voltages. The stage 1 does not necessarily to be present, if there are no failures in the early lifetime. The transition between stage 2 and stage 3 is not fixed and it is difficult to predict or estimate. Generally, power transmission cables have a designed life time of around 40-50 years [2, 3, 4], however due to different service conditions and load profiles, it is rather difficult to provide the exact values. The progress of insulation ageing (deterioration) can be different even for the same cable type installed in different conditions, e.g. different climate.

One possible way to access the condition of power cables is on-site diagnostic tests [19]. The testing consists of several different on-site tests performed at different stages of service life of power cables. Figure 1.6 presents on-site tests, which are intended to reject faulty components or defective parts of the circuit after installation, assembling or repair, e.g. HV withstand test. There are also tests that give an indication of the insulation condition after service life time, e.g. after 40 years. The latter tests should have no impact on cable insulation and are called diagnostic tests.

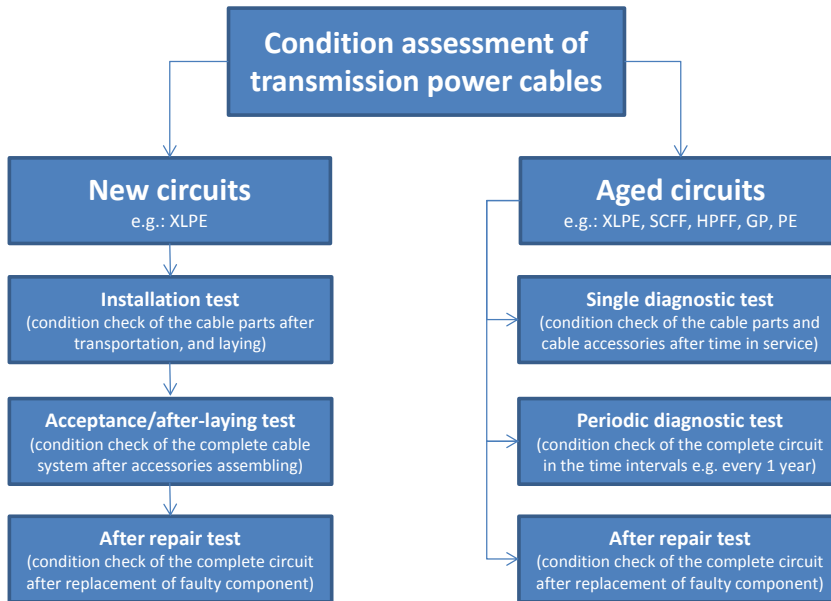


Figure 1.6: Basic overview of the on-site tests performed on transmission power cables to assess their condition.

1.2.1 New cable systems

Early cable failure occurrence is prevented by high quality of the workmanship on-site. In order to check the on-site installation, the acceptance voltage withstand testing is performed on the newly installed cable systems. During on-site tests, both cable insulation and cable accessories are tested at an externally applied over-voltage condition just before putting them into operation [7, 8] (Figure 1.7). The test intends to reject any faulty component of the power cable system. The test is called successful if no breakdown was registered in any part of the cable system during testing time. Failure statistics of new cross-linked polyethylene (XLPE) cables at different voltage levels show that early failures occur during the first three years since the initial operation, 80% of these failures are related to local installation defects in cable joints and terminations [7]. Experience presented in [7] shows that 12% of all on-site acceptance tests on newly installed circuits resulted in breakdowns mostly in cable joints and terminations. The majority of problems occur due to poor workmanship during assembling, e.g.:

- Wrong assembling measures.
- Assembly cleanliness.
- Wrong materials or tools used.
- Missing or wrongly applied electric field distribution elements of joints and terminations, e.g.: spacers, fillers, semi-conductive materials, insulating tapes or defective deflectors.

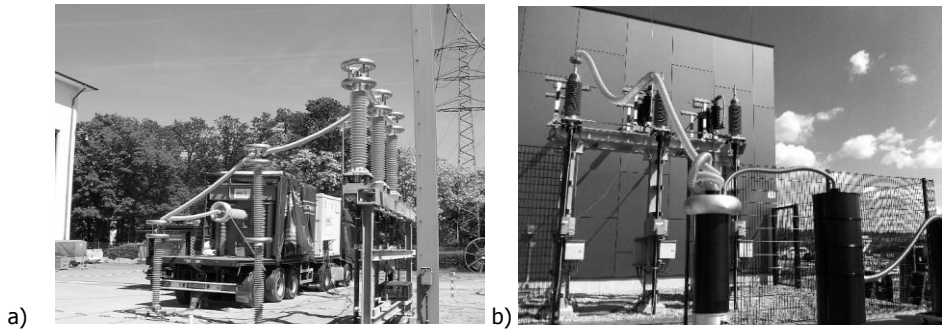


Figure 1.7: Example of on-site testing of newly installed HV power cable circuits: (a) continuous AC voltages by resonance test system [ref. IPH Berlin website], (b) acceptance test using a damped AC (DAC) system.

The trend in Figure 1.8 shows, that there is a high failure rate of new XLPE cables in the range of 60 kV to 219 kV, and the highest number of failures appears during the first 3 years from installation. Assuming that cable systems were tested properly after installation and have passed the tests successfully during the commissioning process, there must have been some hidden defect(s), which had not been detected by the applied testing procedures.

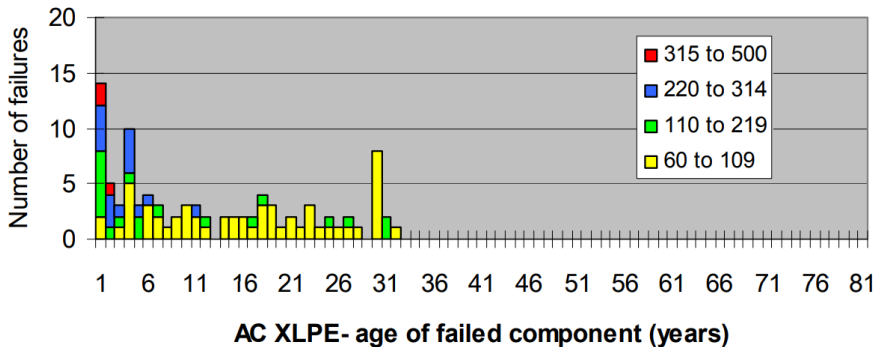


Figure 1.8: Trend in internal failures for XLPE HV power cables at different nominal voltage ranges [3]. These defects could have developed slowly and resulted in failure during operational service in the first year(s) of operation as it is reflected by the statistics in Figure 1.8.

1.2.2 Service aged cable systems

Condition assessment (evaluation) of cables in service can be described as activities focused on measuring or observing the key condition indicators (diagnostic parameters) of the primary cable components such as cable insulation. Comparing these measurement results to the existing standards and knowledge helps provide information about actual cable condition. Condition evaluation may be continuous or periodic. Condition assessment techniques may not cover all failure modes and a cable may fail without warning. Therefore, the way of “examination” of aged power cable systems should be adequate to the particular situation and be non-destructive.

Different approaches are used by power utilities, e.g. visual inspection of the cable circuits (if possible), Dissolved Gas Analysis (DGA) of oil for SCFF, HPFF cables, dielectric loss estimation or analysis of the polarisation-relaxation phenomenon and counting the oil leakages (Figure 1.9).

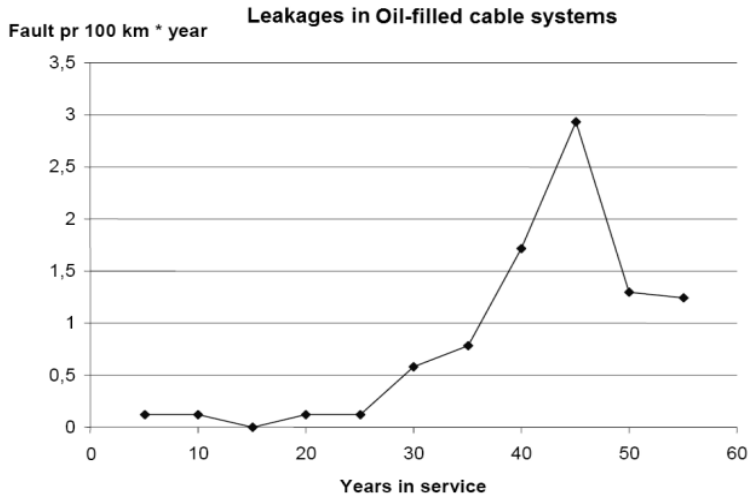


Figure 1.9: Failure rates in SCFF (oil) transmission cables [9].

More detailed information about different diagnostic methods can be found in references [9, 10]. Condition assessment methods of cable systems depend basically on two factors: the type of power cable system and the cost/time necessary to evaluate the condition status of the cable circuit.

An investigation done at several power utilities, experienced in service life management of existing AC underground cables, shows that on-site condition assessment of aged cable circuits can help to discern cables, which are qualified for e.g. replacement and cables which can be still used without the risk of energy transmission interruption [3]. Around 51% of the utilities in the survey have introduced replacement programs for aged self-contained fluid filled (SCFF) transmission cables because of oil leakages. Oil leakages create energy delivery interruptions and are strictly related to the age of a cable (Figure 1.9). In this particular situation a cable fault is understood as any interruption (e.g. lower oil pressure due to the leakage), which puts the cable out of service. It is important to note that these interruptions are not always related to insulation breakdowns. In the investigated utilities, decisions about SCFF power cables replacements were mostly made based on the age of the assets and the number of oil leakage failures in a single cable link per year. Condition assessment results (cable diagnostics data) were taken into consideration in 50% of total investigated replacements and were considered an effective decision supporting tool [3]. In a considerable part of the investigated SCFF cable population on-site inspections and diagnosis confirmed slow ageing of HV terminations and cable insulation and no serious internal defects, which allowed further use of these cable systems after a successful repair of the leakage. Therefore, in such situations even the numerous oil leakages and old age of the diagnosed cables did not always result in rejecting the cable system.

A different approach applies in maintaining the reliability of assets refers to aged gas-pressurised cables. In this type of cable, there is no visual evidence of the failure, such as oil leakages, and the general number of failures is relatively low in comparison to e.g. SCFF circuits. For example, the population of 150 kV external gas pressurised cables in The Netherlands reaches an average age of a single cable section of 30 years [11]. The study of the failure type and failure occurrence rate shows that, the character of the failures in gas-pressurised cables can vary from almost “random” occurring failures to distinctive ageing process related defects. An example presented in Figure 1.10b shows failure records of the gas-pressurised cable population in The Netherlands up to 2009. The total numbers of failures of this population is relatively low, i.e. 5 internal insulation failures of the cable per year at different ages.

Evaluation of the actual condition could be difficult when based only on the statistically calculated failure probability due to the low number of failures in this case. In The Netherlands high voltage some power network operators apply non-destructive diagnostic tests to assess insulation of gas-pressurised cables, e.g. damped AC (DAC) testing and PD diagnosis, dielectric losses measurements or dielectric spectroscopy. The obtained diagnostic parameters are sensitive to both thermal and electrical processes in the cable insulation.

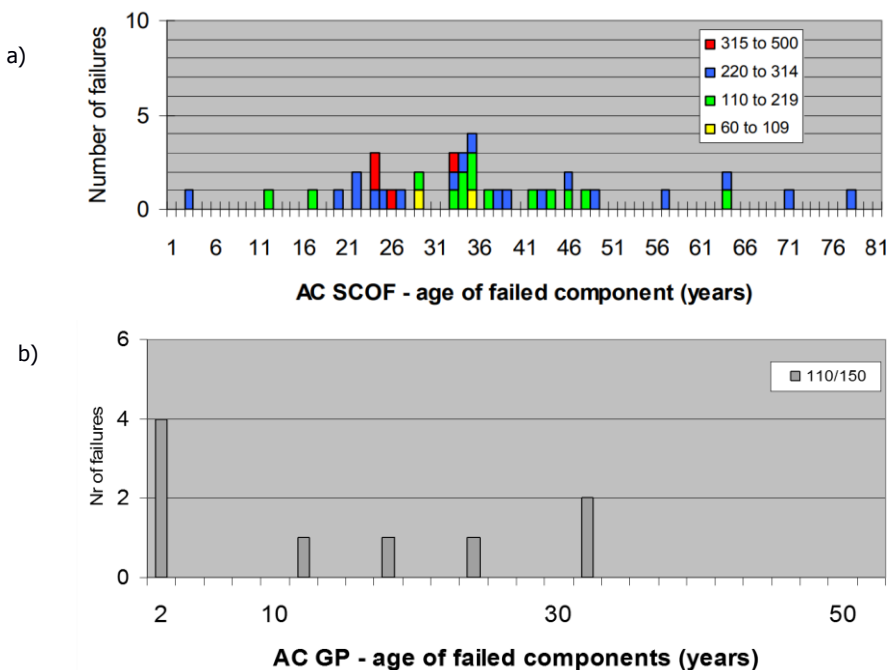


Figure 1.10: a) Trend in internal failures for Self-Contained Oil-Filled (SCOF/SCFF) HV power cables at different nominal voltage ranges [3]. b) Trend in internal failures for 110 kV and 150 kV gas-pressurised power cables in The Netherlands-situation till 2009 [11].

The increasing number of repairs on aged cable systems also forces the use of an effective non-destructive solution to assess the transmission cable status and check the quality of the

repair. Repair costs of transmission links can be very high, and the repair itself can be time consuming (depending on the type of cable and type of failure), when failure occurs. After repair, the cable system should be tested to check the repair quality and to ensure reliability of the repaired section prior to energising. The testing method should be selected in such a way, that the remaining life-time of the remaining part of the cable system (healthy part) should not be threatened [8, 10].

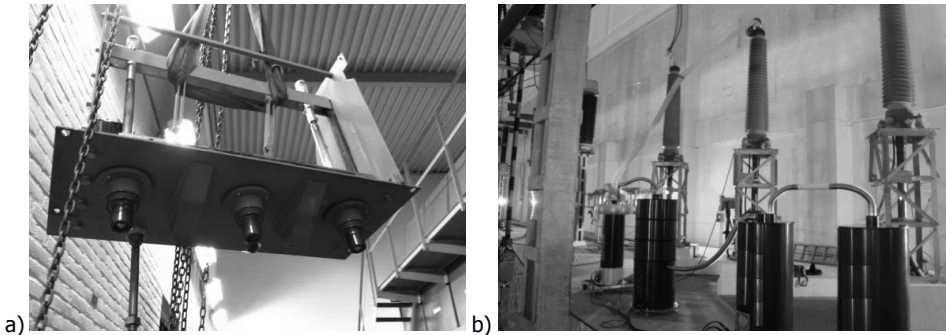


Figure 1.11: Different approaches in condition assessment of service aged power cable system components: a) Visual inspection of 29 years old 50 kV cable terminations compartment (Coq type), b) Example of on-site off-line PD and dielectric loss non-destructive diagnostics on 220 kV, 20 years old power cable with damped AC (DAC) system.

1.3 On-site testing methodology

The quality of cable system's components has an impact on the availability of the electricity supply. To obtain full information about the technical status of the cable system, it is important to answer the following questions:

- What are the conditions of cable components, e.g.: terminations, joints, cable insulation?
- Is there any degradation process visible in the cable system components?
- Can the particular components of the cable system withstand service conditions with minimum risk of breakdowns?
- Are there any threats of potential failures in near future, e.g. next year or in five years, in any of the cable components?
- Will over-voltage service conditions like, e.g. switching surges or short-circuits, cause deterioration or defects, which can be a threat for the cable reliability?

To answer these questions, various types of on-site tests can be applied to power cables, e.g.: low/high voltage, on-line/off-line tests, electrical/non-electrical tests or destructive/non-destructive test. Detailed information about various testing methods for HV/EHV cables can be found in [10].

PD inception voltages of some defects can be above nominal voltage U_0 , so these can be only detected during the overvoltage condition. Thus, PD monitored voltage withstand tests at elevated voltages can detect:

- PD related defects.
- Defects that are sensitive to the withstand test duration and are visible after some time after test starts.
- Defects sensitive to integral insulation changes caused by e.g. moisture.

This thesis focuses on three testing approaches, being on-site voltage withstand tests, on-site off-line partial discharge (PD) diagnosis and dielectric loss on-site estimation.

Voltage Withstand Test

HV on-site withstand tests are used for [7, 8, 10]:

- Commissioning of the equipment on site to demonstrate that transportation, installation and erection have not caused any new dangerous defects in the insulation.
- Checking the quality of repair of the equipment and confirming that all dangerous defects in the insulation have been eliminated.
- Diagnostic purposes to demonstrate that the insulation is still free of dangerous defects and the life-time expectation is sufficiently high.

The application of an overvoltage to the insulation is the oldest method of qualifying a cable for service conditions. This test is related to the nominal voltage (U_0) or above nominal cable voltage (over-voltage) conditions. This simple test can be used to test whether the cable's insulation holds the required voltage with a duration specified in applicable standard, e.g. according to IEC standard 1h. at $2.0 \times U_0$ for 110 kV cables. National standards, e.g. the NEN 3630 Dutch Standard, requires 10 min test at $2.5 \times U_0$ for the same cable. So, there is a worldwide discussion whether a higher voltage or a longer test duration is more effective for qualifying newly installed cable systems. Moreover, tests based only on a breakdown criterion are considered insufficient in order to reliably qualify the tested cable [7, 8]. An external voltage source is necessary for the voltage withstand test to energise the cable capacitance. For HV withstand testing two types of AC voltages are utilised nowadays [4]:

1. Continuous AC voltage (AC).
2. Damped AC voltage (DAC).

For continuous AC, the capacitance of the cable produces high power requirements for the test power generator to compensate losses during cable resonant voltage testing. For continuous AC voltage, a mobile resonance test-set is used nowadays with a variable test voltage frequency of 20-300 Hz. Another type of withstand test is the so called "soaking test". This test is performed on new circuits or after-repair circuits at nominal voltage (50/60 Hz power network supply) obtained by connecting a new circuit for e.g. 24 h to the network without load [4]. The test is called successful if no breakdown occurred in any of the cable system components. However, such tests prove that this type of withstand test is not efficient as many installation related defects have partial discharge inception voltage (PDIV) above nominal voltage U_0 [7, 8]. Since 1999, the damped AC (DAC) systems have been used for

testing and diagnosis [12, 13]. Since 2015 the DAC method has been the standardised method by IEEE400.4 [14]. This method can provide a damped AC overvoltage withstand test with a fixed number of multiple DAC excitations. A single DAC excitation is a process which consists of:

- The charging period ranging from a few seconds up to a few tens of seconds (the duration depends on the capacitance of the tested cable).
- The switching period (few microseconds).
- Damped AC voltage, which is obtained through the resonance effect between cable capacitance and fixed system inductance.

The DAC frequency depends on the system inductance and the cable capacitance (given by cable parameters and cable length), the duration of the oscillation (range of several hundreds of milliseconds) depends on the damping effect of the cable. Withstand tests executed with DAC voltages can be performed simultaneously with PD diagnosis. In this way, monitored withstand tests can be executed on the test object. Diagnostic parameters characteristics as PD amplitude, intensity and location are used to qualify (assess) the circuit. In particular, partial discharges are detected according to IEC 60270 standard and evaluated. In such a way, the real condition of the cable insulation and accessories can be assessed by measuring the occurrence of PD related defects. This information is very important as the insulation breakdown can occur later during cable energising or a long service operation, but not necessarily within the withstand voltage test duration of e.g. 1 hour. A DAC voltage withstand procedure involves PD measurements during:

- Increasing the DAC test voltage level up to the maximum test voltage level of e.g. $1.7-2.5U_0$ as some defects have PDIV at higher test voltages.
- The over-voltage withstand test to assess the effect of the maximum voltage and time.
- After the withstand test to confirm non-destructive character of the just performed DAC voltage withstand test.

As a result, data which are obtained during DAC voltage testing provide the following information:

- Effect of over-voltage condition (breakdown yes/no criteria).
- Presence of PD related and breakdown related defects in cable and accessories.
- Characteristics such as PD amplitude, PD intensity, PD occurrence, PRPD patterns.
- Location of the PD sources in the cable (using Time Domain Reflectometry analysis).
- Information about the non-destructive character of the performed withstand test.

Non-monitored vs. monitored voltage withstand test

Due to different purposes of withstand testing at different stages of cable service life or due to different possible defects present in insulation and accessories, the following aspects regarding voltage withstand testing have to be considered prior to test execution:

- The specific information about the cable system, e.g. age and condition requires various testing approaches to over-voltage application.
- Maximum test voltage level and duration (specified by, e.g. IEC standard in case of new circuits).

- Non-destructive evaluation of the condition of the aged cable systems based on withstand tests.

Such tests consist of a combination of measurements of diagnostic parameters such as partial discharges and dielectric losses. In this mode, besides the yes/no criterion, additional criteria are considered as diagnostic parameters, e.g.: PD location, PD level, PD intensity and PD pattern characteristics observed while increasing the test voltage and the voltage withstand test itself. The test can be terminated, e.g. if PD parameters fall out of the specified safe value ranges. It is an especially important aspect for “mixed” cables, where in one cable link a very old part and a new part of cable coexist as a consequence of repairs. Table 1.1 shows major differences between monitored and non-monitored voltage withstand testing.

Table 1.1
Differences between monitored and non-monitored voltage withstand test.

on-site non-monitored withstand test	on-site monitored withstand test
<p>Process in which the behaviour of the newly installed cable system under electrical field stress is investigated (voltage withstand test) with application of external voltage source.</p> <p>Applicable voltage sources: AC/DAC</p> <p>Over-voltage: Yes</p> <p>Testing is based on the application of electric stresses with a goal to indicate with pass/fail criterion the quality of the whole cable system being under the test and qualify it to service operation. Voltage and test duration depends on the type of the test object (voltage rating) and the recommendation used, e.g. IEC standards for on-site testing of HV power cables.</p> <p>Diagnostic parameters: No</p> <p>Test criteria: breakdown during the test</p> <p>Experience in diagnostic data analysis :No</p>	<p>Process in which internal cable defects and dielectric insulation properties are evaluated under electrical field stress generated by external voltage source.</p> <p>Applicable voltage sources: AC/DAC</p> <p>Over-voltage: Yes, but in case of service aged circuits it is not obligatory due to diagnostic parameters.</p> <p>Diagnosis is based on the application of electric stresses in combination with selected diagnostic parameters to indicate/localize/identify a defect. Voltage and test duration depends on the cable condition and its failure history. Based on the interpretation of the diagnostic, information about the defect(s) impact on power cable reliability can be obtained.</p> <p>Diagnostic parameters: Yes</p> <p>Test criteria: breakdown and diagnostic parameters like: PD parameters and PD location, dielectric loss, leakage-currents, insulation resistance.</p> <p>Experience in diagnostic data analysis :Yes</p>

Results shown in [15, 16, 17] on on-site condition assessment of service aged HV/EHV power cables, show that the PD measuring method is reliable in retrieving information about the ageing status of the insulation and cable accessories. This approach is getting more and more popular together with the standard voltage withstand test and is called “monitored voltage withstand test/diagnosis” even though on-site PD measurements are actually not mentioned by IEC standards and only described in IEEE 400.4 (2015). According to the data presented by IPH Berlin in 2007, the total number of after-installation tests with PD measurements was

clearly increasing [15], for example in 2000 the company performed 25% of the total number of the acceptance tests in parallel with PD diagnosis, whereas in 2006 75% of the total acceptance tests were accompanied by PD measurements. In 2015, IPH Berlin claimed that almost 90% of the total performed acceptance tests in Europe were monitored by parallel PD measurements.

On-site PD diagnosis

Two approaches to on-site PD measurements are used nowadays (Figure 1.12): conventional (classical) PD detection (according to IEC 60270) and non-conventional PD detection. The advantage of PD measurements in compliance with IEC 60270 is a specified calibration procedure which ensures reproducible and comparable PD test results. Measurements can be performed with different measuring systems which give the reading output in pico Coulombs [pC] of the measured apparent charge. However, the main drawback of conventional PD measurements is that the signal/noise ratio is strongly reduced by the limitation of measuring frequency below 500 kHz. Measurements with conventional systems operate in the frequency range below 1 MHz. Narrow-band measurements in the 9-30 kHz are characterised by a centre frequency between 50 kHz and 1 MHz, whereas wide-band measurements are in the range <100 kHz-1MHz>. Conventional systems utilise a coupling capacitor connected in parallel to the test object in order to measure the charge transfer and voltage drop occurring at the circuit during the discharge.

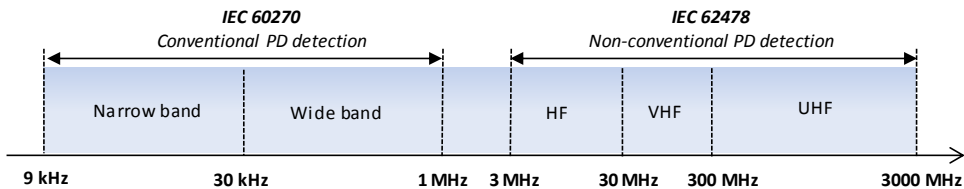


Figure 1.12: PD detection frequencies range for conventional and non-conventional PD detection.

Secondly, non-conventional detection, e.g. radio frequency (RF) technique detects the transient electromagnetic phenomena generated by charge displacement in the discharge area (locally). PD pulses are characterised by rise times in the nanosecond range. Therefore, the resulting frequency spectrum may cover several hundreds of MHz and more. This high frequency spectrum is well detectable by means of inductive and capacitive sensors. The measuring system can be applied locally on power cable accessories like joints and terminations. Figure 1.13 presents a basic configuration where PD sensors are installed around the ground connections of the accessories. With non-conventional PD detection it is not possible to calibrate the system and test object in accordance to IEC 60270, therefore PD readings are displayed in volts, or more often in mV. Selecting centre-frequencies with a proper transfer can be done by determining the transfer function of cable joint or termination in combination with the HF/VHF/UHF partial discharge detection system. After certain sensitivity of the measuring system is obtained, the performance check can be done to verify the detection on a particular test object in specific on-site conditions. This method can be utilised both for on-line and off-line PD measurements.

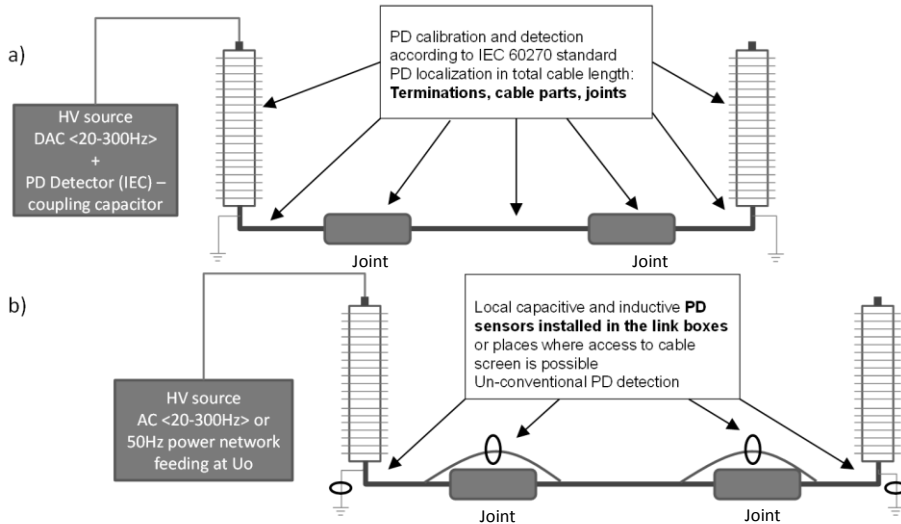


Figure 1.13: Principles of voltage testing and PD measurements a) conventional (off-line) PD detection in Pico Coulombs [pC], b) un-conventional PD detection (on-line/off-line) in volts [V].

On-site dielectric loss diagnosis

Dissipation of energy in insulation under electrical stress is caused by several dielectric phenomena. The most important are [18]:

- Conductive losses caused by finite bulk resistance of the insulation and other leakage currents.
- Polarisation losses arising from dipole orientation under the applied field.
- Interface losses between materials with different dielectric constants (or relative permittivity).
- Partial discharge (PD) losses.

These processes contribute to increase of dielectric losses, which can be measured as the dissipation factor or $\tan \delta$. This diagnostic parameter can be used to measure integral insulation degradation. In the past, the dielectric losses could be measured only with laboratory methods, e.g. Schering-Bridge, which were very sensitive to temperature and moisture and therefore not usable in the field. Other solutions to measure dielectric losses are based on the analysis of gas content in impregnating/insulating medium, e.g. DGA (Dissolved Gas Analysis). This method is applicable mostly for SCFF or HPFF cables and oil filled cable terminations. The content of gases in oil samples, e.g.: methane, butane, which are related to certain ageing phenomena and can be determined in the laboratory. Assessment procedures involve on-site acquisition of a small sample of oil during the inspection of the oil reservoir tanks for laboratory analysis, therefore this method can be considered as “semi-on-site”.

Estimation of dielectric loss from DAC voltages

In case of DAC voltages test method, the estimation of dielectric loss parameter (dissipation factor) is based on the calculation of the DAC test voltage attenuation coefficient. During the on-site voltage testing of HV cables the obtained damped sine wave is characterised by a

certain damping factor (Figure 1.14). It is the attenuation factor β that depends on the cable impedance and the internal DAC system resistance (determined during factory calibration).

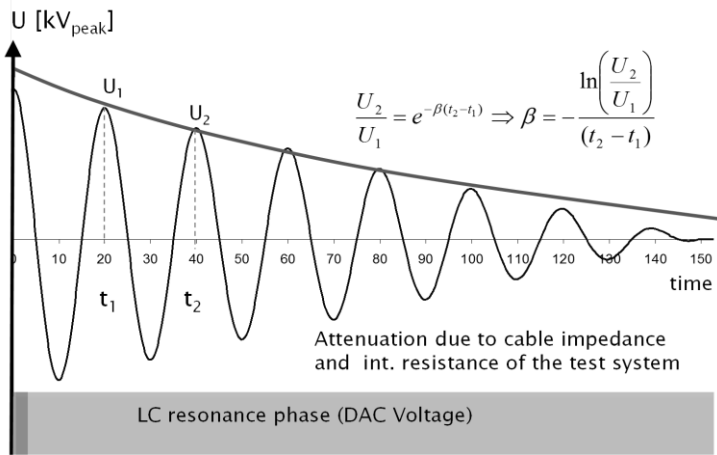


Figure 1.14: Attenuation coefficient calculation principles.

For the calculation of the attenuation coefficient two peaks (positive or negative) are taken from the obtained DAC voltage. When combined with the corresponding time instants, it will give the value of the attenuation coefficient. The calculated value of the attenuation coefficient β , together with the total equivalent internal system resistance R_1 (described in details further in this thesis), oscillating frequency ω and inductance L will give the value of the dielectric losses called DL in the tested cable according to equation below [14].

$$DL = \frac{2\beta}{\omega} - \frac{R_1}{\omega L} \quad [1-1]$$

1.4 Asset management for transmission cables

Asset management (AM) refers to certain strategies to obtain the required reliability of the power network [1]. In general, AM decisions for transmission power cables focus on cable systems reliability. One of the goals is the constant low failure rate in conjunction with economic, environmental, societal and technical factors. In particular, five main processes for AM decisions can be specified to achieve this goal:

- **Refurbishment**-replacing some components of the old system to achieve enhanced assets reliability, functionality and availability.
- **Upgrading**-replacing the aged cable system components with new ones to restore to “as new” condition.

- **Replacement**-complete change of the aged circuits, e.g.: old oil filled cables with extruded cables to achieve, e.g. lower pollution of the environment, more capacity.
- **Repairs**-replacement or fixing of small portion of the circuit that is faulty and may influence cable reliability.
- **Maintenance**-with minimal cost keeping aged assets running.

The asset management decision process regarding servicing aged systems is usually dictated by a long-term replacement policy of the oldest or the cables in the worst condition (Figure 1.15). Power utilities have to select which particular section or complete circuit should be replaced in the first place. From a technical point of view, the prioritisation of assets' health in terms of: a critical, semi-critical or safe asset is based on:

- Actual condition of the assets-analysis of different diagnostic parameters, e.g.: dielectric loss and PD or a combination of both.
- The criticality of the equipment in the network.
- Failure rate.
- Expected remaining life time at particular service conditions.

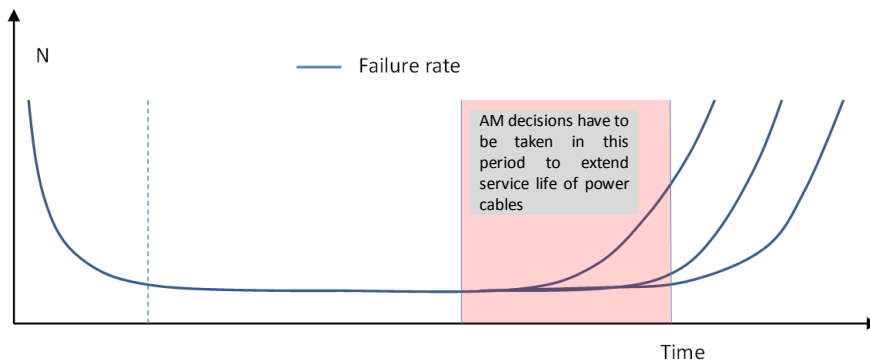


Figure 1.15: Impact of the AM decision on failure rate (life time) of power cables.

All information inputs should be correlated and investigated in order to specify the optimum sequence of replacement/refurbishment for the individual cable section. In order to make a judgment whether an asset has reached the end of its useful life, it is important to set up the acceptable limits for particular service life stages. Once the asset condition falls outside such limits, action is necessary as presented, e.g. in Table 1.2. Furthermore, the ageing models that indicate the degradation rate of cable insulation can be also used to support final decisions. Ageing tests on cable samples taken out of service or cable system components reaching breakdown or the moment of harmful changes in the insulating material, should provide the reference values to support the on-site condition assessment on the similar type of cable/insulation type and to understand the ageing processes.

Table 1.2:
Example of condition indexing (CI) and condition related AM decisions [1].

Index	Status	Condition	AM decision
A	Very good condition, stable	New or Aged: no defects or aging symptoms	Minimal maintenance – go for optimal availability and reliability
B	Good condition	Aged: degradation observed, possible presence of harmful defects	No impact on the reliability – keep status B, against minimal costs and maintain optimal availability
C	Stable, poor condition		Reliability decreased. Refurbish to status B or stabilise to prevent fast aging. Maintain optimal availability by periodical condition assessment
D	Instable situation	Defect present, progressing aging	Very low reliability. Instable situation, end as quick as possible.
E	End of life cycle		No operation recommended. Maintenance aimed to prevent environmental pollution and safe conservation. Extension of life time or availability is no issue.

The technical impact on final AM decisions is the result of an interaction with economical and societal aspects, which are different for each company. Some power utilities’ strategies are shaped by public service, minimum cost; others may be shaped by maximum profit or parameters such as cash flow, return on investment etc. For others, public image may take priority [1]. The most critical (unreliable) asset will be weighted with those criteria important to the business policy. Therefore, condition data describing actual status are crucial for asset managers in making the final decision. Based on the information provided during periodic or condition based inspection, the actual condition of the tested cable and components can be used to schedule necessary maintenance activities and to determine the reliability of the particular asset in the total network configuration.

1.5 Objectives of present study

HV/EHV cables should be reliable under all operational conditions and stay defect free in service. For this reason, the testing system shall be designed in such a way that besides overvoltage test conditions, diagnostic parameters can be measured and evaluated.

The purpose of the investigation presented in this thesis is to develop a standardised uniform test procedure using DAC for both newly and aged transmission power cable systems in the field. Additionally an AM (asset management) decision support model will be developed based on both service and operational conditions of power cable service. To achieve this goal, research results from on-site tests obtained with DAC method in the field as well as in the laboratory. Accelerated ageing tests on oil-impregnated insulation will be compared and verified with the Arrhenius¹ formula. Results of both the laboratory and on-site test will be used to predict cable life time. On-site diagnosis on HV and EHV cables contained in this document are based on four years of practical research and diagnosis in the field of DAC voltages. All laboratory investigations on the detectability of assembling errors are conducted on real full size cables and cable accessories. Furthermore, the following research was performed:

1 The Arrhenius equation is formula for the temperature dependence of the reaction rate constant, and therefore, rate of a chemical reaction.

- Identification of the typical joints and terminations assembly defects that are related to poor workmanship onsite.
- Evaluation and verification of PD detection capabilities of the DAC method for different DAC frequencies that depend on the cable length.
- Analysis of the PD measurements results ranging from newly installed to aged cable systems in the field.
- Statistical analysis of PD detection and dielectric loss measurements performed on service aged oil impregnated paper insulated 50 kV and 150 kV gas-pressurised power cables.

1.6 Structure of the thesis

The research in this thesis is structured in the following way:

- Chapter 1:** Introduction to transmission power cables, on-site testing methodology and problem definition. With reference to the latest IEEE 400.4 2015 guide, discussion about off-line monitored/non-monitored voltage withstand testing. Applicability description of the two major diagnostics parameters used nowadays for on-site tests of HV/EHV power cables.
- Chapter 2:** Overview of the most important assembly defects in HV power systems which may lead to cable failure. Review of major installation related defects of extruded cable accessories and defects symptoms.
- Chapter 3:** Ageing-related defects in HV power cable systems and symptoms.
- Chapter 4:** Damped AC method: voltage generation, technical aspects, features, applicability, available diagnostic parameters.
- Chapter 5:** Investigation of installation defects in extruded cables. Laboratory investigation on detectability of different defects for different energising sources: continuous AC 50 Hz and DAC at different frequencies.
- Chapter 6:** Examples of on-site tests and diagnosis on HV/EHV power cables. Examples of condition assessment approach for newly installed and service aged transmission cables by on-site diagnostic tests. Procedures for testing, result analysis for the DAC method.
- Chapter 7:** Generation of the “insulation life consumption model” to support asset management’s decisions based on two different types of data:
- Operational cable parameters, e.g.: cable load, cable temperature
 - On-site diagnostic parameters: dielectric loss measured with DAC method
- Chapter 8:** Conclusion and recommendations.

2. Transmission power cable accessory installation and assembling related defects

Cable installation and assembly failure refers to the situation when one or more cable system components such as cable joint or termination fails because it cannot withstand operational conditions. This happens as a result of local lower dielectric breakdown strength. Lower dielectric voltage breakdown strength is related to dielectric material condition.

“Most failures in paper insulated cables are due to third party damage and other exterior failure causes (67%), followed by oil leakage of SCFF cables (12%). Overloading is not considered to be a failure cause at all (0%). Regarding high voltage cables with extruded insulation, only 7% of all failures are due to ageing. Third party damage, water treeing and other causes such as poor installation, manufacturing and construction, rank higher with 65%, 13% and 15% respectively [9].

Based on the literature study and onsite experience, several most common assembling defects are explained in this chapter. Some of them are simulated in the HV laboratory and further investigated in chapter 5.

2.1 Accessory assembly

Installation and assembly defects are related to poor workmanship. Considerable amount of assembly defects result in high electric field distribution inside the cable accessory [3, 4, 17]. HV/EHV cable accessories that are not free of these defects should fail during over-voltage acceptance tests. However, sometimes a defect is not detected and causes a failure, e.g. a few months after installations. Our experience collected during acceptance tests (after-laying of new circuits) pointed out that mainly poor workmanship is responsible for cable system failures that occur during after laying testing. Investigation results presented in [7] confirm that *“12% of the total number of performed tests resulted in breakdowns mostly in joints and terminations during voltage withstand tests at maximum test voltage level or during voltage increasing. While some of the installation defects are intermediate failures, other develop slowly and need more time to develop into a failure under operational conditions”*. Most of HV and EHV cables have extruded polymer insulation (XLPE) nowadays. The examples of installation defects which will be presented in this thesis refer to accessories for this type of cable only.

2.1.1 Assembling process

Assembling of cable accessories is a process where two cable parts are galvanically connected. Their integrity is ensured by application of cable joints, which are also called “splices”. Splicing or jointing of high voltage electrical cables is required in order to maintain the electrical continuity of the conductor and shields, as well as to maintain the insulation levels of the two electrical cables joined together. By jointing two separate conductors, insulation is also built up over the exposed conductors to provide insulation properties similar to those of the cable insulation. Cable shields are jointed to confine the electric field to the insulation [4]. Different types of joints are used, e.g. stop joints (prevent oil circulation in the cable in case of SCFF and XLPE cables connection), transition joints (connect different types of cable within one circuit), straight-through joints and cross-bonding joints. More information about joints can be found in [4]. Before the two cable parts can be “connected” they need to be carefully prepared prior to the jointing process. In general terms, such a process is called “cable peeling or cable preparation” and it is performed in compliance with standardised procedures and measures aimed for particular types of cables and joints. For instance, in the case of XLPE cables, the cable’s outer protection (cable sheath) as well as field-smoothing layer have to be removed during the peeling. The exposed conductive layers, e.g.: semi-conductive screen (semicon), outer and inner screens, produce a concentration of field. Due to the presence of tangentially distributed electrical field stress, electric field is built up in the area around the cable dielectric and the insulation boundaries [4]. Application of a joint (including grading elements) ensures not only proper electric field distribution in the area of galvanic connection, but also stable electrical and thermal conditions. Figure 2.1 presents the process of cable preparation prior to jointing (splicing) [4]. Solid dielectric insulated cables are jointed in one of the two ways:

1. Hand wrapping with insulation tape.
2. Slipping a pre-moulded cable splice on the joint/terminated conductors.

In case of hand wrapping, a highly-skilled cable joiner, is required. A cable joiner/splicer must select the proper tape for each stage of the insulation building process and make sure that no air voids or contaminations are present in the final joint.

Pre-moulded or slip-on cable splices for solid dielectric insulated cables are easier to install than for example oil-filled cables. This type of cable splice is designed and manufactured in order to provide the insulation levels and electric field distribution required for a given size of electrical cable. Therefore, the manufacturer is able to test the insulation level and electric field control prior to shipping. This type of cable splice can be installed in less than half of the time required for a hand-wrapped cable splice, although peeling and cable smoothing is also required. Assembly of cable accessories is also related to cable terminations (sealing ends). Here cable ends are connected to the electrical network system with different types of terminations, e.g. transformer sealing ends inserted directly into transformer body, outdoor terminations connected to overhead lines, GIS terminations (gas insulated and integrated within switch gear body). More information about terminations can be found in [4]. Cable termination functionality and internal construction can be compared to “half” of the construction of a cable joint. In case of a termination, the electric field distribution needs to be altered (distributed) in the same way, too. Field steering elements of e.g. polymer insulated power cable terminations have one deflector applied over the “peeled” edge of the

outer semi-conductive layer. In this way, the enhancement of the field at this point is limited. A complete sealing end is placed in a synthetic or porcelain cylindrical insulator. The insulator tube is filled with an impregnating medium or kept under pressure of gas e.g. sulphur hexafluoride (SF₆). Various terminations and joint types can be found in CIGRE documents [23].

General jointing procedure for XLPE HV/EHV cables

1. The sheath is stripped back to the outer semi-conductive layer.
2. The conductor is exposed by cutting back the cable insulation in a straight line.
3. The outer semi-conductive layers are removed over the same length from both sides and the stripped edges are carefully prepared as well as conductor edges in the area where they come in contact with the joint insulation.
4. The body of the joint is pushed on one of the cable in "park position".
5. The conductors are connected and HV electrode is applied.
6. The joint body is placed centrally over the conductor connection with hydraulic system and use of lubricant (placed over cable insulation and semi-conductive layer.
7. The outer semi-conductive layers of both ends of the cable are connected with the semi-conductive coating (varnish) of the joint body and external housing is assembled.

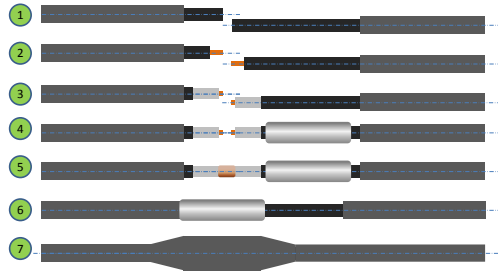


Figure 2.1: Example of assembly process of a slip-on joint for XLPE HV cables [4].

2.1.2 Electric field distribution in cable system

Cable joints and terminations are designed in such a way that the electric field intensity does not exceed the permissible limits inside the cable accessory. From an electrical failure point of view, electric stress distribution is of great importance. The tangential component of the electric field provides stress in parallel to the surface of the dielectric material and has a big impact on the cable accessory defect development. High voltage cables almost always have a coaxial configuration with conductors of inner and outer radii of a and b , respectively. The capacitance C (F/m) of such a cable is given as:

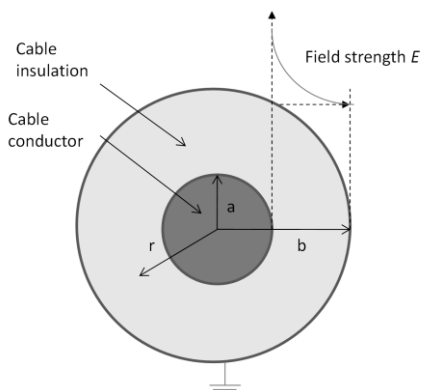


Figure 2.2: Field strength distribution in power

$$C = \frac{2\pi\epsilon_r\epsilon_0}{\ln\left(\frac{b}{a}\right)} \quad [2.1]$$

where $\epsilon_0 = 8.854 \times 10^{-12}$ F/m and ϵ_r = relative permittivity or dielectric constant of the insulation. For XLPE insulation, $\epsilon_r = 2.3$. By application of Gauss's Law, the electric stress E in the coaxial cable insulation at a distance r from the cable centre is given by:

$$E_r = \frac{V_T}{r \ln\left(\frac{b}{a}\right)} \quad [2.2]$$

wherein V_T is the applied voltage (phase to ground), r is the continuous coordinate and b resp. a is the external/internal radius of insulation layer. This equation clearly states that the field is purely radial and is confined within the outer conductor. Its value is maximum at $r = a$ and is minimum at $r = b$ (Figure 2.2).

In the above stress distribution, it was assumed that the conductor surface was smooth. However, the effects of the radius of the wires in a stranded, un-compacted conductor or other interruption, e.g. manufacturing impurities, may increase the local electric field intensity. In high and medium voltage cables, it is typical to apply a semiconducting screen to a stranded conductor in order to obtain a smooth surface. This screen would be a carbon paper tape on paper cables or an extruded semiconducting polymer in case of polymeric cables. This helps to keep the maximum stress near the conductor area and a radial field distribution in the cable [4].

However, the electrical stress is distributed in a different way in a complete cable system and the highest electrical field intensity is always at the cable ends. The disruption of the normal radial field distribution in the cable occurs due to a change in the cable geometry in cable accessories. Prior to jointing or terminating, the outer semi-conductive screen is removed to provide sufficient distance between the conductor and the screen in order to reduce the electrical stress at the cable edge. The electrical field intensity is greatest where the equipotential lines are concentrated. To alter and distribute the field of highest density, stress control is required to reduce the electrical stress intensity below levels at which the air would break down or discharges would occur in the insulation or over the surface of the insulation. In the nominal cable conditions, the operational electric stress on the outer conductive layer of the joint/termination should not exceed 6-7 kV/mm [4] for HV cables.

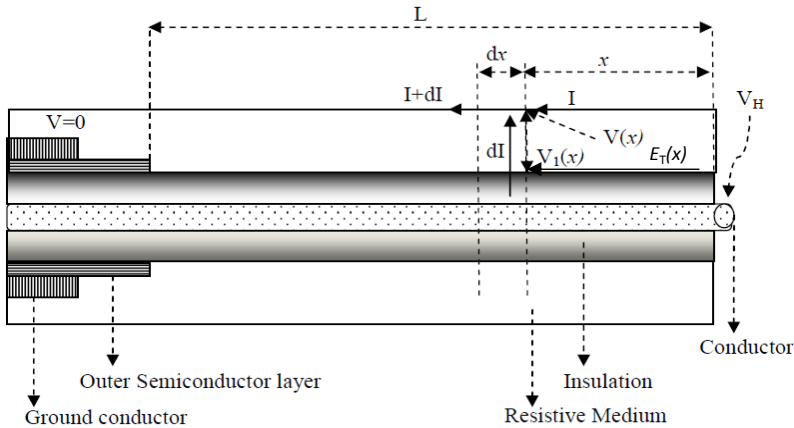


Figure 2.3: Exposed HV power cable end [24]

The tangential stress E_T (Figure 2.3) along the cable insulation surface at distance x (from the edge of the exposed cable end) can be calculated using the following equations [24]:

$$\frac{dV(x)}{dx} = -RI(x) \tag{2-3}$$

$$\frac{dI(x)}{dx} = j\omega RC V_H - j\omega CV(x) \quad [2-4]$$

In the equations 2-4 and 2-5, ω is the frequency of the AC voltage, C is the cable capacitance and V_H is the voltage applied to the conductor, R-resistance of dielectric and I-current. From equations [2-3] and [2-4] we can make one differential equation:

$$\frac{d^2I(x)}{dx^2} = 0 - j\omega C \frac{dV(x)}{dx} = j\omega RC I(x) \quad [2-5]$$

Equation 2-6 has a solution of the form:

$$I(x) = A_1 e^{\gamma x} + A_2 e^{-\gamma x} \quad [2-6]$$

$$\text{Where } \gamma = \sqrt{j\omega RC} \quad [2-7]$$

Where A_1 and A_2 are constants. From equations 2-4 and 2-6, $V(x)$ can be expressed as:

$$V(x) = V_H - \frac{R}{\gamma} (A_1 e^{\gamma x} - A_2 e^{-\gamma x}) \quad [2-8]$$

$$\text{At } x=0, V(x) = V_H \quad [2-9]$$

and

$$V_H = V_H - \frac{R}{\gamma} (A_1 - A_2) \quad [2-10]$$

$A_1 = A_2$ also, at $x = L, V(x) = 0$, or:

$$0 = V(x) = V_H - \frac{R}{\gamma} (A_1 e^{\gamma L} - A_2 e^{-\gamma L}) \quad [2-11]$$

Based on the equation [2-10] and [2-11] it can be written as:

$$A_2 = A_1 = \frac{\gamma V_H}{2R \sinh \gamma L} \quad [2-12]$$

By expressing equation [2-6] and [2-8] with equation [2-11]:

$$I(x) = \frac{\gamma V_H \cosh \gamma x}{2R \sinh \gamma L} \quad [2-13]$$

$$V(x) = V_H - \frac{V_H \sinh \gamma x}{\sinh \gamma L} \quad [2-14]$$

The tangential stress $E_T(x)$ along the cable insulation surface at distance x from the cable can be expressed as:

$$E_T(x) = \frac{-dV(x)}{dx} = \frac{\gamma V_H \sinh \gamma x}{\sinh \gamma L} = RI(x) \quad [2-15]$$

Moreover, the voltage $V_1(x)$ appearing across the cable's insulation at distance x from the cable's end is expressed as:

$$V_1 = V_H - V(x) = \frac{V_H \sinh \gamma x}{\sinh \gamma L} \quad [2-16]$$

For the control of the field distribution in the cable accessories (Figure 2.4), two solutions are used to reduce total electric field magnitude $V(x)$ and magnitude of the tangential component E_T :

- 1) capacitive control.
- 2) geometrical control.

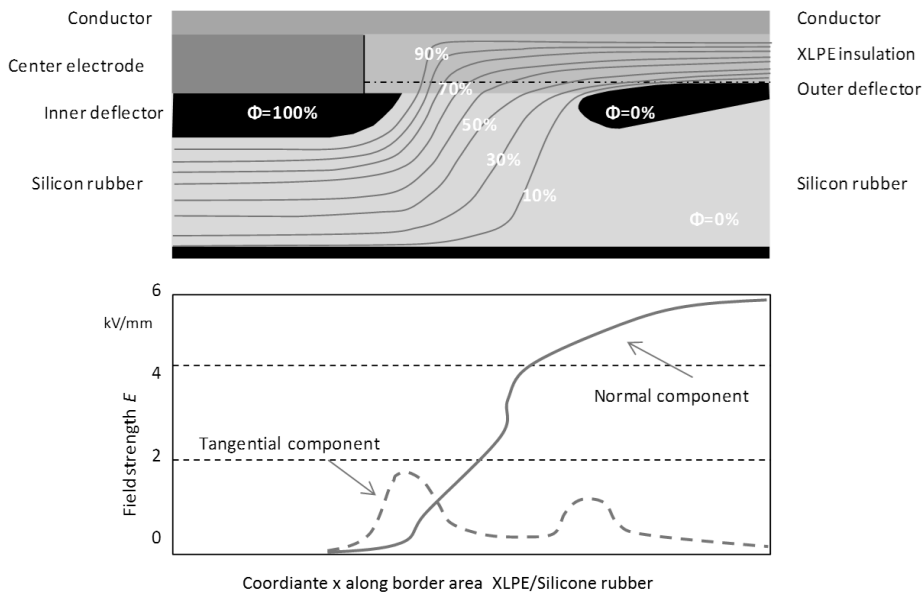


Figure 2.4: Calculation of the potential distribution and field patterns in prefabricated slip-on joints for XLPE cables [4].

Geometric-capacitive field control

This solution is based on the principle of the volume capacitance at the end of the conductive layer. The electric field is reduced by “emphatically” lengthening and expanding the outer conductive layer by the formed shape of elastic semi-conductive and conductive silicon-rubber compounds or EPR/XLPE called control funnel or control deflector [4]. For modern extruded cables, e.g. XLPE cables, control deflectors have the prefabricated slip-on design, e.g.: pre-moulded rubber stress relief cones for terminations and pre-moulded one-piece rubber for joints. Within these prefabricated accessories all field control elements are included. Jointing or cable termination assembling work is limited to slipping-on the elastic bodies onto the prepared (peeled) cable cores. Control elements of sealing ends have normally only one deflector, which is fitted over the stripped edge of the outer semi-

conductive layer. Joints consist of two deflectors with field smoothing cover of the joint provided to maintain outer screening.

Capacitive field control

Shown in Figure 2.5-is based on the fact that the distribution of the electrical field can be changed by applying the artificial equipotential surfaces into the field zone in the form of the conductive/semi-conductive layers. In cable joints/terminations, it is achieved by cylindrically formed capacitors connected in series. For paper insulated power cables the “capacitors” have the form and shape allowing for smooth control of the electrical field radially and axially and are made of oil-impregnated paper strips belted around the connection point. This solution is used for paper insulated cable systems and is done completely and manually in the field. In the past, a lapped field control was used for extruded cables consisting of polypropylene foils, cross-linked PE types and self-amalgamating EPR types (onsite moulded) [25]. Nowadays, the capacitive stress control elements are produced in the factory on tubes of a suitable diameter, delivered on site in an impregnated status.

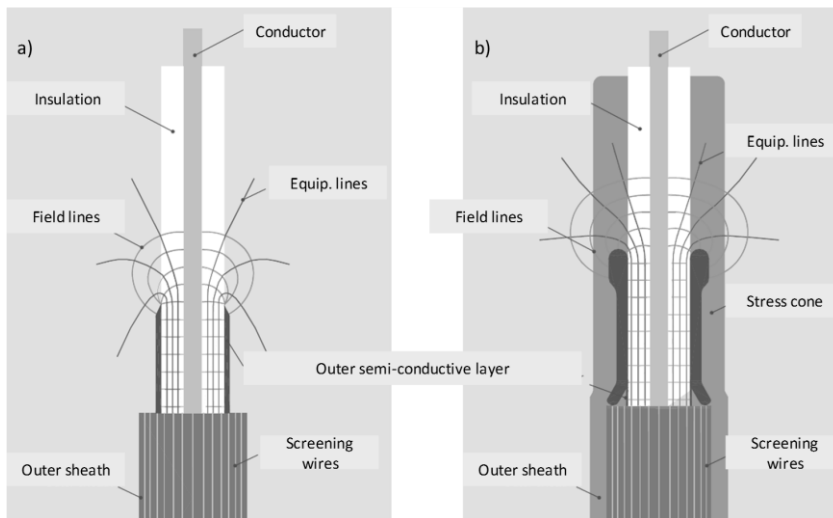


Figure 2.5: a) Example of electrical field without stress control. b) Electrical field with capacitive stress control [4, 86].

2.1.3 Electric field enhancement

The electrical field along interfaces (part of the field parallel to the interface) is always a critical point as the dielectric strength of this interface is practically lower than the strength of solid insulation. The electrical strength of this interface depends mainly on the mechanical design of the joint/termination but also, to a great extent, on proper on-site assembly. During the assembly process it is important to avoid any contamination or mechanical damages to the exposed stress cone. Impurities may change the distribution of the electric field equipotential lines making them more intense (cumulated) and locally concentrated. The abnormal concentration of these lines in the interface structure between two materials is shown in Figure 2.6.

Voltage applied across dielectrics in series will divide in inverse proportion to the dielectric constant of the material (Gauss's law). Thus, when the gas filled void is in series with the cable insulation, a portion of the voltage will appear across the gap/void. The surface of the insulation or cable will then have a voltage-to-ground equal to the voltage across the void/gap. This voltage can approach the full conductor potential when the volume of the void/gap is large and will approach ground potential. The magnitude of the electric field that gives rise to the dielectric breakdown in dielectric materials is called the breakdown strength. As a result of greater electrical field strength in this point a discharging process may occur in e.g. micro voids and across contaminated dielectric surfaces. Local deterioration by a discharging process may finally breakdown the dielectric as a result of irreversible chemical and physical changes.

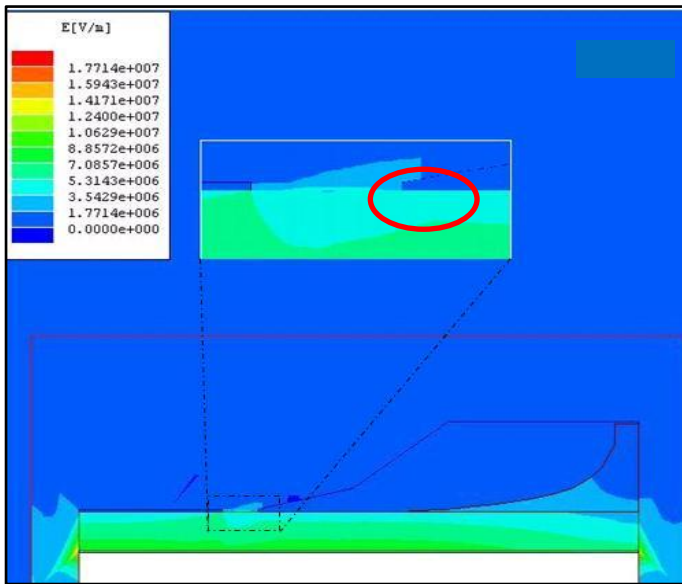


Figure 2.6: Example of electric field enhancement simulation for a joint with a missing semi-conductive screen layer close to the joint housing edge. Electric field plotting for inhomogeneous radial conditions with 15 mm (approx. 2 cm²) missing layer (gap) under HV test at 0.5xU₀ (150 kV XLPE cable), with field enhancement at the defect edges close to joint housing approx.: 3,5 kV/mm.

Figure 2.7 shows a theoretical example of a distorted field distribution as a result of a gas filled void in the dielectric material. In the case of a gas-filled cavity or trapped air, bubbles can arise in damaged semi-conductive screens or at the interface between the screen and the cable insulation. The thickness of the dielectric material is marked in Figure 2.7 as d and it contains a cavity in a form of a disc of thickness- t . In the analogue circuit, the capacitance C_c represents the cavity, C_b corresponds to the capacitance of the dielectric which is in series with C_c , while C_a is the capacitance of the rest of the dielectric. Assuming that $t < d$ and that the cavity is filled with gas, the field strength across C_c is given by equation [2-17] [18]:

$$E_c = \varepsilon_r E_a \quad [2-17]$$

where: ε_r is the relative permittivity of the dielectric.

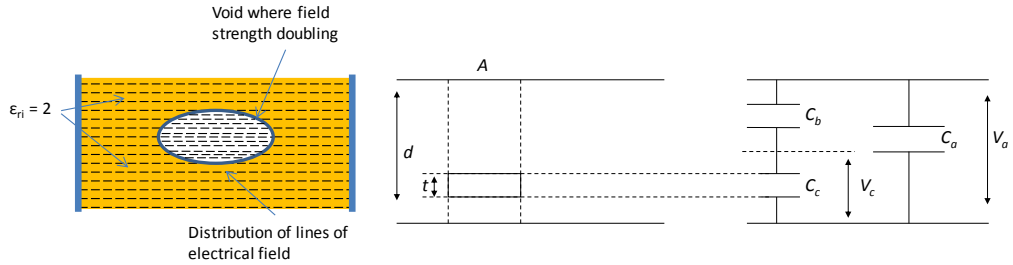


Figure 2.7: Equipotential lines distribution in dielectric material and gas filled voids under electrical field (left) and its equivalent circuit (right).

The discharge inception voltage applied across the dielectric can be calculated in terms of the cavity breakdown stress. Taking into consideration that for example breakdown stress of the gas-filled cavity is: E_{cb} , and considering the cavity as a series capacitances with the healthy part of the dielectric, it can be written:

$$C_b = \frac{\epsilon_0 \epsilon_r A}{d-t} \quad [2-18]$$

$$C_c = \frac{\epsilon_0 A}{t} \quad [2-19]$$

The voltage across the cavity is :

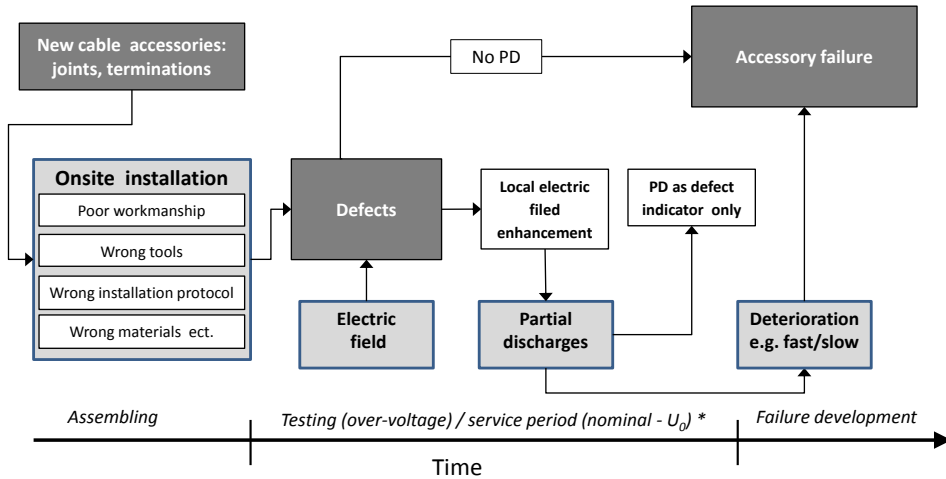
$$V_c = \frac{C_b}{C_c + C_b} V_a = \frac{V_a}{1 + \frac{1}{\epsilon_r} \left(\frac{d}{t} - 1 \right)} \quad [2-20]$$

In case of a protrusion in the semi-conductive layer, the risk of electrical “over-loading” of the dielectric area is high due to the greater concentration of the equipotential lines. The effect of this field distortion manifests itself as changes in the material by an initial hollow channel formation (μm long). After a channel is created, the gas fills the space created by channel discharges. It is called: “channel growth initiation” [17]. The final form is called “electrical tree” or “tracking” and results in dielectric breakdown. The difference is that deterioration caused by electrical trees goes inside (cross-erosion) the insulation rather than onto the insulation surface-which is more suitable to be described as tracking or surface treeing driven by tangential components.

2.2 Typical installation and assembly defects

Distortion of the electric field distribution through installation/assembly defects in the cable accessory can be a source of cable system breakdown. Several interactions are possible between the defect type/location, breakdown and pre-breakdown (Figure 2.8). The type and design stress level of the accessories can be related to the specific type of defect and the local electric field enhancement [26]. The interaction between the applied AC voltage stress and the breakdown depends also on the type of defect itself. With pre-breakdown phenomena such as partial discharges, they also depend to a great extent on the defect physical features, e.g.: shape, size, and localization in the dielectric material. It is known that high non-homogeneities like sharp edges, cavities and impurities are mostly accompanied by the

inception of partial discharges. It is also important to understand that in the case of PD presence, the duration and the level of voltage application are crucial for the occurrence of a breakdown.



(*) – additionally to electric stress during operational service: thermal, mechanical and environmental stress is added and may influence deterioration process

Figure 2.8: Failure process as a result of the assembly related defects.

2.2.1 Voids, contaminations on the dielectric surface

Typical defects that can create so-called assembly failures of accessories are voids or contamination located at the interfaces between field control elements and cable insulation. These might occur through incorrect or unclean assembly of these elements or mechanical damages. Voids can also occur when the water/silicon based installation gel is not correctly distributed or extensively used during the jointing process (Figure 2.9). Other factors consist of: surface roughness of the peeled cable (smoothing process), forces used to push a joint or a termination slip-on deflector/stress cone into the final position. Moreover, a certain elasticity of the joint elements that would assure good contact at the interfaces is required. For example, air bubbles introduced through lubrication may disappear after the gel vapours, however locally created ionization released by partial discharges present in air bubbles may have already produced a small portion of insulation degradation or initiation of electrical tracking over the cable insulation surface.

With the cable “peeling” process, care must be taken when removing the semi-conductive screen prior to jointing or cable termination. Any damage or nick to the insulation may result in creating a kind of unscreened, air filled voids (bounded cavity) that stay shielded (altered) under the joint body or termination stress cone. Mechanical damages to aluminium/copper cable cores may increase the temperature of the galvanic connection inside the joint as the micro space is created under the shielding connecting electrode and discharge activity is present. Any damage to deflectors and stress cones may reduce electrical breakdown strength of the accessory as the geometry and electric field distribution may change. In Figure

2.9a locations of the defects are depicted. In Figure 2.9b a photo is shown of a 150 kV XLPE cable prepared for the jointing process. It is extremely important to keep the exposed XLPE insulation clean at this moment of the jointing process to avoid contamination.

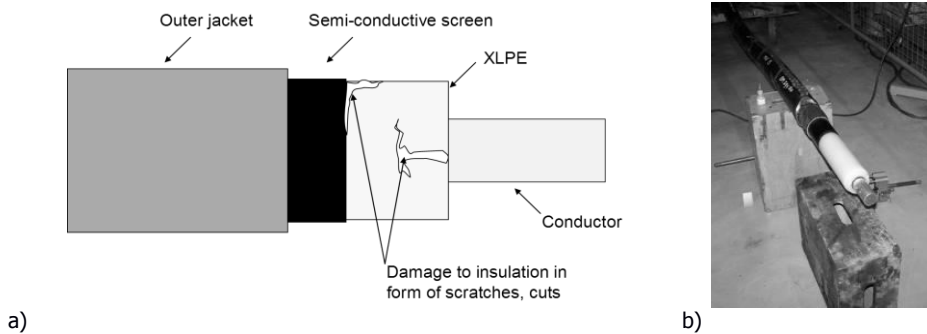


Figure 2.9: a) Example of damage to insulation during cable peeling and jointing. b) Real situation (peeled cable insulation).

2.2.2 Dielectric surface mechanical damage

Cable insulation must be clean and dry before jointing procedures. Due to the fact that cable preparation (peeling) is performed on-site-usually in special tents or containers, some dust or contamination from, e.g. tools and surroundings can be transported onto the surface of the insulation or inside joint termination elements. It can result in distortion of equipotential lines inside the accessory body and enhanced field stress between the insulation of the cable and, e.g. deflector body. Common contaminants include sand, peeling scraps on outside surfaces and semi-conductive particles left on the surface of the insulation after the conductive screen has been removed. If these contaminants remain on the insulation surfaces while being jointed or terminated, a conductive path can occur, and the difference in potential between the energized conductor and earth screen will make the current flow through the contamination, resulting in, e.g. surface partial discharge. (Figure 2.10)

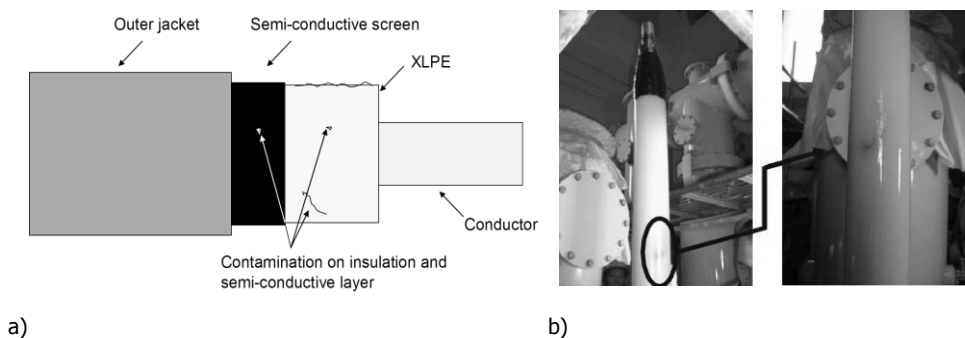


Figure 2.10: a) Example of potential contamination of the insulation surface. b) Real situation, example PD tracking on the surface of XLPE cable sealing end [27].

2.2.3 Remaining semi-conductive screen

In a cable joint, a field control deflector limits field concentration in the ends of the power cable. This control deflector represents the extension of the outer semi-conductive screen at the cable end. For this purpose, the outer semi-conductive screen on the cable end has to be peeled for the connection between the end of the outer semi-conductive screen of the cable and the control deflector in the cable accessories. An improper peeling process can result in a “remaining” semi-conductive screen, which is deposited on the interface between cable insulation and joint body. This interface represents the weak spot in an accessories construction, where the tangential field on that interface must be kept as low as possible. This situation is shown in Figure 2.11. This unwanted extension of the semi-conductive screen in the cable accessory will produce electric field enhancement in the edge of the semi-conductive screen, that can result in partial discharge activity at the boundaries between the cable insulation and the accessory insulation. Wrong peeling could be a result of wrong measurements of the distances between the stress cone and joint insulation body and, e.g. wrong tools used to peel the cable.

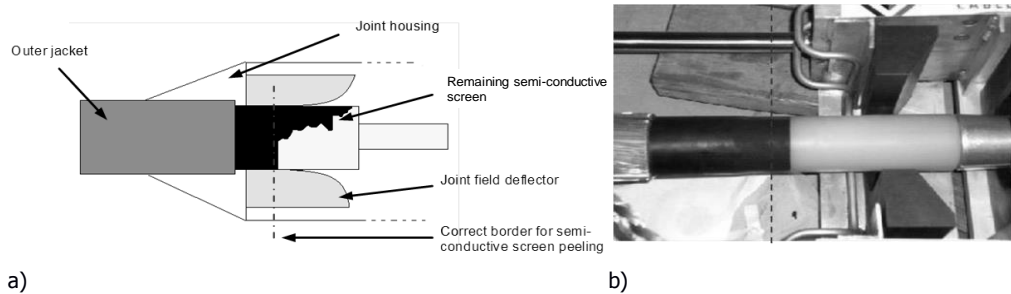


Figure 2.11: a) Example of incorrectly peeled and jointed cable with a remaining semi-conductive screen layer b) Real situation.

2.2.4 Missing semi-conductive screen

This defect represents a situation where partly unshielded cable insulation is inserted into a joint body. When the connection between the joint deflector and cable semi-conductive screen is missing, surface discharge will occur under electrical tangential field stress. The intensity and amplitude of discharges depend heavily on the missing spot size, applied voltage and field intensity created at this point. Such defect may occur as a result of improper cable finishing or use of solvents or cleaning chemicals that are not suitable for the particular type of cable accessories. A missing semi-conductive screen can also be a result of incorrect measurements or, more often, high pressure between the body of the deflector and the cable. Pre-moulded/pre-fabricated joints are applied with the help of a hydraulic system that mechanically connects two cable parts. During this process it is important to reduce the pressure inside the joint body prior to inserting the cable ends fully into the joint body. When the pressure created inside the joint distorts the geometry of the joint deflector or joint housing ends, it will result directly in micro-scratches over the semi-conductive screen. The correct application of the joint requires silicon based grease (gel) to maintain smooth slip of the cable into the joint body. Without a smooth insertion of cable ends, the mechanical

contact between semi-conductive screen and cable joint may result in the removal of part of the screen and exposed insulation (Figure 2.12).

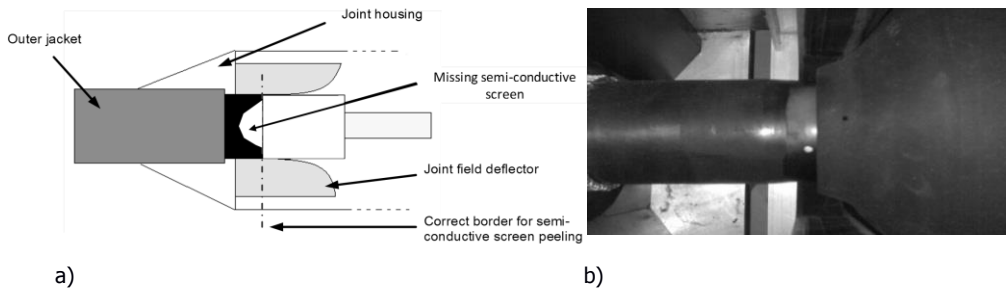


Figure 2.12: a) Example of a incorrectly peeled and joint cable with a remaining semi-conductive screen layer. b) Real situation.

2.2.5 Damages to the slip-on stress cone

Nowadays, slip-on stress cones, slip-on joints and various extrusion moulded joints and terminations are used (Figure 2.13). They consist of pre-fabricated elements for electrical field stress controllers, e.g. deflectors. The deflector is fitted over the stripped edge of the outer semi-conductive layer and reduces electrical field intensity in this place. For this type of accessory, the semi-conductive insulation (layer) is removed from the cable insulation with a special knife-like stripping tool. The exposed insulation surface is cleaned and smoothed by

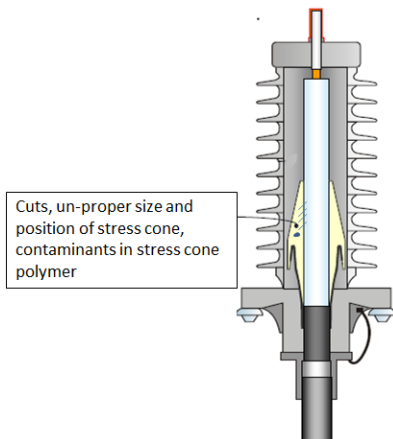


Figure 2.13: Out-door termination with slip-on stress con [4].

polishing. All traces of indentation or scratches along the surface should be removed, since they can lead to field enhancement and discharge activity under nominal voltage conditions. The field pattern is important in case of normal and tangential components of the electrical field in particular, the tangential component of the field at the interfaces being of particular importance in, e.g. slip-on/pre-moulded deflectors. A tangential component of the electrical field is locally enhanced at the interface between the cable insulation and the joint insulation. The tangential component's value can increase if the defect and roughness of the inner or outer deflectors occur and due to the lack of the semi-conductive layer in this

region or a distorted geometrical structure of the deflector itself. This lack of a semi-conductive layer close to the connection point between the deflector body and cable insulation may distort proper field line distributions. The local electrical field may become higher than permissible maximum field strength inside the joint/termination [25]. Finally, it can initiate a breakdown at the interfaces through electrical treeing over the dielectric or joint body surfaces.

2.2.6 Incorrect joint connector assembly

Connector related problems are mostly caused by two reasons: poor interface and conductor damage before applying the connector. The result is the increased resistance and heat production. By not taking care or using incorrect methods, conductors can be quite often nicked. In case of aluminium conductors in particular, it can result in individual strands breaking free, leading to a resistive “hot spot” around the connector area, causing thermal failure. The incorrect joint connector assembly produces local heating and insulation deterioration when the permissible temperatures are reached. An important part of the connector assembly for particular types of joints is also the heat-sink/shield, especially the connection between the metallic heat sink and the connector is of great importance for thermal stability inside the joint body (Figure 2.14). High temperature can create the so-called “thermal-runaway” effect. This situation refers to the phenomenon when the increase of temperature causes changes that lead to even further increases in temperature. Under high temperature, the conductivity of the dielectric material may change which results in an increase in the current flow. Chemical changes such as melting and decomposition through the chemical chain bonds scission may result in higher conductivity and in the same higher current flow. As a result, a higher temperature is released in the region of the so called “hot spot”-conductor connector assembly.

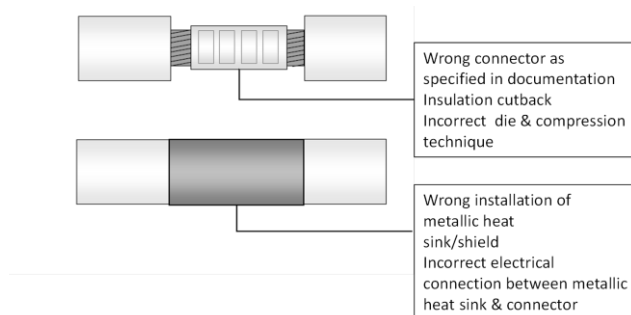


Figure 2.14: Conductor connector assembly for joints [4].

2.2.7 Imperfect sealing of joints and terminations

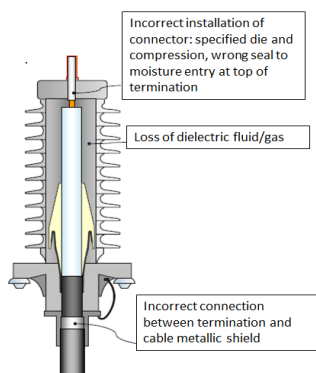


Figure 2.15: Out-door termination with slip-on stress con [4].

Sealing of the cable terminations is very important because of 4 aspects (Figure 2.15): possible moisture penetration (top of termination end pit) due to loose elements, wrong size and dimensioning and wrongly selected materials causing fast corrosion, possible contamination of dielectric medium: oil or gas, chance of the leakage of dielectric medium due to incorrect sealing. Imperfect sealing causes water penetration and an increase of conductivity (leakage current) and condensation. Moisture penetration inside the joint can change local field distribution and PD activity as water can involve metallic particles and

contaminants. In the terminations, sealing water may produce corrosion of internal metal parts and bottom termination flange (from the inside). These assembly defects or errors do not produce direct breakdown under after-laying test voltage levels or service, however they accelerate and initiate deterioration processes inside the terminations. The effect of imperfect sealing could be, e.g.: leakage current, discharge activity and lower breakdown strength of insulation medium inside the termination. The final failure may occur even up to several years after the installation. A breakdown can be driven by two different processes: gas content increase (pressure) due to discharging activity inside oil where carbon, methane, and ethane gases are released or through a conductive path (contamination, tracking) to earth potentially inside termination walls (short-circuit).

2.3 Installation and assembly defects symptoms

Literature [17, 26] and onsite investigations confirm the fact that a large number of accessory installation and assembly defects are related to incorrect electrical field distribution (enhancement) that plays a major role in failure development. Related PD activity can be a symptom of the defects created during jointing/splicing but also PDs can be directly responsible for the development of a failure. The overview of typical defects shows that in situations where local dielectric breakdown strength is exceeded, PD activity is responsible for the intermediate and final stage of the deterioration process. Some defects as, e.g. moisture penetration to termination body, are not directly detectable through PD activity. It can take several months or even years to contaminate the insulating medium and to produce a conducting path to earth or high pressure inside termination (through PD activity ionization process) leading to an explosion. Thus, PD, temperature monitoring, DGA (Dissolved Gas Analysis) can be used to recognize, detect and localize some of the installation and assembly related defects for HV power cable accessories. It has to be noted that PD behaviour is a stochastic process (sometimes random process) and it strongly depends on voltage level, defect type and local conditions such as temperature or gas pressure inside void. On the other hand, correct condition assessment of a suspicious accessory has to be confirmed by a sensitive and reliable on-site PD detection system. For a new installation, on-site acceptance tests can be performed to check the quality of the installation work. This after-laying high voltage test should be able to detect, localize and identify the defects. Nowadays, it is observed that more and more after-laying tests are performed as the “monitored withstand test mode”. Besides the effect of the voltage on dielectrics, partial discharges activity is also measured to trace discharging defects inside the joints and terminations. Moisture content in cable insulation can be also indicated by dielectric loss measurements. However, localization of the weakest part of cable is not possible in this case. Table 2.1 summarizes the possible defects, inducing factors and related symptoms.

Table 2.1
Defects, inducing factors and symptoms

Reasons	Inducing factor	Possible defects	Symptoms
Transportation, handling installation	<ul style="list-style-type: none"> - Human handling - High pulling forces - Small bending radius - Wrong tools - Defect of pulling rollers or pulling hydraulic equipment resulting in high pulling/pressure forces on cable and joint - Dust, environment impact 	<ul style="list-style-type: none"> - Insulation deformation: cracks, voids - Low dielectric breakdown strength - Elongated and overstressed insulation and mechanically stressed insulation - Conductor replacement against insulation, deformation of accessories body - Cable sheaths damage 	<ul style="list-style-type: none"> - Enhanced field - Local over-heating - Low breakdown strength - Contamination - PD
Accessories installation and assembling	<ul style="list-style-type: none"> - Human handling - Poor workmanship - Lack of knowledge and/or experience - Wrong tools - Wrong assembling protocol and dimensioning - Incorrect material used e.g. terminations sealing materials sensitive to corrosion in particular conditions 	<ul style="list-style-type: none"> - Wrong electrical field distribution inside joints and terminations, - Voids - Contamination - Impurities - Various distortion of semi-conductive screen layers - Defects of stress cones, deflectors, insulation surface, field grading components - Interfaces - Water ingress 	<ul style="list-style-type: none"> - Local over-heating (hot-spots) - Enhanced field - Low breakdown strength - Increased leakage current - Increased dielectric losses - PD - Increased or decreased pressure of insulating medium in cable terminations - Gas content in the insulating medium (in the oil)

2.4 Conclusions

1. Human related mistakes made during installation and assembly errors are major reasons for cable accessory assembly related failures.
2. For most of these defects, incorrect field distribution is responsible for failures followed by PD activity.
3. Some installation defects, e.g. imperfect sealing of the terminations, cannot be detected directly during acceptance on-site tests, as the effect occurs after a few months or even years after the installation (moisture content, leakage current).
4. Damages to the cable insulation, joint body and terminations during failure are irreversible and in the majority of cases the whole component needs to be replaced.

5. PD activity characteristics is a known phenomenon for status assessment of the dielectric materials, PDs can also be used to asses, localize and identify some of the assembling and installation problems.
6. Evaluation and analysis of PD characteristics may help to recognize the type of particular installation and assembly defects for the known type of component.

3. Transmission cables ageing related defects

Based on a survey done by CIGRE Group from 2008 [9], it was stated: “At the moment, high voltage paper insulated cables do not seem to fail so much due to ageing. Only 12% of the total number of cable failures in paper insulated high voltage cables are ageing related failures”.

Ageing defects are natural effects of deterioration of the cable systems under service conditions. Ageing of the solid insulating materials and systems, according to IEC standards and IEEE guides, is described as follows: “occurrence of irreversible deleterious changes that critically affect performance and shorten useful life”. This degradation strongly depends on the service conditions such as: load, number and type of defects developed during years of service, repair quality and an environmental factor, e.g. soil thermal resistivity, over-voltage conditions. Ageing failures are the result of cable service stresses. Four major cable stresses can be specified according to [26, 28] and these are electric stress, thermal stress, mechanical stress and environmental stress. Apart from the nature and the source of stresses in the cable, there are two groups of ageing stresses (Figure 3.1). One of them can cause irreversible changes in the properties of insulated material. This type of ageing is referred to as intrinsic ageing and may affect a large volume of the insulation, e.g. thermal ageing of paper and oil. The second group of ageing factors refers to: contaminants, protrusions, voids in the materials or at interfaces and they produce degradation mainly through PD activity. This type of ageing is referred to as extrinsic ageing [26]. Extrinsic ageing usually results in local changes in the insulating material, e.g. physical insulation damages visible after breakdown in the region of the defect’s presence.

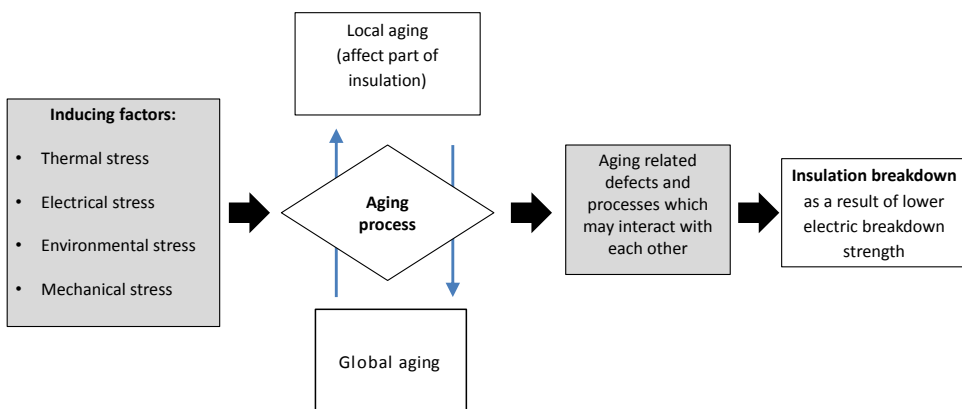


Figure 3.1: Aging of power cables.

3.1 Ageing of oil impregnated cable insulation

Ageing of paper insulated cables is a complicated process. Oil impregnated paper under stresses such as: thermal, electrical and mechanical stress loses electric and mechanical strength but the process is not constant and predictable. This ageing process is not related to one major stress but to a combination of various stresses acting synergistically throughout the cable service time [26]. Ageing of the impregnated paper goes through three different processes, namely:

- Thermal degradation (pyrolysis).
- Oxidation (gasification).
- Hydrolytic degradation.

In the case of paper insulated power cables, hydrolytic degradation is the main degradation mechanism leading to lower breakdown strength and irreversible deterioration of the insulating paper. The combination of ageing stresses (correlated with each other) makes a particular ageing factor difficult to distinguish.

3.1.1 Cellulose chains breaking (de-polymerization/scission)

Thermal degradation, which is also called “pyrolysis of cellulose”, in the absence of oxidizing agents and moisture, results in breaking of the glycosidic bonds and creation of openings of the glucose rings [29]. During thermal stressing of the paper structure, moisture is produced at the beginning of the process as an effect of the chemical decomposition of paper together with oxygen (de-polymerization) (Figure 3.2). Free glucose molecules, moisture, carbon oxides and acids are also formed during thermal stressing of paper over the years of service. In the later stages of degradation, moisture can also be absorbed, e.g. during formation of the acetic acid that consumes the moisture [30]. Under temperature stressing, due to the nominal current load or extensive over-loads or repetitive thermal cycles, a degradation effect is recognized mostly through the modification (scission) of the cellulose chain bonds. It results in a decrease in the average molecular weight of the chains, and therefore is followed by a reduction in the tension strength. As a result, the insulation paper loses mechanical strength, resulting in a lower degree of polymerization and lower breakdown strength. Thermal degradation is in some cases an “initiator” of the other two ageing processes called: gasification and hydrolysis or hydrolytic degradation. Pyrolysis can take place without access to oxygen or moisture. During normal operation when the temperature is below 140⁰C, pyrolysis processes are considered to be of little relevance.

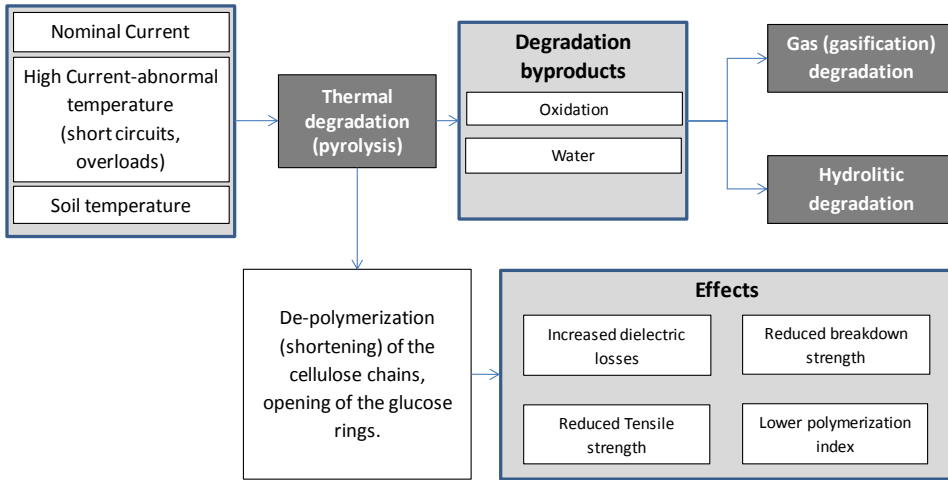


Figure 3.2: Thermal degradation in paper insulated cables.

3.1.2 Water content (hydrolysis)

Another compound that is released during thermal stress is water. Water is related to the hydrolytic degradation process. Water is a harmful medium for power cables with impregnated paper insulation because it is attracted to places with a higher electrical stress (water can be easily polarized). Water accelerates the deterioration of both insulating oil and paper insulation and leads to more water content in the process of thermal ageing (heat catalysed). Water increases the insulation conductivity, and at the same time lowers the electrical resistance, increasing dielectric losses and decreasing dielectric breakdown strength. (Figure 3.3). Hydrolytic degradation is produced by water and acids attracting the glycosidic bond between glucose monomers yielding the formation of free glucose [29]. The result is a reduction in the degree of polymerization and weakening of the mechanical properties. Once the paper insulation has been degraded by water, it can never (unlike the oil) be returned to its original condition. Water which is released from the paper is condensed in the cellulose pores or absorbed on the surface (between layers) partly by paper and partly

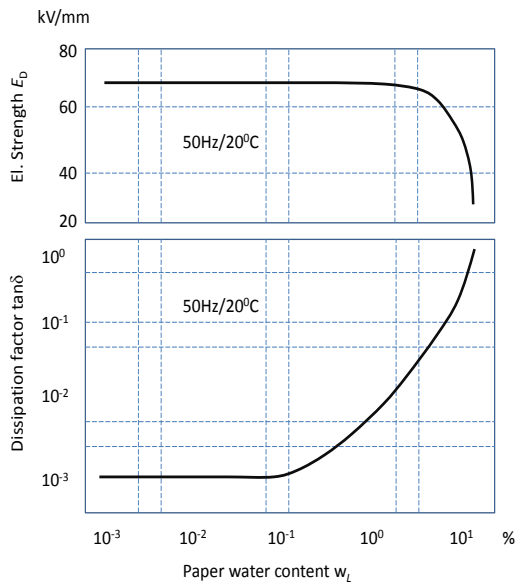


Figure 3.3: Influence of moisture on the dissipation factor and breakdown field strength of oil impregnated cable paper [4].

by the oil film between paper layers. Water causes higher conductivity of paper, resulting in a bigger volume of paper (paper swell). When the cable temperature rises above safe operational limits, e.g. abnormal circuits temperatures and during over loads, water saturation solubility w_L of the oil increases exponentially according to equation [3-1]. It means that paper can absorb more moisture (paper acts as a sponge) [4].

$$w_L = w_{L0} \exp\left(\frac{-H}{T}\right) \quad [3-1]$$

Where: H, w_{L0} -oil solubility coefficients T-absolute temperature

However, when the cable core temperature rises above 125⁰C [30], decomposition of paper is much faster and water absorption is limited. It is partly because the fact that the gases, particularly carbon dioxide and carbon monoxide, are released much faster but also due to the water content in the residual gas composition and the fact that the mobility of charge carriers increases. The presence of water is very destructive after reaching 125⁰C as it produces an accelerated weakening of paper and may result in embrittlement and tearing under thermo-mechanical tension. In other words, the volume of water extends the paper absorption capability and creates additional pressure between paper layers. Under pressure, water migrates to gap sites and disrupts the hydrogen bonds between cellulose molecules, destabilizing the paper matrix. Such degradation is primarily a combination of hydrolytic breakdown and thermal scission of the glycosidic bond. A combination of thermal and hydrolytic ageing has a synergistic nature (ageing processes interacts with each other) and results in additional effects, e.g.: free glucose monomers, reduction of tensile strength.

3.1.3 Gas content (gasification)

An additional type of ageing in paper-oil insulation is related to gas formation and is called gasification of the insulation. One of the types of gasification is oxidation. Oxidation takes place when oxygen attacks carbon atoms in the cellulose molecule. Aldehydes, water, acids and carbon monoxide might be produced as a result of the oxidation [30]. Gasification also relates to thermal decomposition of the oils visible through the production of various types of gasses e.g.: methane, ethane, during the cable insulation ageing process. The source of these gases is mostly the ionization process (PD activity) which occurs in trapped voids in paper pores, cracks and gaps. Discharges occur under electric field stress but also as a result of oil contamination with conductive and semi-conductive particles. Gasification becomes a threat for the insulation especially if the electrical field stress and the pressure inside the gas filled cavities and voids creates conditions suitable for partial discharges initiation.

Gas content in paper and oil has an impact on the total volume of insulating paper-the radial and axial expansion. In SCFF cables, where the pressure of oil is only around 1 bar, which is not enough to act against the radial expansion of insulation, this effect may produce irreversible damage to the cable lead shield. Figure 3.4 presents this gasification process combined with hydrolytic degradation.

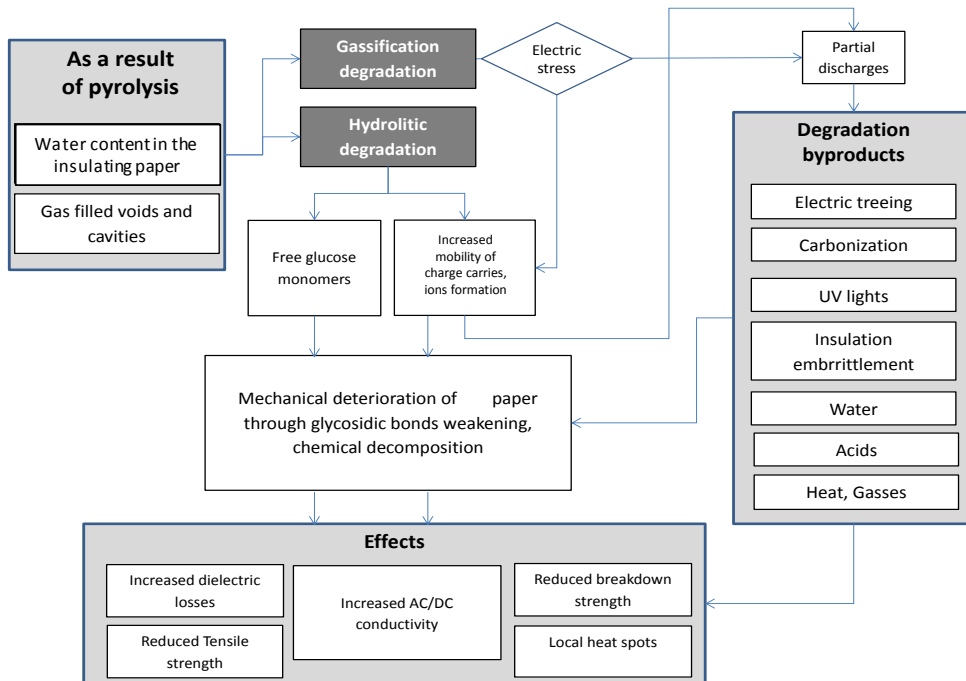


Figure 3.4: Hydrolysis and gasification degradation in paper insulated cables.

3.1.4 Electrical treeing/tracking

Deterioration of paper oil dielectric due to thermal or electrical ageing (partial discharges) can result in failures. A water-free, well impregnated insulation is not reported to degrade under the application of an electrical stress alone [31]. However, the process of paper insulation degradation occurs due to the electrical field present in the cable. The cause of tracking or treeing is usually the non-homogeneity of the dielectric, which causes the enhanced field stress and initiation of discharging processes. In the aged paper insulation there is no longer a homogeneous insulation structure. Under the effects of an electric field (especially over-voltage conditions), weak areas might be a threat by PD. During the breakdown process of, e.g. the gas filled cavity, there is a conversion of an atom or molecule into an ion by adding or removing charged particles such as electrons or other ions. During the PD process the electrons are released, which additionally increases conductivity in the region of the released gases and the border between void and dielectric material. It accelerates the process of further ionization. Now, a lower electric field is required to initiate another discharge, and the next discharge is initiated faster. Heat and UV light which are generated, interact with cellulose, producing carbonization (effect of heat and UV light) and structural decomposition (chain shortening) called chain scissions [30]. The more gases produced, the faster the weakening of the area surrounding the paper void due to the interaction with cellulose and resulting in additional water release. As a result, hydrolytic degradation occurs but in this case it is mainly driven by electrical stress.

In the paper layers where PD occurs at interfaces, gases may spread along the paper surfaces while creating cable swallowing (gas-pumped paper). It is due to the fact that paper layers are impregnated and an oil film is created between each single paper surface. As a result carbonized paths are limited along the total thickness of the paper layer. The process of branching can be limited until the moment that a single layer is completely bridged across its thickness. During the branching process, compounds such as methane, ethane and carbon are released. They are partly dissolved (absorbed) by the oil film between paper layers and therefore the process of degradation may stop or can be continued in different regions in the next paper layer, having different propagation directions. Examples of these processes are shown in Figure 3.5. The total branching over tens of single paper layers can take a long time (even several years) and depends on the service conditions such as cable temperature and field stress. The final stage of the deterioration process can be visible by the presence of “wax” content between insulation layers. It is the result of low level ionization of polymerized oil molecules and may be detected by fluorescence under UV light. In-depth investigation of the treeing process is only possible through the sensitive PD measurements or a laboratory investigation of the cut pieces of the degraded cable insulation.

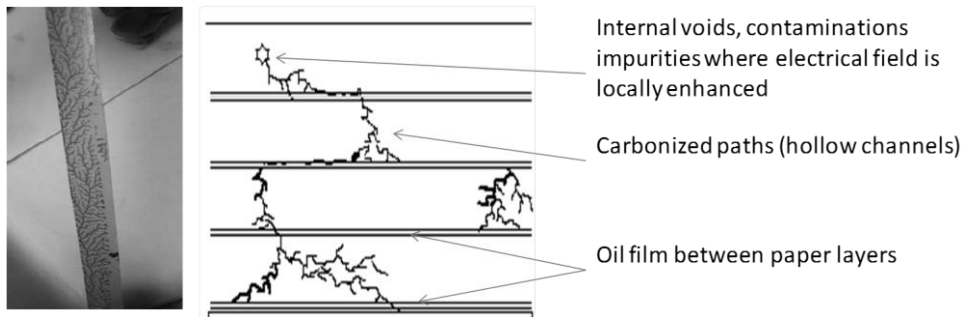


Figure 3.5: Example of multi-layer construction of paper insulated power cables and degradation through the electric treeing process.

3.1.5 Oil contamination

Oil as an organic material can experience changes in its properties, e.g. due to the presence of oxygen or other gases and contaminants. This change is a chain reaction that starts when the hydrocarbon molecules of oil are oxidized to form hydrogen peroxide [29]. Hydrogen peroxide decomposes easily forming free radicals. Free radicals are highly reactive and they easily oxidize forming more free radicals. Insulating oil has a lower electrical strength (approx.: 30 kV/mm) than the combination of paper and oil together (approx.: 70 kV/mm). Considering the fact that between paper layers, pure thin oil film is present, the difference in oil and impregnated paper permittivity results in PD activity (if voids with gases are present). Gasification and contamination of the oil produced by chemical by-products of cellulose degradation leads to increased oil conductivity and lower electric breakdown strength. The final effect of oil degradation is called “black oil” with dielectric breakdown lower than 30 kV/2.5 mm [32]. It is a result of continuous ionization (PD activity) and is reflected in the increased dissipation factor ($\tan \delta$) of oil.

Besides water and gas content in oil, particles can occur in oil as a result of, e.g. carbonization of insulation or contamination from the reservoir oil tanks and corrosion (SCFF or HPFF cables only). Conductive particles can accelerate the ageing process in, e.g. HPFF cables where oil is used as a cooling and pressurizing medium to avoid void formation. When oils contain conductive particles, these particles circulate in the cable systems under the influence of the electric field and become polarized. When the electric field: E is applied, these particles become polarized. If the particle has a permittivity: ε_2 , greater than that of the oil, ε_1 , (as is generally the case), a force will act on the particle forcing it towards the area of maximum electric stress between the electrodes. For a spherical particle of radius r the magnitude of the force F is given by the equation 3.2 [4]:

$$F = \frac{1}{2} r^3 \frac{\varepsilon_2 - \varepsilon_1}{2\varepsilon_1 + \varepsilon_2} E^2 \quad [3.2]$$

Because of the high permittivity of water, this force is greatly enhanced if the particle is moist or wet. Other particles will be attracted into the region of the highest stress until particles are aligned end to end by the field. In this way, a short circuiting bridge can be formed between the electrodes. The current flow along these bridges will cause localized heating leading to a breakdown. If the particles are metallic, then $\varepsilon_2 \rightarrow \infty$ and a single metallic spherical particle between the electrodes can increase the electric field at its surface by up to three times. In some cases, this enhancement might be, enough to initiate PD at the interface between particle and insulation. Many studies have been made on the movement of the particles in electrically stressed oil but there is no accurate quantification of how they affect dielectric strength. However, it is accepted that particle contamination severely reduces dielectric strength and provides a good indication of the condition of oil [32, 33].

3.2 Ageing of XLPE cable insulation

Degradation of cross-linked polyethylene can be described by three types of degradations [4, 34, 35] (Figure 3.6):

- Chemical degradation of insulation and trapped charges.
- Physical degradation (irreversible changes in dielectric structure).
- Electrical degradation (tracking, electric treeing).

Solid dielectric insulated cables: XLPE and EPR are not affected by thermal ageing at normal operating maximum temperature below 90°C [4]. Gasification can occur when XLPE insulation is operated above 130°C, but it will not intrinsically affect the breakdown strength. The effects of the temperature are considered when operating XLPE insulation at high temperatures and are subjected to thermal-cycling (thermo-mechanical stresses). These types of stresses are generated by the expansion and contraction of the insulation.

Thermal ageing of PE and XLPE insulation begins at temperatures between 150°C and 225°C ,where free radicals may attach to the backbone of the other polymer chains causing crosslinking. This crosslinking may decrease mechanical strength, density and crystallinity [35]. At temperatures higher than 225°C, the formation of trans-vinyl groups can be observed. The formation of trans-vinyl groups indicates rearrangements of radials. At very high

temperatures above 350°C, polyethylene degradation takes place through de-polymerization and incomplete thermal cracking, forming coke [34].

As opposed to MV XLPE power cables, HV and EHV XLPE cable systems are better protected against moisture penetrations (water barrier membranes). The water treeing phenomena is almost never a problem in new generation of HV/EHV cables. As a result, this type of deterioration is not discussed in this section.

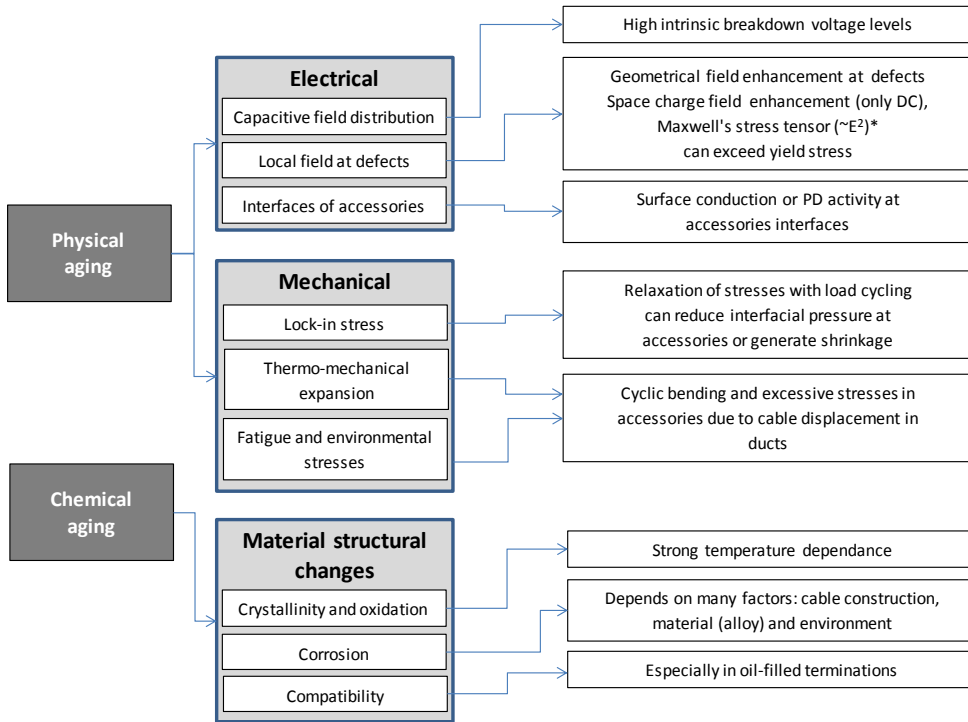


Figure 3.6: XLPE HV/EHV cables ageing factors and effects. (*)-Insulating materials with high permittivity and high breakdown strength would yield large electrical energy density. The stored energy W is expressed as a function of the dielectric permittivity ϵ and the square of the applied electric field E , $W = \epsilon E^2 / 2$ [34].

3.2.1 Chemical decomposition

Chemical decomposition of XLPE insulation is related to breaking of the long polymeric chains (de-polymerization). In this process, under the impact of the different compounds, the cross-link bridges can be damaged or created. Chemical reactions between oxygen, polyethylene and temperature can result in crystallization of the insulation (making it stiffer). Oxygen presence can initiate PD activity and this process depends strongly on the intensity of the interaction between oxygen and additional stresses such as temperature or UV radiation [34].

3.2.2 Physical decomposition

The major by-products of thermo-oxidation are carbonyl groups. The overall results of thermal ageing are the oxidation reactions, cross-linking, chain scission, variations in crystallinity and variations in the insulation melting point. Current over-loads, abnormal operational temperatures (above 200°C) resulting from short-circuit or overloads can produce known effects such as the cable insulation melting. In this process, the weakened (softened) polyethylene loses its thermo-elastic properties. As a result, the heavy conductor can “sink” into the insulation. This effect is known as conductor sagging or replacement. The final stage of this process results in voids between the inner conductor screen and XLPE insulation layer and a total breakdown initiated by void PD erosion mechanisms.

3.2.3 Electrical erosion/treeing

Studies have shown that pure electric design stresses used in transmission cables have negligible effect on the chemical and physical properties of polymers [31, 35, 36]. Electrical ageing is invisible at low fields below a critical/threshold field. An increase in electrical ageing rates may occur when C-C bonds are broken above that critical field. Free radicals are shown to accelerate the bond breaking process. Below the critical field (in the 10 kV/mm range) even if any C-C bonds are broken and even if few radicals are generated, the lifetime will not be reduced [37]. Electrical ageing of polymers is still poorly understood although it has a considerable influence on the lifetime (breakdown strength) and therefore on the reliability of extruded cables.

Generally, electrical ageing in transmission XLPE cables can be explained by the electrical treeing process which occurs in the form of electrical PD treeing as a rapid degradation phenomena. An imperfection can cause local field enhancements of up to several hundreds of kV/mm, even with an average field of 10-20 kV/mm. The local field enhancement may give rise to electrons having energies of some eV. Electrons with this high energy are able to cleave bonds directly or excite polymer molecules. The excited molecule will emit photons when returning to zero potential. This radiation can cleave bonds or excite new molecules. This bond cleavage could lead to void formations or electrical tree initiation, especially in combination with oxidation. In the end, electrical treeing results in the so called erosion breakdown. The total process of tree formation can be divided into three stages (Figure 3.7). This process can be initiated by several different sources and hardly ever by itself in defect-free XLPE cables [31]:

- Metallic particles, contaminations produce tracking, treeing discharges.
- Purity of polyethylene, extrusion process may have an impact on the production of voids (micro voids).
- Mechanical damages (bending, pressing) will result in cracks, voids.

Similarly to the discharge processes in paper cables, treeing produces gasses, e.g.: hydrogen, methane and additionally low-molecular hydrocarbons. XLPE materials do not produce the conductive paths on the channel walls or surfaces of the bound voids or cavities as the XLPE has a high density structure. As a result, they cannot de-stress the discharge space of a

polymeric dielectric as polyethylene. If the accumulation of gasses increases, low inception PD activity can occur. In the process of electrical treeing, ionization is followed by UV light, which makes the polyethylene surface brittle locally and accelerates in-depth erosion phenomena, which isn't fully understood yet. Therefore, the brittle material cracks and is less resistant to pressure of locally distributed gasses.

The inhomogeneous areas of the insulation create an enhanced electrical field. In situations where the erosion process is already in an advanced stage as represented by, e.g. "stage 2" in Figure 3.7, the volume of polymer occupied by discharging interacts with heat. Thermal interaction with C-C bonds of polyethylene reduces its strength. As a result, the local crystallization of the polyethylene material around pits can occur. In the final stage, the crystals and the clusters grow on the surface or through the insulation. The pits formed in close distance to crystals penetrate the polyethylene structure even faster as the area around crystals becomes conductive. Through the enhanced field, more and more ions accumulate at the interfaces between healthy polyethylene and crystallized and carbonized parts at the same time.

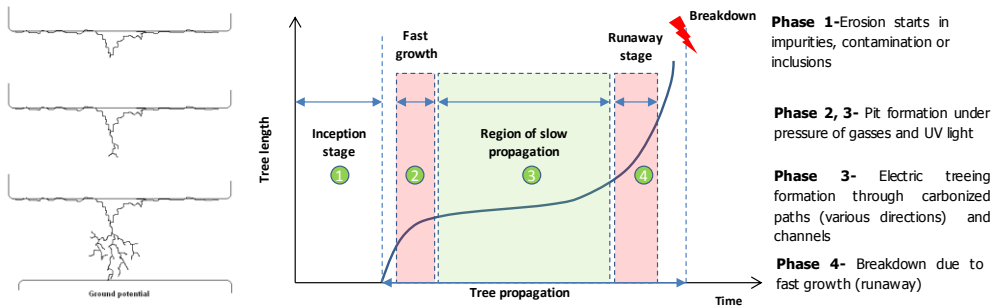


Figure 3.7: Stages of erosion breakdown through one layer of polymeric insulation [36].

It was found that the shapes and the propagating characteristics of erosion breakdown (treeing direction) followed by PD phenomena in pure polymers are influenced by some combined factors. These factors are: the micro pores (micro voids structure in polyethylene), residual mechanical stress, and micro-pores and impurities in amorphous materials. Because gas pressure acts in all directions, the propagating direction of a single branch of a tree is barely effected by the direction of the applied electric field. As a result, the channel of the branch tree propagates in a very broad direction (Phase 3), even deviating from the direction of the applied electric field.

The total process of erosion degradation by partial discharges in extruded insulation is faster than in oil impregnated paper insulation. This process depends on several parameters such as: electric field stress level, purity of polyethylene, micro voids content, and the temperature of the cable.

3.3 Mechanically induced defects (all types of insulation)

Mechanical stress is understood as an external mechanical force which continuously or temporarily acts on any of the power cable's components. This stress results in irreversible physical changes in the cable system insulation, that can lead to cable failure. The mechanical stresses are mostly induced by third party (human handling) factors which represent around 70% of total external faults in transmission cables, e.g. through digging activity [10]. Considering service conditions, mechanical stresses caused by soil (ground) or thermo-mechanical effects of the cable itself, are both very destructive. They can start an ageing process and "participate" in the final cable breakdown process.

3.3.1 Mechanical defects due to soil/ground movements

Soil is a quasi-elastic medium. Therefore, the impact and load of heavy vehicles and self-ground movements are considered as sources of mechanical stress to a cable system. Rolling on asphalt macadam surface above a cable duct may result in lowering of the ducts and therefore cable movement. For example, car wheels produce temporary depressions in front of it of similar shape and curvature to that of the wheel. Due to the ground elasticity, the soil will recover gradually and return to its original geometry as soon as the wheel rolls forward. The time necessary for recovery to the original state depends on soil structure and the rate of load cycle. Two surf-riding examples can be distinguished [10].

External longitudinal-motive force. It arises from the vehicles braking motive forces as it is presented in Figure 3.8. The braking phase is divided into 3 stages: A, B, C. At each stage the resultant force "S" acts on soil with a different value. At stage "A" when the vehicle starts braking, the biggest resulting force S_1 is produced because of the highest kinetic force and the load. This action puts the highest pressure onto macadam and cable ducts (by indirect contact) and therefore push it to a lower position in comparison to where the macadam is not stressed. At Stage "B" the speed of the braking vehicle is already lower and as a result, the force S_2 is weaker. At the last stage "C", the vehicle speed is almost zero and the force of gravity "G" is the only one acting on the soil. The cable duct is forced forward by the horizontal component of the force and downwards by the vertical component. As a consequence, the static friction between the cable and the duct is broken.

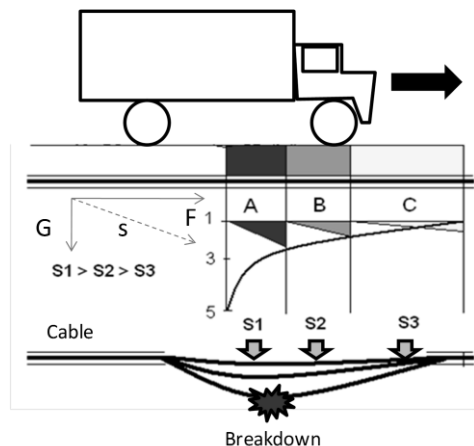


Figure 3.8: Forces induced due to longitudinal motive force.

External cross-motive force. It depends on the soil type and composition. Cross-cycling load on particular "weight spots" results from the vehicle wheel vertical force and gradually lowers the level of soil. Accelerating factors are also water and broken rain drains, where leaking

water is jetting sand and soil. As a result, both the soil level and cable ducts decrease their levels. It can lead to mechanical failures of the cable caused by mechanical overstressing and bending. Cable movement in softened soil/grounds can induce mechanical forces similar to those induced by thermal cycling. The cross-pressure of the ground to cable may also result in the so-called “squeeze” effect for directly buried cables. Deformations under the external force on the cable PVC jacket and external sheath can result in loose contact between the insulation body and external sheaths. This can lead to gaps and free spaces and mechanical damage to the insulation [10].

3.3.2 Thermo-mechanical related defects

The effect of thermal stress is also important from a mechanical point of view due to internal forces induced during thermal stressing. This mechanical stressing is more severe to SCFF cables than XLPE cables due to oil impregnated insulation, physical structure and expanding abilities during thermal cycles [37]. Due to different temperature characteristics during service life, e.g. higher cable temperature during the day and lower during the nights, the cable is in a constant process of cooling (decreased current load) and heating (increased current load) (Figure 3.9). It results in so-called heating cycles and relates to thermo-mechanical movements. Therefore, during 24 hours of daily service² the cable shrinks and expands producing longitudinal forces. Such induced forces interact with the cable joints more so than terminations and may result in [37]:

- Back-to-back forces and shifting of cable body into joint body.
- Radial expansion resulting in an increased volume of insulation and forces to cable sheath.
- Displacement of the conductor against insulation, in the worst case scenario.

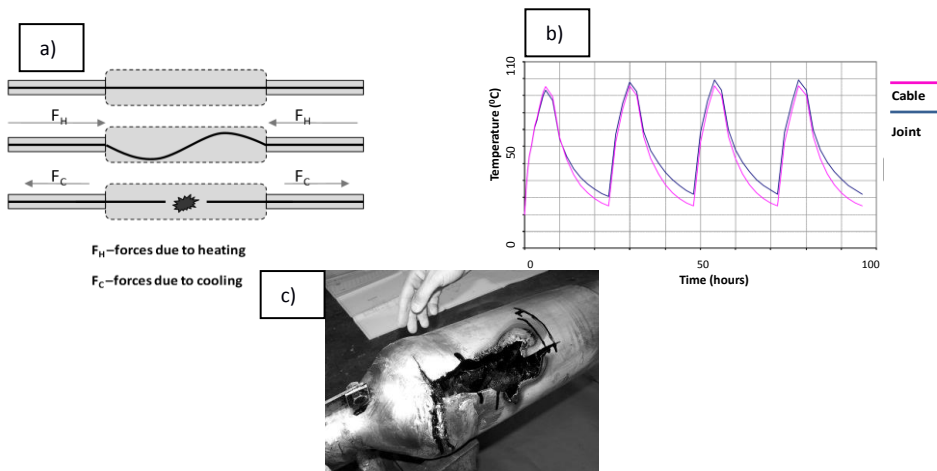


Figure 3.9: a) Experimental loading cycles (8 hours on, 16 hours off) on a 400 kV 2500 mm² Cu cable and joint [37]. b) Theoretical visualization of the effect of thermal cycling. c) Internal mechanical defect of the 110 kV SCFF cable.

² Valid for cables exposed to thermal cycling. In cables with constant load thermo-mechanical forces are not present

Load cycling has severe impact on splices and terminations as they may be physically restrained and may experience significant compressive or tensile forces. Such forces may cause components within the splice or termination to shift, resulting in joint body replacement. As a result, the electric field distribution is no longer homogeneous. Repetitive shifts and movement may create, e.g. voids or gaps at the border between semiconducting and joint body or tears and cracks due to created forces. As a result of these deformations, the geometrical structure of the cable insulation is also deformed. Depending on the time constants and duration of the cooling period, when permitted operational temperatures (Table 3.1) are exceeded, cable movements can occur more rapidly as the effect of higher cooling and heating forces, e.g. over-loads. However, cable systems are designed to handle thermo-mechanical movements, in case of long-term processes and combinations of other mechanical phenomena, e.g. soil movements and the effect of temperature changes within a cable system may lead to insulation mechanical damages, e.g. conductor displacement and breakdown followed by PD activity.

Table 3.1:
Permissible cable conductor temperatures comparison in HV/EHV power cables [4].

Insulation	Impregnated paper	XLPE
Operating temperature [°C]	85/90	90
Short-circuit temperature [°C]	160/180	250

3.4 Defects symptoms

Ageing defect symptoms can be divided into three separate groups:

Indicate localized ageing insulation changes/ defects: (local defect due to enhanced electric field and discharging phenomena in this region)-indicator PDs, increased local temperature.

Indicate integral long-term ageing changes/defects: Developed slowly, irreversible, affect large amount of insulation, driven by many separate service factors-Increased dielectric losses (dissipation factor), increased temperature (X-rays), gas content (DGA), lower polarization index (PI).

Visual effect of ageing-crack of PVC jackets, leakages of oil from SCFF, HPFF cable system, corrosion, fatigue of cables, prolonged jackets.

In Table 3.2 major defects and inducing factors are highlighted.

Table 3.2
Defects, inducing factors and symptoms

Source	Inducing factor	Possible defects	Symptoms
Aging	- Electric field - Temperature - Thermo -mechanical forcers (combination)	<u>Paper insulation</u> - Gasification (HPFF, SCFF) - Electrical treeing - Moisture - Carbonization, PDs - Oil contaminations <u>XLPE insulation</u> - Insulation crystallization - Leaning - De-polymerization - Treeing/tracking - Brattling <u>Both</u> - Fatigue and creep of metal, alloy sheaths (mechanical)	- Lower breakdown strength - Lower tensile strength - Lower polymerization degree - Local/global over-heating - Thermal runaway, dry-outs - Increased conductivity - Lower insulation resistance - Deterioration of cable sheath - Oil leakages -SCFF only - Gas migration to metal pipes-inter. GP cables only - Increased dielectric losses - PD
Third party damages*	- Human factor	- Insulation and or conductor mechanical distortion (damage) - Holes in cable e.g. digging - Cracks - External jacket damages - Cable shield damage	- Cable breakdown or cable "dripping" - Total loss of cable path continuity - Oil leakages - (SCFF, HPFF cables only)
Environment	- Natural factor	- Swelling of the external jackets due to moisture - Corrosions - Water ingress - Mechanical damage through tree roots	- Lose of cable sealing integrity - In same situations increased dielectric losses - Oil leakages-(SCFF, HPFF cables)

(*)-Not related directly to ageing but may implicate ageing process

3.5 Conclusions

1. During cable insulation ageing, e.g. pyrolysis, hydrolysis contribute to each other, and in some situations it is impossible to determine the major leading service degradation factor.
2. Major degradation mechanisms are initiated by voids, impurities or mechanical deformation of insulation homogeneity which leads to PD activities under distorted electric field stress.
3. Dielectric loss measurements (dissipation factor) can be an indicator of long-term material changes due to ageing. Ageing by-products, e.g. water ingress can slowly change resistivity of the cable and this results in increased resistive current over the insulation.
4. Partial discharge diagnosis can provide information about weak spots in service aged cables and it can also be an indicator of temporary ageing transition processes such as void formation during the cooling process of paper insulated cables (thermal cycles).
5. For cables with an impregnating medium as in SCFF or HPFF cables, laboratory oil analysis, e.g. DGA (Dissolved Gas Analysis) can be an indicator of chemical decomposition of insulation.
6. Dielectric spectroscopy and insulation temperature analysis may reveal information about the chemical and physical changes driven by ageing processes in XLPE insulation.
7. PD activity inside the polyethylene insulation will lead to an irreversible erosion process. In oil impregnated paper insulation, the electric trees development is slowed down by oil that can fill carbonized spaces and gaps. As a result cables with oil impregnated paper insulation can “survive” longer with PDs activity in comparison to XLPE cables.

4. DAMPED AC

Damped alternating current voltage, which is also known as the damped AC voltage (DAC) was introduced at the end of the 80's as an alternative for on-site testing of XLPE HV/EHV cables and described in several publications [38-42]. As a consequence of the introduction of the extruded HV power cables and risks of e.g. space charge accumulation correlated with HV DC on-site testing on these cables, there was a need for a new effective on-site method. The results provided by on-site and laboratory experiments [40] show the applicability and effectiveness in detecting several installation related defects. Since the beginning of the 90's, the approach of the voltage oscillating wave for HV testing on-site has been continuously investigated and developed. Since the end of the 90's, the experiences in on-site application of the damped AC method on MV cables has been growing continuously. Technological development in power electronics and advanced signal processing of data acquisition have made the damped AC a popular method for on-site testing of various types of power cables, e.g.: after-laying test, maintenance or diagnostic tests. Nowadays, the damped AC method is better known as the DAC voltage method and is successfully used for on-site testing and sensitive partial discharge diagnosis for all type of power cables with paper or extruded insulation.

4.1 Damped AC resonance

In systems that generate damped AC voltage, the required test voltage across the test object U_0 is fed by an external voltage source. The Charging (energizing) process runs until the required V_T voltage level is reached. After this period, the voltage source is switched off after the energizing phase and the switch (Figure 4.1) discharges the RLC circuit (where: R_1 -system losses (resistive losses of the system), L-System inductance, C-test object capacitance).

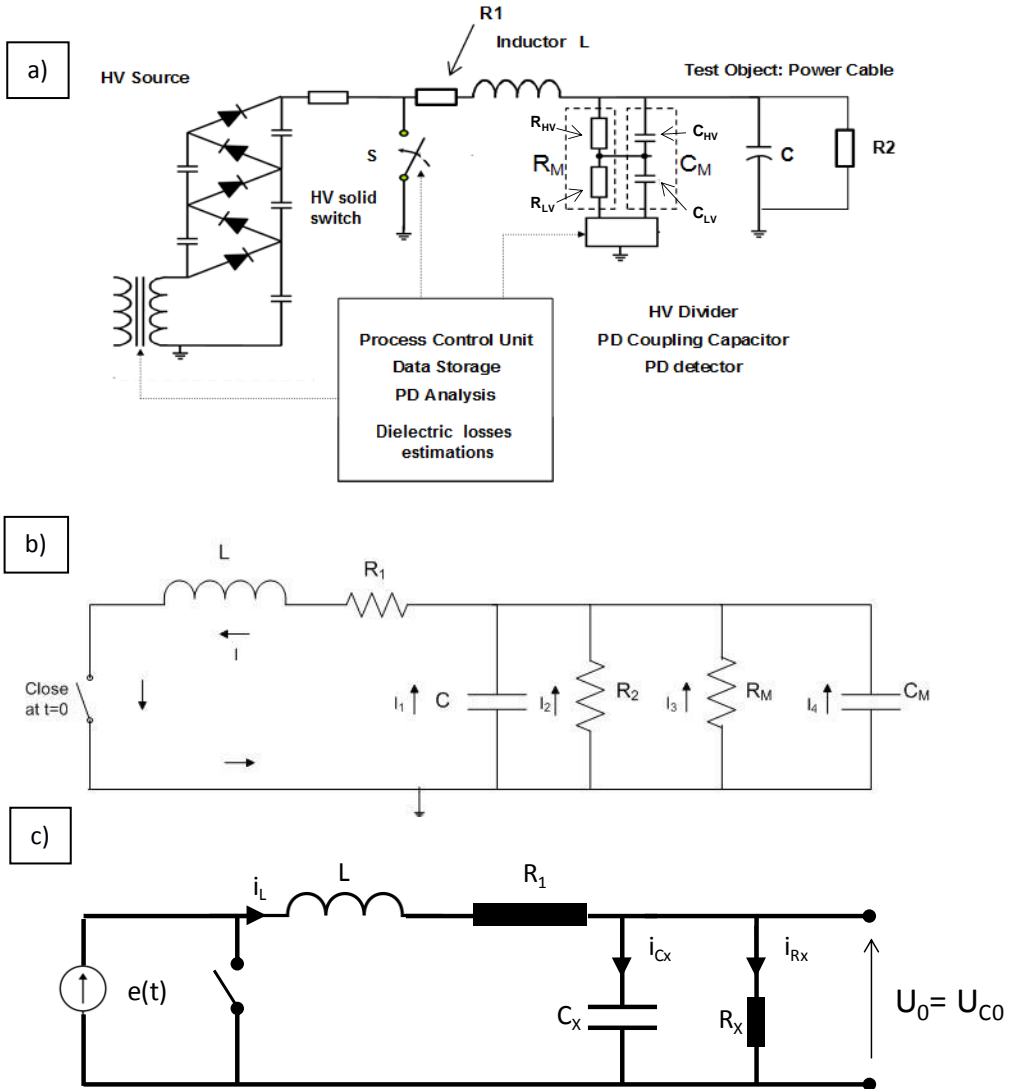


Figure 4.1: a) Real DAC voltage testing and diagnosis system scheme [43]. b) DAC schematic model [44]. c) Simplified schematic model of DAC circuit where C_x and R_x are introduced. U_0 is voltage on the capacitor (cable) and U_{C0} is voltage on the capacitor (cable) in moment of $t=0$ (switching).

In this model in Figure 4.1b, R_1 represents the total series resistance of the primary loop (system losses), whereas R_2 represents the losses in the test object and C represents cable capacitance (test object capacitance). The resistive divider is represented by R_M [4-1], and the coupling capacitor in series with measuring capacitor of the quadrupole is represented by C_M [4-2].

$$R_M = R_{\text{HIGH-VOLTAGE ARM}} + R_{\text{LOW-VOLTAGE ARM}} \quad [4-1]$$

Where : $R_{\text{HIGH-VOLTAGE ARM}}$ is the resistance used to divide the high potential and $R_{\text{LOW-VOLTAGE ARM}}$ is the resistance used for the signal reading with the digital oscilloscope card.

$$C_M = \frac{C_{\text{HV}}C_{\text{LV}}}{C_{\text{HV}}+C_{\text{LV}}} \quad [4-2]$$

Where: C_{HV} -is the HV coupling capacitor, C_{LV} -is the measuring capacitor of the quadrupole unit.

In general the energy storage elements in the RLC circuit can be described in terms of a frequency dependent reactance:

$$X_L = 2\pi fL \quad [4-3]$$

$$X_c = \frac{1}{2\pi fC} \quad [4-4]$$

L -inductance, C -capacitance, f - frequency

For the so-called resonance phenomenon to occur these reactances must be equal. A repeating exchange between the stored energy in the magnetic field and the stored energy in the electric field of the inductor and capacitor respectively, make the voltage and current oscillate. In real LC circuits, there is always a resistive element R_1 i which produces damping of the resonance AC oscillations. Energy consideration is as follows:

$$W_L = \frac{1}{2}Li^2 \quad [4-5]$$

$$W_C = \frac{1}{2}Cv^2 \quad [4-6]$$

The frequency of oscillation is the resonance frequency, which follows the resonance condition:

$$X_L = X_C \Rightarrow f_0 = \frac{1}{2\pi\sqrt{LC}} \quad [4-7]$$

4.1.1 Mathematical model

The circuit presented in Figure 4.1b can be simplified into the circuit of Figure 4.1c, substituting:

$$C_x = C + C_M \quad [4-8]$$

$$R_x = \frac{R_2 R_M}{R_2 + R_M} \quad [4-9]$$

Now, we can describe the DAC circuit presented in Figure 4.1c with the following equations: [4-10], [4-11], [4-12], [4-13]:

$$e(t) - R_1 i_L - L \frac{di_L}{dt} = U_{C0}(t) \quad [4-10]$$

$$C_x \frac{dU_{C0}}{dt} = i_{Cx} \quad [4-11]$$

$$U_{C0} = R_x i_{Rx} \quad [4-12]$$

$$i_L = i_{Cx} + i_{Rx} \quad [4-13]$$

Equations [4-10] to [4-13] can be transformed using Laplace transform. We can assume that at the moment of closing the switch $t=0$, we have :

$$e(t) = 0 \quad [4-14]$$

and we assume that before the switch closing, there was a steady state obtained in the circuit and that means the following assumptions:

$$i_L(0) = \frac{U_{C0}(0)}{R_x} \quad [4-15]$$

$$i_{Cx}(0) = 0 \quad [4-16]$$

Transforming equations [4-10] to [4-13] our Laplace transform will result in the following form [4-17]. Mathematical derivation can be found in Appendix B.

$$U_{C0}(s) = \frac{s + \frac{R_1}{L} + \frac{1}{R_x C_x}}{s^2 + \left(\frac{R_1}{L} + \frac{1}{R_x C_x}\right)s + \frac{R_1 + R_x}{R_x} \frac{1}{LC_x}} U_C(0) \quad [4-17]$$

Now we can use an inverse Laplace transform [4-18]. Mathematical derivation can be found in Appendix B

$$U_{C0}(t) = U_{C0}(0) \sqrt{1 + \left(\frac{3\alpha}{\omega_1}\right)^2} e^{-\alpha t} \cos(\omega_1 t + \theta) \quad [4-18]$$

Additionally we can assume that:

$$\frac{R_1}{L} = \frac{1}{R_x C_x} \quad [4-19]$$

and

$$\omega_1 = \omega_0 = \sqrt{\frac{1}{LC_x}} \quad [4-20]$$

$$\alpha = \frac{R_1}{L} = \frac{1}{R_x C_x} \quad [4-21]$$

$$\theta = \arccos = \frac{1}{\sqrt{1 + \left(\frac{3\alpha}{\omega_1}\right)^2}} \quad [4-22]$$

The values of α and ω_1 are relatively small and therefore θ is also small and practically we can express our DAC voltage in the simplified circuit in Figure 4.1c with the following expression [4-23].

$$U_{C0}(t) = U_{C0}(0)e^{-\alpha t} \cos(\omega_0 t) \quad [4-23]$$

In the real DAC systems R_1 is obtained by a calibration of the system in the factory so this value is known. Due to the fact, that the internal resistance R_1 is only valid for one voltage level and one frequency, an extensive calibration procedure is necessary to determine this R_1 value at different voltages and frequencies. To obtain these internal resistance values, several capacitors are used and successively switched in series and parallel, to vary the total capacitance (and thus the frequency) in a complete range of system voltages. Since the dielectric losses of the test capacitors are known, the internal resistances can then be calculated using equation [4-24], where R_1 will be the only unknown variable left.

$$R_2 = \frac{L}{2\beta LC - R_1 C} \quad [4-24]$$

$$\tan \delta = \frac{1}{\omega R_2 C} \quad [4-25]$$

The attenuation factor β is determined from the measurement results. Due to the exponential damping, the value of an arbitrary peak can be calculated. This is done through measurements of two voltage peaks (e.g. peak 1 and 2), so the attenuation of DAC can be calculated from the following equation [4-26], [4-27].

$$U_x = e^{-\beta t_x} \quad [4-26]$$

$$\frac{U_2}{U_1} = e^{-\beta(t_2 - t_1)} \rightarrow \beta = -\frac{\ln\left(\frac{U_2}{U_1}\right)}{t_2 - t_1} \quad [4-27]$$

When equations: [4-26] and [4-27] are entered into each other, the relation of R_1 to the dielectric losses (DL) will be the result, equation [4-28]:

$$DL = \frac{2\beta}{\omega} - \frac{R_1}{\omega L} \quad \text{wherein: } \omega = \omega_0 \quad [4-28]$$

4.2 DAC testing voltage

DAC voltage withstand testing is performed as a sequence of a pre-defined number of DAC excitations. One DAC excitation consists of the following phases (Figure 4.2 and Figure 4.3) [14]:

Energizing phase. This is the energizing process during which the test object is charged to the specified test voltage level V_T with a rising unipolar DC voltage source. Charging time takes a few seconds and depends on the test object capacitance and required voltage level.

Switching phase. The switching period ($< 1 \mu\text{sec}$). Fiberglass controlled cascade of thyristors are used to noiselessly separate the charged circuit from the voltage generator and ground it via an internal coil.

LC resonance phase. The oscillation voltage period described with equation [4-23] during which dielectric loss and partial discharge parameters can be measured.

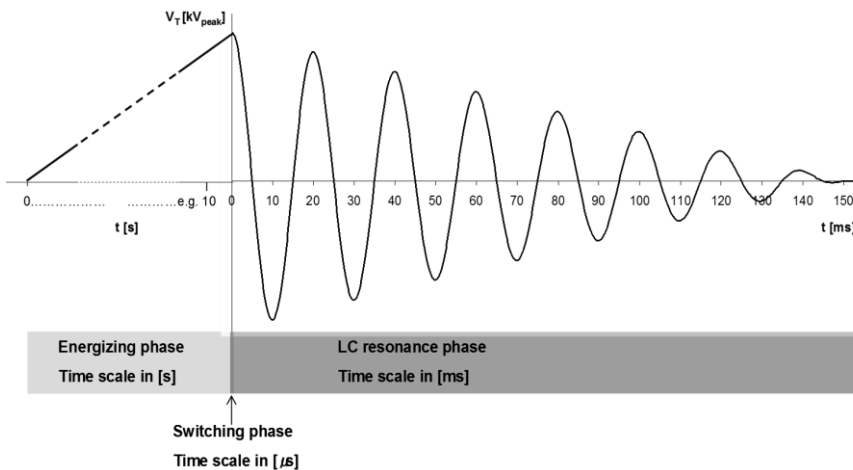


Figure 4.2: Typical example of a DAC excitation. The maximum DAC voltage level is determined by the charging peak value V_T [14].

During the energizing phase, the test object is stressed with a slowly increasing uni-polar voltage. The charging time depends on the maximum available load current of the voltage supply, the test voltage and the capacitance of the test object. Due to a continual increase of the electric field, no DC stress is applied to the test object [38, 39, 42]. In contrast to the situation where pure HVDC stress is applied to insulation and according to [18, 38], the initial voltage distribution will be capacitive and slowly relax to a resistive distribution with the time constant of a typical XLPE insulation (permittivity $\epsilon_r \epsilon_0$ times volume resistivity ρ): $2.3 \times 8.85 \times 10^{-12} \text{ F m} \times 1014 \Omega \text{ m} = 2035 \text{ s}$.

As a result, in a hypothetical case of pure HVDC stress (constant voltage level only), the time constant needed for this transition would be over 33 min. Moreover, there is no risk of steady DC conditions due to relatively short duration of bi-polar stresses, which are followed by

damped AC voltages. Typical DAC test voltage resonance frequencies are presented in Table 4.1 for two types of cable insulation: oil impregnated paper and XLPE.

Table 4.1
Examples of DAC test voltage frequencies obtained for different types of cable capacitance and insulation of two typical 220 kV power cables (charging current-10 mA, fixed inductance-8,9 H).

Cable length [km]	XLPE (C=200pF/m) [Hz]	Oil filled (C=350pF/m) [Hz]
0.25	238	180
0.5	168	127
1	119	90
2	84	63
4	59	45
8	42	31
16	29	22
20	26	20

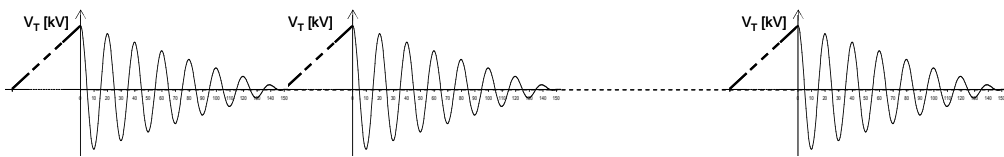


Figure 4.3: Damped sinusoidal AC voltage excitation sequences-number of DAC excitations (N_{DAC}). The duration of the test is determined by a number of DAC excitations which have been applied to the power cable under the test at a selected DAC maximum test voltage level. The maximum DAC voltage level is determined by the voltage peak RMS-values of V_T ($V_T/\sqrt{2}$) of the 1st DAC cycle.

4.2.1 DAC voltage test procedure

DAC voltage testing requires a number of parameters that have to be taken into account. To perform testing with DAC voltage, the following parameters related to the test circuit and test execution need to be set. All parameters describing DAC method is presented in Appendix A.

- Amplitude for one DAC voltage step for the voltage increasing phase- (ΔV_T)
- Number of DAC excitations per voltage step- (N_{DAC})
- Maximum voltage withstand test level
- Number of DAC excitations at the maximum test voltage level (e.g. for voltage withstand testing)

To obtain repetitive test procedures, a fixed number of DAC excitations per voltage step shall be kept. During the voltage withstand test, a fixed test duration or fixed number of DAC excitations shall be performed for three cable phases. Only tests performed with similar test parameters can be compared to each other. Analysis of the test voltage levels, test circuit parameters, and the evaluation of these parameters between particular cable phases should

be based on the comparative basis. An example of a voltage test procedure is presented in Figure 4.4 and Table 4.2. All test parameters according to IEEE 400.4 (2015) are described in Appendix A.

Test procedure according to IEEE400.4 (2015)

During voltage testing with DAC, the maximum test voltage is reached by increasing the test voltage in steps from 0 kV to the test voltage level- V_T . The full testing procedure involves a number of voltage increments. It is done by continuous test voltage increases from 0 kV until the nominal voltage of the test object- U_0 is reached in fixed voltage steps: ΔV_T -e.g. $0.2 \times U_0$. This testing phase is related to the voltage increasing phase (Figure 4.4). After the nominal voltage level is reached and no breakdown has occurred, the over-voltage testing can be applied through further test voltage increasing until the maximum test voltage level. At the maximum test voltage level (withstand voltage level) 50 DAC excitations are performed. The duration of the voltage withstand test depends on the number of DAC excitations and the test object charging time t_{ch} expressed by equation [4-29].

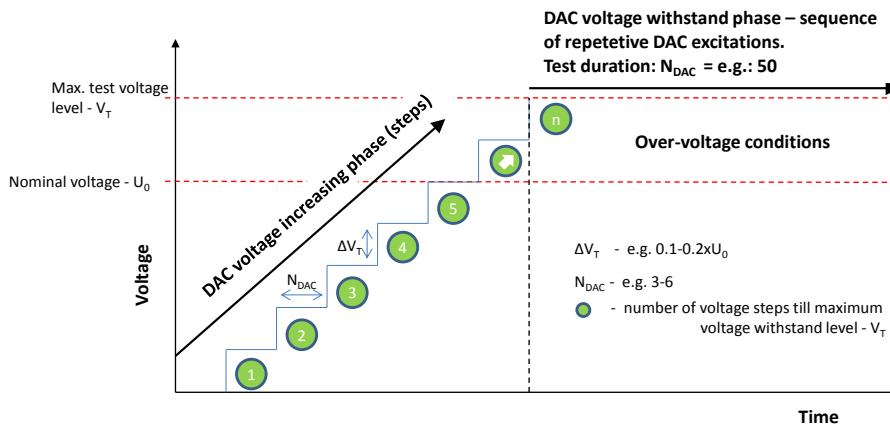


Figure 4.4: Schematic overview of the DAC voltage application procedure according to IEEE 400.4:2015 [62].

Each DAC voltage step consists of a sequence of excitations- (N_{DAC}) as presented in Figure 4.4. The duration of DAC oscillations depends on the damping (attenuation) factor β described in the previous section with equation. For short cables, the charging time is shorter as the cable capacitance C is smaller, thus the number of DAC excitations will be different for short and long cables during a, e.g. 1 hour test. The average time necessary to perform one DAC excitation is presented in Figure 4.5 and is based on the assumption that I_{load} (loading current) is relatively low and depends on the device. Typical values of loading currents for commercially available systems are between 5-12 mA and the DAC system inductances are in the range of a few henrys (H).

$$t_{ch} = \frac{V_T C}{I_{load}} \tag{4-29}$$

Where V_T -test voltage level, C -cable capacitance, I_{load} -charging current of DC source.

Damped AC

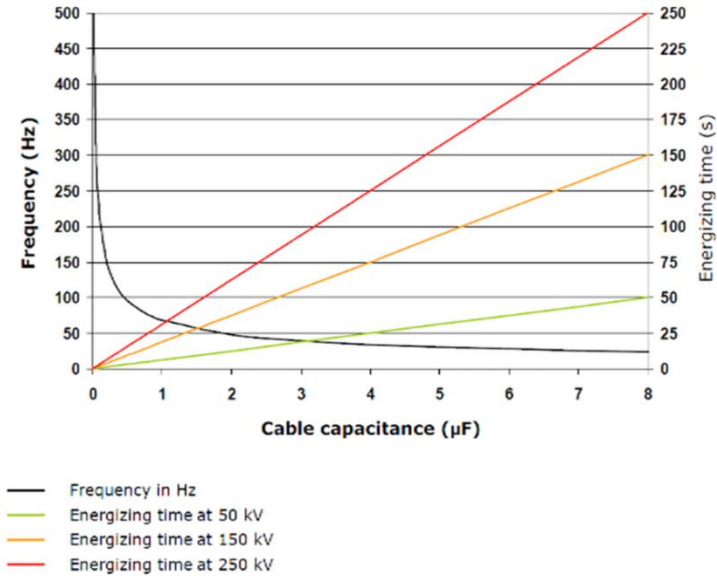


Figure 4.5: Examples of different energizing (charging) duration. DAC frequency vs. cable capacitance (single phase) for three different test voltage levels. Assumption: internal inductance of DAC system-5.5 H and charging current of DC source-8 mA.

Table 4.2

Example of DAC test procedures as used in The Netherlands for diagnostic tests with a specified number of voltage steps at maximum withstand test voltage level for: a) 50 kV (voltage level according to Dutch NEN3620 norm)-b) 150 kV power cables (voltage level according IEC 60840).

a)	Rated voltage 30/50kV				b)	Rated voltage 90/150kV			
	xU_0 ($\Delta VT = 0.2$)	kV (rms)	kV (peak)	number of DAC excitations - N_{DAC}		xU_0 ($\Delta VT = 0.2$)	kV (rms)	kV (peak)	number of DAC excitations - N_{DAC}
	0	0		1	0	0.0	0.0		1
	0.3	7.5	10.6	3	0.3	27.0	38.1		3
	0.5	15	21.2	3	0.5	45.0	63.5		3
	0.8	22.5	31.8	3	0.8	72.0	101.5		3
	1	30	42.4	10***	1	90.0	126.9		10***
	1.3	37.5	53	3	1.3	117.0	165.0		3
	1.5	45	63.6	3	1.5	135.0	190.4		3
	1.8	52.5	74.2	3	1.7	153.0	215.7		50*
	2	60	84.9	3					
	2.3	67.5	95.5	3					
	2.5	75	106.1	50*					

(***)-number of DAC excitations at U_0 can be different. It is common to increase the number of DAC excitations at nominal voltage [45, 47].

(*)-number of DAC excitations recommended by IEEE400.4 at maximum test voltage level.

4.2.2 Voltage withstand test

A cable voltage withstand test is a test performed at a certain voltage level and with certain duration mostly specified by national or international norms. The goal of this test is to check if the insulation of the cable system (cable insulation and cable accessories) can withstand applied over voltage without breakdown. The successful (no-breakdown recorded) voltage withstand test should ensure no-failure services after putting the cable into operation. If any breakdowns occurred during voltage withstand testing, the cable system is not accepted and the faulty component has to be replaced and the complete cable system has to be tested again. Two modes are possible for voltage withstand tests with DAC voltages:

Non-monitored DAC withstand test-a number of DAC excitations is applied and the ability to hold the maximum DAC voltage is based only on the breakdown criterion (Figure 4.6). This test is also called a simple test as it does not involve any diagnostic monitoring parameters. The goal of a non-monitored, simple DAC withstand test is to make the weak points in the cable insulation fail during voltage application (with minimal fault current) at a time when the impact of the failure is low (no system or customers affected) and repairs can be made more cost effectively. The failure may occur during the voltage increasing or during the withstand voltage test (Figure 4.6). After the failure has occurred during voltage increasing or the voltage withstand test, the failure should be located through a fault location process (another system based, e.g. on arc reflection method³), repaired and the circuit has to be re-tested. The results of these tests are described as either pass or fail. The maximum test voltage for non-monitored withstand test can be applied according to the required norm or standard, however it must be noted that for service aged power cable, the test voltage should be adjusted in such a way that testing will not cause additional ageing on the healthy part of the insulation system, including joints and terminations. Up to now, there is no IEC standard describing the maximum test voltage level for the service aged HV cables. The IEEE 400.4 (2015) guide refers to the 80% rule-the maximum test voltage level for the aged cable shall be no more than 80% of test voltage for a new cable.

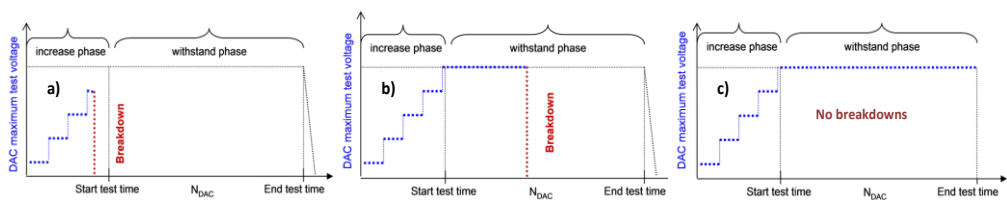


Figure 4.6: Non-monitored simple voltage withstand test possible scenarios: a) Breakdown during voltage increase, b) Breakdown during voltage withstand test, c) No breakdown [14].

Monitored DAC withstand test-in this mode, besides a breakdown criterion, diagnostic parameters, e.g. partial discharges and dielectric losses can be used. Evaluation of PD parameters is used to detect weak spots in the cable system during the DAC test (Figure 4.7).

³

Arc reflection method (ARM) - cable fault localization method based on the pulse reflection from the burning arc which transform the high resistance fault into low resistance fault ($R_{Fault} < 100 \Omega$) and therefore traceable through reflection method.

PD attributes are expressed by diagnostic properties such as PD amplitude, PD intensity, PD occurrence, PD phase-resolved patterns and additional PD location⁴.

Due to the additional information as provided by PD detection, these parameters can improve the evaluation of the insulation condition. If PDs are detected during voltage test execution, evaluation of the detected PDs is necessary. Expert knowledge about PD behaviour in different types of insulation with different PD behaviour is necessary to obtain a reliable picture of the tested object. Important aspects are background noise level at the test location, proper test setup installation, calibration and quality of the connection between the cable terminations and DAC test system.

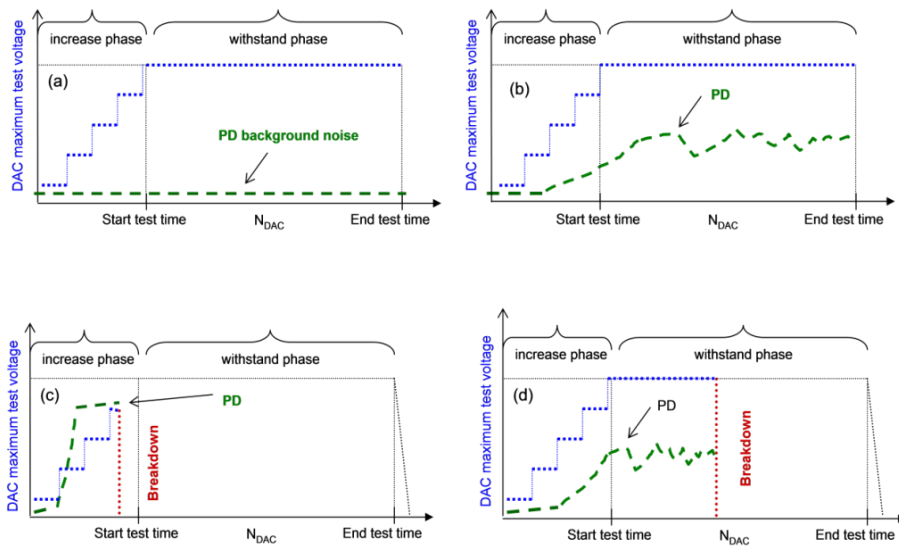


Figure 4.7: Monitored voltage withstand test and example of possible test scenarios. a) No breakdown, no PD detected above noise level, b) No breakdown, PD detected, c) Breakdown during voltage increasing, PD detected, d) Breakdown during voltage withstand test, PD detected [14].

PD measurements and related decision process

When PD measurements are taken into consideration during DAC testing voltage test (increasing phase and voltage withstand phase), a decision process needs to be prescribed in case of various test scenarios. This approach is especially important for the service aged cable circuits when the breakdown is not always necessary. For the acceptance after laying tests for new cables or diagnostic test performed as PD monitored voltage withstand test, the scenarios depend on the goals of the test. Even with the increasing PD amplitude of the internal PDs, the test can be continued to evaluate PD character and check if a breakdown occurs during the test. On the other hand, if PD evaluation gives a clear indication of the weak spots in the cable insulation, then the cable condition is directly known. Figure 4.8 presents an example of the schematic procedure of the decision process. Figure 4.8 various scenarios are considered regarding PD detection results and the further decision process. For the increasing and withstand voltage stage, two options are possible:

- PD detected.
- PD not detected.

⁴ Only for the internal detectable PD in the cable insulation or cable accessories localized in TDR.

In situations when PDs are detected and localized, decisions about further action(s) needs to be taken. A further step involving TDR analysis (described in the next sections), phase resolved PD patterns analysis and analysis of the characteristics of PD (PD occurrence, PD intensity, PD amplitude). If PDs are localized during the increasing phase of the DAC voltage in one or more of the faulty cable components, information about the cable condition can be given even before the withstand voltage test phase takes place. Thus, a decision about performing the next step actually depends on the PD analysis, the experience of the operator and agreement between cable owner and test executor. If the PD level is voltage dependent and an additional over-stressing increases the number of PDs, further cable testing may result in a breakdown. A breakdown of the faulty cable may have an impact on the service life time reduction especially for the service aged cables [8, 10]. On the other hand, the cable owner can make an agreement to execute the withstand test even though the PDs were successfully localized. However, if no breakdown was recorded at voltage withstand test but PDs were localized in the cable system, 100% service reliability of the cable system cannot be ensured anymore. The surveys presented in IEEE400.4 [14] concluded that during testing of the HV cables with DAC method, 40% of survey responders have observed during DAC test an insulation breakdown, and in more than 70% of these breakdown cases, the PD was detected before breakdown.

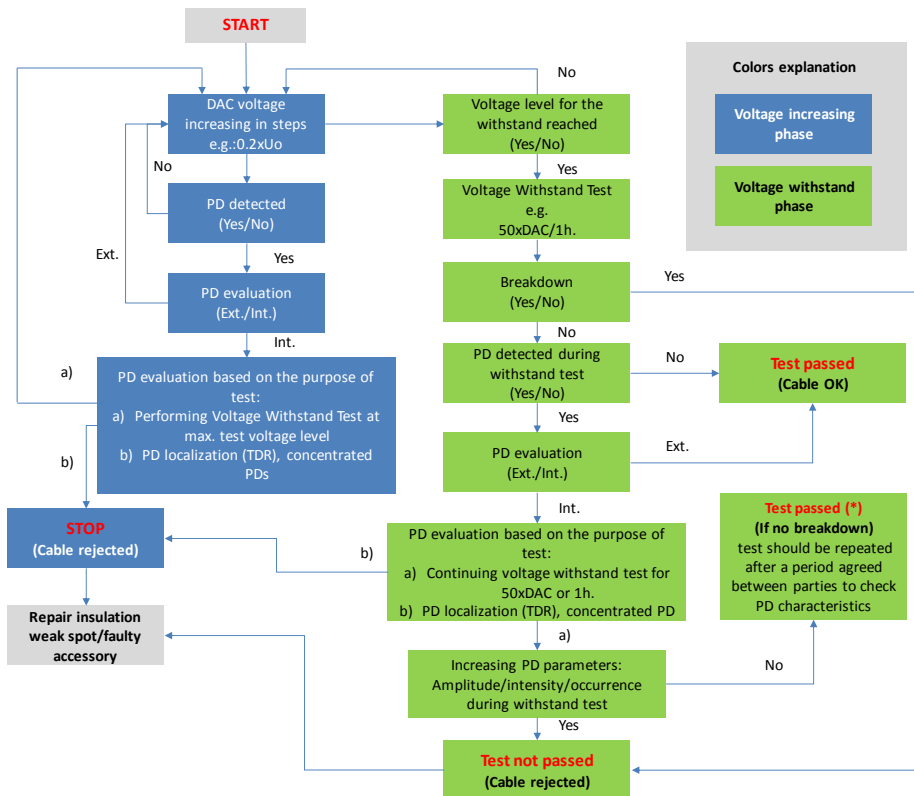


Figure 4.8: Example of test results interpretation for PD monitored DAC withstand test. Note: Breakdown both for the increasing test voltage phase and the withstand voltage phase rejects cable (test not passed/cable not O.K.).

The optimal solution is to replace the faulty component (indicated by PD activity or due to a breakdown) and repeat the test procedure. However, it is also known, that there are some homogeneous defects, e.g. water related defects, that will not produce PD activity before or during the breakdown. Finally, the best possible test scenario is when there is no PD detected and there is no breakdown recorded during the increasing and withstand phase of DAC testing.

For these reasons, it is of great importance to discuss all possible test scenarios and test parameters with the cable owner prior to test execution. This knowledge may help to qualify the cable under the test and make a final decision about further service. In many situations (especially when the breakdown did not occur but PD was detected), advice about repeating the PD measurements is taken to check the PD characteristics after some time in service. If after e.g. 3 months, PD are still detectable and could be localized in the same position as during the first measurements, usually a decision about the replacement of the faulty component is taken directly. A very important parameter is PD inception voltage level. A decrease of inception voltage of PD related defect is a good indicator of the insulation degradation progress in time.

4.3 Partial discharge measurements using DAC

The original PD current pulse, which occurs in a HV power cable, cannot be measured directly as the PD source is not accessible. However, the transient voltage drop that appears across the test object (cable) terminals can be detected and measured by the external measuring circuit in the DAC testing system. In principle, there are two methods available for the detection of partial discharges: the conventional (classical) method described in IEC 60270 standard and non-conventional PD detection method described in IEC TS 62478. During the past 15 years, it has been shown that adding PD diagnosis can significantly increase the effectiveness of the withstand testing [8, 52]. PD diagnosis informs us about the quality of the cable system in terms of PD phenomena and related defects. In the combination with non-destructive DAC energizing, the PD diagnosis provides a powerful method to assess the cable condition at various voltage levels.

4.3.1 IEC 60270 PD detection with DAC

With the conventional method an external circuit is applied which incorporates a coupling capacitor fitted in parallel to the HV equipment (test object). When PDs occur in the HV equipment, they appear to the external circuit-coupling capacitor. Then, a displacement current charge flows into the HV measuring circuit. Partial discharges that occur in the test object will produce current or voltage pulses. The conventional PD detection method is based on measurement of the charge displacement q . Pulses generated at a partial discharge location propagate over the cable length until one of the cable ends connected to the measuring circuit. This measuring circuit is described in reference [53] and Figure 4.9.

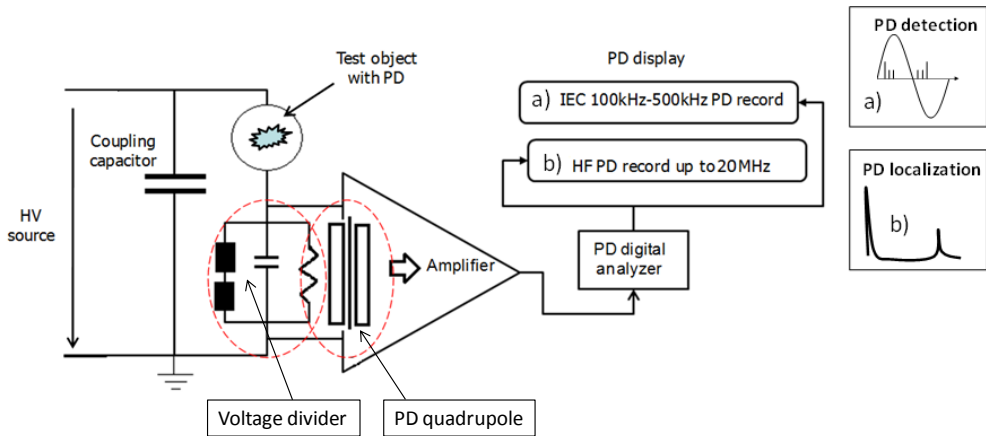


Figure 4.9: DAC PD detection circuit of DAC systems.

Digital PD signal processing

Most DAC systems utilize fast analogue-digital converters to process the PD signal which are detected with a coupling capacitor. Digitalization of the input signal received from the test object is performed in real-time mode without any analogue pre-processing. With analogue pre-processing the PD pulses are first quasi-integrated in an analogue manner using a band-pass filter to create the apparent charge pulse. The band-pass filtering and the peak detection are performed after the A/D conversion by the application of an FPGA (The Field-Programmable Gate Array) for example. With this approach, the recorded signal can be sufficiently de-noised (Figure 4.10). Application of digital conversion in the diagnostic system makes it possible to record such parameters of PD pulse as:

- Instant time of t_i of PD occurrence.
- apparent charge q_i at t_i .
- test voltage magnitude u_i at t_i .
- phase angle φ at t_i .
- phase-resolved PD pattern analysis 2D or 3D.
- Location of the PD pulses using TDR analysis.

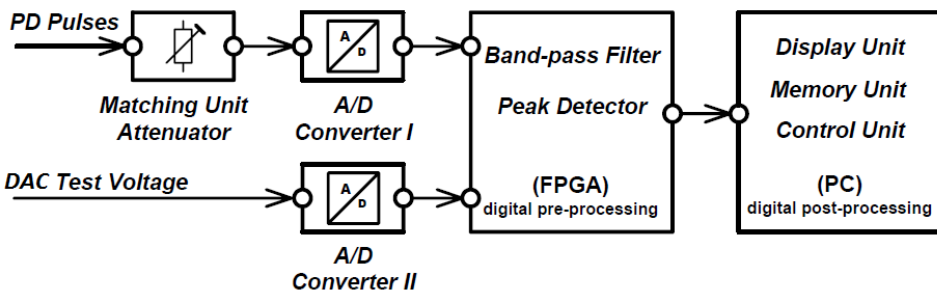


Figure 4.10: Digital pre and post processing of PD pulses with DAC systems [54].

DAC measuring systems utilize the conventional PD detection circuit described above and PD detection is performed in two frequency ranges [5, 6]. The first range is described by IEC 60270 recommendations: 100 kHz- f_1 (lower PD detection frequency) and 500 kHz- f_2 (upper frequency limit). The frequency range between $< f_1-f_2 >$ is used for the PD detection and visualization (Figure 4.11a). In the high frequency (HF) range, up to 20 MHz (fast record) with 100 MHz sampling, PD localization is performed using TDR (Time Domain Reflectometry). Figure 4.11b shows HF (High Frequency) record of PD pulses. In this record, all PD pulses from a single DAC excitation are saved. (Figure 4.11b).

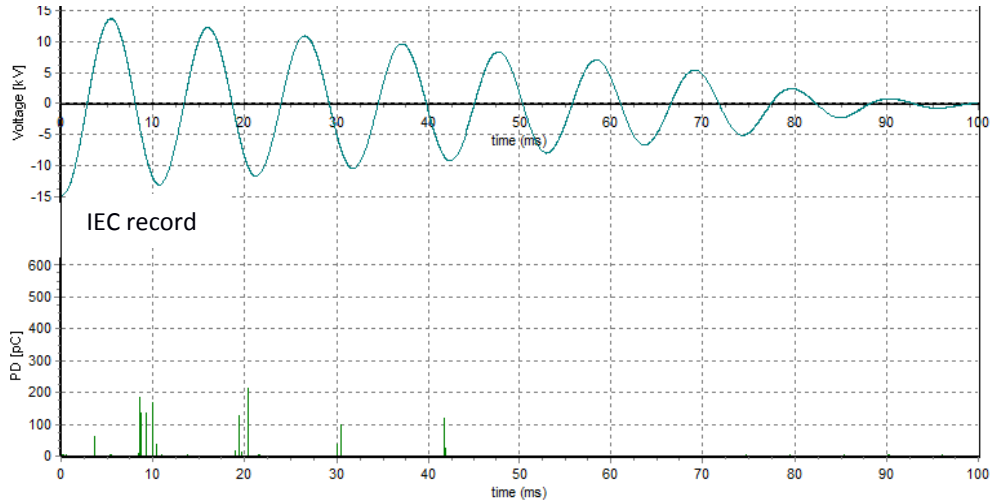


Figure 4.11a: IEC partial discharge record at DAC.

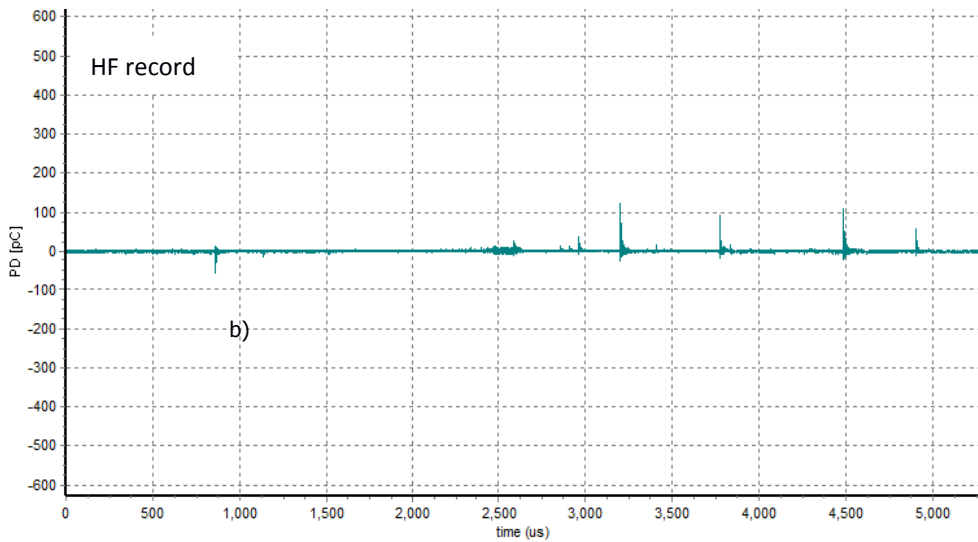


Figure 4.11b: HF partial discharge record at DAC.

4.3.2 DAC circuit calibration

Document IEC 60270 [53] specifies the calibration method based on the simulation of the internal charge transfer between the PD source and the terminals of the diagnostic system by means of an external charge injection unit. Based on this calibration procedure, the apparent charge of a PD pulse is defined as:

“that charge which, if injected within a very short time between the terminals of the test object in a specified test circuit, would give the same reading on the measuring instrument as the PD current pulse itself.”

The PD calibrator unit is a pulse generator connected in series with calibrating capacitors. In order to simulate the transient voltage across the PD defect, the pulse generator creates equidistant voltage steps of known magnitudes U_0 [54]. If the value of the calibrating capacitor C_0 is substantially lower than the value of the virtual test object capacitance C_a , the calibrating charge injected in the test object terminals can simply be expressed by the equation 4-30 [54]:

$$q_0 = C_0 * U_0 = C_a * U_1 \tag{4-30}$$

U_1 is the voltage at the test object C due to calibration.

Figure 4.12 shows the circuit for calibrating apparent charge according to specifications described in [54].

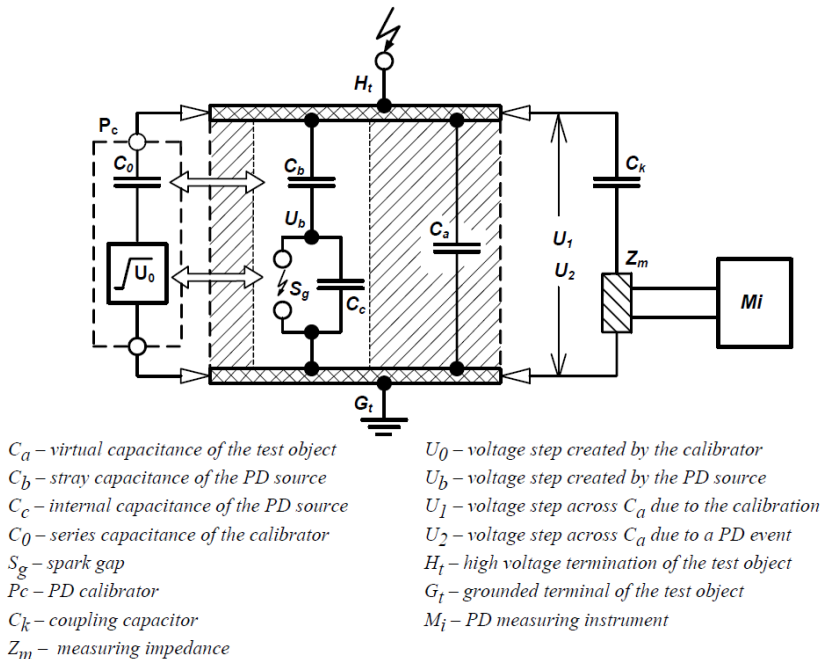


Figure 4.12: IEC 60270 circuit for calibration of apparent charge [53].

Calibration of a DAC measuring circuit means the tuning of the DAC system and test object in specific measuring on-site conditions. For long cables or cables with many cross-bonding joints PD pulse can be strongly attenuated and the far cable end not visible.

With DAC systems two calibration procedures are performed:

- Calibration of the PD reading; in accordance with IEC60270 recommendation a PD pulse calibrator as defined in the IEC 60270 has to be used (as described above).
- Verification of the PD pulse propagation velocity. In XLPE cables, the pulse velocity can be in the range between: 80-89 m/μs whereas in oil impregnated paper cables the pulse velocity can vary between 72-80 m/μs. The mentioned speed here is the V/2 (V over 2) speed and not the actual pulse speed. Injection of the pulse can be done with the same IEC calibrator and the PD pulse propagation velocity is required for TDR analysis measured. During TDR analysis, PD source locations can be calculated based on the calibrated value of PD pulse velocity in particular measuring conditions and a particular type of cable insulation. Moreover, based on the attenuation of the reflected pulse (from remote cable end) it is possible to check (verify) the cable length. (Figure 4.13).

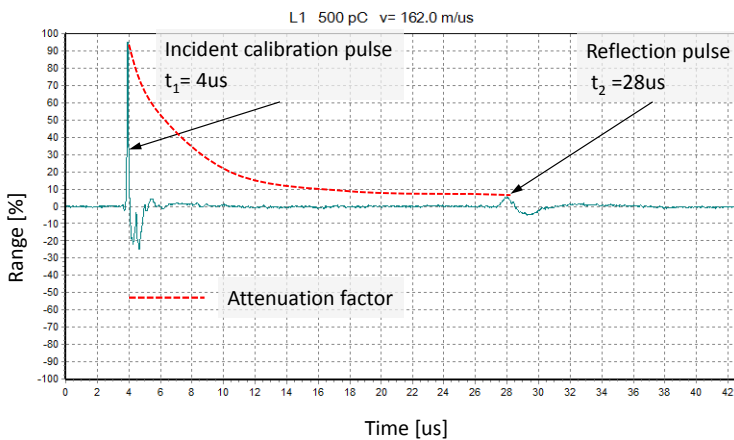


Figure 4.13: Example of the calibration pulse at oil filled 50 kV power cable with length of 1950 m.

For this pulse velocity estimation process, the calculation of time differences between original injected (incident pulse) and its first reflection is done. This pulse is injected from the external calibrator unit. Figure 4.13 shows an example of 500 pC pulse injected and reflected at the open end of an oil filled paper insulated 50 kV cable. The estimated pulse velocity is calculated with the equation [4-31] based on the fact that the calibration pulse runs 2x times over the cable length.

$$V = \frac{2l}{\Delta t}, \text{ where } \Delta t = t_2 - t_1 \quad [4-31]$$

According to references [48, 55], the sensitive PD detection is possible for power cables with lengths of up to several kilometres (Figure 4.14). In cases of cable lengths longer than 10 km,

the PD detection sensitivity is decreased due to the attenuation phenomena and dispersion phenomena of PD pulses traveling through the cable length.

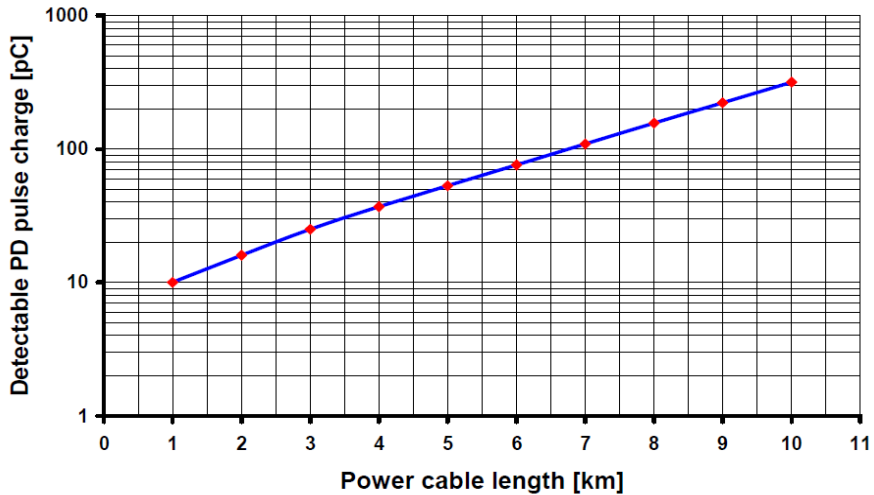


Figure 4.14: Example of PD detection sensitivity versus the cable length calculated on the basis of a reference value of 10 pC achievable for a power cable of 1 km length [48].

PD localization might still be possible, but with an increased threshold level. The PD detection threshold limit refers to the minimum PD magnitude which can be detected (visible) with the measuring circuit calibrated in particular on-site conditions. The PD pulse dispersion can be influenced not only by cable length, but also by the number and type of joints and type of cable terminations.

4.3.3 PD parameters measured with DAC (according to IEE400.4)

If the monitored test voltage mode is used, several PD parameters can be measured-Table 4.3.

Table 4.3
PD parameters obtained with on-site DAC measurements.

Parameter	Description
PDIV [kV]	Partial Discharge Inception Voltage-at this voltage first repetitive discharges are visible.
PDEV[kV]	Partial Discharge Extinction Voltage-at this voltage an internal discharges stop their activity and become undetectable. PDEV determines the highest "safe" voltage at which the test object is "PD-free".
PD magnitude [pC] at different voltage	Related to size of defect gives information about PD destructivity. The higher PD amplitude, the more harmful defect is.
PD pattern (PRPD)	Phase-resolved PD Pattern of discharging pulses that occurs during DAC voltage excitation.
PD intensity [N]	Number of PD pulses recorded in one DAC excitations.
PD location	Location of discharging sources in the cable system through Time Domain Reflectometry technique. Based on this parameter, it is possible to pinpoint the faulty part of cable circuit.

PD inception and extinction voltage

Partial Discharge Inception Voltage (PDIV) is one of the most important diagnostic parameter. It shows at which test voltage level the first PDs above the background noise level occur in the tested insulation system. It is related directly to the type of discharging defect and the defect volume and voltage conditions. It is usually estimated by slowly increasing the test voltage level and recording the PD amplitude. PDIV determines also the voltage level at which PDs are repetitive and stable. Figure 4.15 shows the important aspect of determining PDIV and PDEV (PD Extinction Voltage). In Figure 4.15 according to cable specific

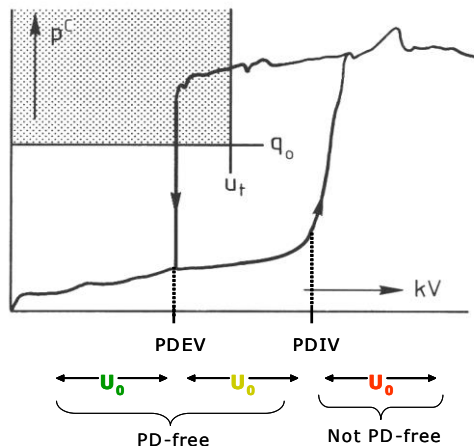


Figure 4.15:PD measurements in a function of test voltage [18].

acceptance values: q_0 and U_t any particular discharge larger than q_0 measured below the selected test voltage U_t leads to rejection of the object under test (shaded area).

PD inception voltage PDIV and PD extinction voltage PDEV referred to U_0 (nominal voltage of the cable) are important indicators of PD presence during network operation. In Figure 4.16 an example of PDIV and PDEV records with DAC voltage is shown for 110 kV, 30 year old oil filled paper insulated power cable. It can be concluded that PDIV is in the range of $1.4 \times U_0$ while PDEV is much lower and equal to $1.2 \times U_0$.

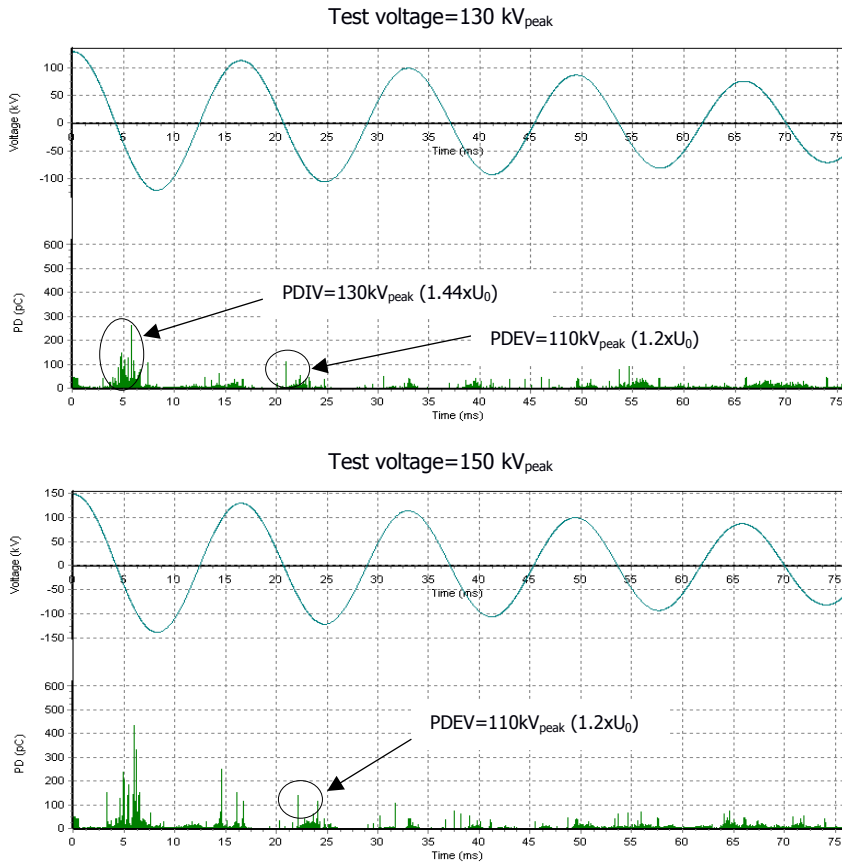


Figure 4.16: Evaluation of PDIV and PDEV for 110kV oil-filled power cable.

PD magnitude

Analysis of PD magnitude in [pC] is an important part of quality control and condition assessment of power cables. For example, for the same type of power cable, PD levels can be compared with each other measured as a function of test voltage. Such a measurement is important to reveal:

- Information about a defect under voltage characteristics e.g. according to the IEC 60270 voltage withstand test requirements.
- PD characteristics of a discharging defect. Insulation damage is caused by the energy dissipated by high energized electrons or ions, ultraviolet light from the discharges, ozone which attacks the void walls, cracking due to the chemical breakdown processes, and liberated gases at high pressure.
- q vs. V (PD level-Test voltage level) graphics help to monitor the PD trend.
- The relation between PD and dielectric loss characteristics.

In Figure 4.17 an example of q vs. V graphics are presented as measured with DAC voltage for HV XLPE power cable during the acceptance test.

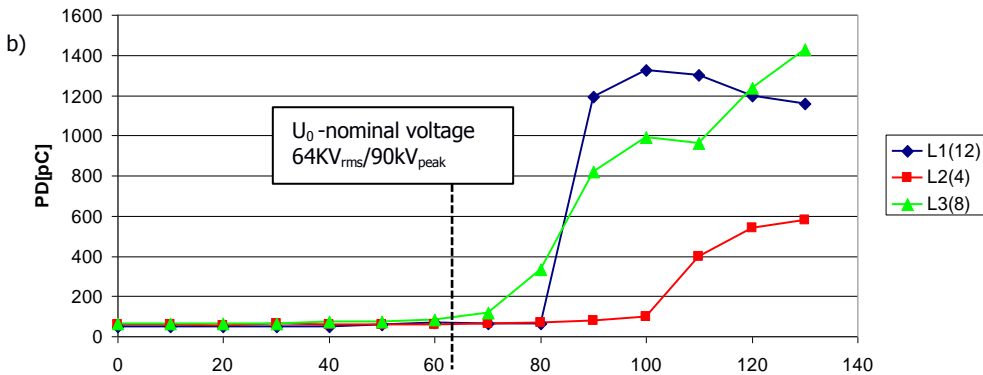
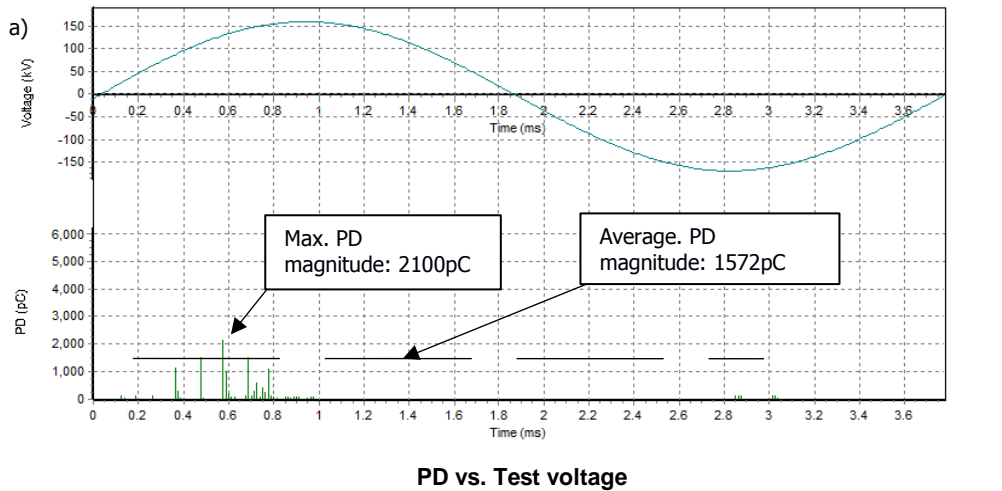


Figure 4.17: a) DAC PRPD at test voltage level of 150 kV . Maximum and average PD magnitude can be derived (selected for the one voltage period). b) q vs. V graphics obtained during site acceptance test on 110 kV XLPE power cable. Different PDIV has been observed for particular cable phases.

PRPD patterns and PD intensity

Records of PD pulses as a function of the voltage phase angle ϕ create the so called phase resolved PD pattern (PRPD Pattern). This pattern is also called “PD fingerprint”. When the maximum permissible PD level is exceeded, it is often important to know the cause of the discharge. Studies of PD patterns may provide an experienced test engineer with valuable information about PD source. It is known that the shape of these patterns has a strong relationship with the type of discharging defect e.g.: corona discharges concentrate at 90° and 270° . Internal discharges can be symmetrically and asymmetrically located in 1st and 3rd quarter of the voltage sine period. Record of PD pulses within single voltage DAC excitation can be displayed as a 2-dimensional (2D) PD pattern (Figure 4.18). Single PD pulses in the form of straight lines/colours is positioned in the 1st, 2nd, 3rd or 4th quarter. Some DAC systems also have an option to create PDPR patterns by mapping the highest intensity of the PD with

colours. The more intensive the colour is recorded the more PDs appeared in a certain position of the voltage sine.

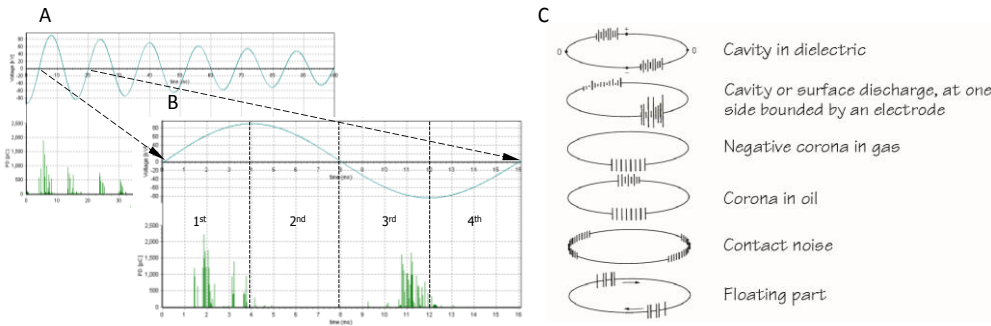


Figure 4.18: a) Full mode-PRPD pattern in time domain displayed at several DAC voltage periods, b) Single period mode-PD pattern displayed only at 1st, 2nd, 3rd and 4th quarter in the time domain for one DAC excitation expressed with line thickness/colors, C) Phase-resolved patterns for different PD sources [18, 56].

PD location (TDR)

PD mapping shows the map of the localized PD pulses in a cable system. PD mapping indicates which cable parts or cable accessory produce PDs and how many PDs was localized under voltage levels. For the localization of PD sources, TDR (Time Domain Reflectometry) principles are applied on the recorded PD pulses in time domain. Particular data necessary to calculate location of PD sources are obtained through (Figure 4.19):

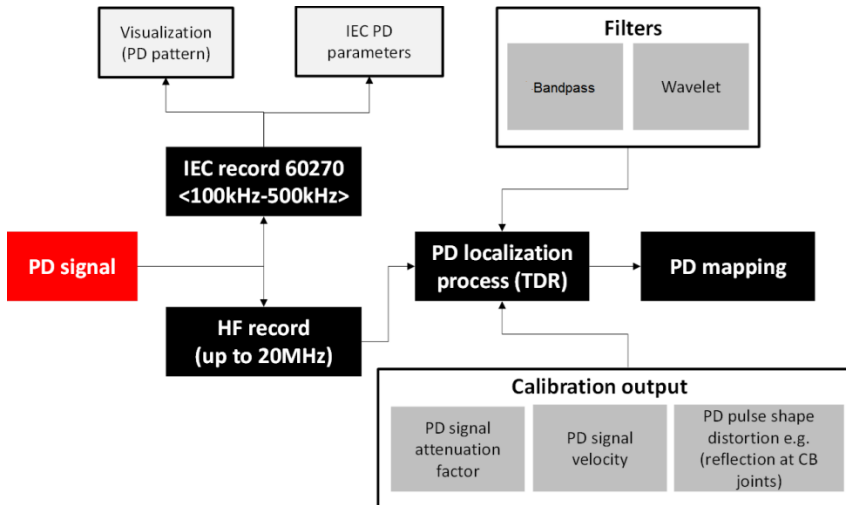


Figure 4.19: PD mapping process (PD localization process).

The principle of using TDR is based on the PD pulse propagation in cable. A PD pulse travels with a certain speed through the cable to near and far cable ends (Figure 4.20). The pulse traveling towards the near end is called “incident pulse” and incident pulse reflection from the far cable end is called “reflected pulse”. A pulse is transmitted down the cable towards both ends. When pulse (representing discharging defect) reaches the near end (place of the connection to the measuring device), it is recorded by a measuring capacitor. A second pulse “reflected pulse” appears after a certain traveling time. Reflection occurs when the impedance of the detector is much higher than the cable’s impedance. In Figures 4.20 and 4.21 a pulse dispersion due to cable attenuation is presented. By knowing the time difference between the incidence pulse and the reflected pulse Δt_{cal} a distance x_i to pulse source can be estimated with equations [4-32 to 4-35].

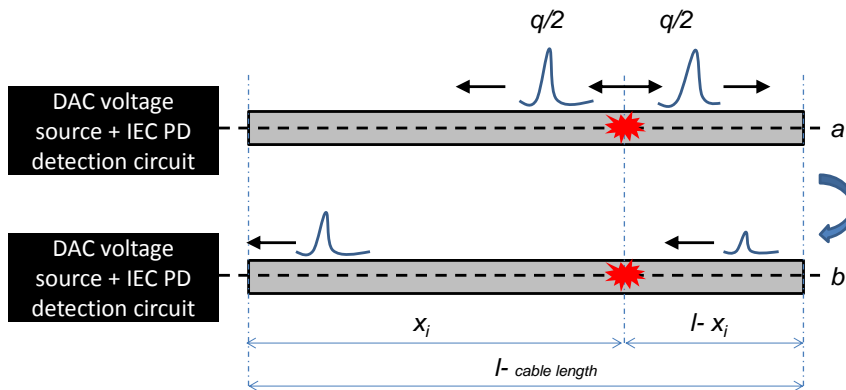


Figure 4.20: Principle of PD pulse localization in power cables. Where l is the length of the cable, Δt is the time difference between the incident and the first reflection of the incident pulse.

$$t_1 = \frac{x_i}{v} \quad [4-32]$$

$$t_2 = \frac{(l-x_i)+l}{v} \quad [4-33]$$

$$\Delta t = t_2 - t_1 \quad [4-34]$$

$$x_i = l - \frac{v \cdot \Delta t}{2} \quad [4-35]$$

Where: v -pulse velocity estimated during calibration, t_1 -record time of incident pulse, t_2 - record time of reflected pulse.

In Figure 4.21 an example of PD mapping of aged 110 kV PE cable (length of 1300 m) is shown. There are several sources of PD activity in the cable insulation. The blue line is a saved calibration pulse injected at the near termination. This pulse travels directly to the diagnostic system through the connection leads and the remote cable end. The orange line is a PD pulse which was originating from the distance of 1065 m. The difference between the calibration pulse and PD pulse from the cable defect is clearly visible.

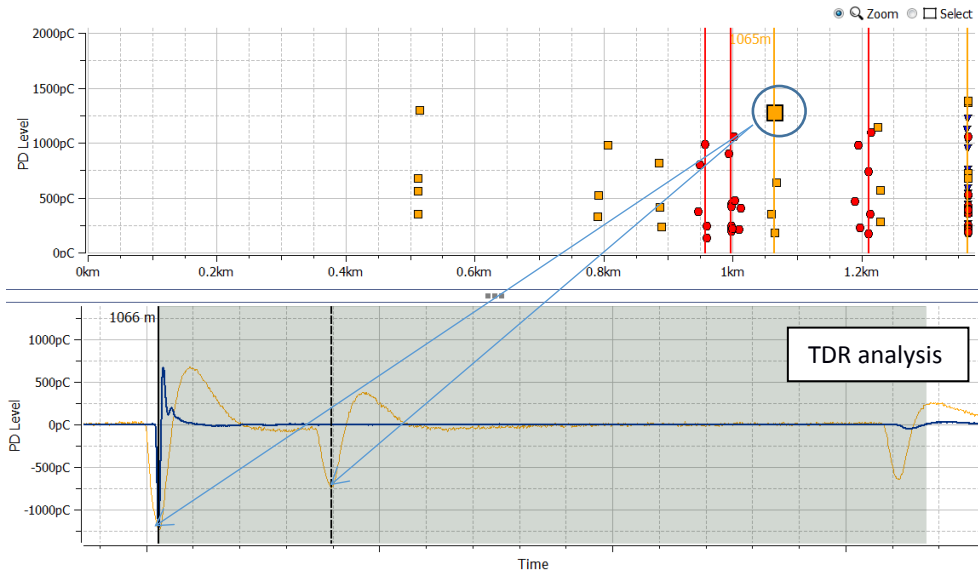
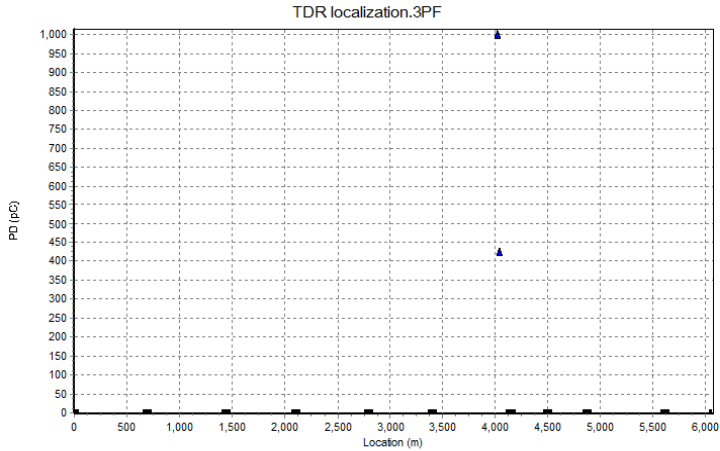


Figure 4.21: PD location (PD mapping) of 110 kV aged PE cable obtained during the maintenance test. Note: PD events localized in cable insulation are represented by: blue triangle (L1), orange square (L2), red dot (L3). Blue line is a calibration pulse.

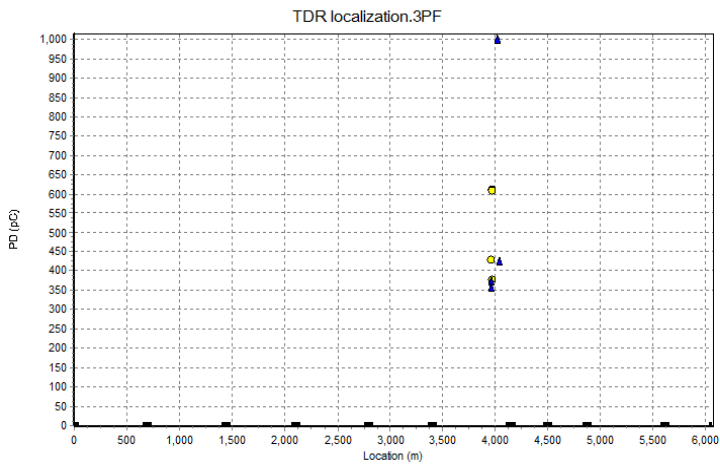
If localization of the discharge sources is strongly concentrated and both the PD amplitude and intensity of the detected PD increase with test voltage level, it is a clear indication of a weak spot (Figure 4.22).

An example of PD mapping obtained from TDR analysis of PD pulses recorded at different test voltage levels is shown in Figure 4.22. Based on this PD mapping, it can be clearly derived that the source of PD location is the cable joint number 6 and the near termination in cable phase L1/L2/L3. Increasing PD magnitude as measured at the voltage range $0.6 \times U_0$ - $1.7 \times U_0$ confirms the faulty joint by increasing the PD magnitude and PD occurrence.



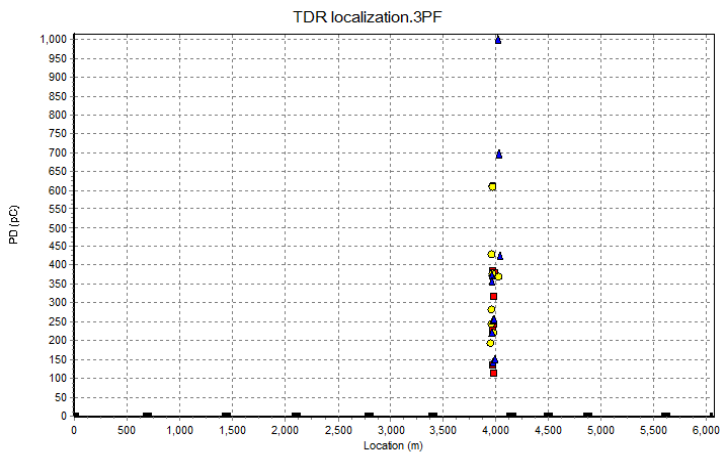
0.6xU₀ concentration of PD pulses at the vicinity of joint no.6, no concentration at other locations at this cable section.

PD occurrence:
2-PD pulses localized in joint no.5 cable phase L3.



1.0xU₀ concentration of PD pulses at the vicinity of joint no.6, no concentration at other locations at this cable section.

PD occurrence:
8-PD pulses localized in the phase L3 and 5-PD pulses localized in phase L2.



1.7xU₀ concentration of PD pulses at the vicinity of joint no.6, no concentration at other locations at this cable section.

PD occurrence:
15-PD pulses localized in phase L3 and 9-PD pulses localized in phase L2 and 4-PD pulses localized in phase L1.

Figure 4.22: PD location (PD mapping) of 110 kV new XLPE cable obtained during the acceptance test. Note: black rectangles represent joints positions.

The influence of the cross-bonding (CB) joints on PD signals

(E)HV cable systems are often equipped with cross-bonding joints at regular distances, e.g. every 1 km. In a cross-bonding joint, the cable sheaths of different phases are exchanged. A cross-bonded cable system helps to balance induced voltage and circulating currents, which leads to a reduction in losses and keeps a thermal balance along the cable lengths [57].

Calibration pulse is strongly reflected at this type of joint due to impedance change of the cable in this point. Therefore, to reduce the attenuation, these joints should be in a “straight-through” configuration (Figure 4.23b) during calibration of the complete circuit and during DAC testing. It is assumed that the pulse velocity does not change neither in CB joint configuration “A” nor “B”. However, it can be seen that the magnitude of the signal reflection at CB joints in configuration “B” is much lower and amplitude of the far cable end pulse reflection is much higher. Thus, especially for the long cable connection, the velocity reading can be more accurate at configuration “B”. In cases of internal PDs detected in cable section, a cross-bonding configuration of joints decreases detection sensitivity. If CB joint is in configuration “A”, then a PD pulse signal is separated through cable sheath in ratio-1/3 due to the fact that PD reflection signal which arrived from the remote end is more attenuated than in “straight-through” configuration “B”-Figure 4.23. A reflection recorded during circuit calibration (signal injection at the near cable end) is shown in Figure 4.23. Differences in PD magnitude as observed in CB joint configuration “A” and “B” are visible.

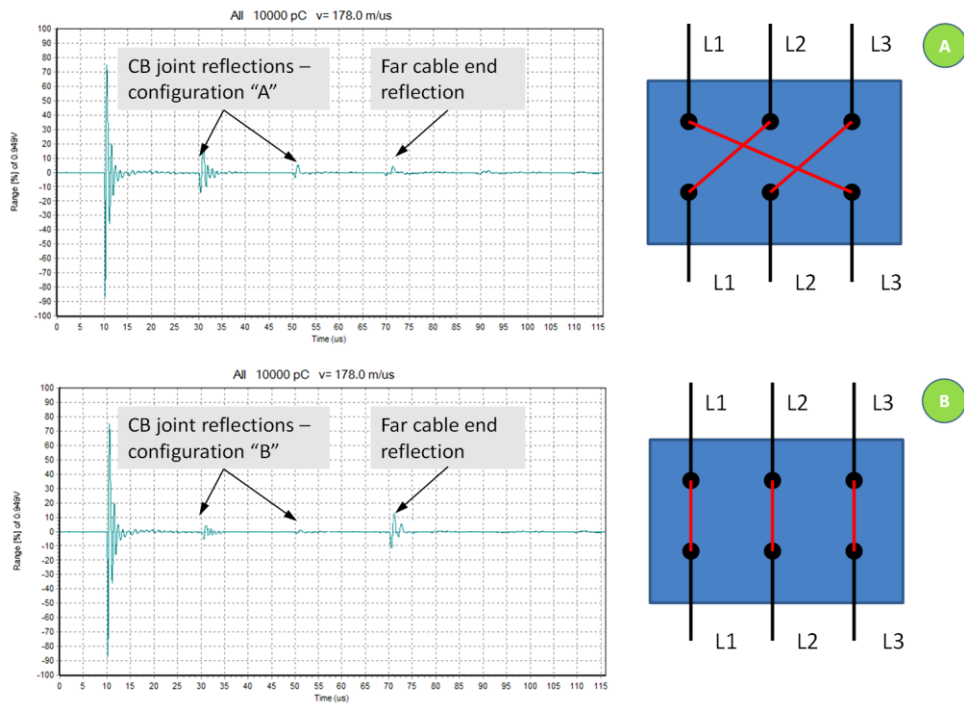


Figure 4.23: Results of PDs pulse measurements on CB (Cross-Bonding) joint configurations A and B.

4.4 Dielectric loss estimation using DAC

With DAC voltages the estimation of the dielectric loss of the cable is based on the calculation of the attenuation factor of the damped voltage sine wave applied to test object. The readings of dielectric loss are based on the loss characteristics of the test object together with the known losses of the measuring device. The test object can be represented by a resistance in parallel with capacitance (Figure 4.1). Thus, to estimate losses R_2 in a measured test object, the internal losses of the measuring system (device) must be known. The value R_1 can be obtained through calibration procedure of the test system at different voltages and frequencies during manufacturing of the system. This calibration procedure is done through a series/parallel configuration of PD free and loss free capacitance connected to the test system and energized with DAC sequences. Under different voltages and different DAC frequencies losses of the system are recorded. Since the dielectric losses of the test capacitors are known, the internal resistances of the measuring circuit can be calculated.

A damped AC voltage wave can be described by the previously mentioned equation [4-18]:

$$U_{C0}(t) = U_{C0}(0) \sqrt{1 + \left(\frac{3\alpha}{\omega_1}\right)^2} e^{-\alpha t} \cos(\omega_1 t + \theta) \quad [4-36]$$

DL (dielectric loss) can be calculated from the damping characteristics of the oscillating voltage wave. The losses of the test object are represented by a parallel resistance R_2 (Figure 4.1b). This R_2 can be estimated numerically out of the measurement results according to the equation:

$$R_2 = \frac{L}{2\beta_{DAC}LC - R_1C} \quad [4-37]$$

Where: L-is the fixed inductance of DAC setup, C,is a capacitance of the test object.

The unknown factor β_{DAC} can be calculated directly from the damping characteristics of the DAC voltage, using the voltage and time of the voltage peaks of different periods (Figure 4.24). DL of the cable sample can be given by:

$$DL = \frac{1}{\omega \cdot R_2 \cdot C} \quad [4-38]$$

During dielectric loss measurements on the power cable, the losses can be directly obtained from the damping factor of the oscillating test voltage (Figure 4.24) calculated between e.g. the first and third voltage amplitude period with equation. The damping factor depends on losses in the test object (R_2) and losses of the measuring circuit (already calculated during manufacturing). Therefore, the change of R_2 relates to change of cable losses. As a result, the lower the value of R_2 , the less damped and longer oscillations are obtained (Figure 4.24). Currently the only published rules and guides for dielectric loss measurements with DAC voltages is IEEE400.4:2015 [14]. Tests are performed on a comparative basis. The purpose of dielectric loss estimation with DAC is to grade tested cables on a scale from high to low-quality. Again, comparative testing will show which cables are better and which are worse and, over time, let users develop their own in-house guidelines, unique to specific situations.

Dielectric loss measurement on a cable sample result in single DL value in [%] respectively in $N \times 10^{-4}$ where the relation is $0.1\% = 10 \times 10^{-4}$. According to reference [14] the measuring threshold value of DL at DAC is 0.1%.

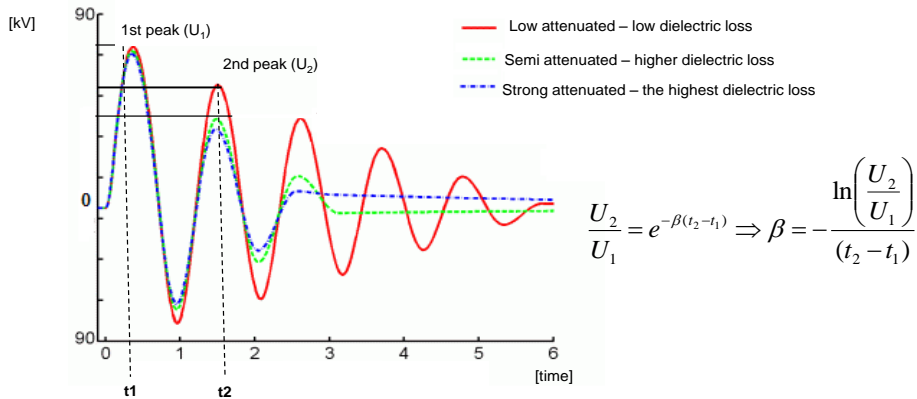


Figure 4.24: Principle of dielectric loss estimation with DAC voltage.

In Figure 4.25 an example of on-site dissipation factor measurements performed on self-contained oil-filled 150 kV cable is presented. In this particular case, the increase of losses between $0.4 \times U_0$ ($40 \text{ kV}_{\text{peak}}$) up to $1.2 \times U_0$ ($150 \text{ kV}_{\text{peak}}$) was observed in all three cable phases. The absolute values for losses oscillate around 1.45% which corresponds to 145×10^{-4} . In this particular case, it can be concluded that all cable phases L1/L2/L3 show a similar increase of dielectric loss in the test range $0.4\text{-}1.2 \times U_0$.

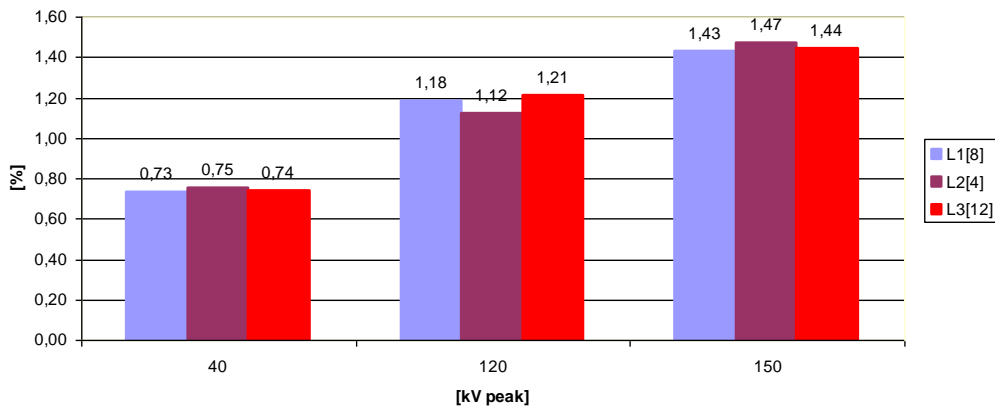


Figure 4.25: Example of dielectric loss measurements with different DAC levels on 40 year old 150 kV SCFF cable. Results show a relatively high loss increase between $0.4\text{-}1.2 \times U_0$ which could be an indication of insulation ageing processes.

4.5 Conclusions

1. DAC voltage is a test voltage created through a resonance effect created between cable (capacitance) and coil (inductance) in a series configuration after charging the cable capacitance with continuously increasing HV voltage with uni-polar DC source: positive (+) or negative (-).
2. Resonance sine wave voltage is damped (decaying) due to the fact that energy stored and transferred between inductance and capacitance is not compensated with the external voltage source at the moment of oscillations.
3. The continuous increasing voltage in the energizing phase results in the AC field distribution without DC stresses and AC sinusoidal damped voltages for the duration of the withstand test. Thus, there is no risk of e.g. space charge accumulation in XLPE insulation.
4. DAC testing when combined with PD and DL diagnosis, provides a tool for the assessment of the condition of both the new and aged power cables.
5. Due to the fact that DAC systems are relatively small, it can be used in a small substation and the areas with a limited footprint.

5. Comparison of AC and DAC voltages for defects detection by PD

Chapters 1 and 2 show that installation related defects are responsible for a large number of power cable failures. These failures may occur both during cable HV acceptance tests (voltage withstand test) or later during the cable “childhood” period-a few weeks or months⁵ after “successful” commissioning procedures. These defects are related to PD activity and breakdown processes. To minimize the risk of unexpected cable failure on-site, HV acceptance tests are performed with the application of external over voltage source. This voltage source should generate voltage at a frequency between 20 Hz-300 Hz as per IEC standard at ten elevated levels. General requirements and a maximum test voltage level for a withstand test should be based on the national or international norms or discussed with the cable purchaser if necessary. The test intends to create such a condition in which a faulty component should fail during the test. A common practice is testing above nominal voltage level e.g. 1.2-2.5xU₀.

In the past few years, we have observed that a voltage application above nominal level gives good results in finding some serious problems in cable joints and cable terminations onsite. These “good” results relate to the situation when installation error(s) produce ultimate breakdown in a faulty component during relatively short cable testing time onsite.

Experience gained during onsite acceptance tests on HV/EHV cable systems presented in several publications [8, 12, 17] confirms that sensitive partial discharge diagnosis can also bring valuable information about the cable system condition. PD detection in combination with localization of PD sources is considered as a more effective method than only simple go/no-go withstand testing.

In this chapter, the applicability of DAC voltages for onsite testing and cable installation related error detection is presented based on laboratory tests. Three known defects that occur during 110/150/220 kV class cable jointing procedures are investigated. Comparison of defect detectability with AC 50 Hz and DAC voltage (various frequencies) on power cables is discussed. For a better understanding of the installation related failures, the electric field distribution in the cable joint under the over-voltage conditions was calculated. These analyses are based on the theoretical defect simulations and are done with Finite Element Analysis (FEA) software.

⁵ Some installation related failures may occur even later e.g. after 3-4 years or longer [2, 3].

5.1 Defects for the laboratory investigation

The investigated defects in this thesis were selected based on the literature and knowledge of cable manufacturers. It resulted in the selection of the most problematic and “most frequently occurring problems” that happen during field jointing of 110-220 kV class XLPE cables. The test set-up used for joint defect investigation consisted of a 100 meter HV 90/150 kV cable with a capacitance of 180 pF/m, with longitudinal watertight solid aluminium conductor, extruded semiconducting copolymer compound, XLPE extruded insulation. The insulation screen was an extruded semi-conductive copolymer compound. The cable was equipped with semi-conductive water blocking tape and copper wire helix, copper contact type counter helix and the outer sheath is PE extruded. The cable was divided into two sections through one click-fit type joint and finished by two outdoor-type terminations. The termination used for the test set-up was Prysmian OTC-170-X. This type of termination is designed to terminate an extruded high voltage cable in outdoor conditions under the heaviest pollution conditions and its maximum U_{max} voltage is 170 kV. A pre-moulded click-fit joint type Prysmian CFJ-170A was used for the investigation (Figure 5.1). This joint type is designed to connect two extruded high voltage cables of the same construction and has separated cable sheaths. The distance between termination 1 and the joint was 90 m, while between the joint and termination 2 it was approximately 10 m. All the components in the cable system were provided by Prysmian Cables and Systems B.V, The Netherlands. The test set-up is shown in Figure 5.2.

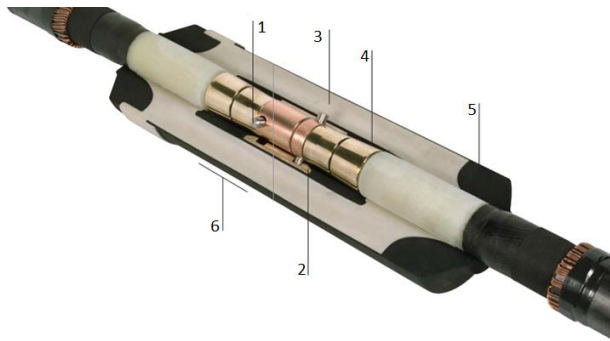


Figure 5.1: Click-fit type joint cross-section. Detailed information regarding cable joint and terminations can be found on the manufacturer’s website [90]. Components: 1-Plugs, 2-CLICK-FIT® locking mechanism, 3-Joint body, 4-Shielding electrode, 5-Stress control cones, 6-Cover.

For the laboratory investigation of the assembling/installation faults, three different cable joint defects were chosen, see Figures 5.3-5.5. Three defects are artificially created in the cable joint and these defects produce PDs. Some of the presented joint defects are already mentioned in section 2 of this dissertation. The first and the second defect represent the surface discharge along the interface of the insulation material. This type of PDs can result in a failure of cable system even if the extruded insulation is totally immune to PD-induced electrical tree initiation. The third artificial defect represents the case of electrode-bounded cavity between the outer semi-conductive screen and the cable insulation, where PDs may result in the erosion discharge process through the insulation layer.

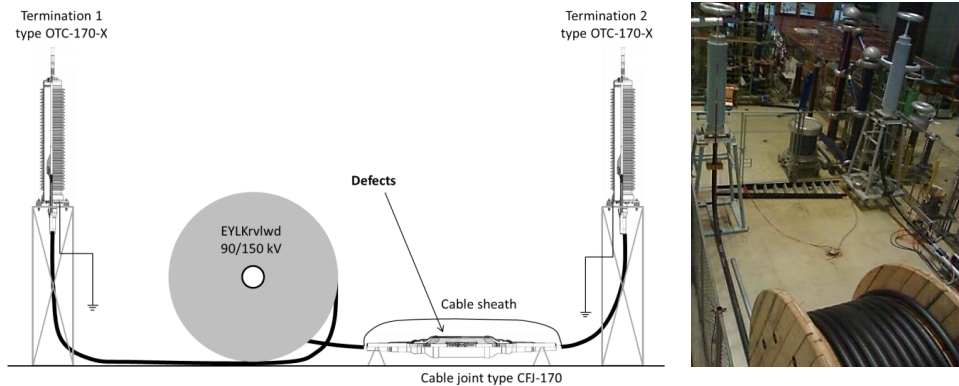


Figure 5.2: Test setup: 100 m XLPE cable with accessories.

Defect type 1: Missing outer semi-conductive screen

This defect occurs mostly when distances of the semi-conductive layers are wrongly calculated (wrong measures). This defect can also occur due to the high pressure and surface tearing through a lack of lubricant when joint deflectors (housing) are applied. The source of this type of defect is poor workmanship. Figure 5.3 shows the location of this defect in the cable joint. For the investigation, three different sizes of defect 1 were created: 5 mm, 10 mm, 15 mm. This artificial defect is created by removing the outer semi-conductive screen of the cable in the small area before entering the joint. As described in section 2, such a defect will produce an electric field enhancement at the edge of the semi-conductive screen which will result in surface discharges along the surface of cable insulation. PD measurement according to IEC 60270 standard were applied to the test setup and to investigate the PD behaviour of this type of defect with two HV sources: AC 50 Hz and DAC (different frequencies).

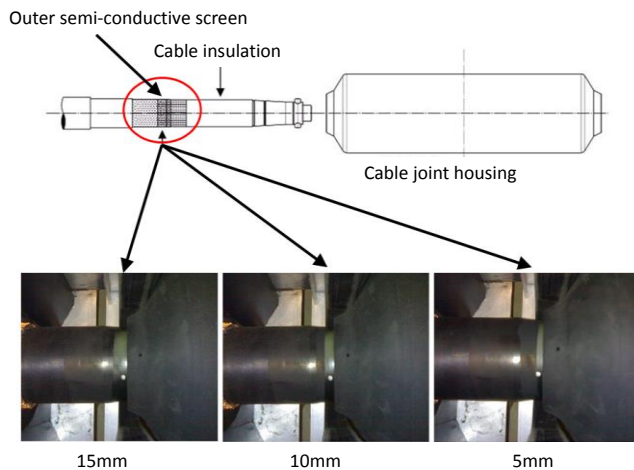
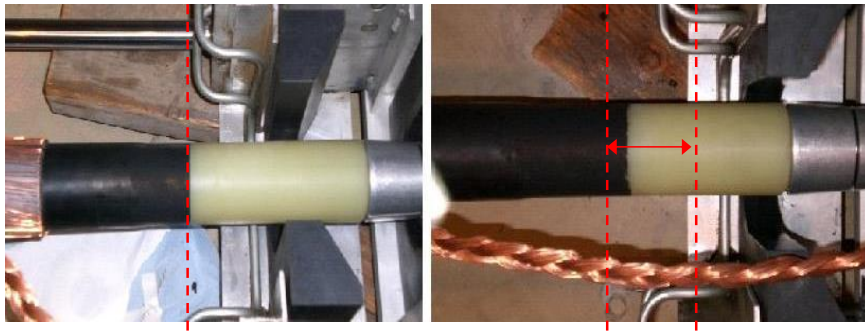


Figure 5.3: Location of the joint defect 1

Defect type 2: Extra semi-conductive screen in the joint

Defect 2 occurs mostly when the distance between semi-conductive layers is wrongly calculated (wrong measures) and an extra semi-conductive screen is applied on the surface of the cable insulation inside the joint body. The source of this type of defect is poor workmanship. Figure 5.4 shows the location of this defect in the cable joint. For the investigation, three different sizes of defect 2 were created: 10 mm/20 mm/30 mm.



0mm (PD-free position)

10 - 40 mm of extra semi-conductive screen

Figure 5.4: Location of the joint defect 2.

Defect type 3: Electrode-bounded cavity

This defect occurs between the cable insulation and the outer semi-conductive screen. This defect may occur due to poor contact between cable insulation and semi-conductive screen as a result of poor elasticity of stress-cone or wrong diameter size. The main reason of this defect is poor-workmanship but it can also be the low quality of manufacturing. When the material of the stress-cone is too stiff or the shape is not completely round, it may result in poor contact under the joint housing. Figure 5.5 shows defect no. 3.



Initial situation

Removed insulation by scratching with the knife

Copper tape glued on the top of the scratch

Figure 5.5: Location of the joint defect 3.

5.1.1 Electric field distribution for defects 1, 2, 3

Before the artificial defects were investigated, the electric intensity within the (simulated) faulty component (joint) was calculated using Ansoft version 9.0 of Maxwell 2D Student Version. This program can be used for analysing the electric fields in the cable joint cross-section by using Finite Element Analysis (FEA)⁶.

All objects in the cross-section model, e.g. presented in Figure 5.3-5.5 have to be assigned for their material properties which consist of:

- The high-voltage conductor is assumed as perfect conductor with the infinite conductivity.
- The inner and outer semi-conductive screen is assumed as material with the conductivity: 10^{-5} siemens/meter.
- The cable insulation material with the relative permittivity: $\epsilon_r = 2.25$.
- The joint insulation is assumed as material with the relative permittivity: $\epsilon_r = 3$.
- The background is modelled as air with the relative permittivity: $\epsilon_r = 1$.

Defect type 1: Missing outer semi-conductive screen

Electric field calculations were performed including a field plotting simulation for normal situations without any defect, and with the defect in three different sizes. The electric field in the cable system is highest close to the high-voltage conductor while the lower stress will be located in the area close to the outer semi-conductive screen.

$$E_r = \frac{CV_T}{2\pi\epsilon_r\epsilon_0 r} = \frac{V_T}{r \ln\left(\frac{b}{a}\right)} \quad [2.2]$$

Where: b and a-external/internal radius of insulation layer, V_T -applied voltage (phase to ground), r-continuous coordinate. Figures in Appendix C show the electric field behaviour for various voltage simulations. In Table 5.1 the simulated electric field stresses calculation are shown for each defect size and different test voltage (AC 50 Hz). Additionally, for each voltage level the average measured PD amplitudes were marked in colour.

Table 5.1
Electric field for different situations of defect type 1 at different voltage stresses. The colours reflect PD amplitude measured with AC 50 Hz up to $1.2U_0$. Green: No PD, yellow: $PD < 700pC$, orange: $1000pC < PD < 5000pC$, red: $PD > 5000pC$.

Voltage Stress (kV _{peak})	Electric Field (kV _{rms} /mm) for each condition			
	No defect	Defect 5mm	Defect 10 mm	Defect 15 mm
28 (0.2U ₀)	1.16	1.24	1.36	1.62
60 (0.5U ₀)	2.49	2.66	2.91	3.47
122.5 (U ₀)	5.06	5.41	5.96	7.09
147 (1.2U ₀)	5.89	5.92	6.01	7.12
208.2 (1.7U ₀)	8.61	9.19	10.13	12.04

At 1.7U₀, only electric field calculations have been done

⁶ In mathematics, finite element method (FEM) is a numerical technique for finding approximate solutions to boundary value problems. It uses vibrational methods (the calculus of variations) to minimise an error function and produce a stable solution.

Defect type 2: extended semi-conductive screen

Material properties which are used in experimental simulation of the defect type 1 are also used for modeling defect type 2. In order to see the effect of defect type 2 in the cable joint, a comparison of normal situation without defect 2 and condition with defect 2 for several voltage stresses was made. In Appendix C, all electric field plotting results are depicted for normal conditions and for voltage stresses: $0.2xU_0$, U_0 , $1.7xU_0$. Defect type 2 in the form of extra length of semi-conductive screen at the boundary between cable insulation and joint insulation will change the electric field distribution and result in field enhancement at the end of defect type 2. In order to see the effect of the size of the defect, several simulations with different sizes of defect type 2 are calculated. Field plotting simulation for different sizes of defect type 2 shows that the length of the extended semi-conductive screen influenced the electric field enhancement at the edge of the extra semi-conductive screen. It can be concluded, from the results of field plotting of defect type 2, that the situation will be more critical for larger sizes of defect type 2 due to higher electric field enhancement. In Table 5.2 the simulated electric field stresses calculation are shown for each defect size and different test voltage (AC 50 Hz). Additionally, for each voltage level the average measured PD amplitudes were marked in colour.

Table 5.2
Electric field for different situations of defect type 2 at different voltage stresses. Colours reflect PD amplitude measured with AC 50 up to $1.2U_0$ Hz: green: No PD, yellow: PD < 80pC.

Voltage Stress (kV _{peak})	Electric Field (kV _{rms} /mm) for each condition				
	No defect	Defect 10mm	Defect 20mm	Defect 30mm	Defect 40mm
30	1.24	1.54	1.68	1.84	2.02
122.5(U_0)	5.06	6.28	6.86	7.52	8.23
147($1.2U_0$)	5.89	6.91	6.93	7.61	8.38
208.2($1.7U_0$)	8.61	10.68	11.65	12.78	13.98

At $1.7U_0$ only electric field calculations have been done

Defect type 3: electrode bounded cavity

The simulation model for defect 3 has equal material properties as used in defect type 1 and 2. Defect type 3, electrode-bound cavity (or rather open multi-channel), is assumed to be filled with air with relative permittivity (ϵ) equal to 1 and has a dimension of 10 mm length and 1 mm depth. In the test set-up, defect type 3 is more complicated in dimension since it is made by removing a piece of XLPE insulation with a knife. The gap was covered with copper tape. Conductivity of the copper tape used in the tests was $6x10^7$ S/m.

Investigation of the effect of electric field behaviour in the cable system due to the presence of defect type 3 is obtained by electric field plotting. It is performed for a normal situation without defect type 3 and with the presence of defect type 3. When defect type 3 occurs in the form of electrode-bound cavities, the electric field distribution changes and the electric field inside the cavity is much higher than the electric field in the remaining part of the cable insulation. If this field enhancement is higher than the breakdown strength of gas inside the cavity, breakdown of gas will occur and produce PDs. It must be noted that the presence of a copper strip covering the air filled gap may have an influence on PD production. It is due to the high conductivity of copper strip (cathode material) and the additional edge effect of the copper strip shape. A PD event in defect type 3 appears with an increased electric

conductivity in one or more of the cavity channels. Channels discharge independently as they slightly differ from each other. A channel discharges when the voltage over the channel, measured between the upper and lower cavity surface of the channel, exceeds the inception voltage and a first seed electron starts the avalanche somewhere in the channel. The inception voltage is approximated with the breakdown voltage for air given by Paschen's law.

According to the Paschen curve [18] as shown in Figure 5.6, it is valid to describe the breakdown strength of small cavities in solid insulation with pressure times distance, (p.d) up to 100 atm.mm. By applying the Paschen curve, the breakdown strength of air-filled cavity of 1 mm distance between electrodes and assumed pressure 1 atm. will be around 4.37 kV_{peak}/mm. This value is close to the results of the electric field enhancement in the simulation at voltage stress at 50 kV_{peak}. Thus, the assumption was that at 50 kV_{peak}, the first PD signals should be observed⁷.

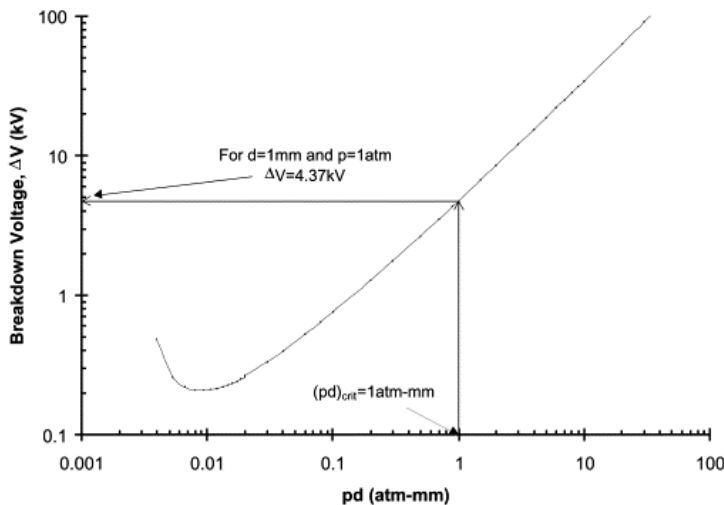


Figure 5.6: Paschen's curve for dry air [18].

The Townsend breakdown mechanism will play a role in case of defect type 3 for the condition of pressure times distance lower than 5 atm./mm. In this mechanism, the cathode material will play an important role in releasing new electrons from the feedback mechanism by positive ions or photons. Furthermore, the transition from the Townsend to Streamer mechanism in electrode bound cavities will occur. These mechanisms are controlled by the over-voltage, where the space charge and surface charges in the cavity may determine the streamer mechanism [58]. A closed cavity has a special PD characteristic as a function of time where the PD pulses tend to decrease or disappear with long duration of voltage stress applied. This phenomenon relates to the reduction of over-voltage due to sufficient supply of initial electrons and an increase of conductivity of the cavity surface, which shield the cavity interior from the electric field. It depends on the part of the AC cycle, which material represents cathode (process of electrons release). The cathode supplies the electrons to support PD activity. In Table 5.3 the simulated electric field stresses calculation are shown for

⁷ Paschen's curve is based on a perfectly spherical void, which is difficult to obtain in real situations, so the breakdown voltage may be slightly different due to the physical shape of the cavity.

each defect size and different test voltage (AC 50 Hz). Additionally, for each voltage level the average measured PD amplitudes were marked in colour. The plot of electric field as a function of voltage applied up to $1.7 \times U_0$ for defect type 3 and without the defect is shown in Figure 5.7. It can be seen from the simulation that the field enhancement in the cavity is approx. ϵ times higher than the normal field in the dielectric⁸.

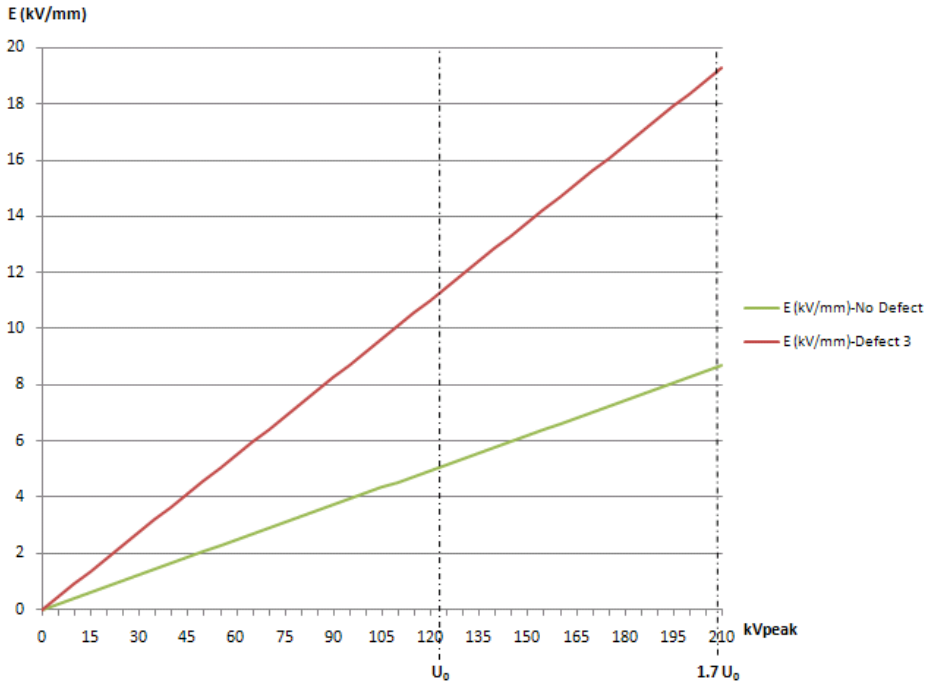


Figure 5.7: Plot of electric field as a function voltage applied for defect 3.

Table 5.3

Electric field for different situations of the defect type 3 at different voltage stresses. Colours reflect PD amplitude measured with AC 50 Hz up to $1.2 \times U_0$ Hz: green: No PD, yellow: PD < 80pC, orange: PD < 2200pC.

Voltage Stress (kV _{peak})	Electric Field (kV _{rms} /mm) for Each Condition	
	No defect	Defect 3
50	2.01	4,5
122,5(U_0)	5.06	11.1
147($1.2U_0$)	5.89	13.4
210($1.7U_0$)	8.61	19.2

At $1.7U_0$ only electric field calculations have been done

⁸ ϵ -permittivity of XLPE insulation equal to 2.25

5.1.2 Effect of the voltage frequency on the electric field and inception voltage in the bounded cavity

The parameter, which drives local conditions in a faulty dielectric is the local electric field stress E_i at the defect, which is directly responsible for discharge initiation. According to equation [5.1] E_i strongly depends on two terms:

$$E_i = E_c + E_q = fE_0 + E_q \quad [5.1]$$

E_0 is the applied electric field, which due to the dielectric permittivity and the shape of the defect area can change into E_c . Also the amount of deposited surface charge contributes to E_i with E_q . The accumulated charge on the cavity walls gives also a source for starting electrons, which are necessary for the following PD ignition and so may have a direct impact on discharge inception voltage (Figure 5.8) For instance for a spherical cavity, occurring due to an ageing process, the field modification factor f is [58]:

$$f = \frac{3 \cdot \epsilon_r}{2 \cdot \epsilon_r + 1} \text{ where } \epsilon_r \text{ is the dielectric constant of the insulation [F/m].}$$

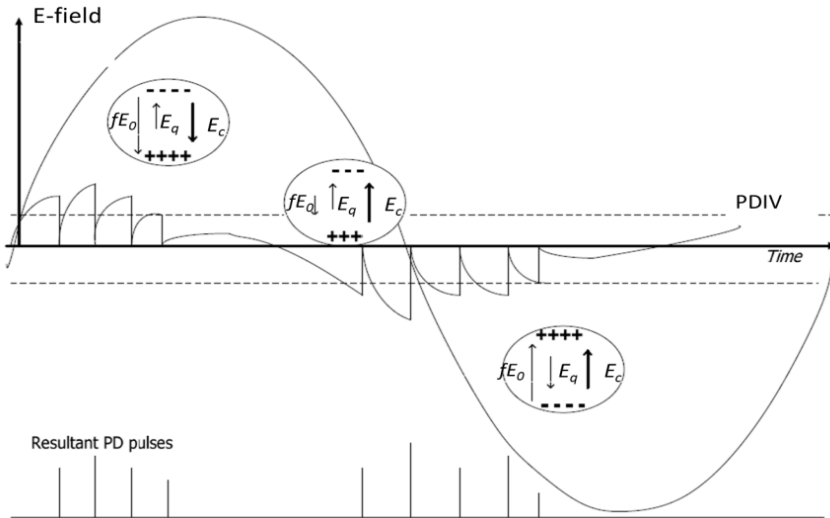


Figure 5.8: Partial discharge process in the gas filled cavity that depends on surface charge deposit in the cavity [58].

The moment when the test voltage exceeds PDIV (Partial Discharge Inception Voltage) a physical PD occurs after so called “statistical time lag”. This statistical lag occurs, when there is no starting electron, that could start the electron avalanche. However, when, e.g. deposited surface charge is present and the surface charge decay time (τ_{cd}) is longer than the duration of the single sine wave period T , the charge does not decay between two consecutive PD events. In this case, the deposited charge will strongly contribute to the field in the cavity and it will reflect in higher PD magnitudes than in case when decay time $\tau_{cd} \ll T$. For short surface charge decay times mainly the field contribution E_c remains, which leads the PD process with

lower PD magnitudes. It is shown in several publications [80, 81, 82] that this phenomenon is related to voltage frequencies below 200 Hz-300 Hz. At higher voltage frequencies, results described in [80, 82] show that PD amplitudes may decrease and PDIV increases with a higher frequency. This phenomenon is implicated through several aspects; one very important aspect is deposited surface charges in e.g. a cavity. The constant time for deposited surface charges can be expressed with the equation [5.1]

$$\tau_{cd} = \varepsilon_0 \cdot D_b/4 \cdot \sigma_s \quad [5.1]$$

Where ε_0 is the vacuum permittivity, D_b is the cavity diameter and σ_s is the cavity surface conductivity.

For example, in a bound cavity, two dielectric time constants influence the initial partial discharge activity: τ_{cavity} , related to charge re-distribution on the cavity surface (shape dependent), and $\tau_{material}$, which is related to charge re-distribution in the surrounding insulation material illustrated in Figure 5.8. Partial discharge activity becomes frequency dependent if the value of one or both of the time constants and/or the value of the statistical time lag is in the same range as the period of the applied voltage. Moreover, the partial discharge activity becomes frequency dependent if the physical changes inside the cavity responsible for PD activity occur fast enough (e.g. within one single period of test voltage) to create a successive PD event during positive and/or negative voltage sine wave at a particular voltage frequency. As a result, we can describe surface discharge decay time inside cavity (τ_{cd}) as a total sum of two dielectric time constants: $\tau_{material}$ and τ_{cavity} .

As a result, surface charge accumulation in a cavity can implicate a PD initiation process, which depends on the voltage frequency f or the duration of one single voltage period T [5.2]:

$$T = \frac{1}{f} \quad [5.2]$$

Three situations can be described [59-60]:

$T \ll \tau_{cd} \rightarrow$ Surface discharge deposited inside the cavity will contribute to electrical field inside the cavity E_c .

$T \gg \tau_{cd} \rightarrow$ Surface discharge deposited inside the cavity will not contribute to electrical field inside the cavity E_c .

$T \approx \tau_{cd} \rightarrow$ Surface discharge deposited inside may contribute to electrical field inside the cavity but it will depend on the amount of charge deposited the in cavity.

AC vs. DAC

Comparing the results of PD occurrence at AC and DAC voltages is complex due to several aspects:

- The damping character of DAC voltage. After voltage charging, during the resonance period, the voltage level decreases with time till 0.
- Relatively short duration of the DAC oscillations (in single excitation)-several hundred milliseconds.
- Repeated excitations.

By comparing, e.g. 50 Hz AC and 50 Hz DAC (e.g. 1 minute), the amount of surface charge inside the cavity should be lower in the cavity in a virgin state at DAC voltages as the ratio of dU/dt^9 is lower for DAC voltage. On the other hand, it must be noted that DAC excitation also consists of the unipolar charging period, when injection of electrons is done through a continually increasing voltage level. As a result of momentary voltage decaying (damped oscillations), the condition for the successive PD might be fulfilled even easier. Thus, in theory, inception conditions should appear faster, e.g. for a gas filled cavity when DAC voltage is applied. On the other hand, e.g. in one minute of 50 Hz AC voltage stress, more positive and negative voltage charging occur. In this chapter we will try to answer this question.

Minimum PDIV and Maximum PDIV

In the investigations and experiments presented in this thesis, in addition to the PD amplitude relation to test voltage and the PRPD patterns, the PDIV delay time is investigated. These two terms: minimum PDIV and maximum PDIV relate to 2 particular situations:

- Long delay of PDIV-situation where the test voltage is low enough not to ignite PD directly but high enough so that after a certain time, the first successive PD event will be recorded (without changing the voltage magnitude).
- Short delay of PDIV-situation where the test voltage is high enough to ignite PD event directly almost without any detectable delay.

In these two situations, different voltage levels will be obtained and theoretically different PD amplitudes. Thus, a long delay PDIV refers to minimum PDIV, and a short delay PDIV refers to maximum PDIV. Measurements of minimum and maximum values of PDIV are performed differently at AC and DAC voltages. At 50 Hz AC the voltage time is counted in seconds before the first PD event occurs. Maximum measuring time was set to 2 min. For DAC voltage, due to the damping effect of the voltage shape, the number of DAC excitations required to the first initial successive PD event is counted. The maximum number of DAC excitations is 30 per test voltage step. The maximum number of the excitations was set to 30 based on our experience and tests performed in the field. These tests showed that joint and termination related defects were detectable within 30-50 excitations at various test voltage levels (discussed in chapter 6).

5.2 Description of the test setup

To energize the complete setup, two voltage sources were used: AC 50 Hz and DAC at frequencies: 60 Hz and 264 Hz and 420 Hz. Based on two different energizing methods, there were two conventional PD detection systems used and both were in compliance with IEC 60270 standards:

- AC conventional PD detection by using TE 571 digital PD detector.
- DAC conventional PD detection by using oscillating wave test system (OWTS) HV150 series.

⁹ Ratio of applied test voltage U magnitude to the duration of the voltage applied

5.2.1 AC energizing method and IEC60270 PD detection

The equivalent circuit for this PD detection is shown in Figure 5.9. This PD detection setup consists of several important components: test transformer, voltage regulator, digital universal measuring instrument (voltage measurement), coupling capacitor, (PD pulses detection), AKV 572 Haefely Trench (coupling quadrupole). Post processing of PD data is performed in the standard TE 571 PD detector. PD pulses are plotted with respect to intensity and phase angle. The TE 571-DSW TEAS software was used to create a fingerprint based on the measured data. By comparing PD data distribution to a normal distribution, standard statistical parameters such as asymmetry, kurtosis and skewness can be calculated additionally. Moreover, parameters calculated for differences between the negative and positive half cycles of the test voltage and the number of peaks in the PD data distribution can be presented.

Test procedure

Withstand voltage testing within parallel PD measurements was applied in 2 minutes for each level of test voltages, in order to record PRPD patterns and average values of PD amplitude. In this way, different defect sizes were compared. Three quantities were analysed: the number of PD pulses, the maximum value of PD magnitudes and the average value of PD magnitudes [10]. These three quantities were plotted as a function of phase angle of sinusoidal AC voltage. After each voltage step, and test time of 2 min. the voltage was switched off and the cable grounded for 10 min.

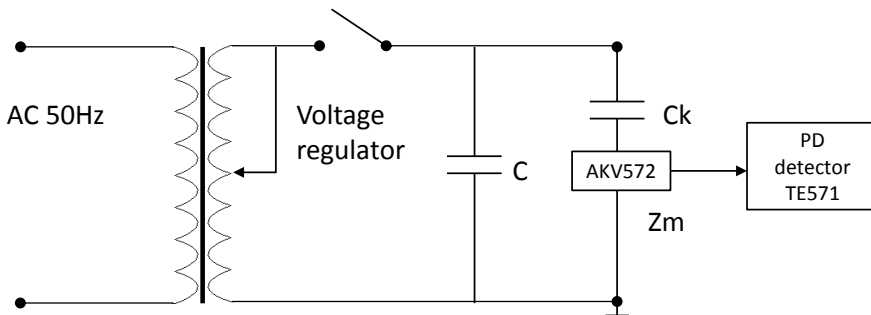


Figure 5.9: Conventional IEC 60270 PD detection circuit with 50 Hz energizing source. C-test object (100 m cable), Ck-coupling capacitor, Zm-coupling quadrupole.

5.2.2 DAC energizing and IEC60270 PD detection

For DAC voltage energizing method, the OWTS HV150 was used for energizing and PD detection (Figure 5.10). The OWTS HV150 series can provide PD diagnosis and dielectric loss measurements for the HV power cable system up to $106 \text{ kV}_{\text{rms}}$ ($150 \text{ kV}_{\text{peak}}$). General aspects of DAC system components and possible diagnostic parameters were discussed in Chapter 4. DAC systems are based on test voltage application in the form of DAC excitation sequences. To find the optimal number of DAC excitations at a particular test voltage level, experimental test procedures were developed with a different number of DAC excitations at the different

frequencies. The goal of the investigation was to check how the number of DAC excitations and voltage frequency may influence the PD detection and related PD parameters.

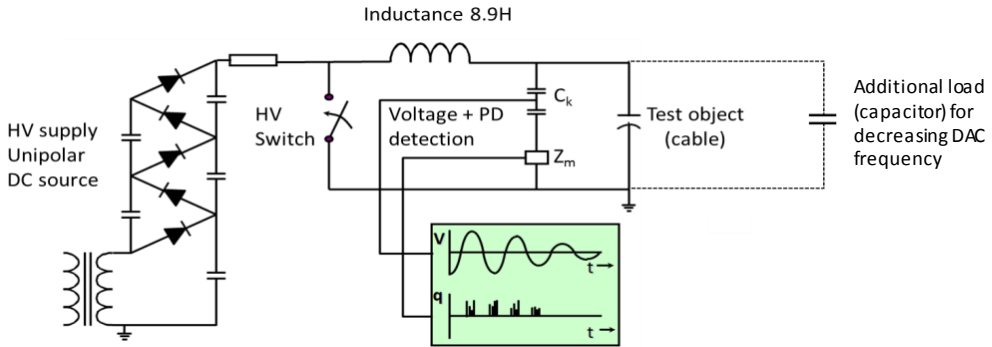


Figure 5.10: Conventional IEC 60270 PD detection circuit with 50Hz energizing source, C_k -coupling capacitor, Z_m -coupling quadrupole.

For DAC voltage investigation three DAC frequencies were investigated (Figure 5.11):

- 60 Hz DAC voltage obtained with additional capacitor of 1 μF . Total test capacitance-1.02 μF adequate to energize 4.3 km long XLPE cable (180 pF/m).
- 264 Hz DAC voltage obtained with additional capacitor of 0.02 μF . Total test capacitance-0.04 μF adequate to 0.23 km long XLPE cable (180 pF/m).
- 420 Hz DAC voltage obtained without any additional capacitor. Total test capacitance-0.02 μF adequate to 100 m long test cable (180 pF/m).

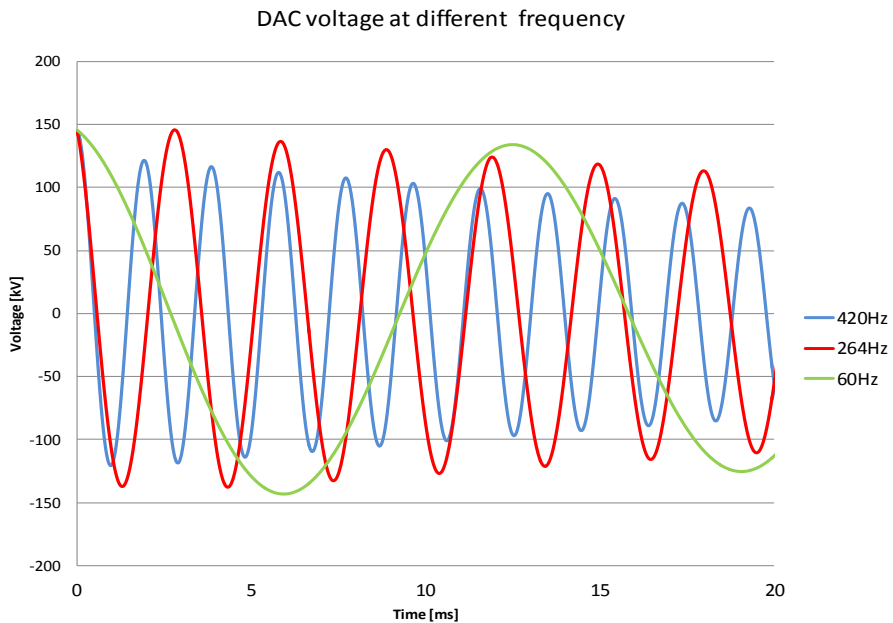


Figure 5.11: Three different DAC voltage frequencies applied for defect investigation.

For the additional test capacitance-the charging time will be longer according to the equation [5.3] below. For this reason, not only DAC frequency have an impact but also various charging times of the unipolar increasing DC stressing may have an impact on PD inception.

$$t_c = (U_{test} * C_{total}) / I_c \quad [5.3]$$

where: $C_{total} = C_{cable} + C_A$ and U_{test} is test voltage, I_c is the charging current-8mA, C_A is an additional load.

An aspect of DAC voltages is the decaying character of AC voltage. Due to the damping of AC voltage oscillations, the test object is stressed temporarily-for tens of milliseconds per single excitation. Thus, the number of oscillations compared to 2 minutes of continuous AC voltage at 50 Hz will be different and dependent on the particular DAC frequencies: 60 Hz, 264 Hz and 420 Hz (Table 5.4). It means that with a continuous AC 50 Hz test voltage, a higher number of AC oscillations will be recorded than with DAC voltage when the same testing time is considered, e.g. 2 min. It must also be noted that voltage charging duration depends on the capacitance (load) of the test object. The longer the cable, the longer the charging time.

Table 5.4
Test Voltage parameters.

Frequency	One voltage sine period duration	Testing time/ number of excitations	Total number of full periods within testing time	Duration of the oscillations
50Hz AC (continuous)	0.020(20ms)	2min	6000	120000ms
60Hz DAC	0.017(17ms)	10/20/30/50 x[DAC]*	97/194/291/485	165ms (1xDAC)*
264Hz DAC	0.004(4ms)		263/525/788/1313	105ms (1xDAC)*
420Hz DAC	0.002(2ms)		425/850/1275/2125	85ms (1xDAC)*

*-Charging time is not counted

Test procedure

The test voltage level is slowly increased with steps of $0.1xU_0$. The first step is the application of 10xDAC excitations. If there are no PDs observed, the voltage is switched off. After a 10 minute break (cable conductor grounded), the voltage is again increased in steps as presented in Table 5.5. Now, a higher number of 20 DAC excitation is applied. During 20xDAC excitations PD parameters are observed again. If there are no PD observed, the previous sequence is applied: system switched off, cable grounded for 10 min, test repeated with higher number of DAC excitations. If after 30xDAC excitations at a particular test voltage level, PDs are not recorded, the test voltage is increased according to test voltage steps (Table 5.5) and the procedure is repeated again.

Table 5.5
 PD amplitude measurement procedure and charging times for different test object capacitance.

[xU ₀]	Charging time t _{ch} [s] for load-C _{total}			N _{DAC} [N]
	0.02uF	0.04uF	1.02uF	
[x90kVpeak]	Defect 1/Defect 2/Defect 3			
0.2				10...30
0.3	0.1	0.2	2.1	10...30
0.5	0.1	0.2	3.5	10...30
0.6	0.1	0.2	4.2	10...30
0.8	0.2	0.3	5.6	10...30
1.0	0.2	0.4	7.0	10...30
1.2	0.2	0.4	8.4	10...30

5.3 Voltage withstand tests after cable installation in the lab

At the beginning, after installation of the cable termination and cable joint, complete setup was tested with continuous AC 50 Hz up to 1.2xU₀ and parallel PD measurements were applied. The duration of the acceptance test was 30 minutes at U₀ (90 kV_{rms}/127 kV_{peak}). At the maximum test voltage of 1.2xU₀ (106,3 kV_{rms} /150 kV_{peak}) the duration of the test was limited to 30 minutes (due to thermal limits of feeding transformer and the risk of transformer damage). After the AC 50 Hz test, DAC testing was performed with a similar procedure, however instead of the time count, DAC excitations were counted (Figure 5.12).

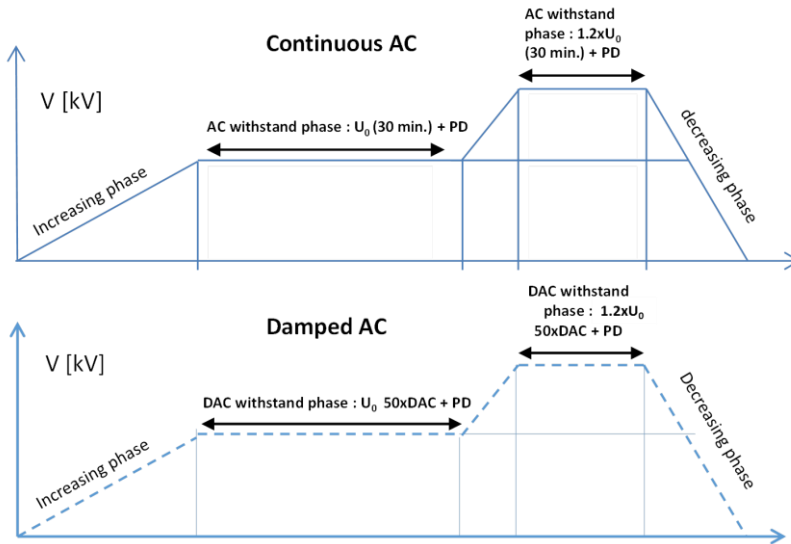


Figure 5.12: Acceptance test procedure with continuous 50Hz AC/DAC voltage.

The increasing phase was obtained by increasing the voltage with 10 kV steps of 30 sec. voltage duration per step and 3xDAC excitations. Note: the solid line relates to AC test and dashed line to DAC excitations. During the acceptance tests, both with AC 50 Hz and DAC 60 Hz/264 Hz/420 Hz, no breakdown was recorded and no PD observed. Number of DAC excitations (50) was chosen based on the recommendations of the latest IEEE 400.4 [14].

5.4 Missing outer semi-conductive screen (Defect type 1): 50 Hz AC vs. DAC

5.4.1 PDIV delay time at 50 Hz AC

After the artificial defect 1 had been created, the cable was joined again with the help of a hydraulic system that was used to position and insert a cable inside the joint body. The complete cable was connected again to the feeding transformer and energized accordingly to the test procedure presented in Section 5.2.1. The voltage was increased and PD activity was monitored. In Figure 5.13 PD behaviour is presented as a function of increasing test voltage for different configurations of defect 1. PDs were measured from 0 kV till the moment of stable repetitive PD occurrence. The measurement was done by slowly increasing the voltage from 0 kV to get the PD inception voltage (PDIV) and then PD measurement was performed at several levels of voltage with 2 minutes duration for each voltage. At $1.2xU_0$ the PD level was increased to 9000 pC for defect type 1 for a length of 15 mm. At a test voltage of $1.2xU_0$, besides high PD level observed electrically, PD activity was also observed through the acoustic signals detectable by human without additional acoustic detectors. For each defect size, a total of 9 measurements were performed to obtain reproducible PDIV delay time results. After each single measurement of PDIV delay time, the voltage was switched off and system grounded for 10 minutes.

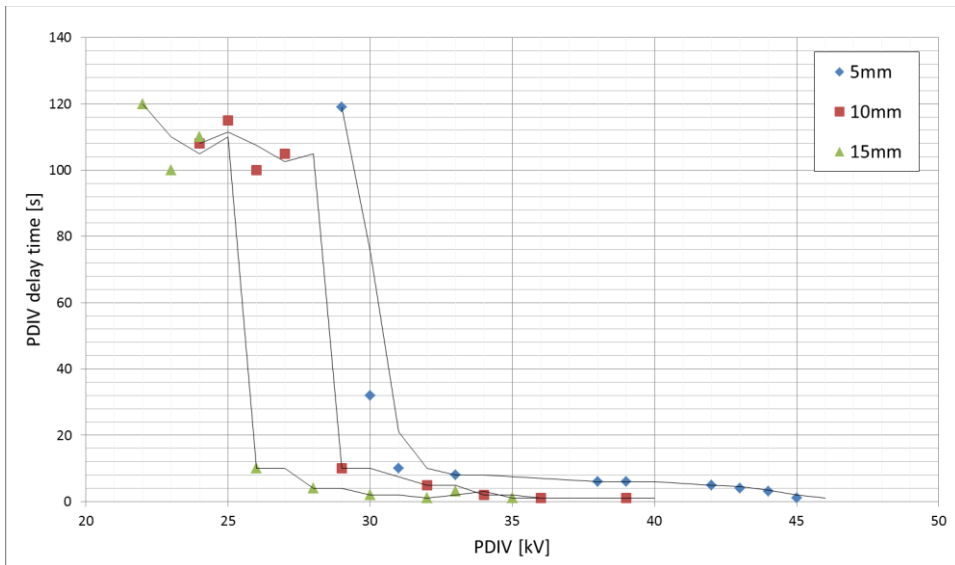


Figure 5.13: 50 Hz AC energizing. PDIV delay time (time necessary to record first PD) at different voltage levels

From the plot presented in Figure 5.13, it can be concluded that for the smaller size of defect 1 (5 mm of missing semi-conductive screen) PDIV was higher than for 10mm and 15 mm sizes. Minimum PDIV obtained after (long delay) time:

- 5 mm defect after approx. 120 seconds of testing with 29 kV_{peak}.
- 10 mm defect after approx. 115 seconds of testing with 24 kV_{peak}.
- 15 mm defect size after approx. 101 seconds of testing with 23 kV_{peak}.

5.4.2 PD magnitude at 50 Hz AC

To check PD behaviour at different voltage levels, for each case sample with defect size 5 mm/10 mm/15 mm, AC voltage was increased accordingly to the scheme presented in table 5.5. Results are presented in Figure 5.14.

For PD magnitude at PDIV, the following values were measured (for the minimum PDIVs):

- Defect 1 size 5mm-25 pC at 29 kV_{peak}.
- Defect 1 size 10mm-50 pC at 24 kV_{peak}.
- Defect 1 size 15mm-31 pC at 23 kV_{peak}.

Figure 5.14 shows that the increase of PD amplitude as a function of voltage is steeper for the larger size of defect type 1. Electric field simulation done with Ansoft software shows an increasing electric field intensity with increasing defect size (Table 5.1). For the largest size (15 mm) of defect type 1, the electric field is the highest and also the highest PD amplitude is recorded. At the U_0 for the joint without defect and size 5 mm, 10 mm simulated electric field is approximately 5 kV/mm. For the same conditions (U_0) defect size 15 reaches 7 kV/mm and almost double the PD amplitude compared to size 5 and 10 mm (Figure 5.14).

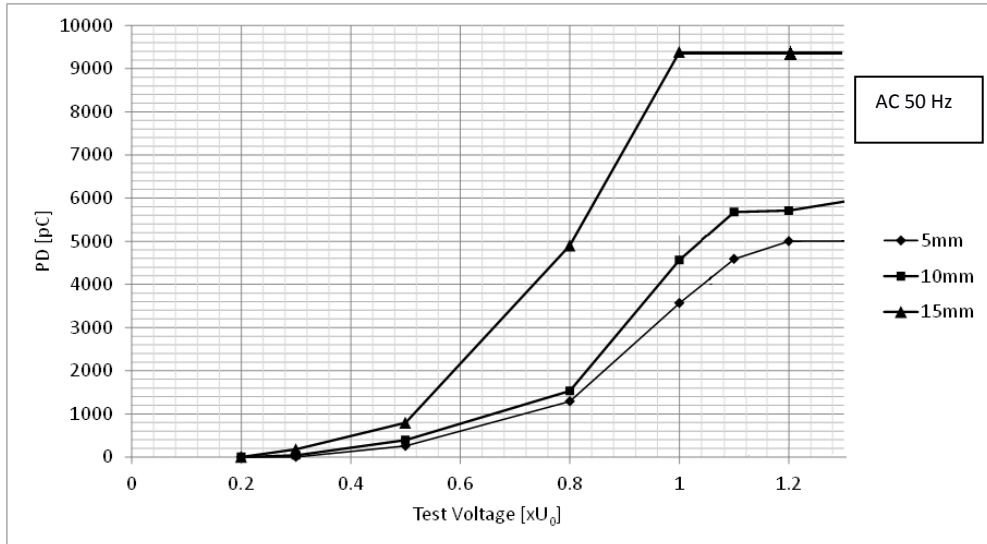


Figure 5.14: PD vs. test voltage for defect 1 at 50 Hz AC voltage. Note: values presented in the plot are the average PD magnitude obtained during 2 min. measurements.

5.4.3 PRPD patterns at 50 Hz AC

Phase resolved PD patterns were monitored through the complete process of testing. PRPD patterns for different sizes of the defect were obtained by measuring for 2 minutes. Figure 5.15 shows PRPD patterns that were observed at maximum PDIV and U_0 for three sizes of defect type 1. PRPD patterns for three sizes of defect type 1 show that at PDIV the asymmetric PRPD patterns occur at negative half period of the 50 Hz AC voltage cycle. It can be seen from Figure 5.15 that at a higher voltage the PD phase-resolved patterns for defect type 1 become symmetrical, occurring at both positive and the negative half of 50 Hz AC voltage cycle.

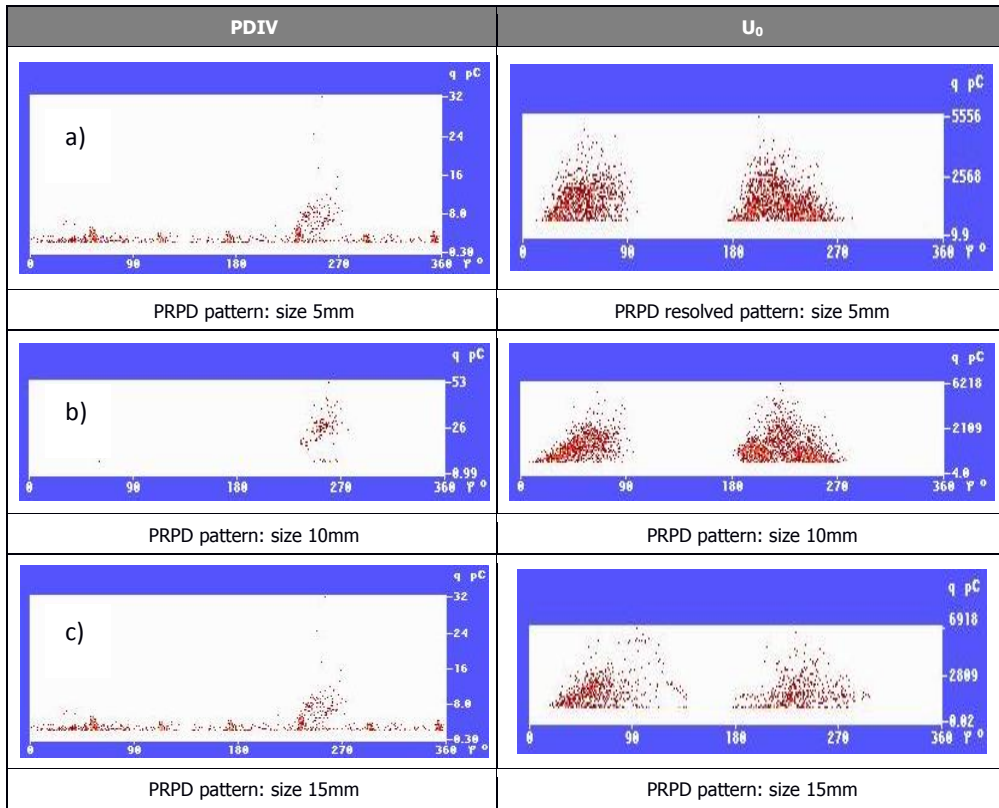


Figure 5.15: PRPD patterns at PDIV short delay PDIV/Max. PDIV left side and PRPD patterns at U_0 right side for different sizes: a) 5 mm, b) 10 mm, c) 15 mm.

5.4.4 PDIV delay time at DAC

At damped AC voltage PDIV delay time was calculated differently than in the case of 50 Hz AC voltage. Here, the number of the DAC excitations was counted before a PD event occurred. The duration of each DAC excitation was related to the capacitance of the test object and voltage level. So, the number of voltage periods could not be directly compared with continuous AC. In Figure 5.16 PD delay time as a function of the number of DAC excitations is presented.

With DAC voltage PDIV was the highest for defect 1 size 5 mm however, there was not much difference between 5 mm and 10 mm defect sizes. The same behaviour was observed with 50 Hz AC voltage. Minimum PDIV (long delay time at 60 Hz DAC):

- For a defect length of 5mm the long PDIV delay time relates to 26xDAC excitations. The PDIV level was 26 kV_{peak}.
- For a defect length of 10mm the long PDIV delay time relates to 30xDAC excitations. The PDIV was 24 kV_{peak}.
- For a defect length of 15mm the long PDIV delay time relates to 30xDAC excitations and PDIV was 20 kV_{peak}.

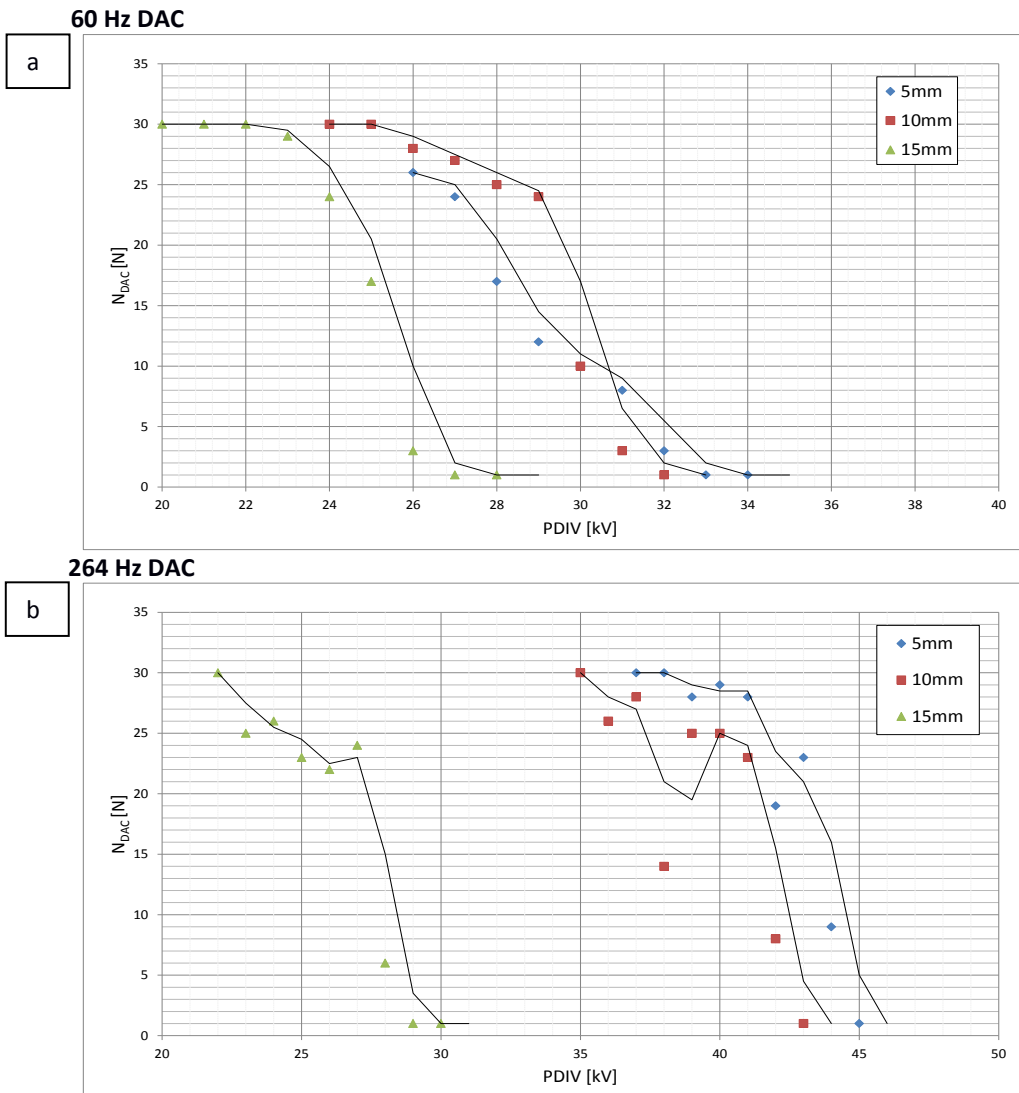


Figure 5.16: PDIV delay time (number of DAC excitations till PD occurrence) at different voltage levels for a) 60 Hz b) 264 Hz c) 420 Hz.

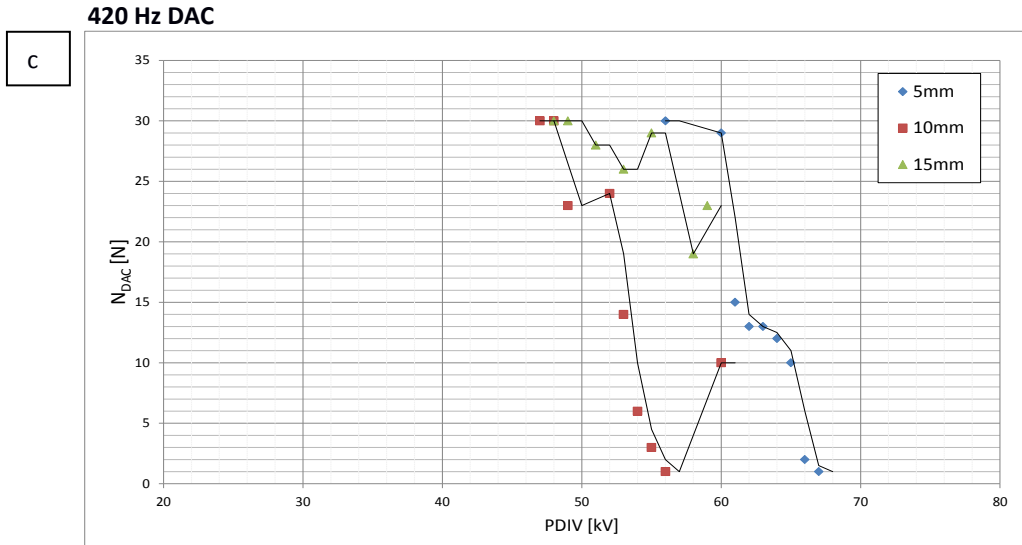


Figure 5.16 (continued): PDIV delay time (number of DAC excitations till PD occurrence) at different voltage levels for a) 60 Hz b) 264 Hz c) 420 Hz.

It can be concluded that for defect type 1, at different sizes the number of DAC excitations has an impact on PDIV delay time and PDIV level. By comparing DAC frequencies and PDIV level it can be concluded that at the lower frequency of 60 Hz the PDIV characteristics (inception level) are similar to 50 Hz AC. For the defect size 5 mm, the lowest PDIV level at 50 Hz was 28 kV (after 2 minutes of voltage application) and the lowest PDIV at DAC 60 Hz was 26 kV (after 26 DAC excitations). A general conclusion derived from the investigation performed on defect type 1 is that at a higher DAC frequency, PDIV is also increasing. Moreover, at higher DAC frequencies to get a clear PD indication, a larger number of DAC excitations is necessary. When we take a look at 60 Hz DAC test voltage, an almost linear decrease of PDIV as a function of DAC excitation number is observed (Figure 5.16 a). At the higher frequency of 264 Hz it can be concluded that the difference between 5 mm and 10 mm defect is still not significant when comparing PDIV levels and the lowest PDIV (longest PDIV delay) is obtained at 37 kV (5 mm) and 35 kV (10 mm). Interestingly, for the larger defect size (15 mm), PDIV level characteristics at 264 Hz stay similar to the tests performed at DAC frequency of 60 Hz.

The biggest changes and influences on PDIV are observed at 420 Hz DAC test voltage. Here, the response (defect sensitivity) to higher frequencies is related to much higher PDIV levels for all the defect sizes. Similar to previous voltage frequencies, the highest PDIV was recorded for the 5 mm defect. Moreover, it can be observed that for defect sizes 10 mm and 15 mm, the difference at minimum test voltage level (longest PDIV delay) is smaller than at 60 Hz and 264 Hz. It is also interesting that for defect sizes 10 mm and 15 mm there is no linear decrease of PDIV with higher number of DAC excitations. As a result, even with relatively high voltage (when compared to 60 Hz/264 Hz), still more excitations are necessary to ignite a stable PDs activity. It is shown that the larger the defect size, the less responsive (less detectable) at higher test voltage frequency it is. For defect size of 15 mm, the shortest delay time was obtained after 19 DAC excitations at 58 kV, and at 59 kV, PDs were detected after 23

DAC excitations. Similar behaviour was observed for defect size of 10 mm where the shortest delay time was obtained after 2 DAC excitations at 56 kV. At the test voltage level of 60 kV, 10 DAC excitations were necessary to ignite PDs.

5.4.5 PD magnitude at DAC

To check PD behaviour at different voltage levels, for each DAC voltage frequency the comparison per type of defect size was done. In this way, the impact of DAC frequency on the PD behaviour can be easily compared. The results of PD level at PDIV are presented in Table 5.6. It has to be mentioned here that adding an extra capacitors to cable can result in lower measured PD amplitude. This lower PD amplitude can be a result of the fact that a part of the PD energy “disappears” in the additional capacitor.

Table 5.6
PD level at lowest PDIV (long delay time) for different DAC frequency and defect sizes.

DAC freq.\size	PD levels for defect 1 for min. PDIV at different DAC test voltage frequencies		
	5mm	10mm	15mm
60Hz	20pC@26kV	28pC@24kV	17pC@20kV
264Hz	21pC@37kV	34pC@35kV	20pC@22kV
420Hz	30pC@56kV	53pC@47kV	15pC@48kV

From Table 5.6 it can be clearly concluded that at a DAC frequency of 420 Hz, even though PDIV level is more than 2x higher than PDIV at 60 Hz, the PD level is lower for the defect length of 15 mm. Thus, it can be assumed that defect type 1, in size of 15 mm is less sensitive to test voltage frequency change than the smaller defects. For 5 mm and 10 mm at 420 Hz the increase of PDIV level is visible and the PD level as well. PD vs. test voltage plots are presented in Figures 5.17 a, b, c. Note: In the plots presented in Figure 5.17 a, b, c the average PD amplitude is presented as recorded per voltage step (accordingly to test procedure presented in Table 5.5).

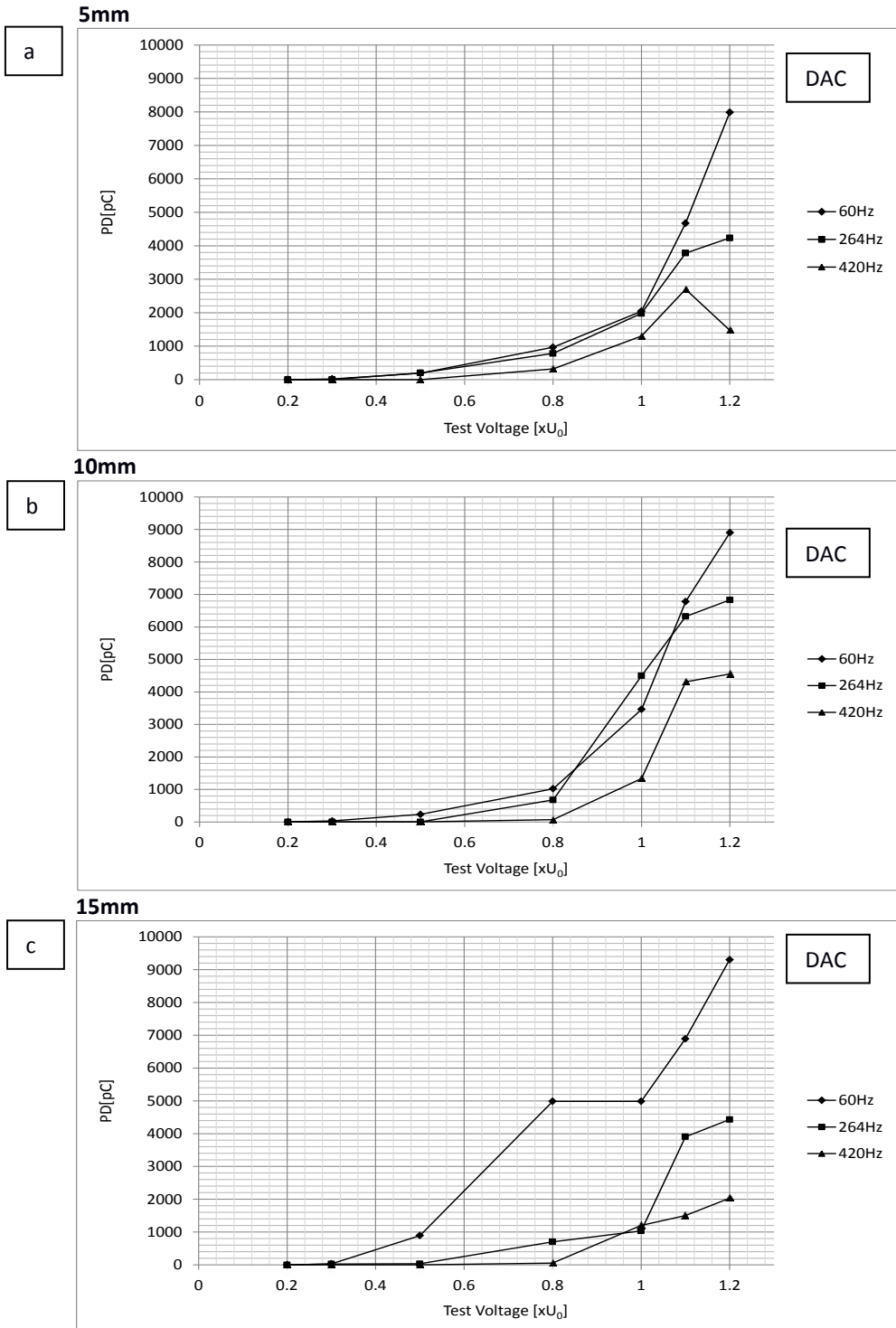


Figure 5.17: PD vs. test voltage for defect 1 at DAC voltage. a) 60 Hz, b) 264 Hz, c) 420 Hz.

5.4.6 PRPD patterns at DAC

With the DAC system the phase resolved patterns are obtained in a different way than with 50 Hz conventional PD detection. Here, after each DAC excitation, a single PRPD pattern for the 1st oscillation is displayed on the screen. At the time of performing the tests, DAC systems displayed the phase resolved patterns as a picture of one excitation). In the 50 Hz AC system each 50 Hz cycle (period) was saved and a picture of several hundred of cycles were displayed in the form of the phase resolved pattern. Nowadays, DAC systems are also equipped with the function of creating the PRPD patterns based on the number of excitations. In Figure 5.18 and 5.19 the results of PD detection with DAC method are presented for defect type 1 of size 5 mm at PDIV and U_0 .

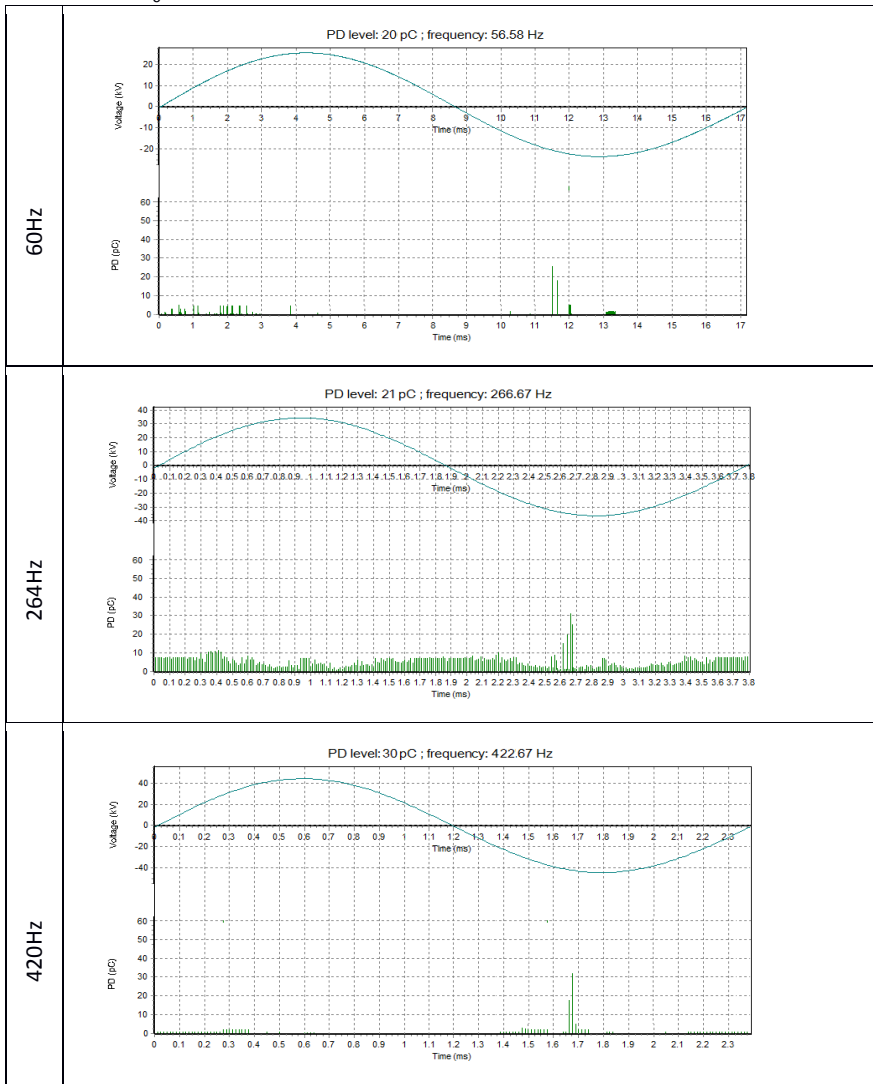


Figure 5.18: PRPD patterns for defect type 1, size 5 mm at PDIV. Note: These are random examples (single excitation) from the measuring process of 30xDAC excitations.

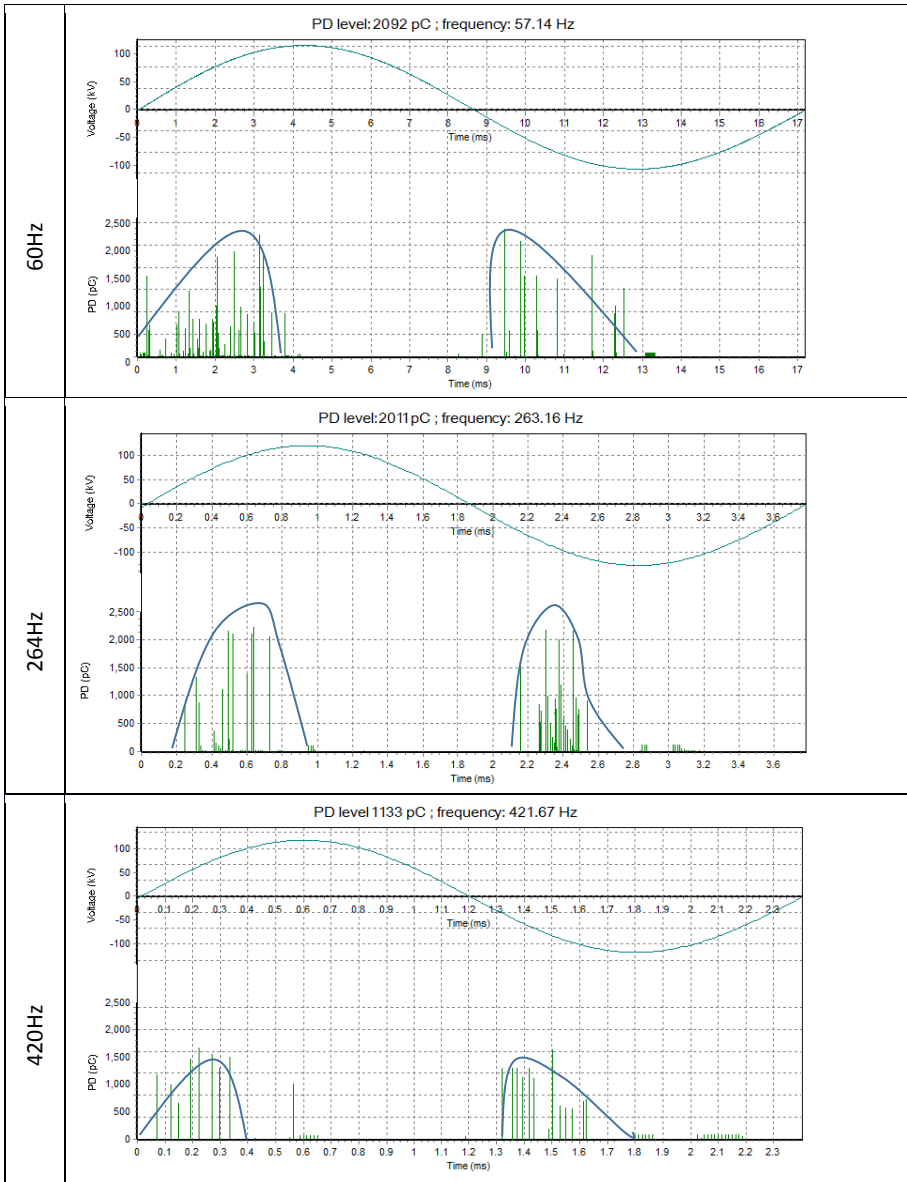


Figure 5.19: PRPD patterns for defect type 1, size 5 mm at U_0 . Note: These are random examples (single excitation) from the measuring process of 30xDAC excitations.

It can be concluded that PRPD patterns show a similarity in the shape and PD occurrence at 3 different frequencies. At PDIV, the PD pattern is recorded only for the negative part of voltage sine (asymmetric) whereas at higher voltages, e.g. U_0 , patterns become symmetric. There is almost no difference at PDIV level for PD level at 60 Hz and 264 Hz and the same situation is for PRPD pattern. Interestingly, at higher frequencies, e.g. 264 Hz and 420 Hz, the intensity of PD pulses is lower than at 60 Hz.

For all sizes of defect type 1, PD magnitude is higher with the larger size of defect type 1. The results obtained at a maximum test voltage level of $1.2 \times U_0$ confirm our assumption about lower intensity (occurrence) of PD pulses at higher frequencies when compared to 60 Hz DAC. In this case, it can be concluded that at 420 Hz DAC, the changes of the local surface discharge process on the exposed semi-conductive screen do not follow positive and negative voltage oscillations and electric field polarity changes at higher frequencies. For each test voltage frequency, the same characteristic pattern was obtained, e.g. at U_0 at positive voltage sine the PD pattern was created through a repetitive pyramid-shape slightly shifted to the right (90°) as presented in Figure 5.19. For the negative half of voltage sine almost symmetric (mirrored) pyramid-the shape pattern was recorded between 180° and 270° . For defect type 1 size 15 mm, the pyramid-shape pattern was less visible and less stable especially for the 420 Hz voltage frequency.

5.5 Extra semi-conductive screen in the joint (Defect type 2): 50 Hz AC vs. DAC

5.5.1 PDIV delay time at 50 Hz AC

Defect type 2 was created as described in Section 5.1. An additional semi-conductive layer was added on the surface of the XLPE insulation. The extended layer according to Ansoft electric field calculation creates a slightly lower enhancement than in the case of defect type 1, thus lower PD activity or PD amplitude similar to defect 1 was expected. Likewise to the previous defect type 1, after the artificial defect type 2 was created (extended layer of 40 mm above the proper measures) the cable was jointed gently again with the help of a hydraulic system attached to joint housing and cable. The longest semi-conductive extension was selected to be first tested due to several issues.

Prismian Cables and Systems experts assumed that even according to the electric field calculation and relatively high field enhancement produced by defect type 2, the chance of PD occurrence can be low. This assumption is based on the fact that for defect type 2 there is a higher local breakdown strength of the combination of dielectric materials. In the case of defect type 2, the presence of air in the interfaces between the cable insulation and the joint insulation is restricted by the elastic properties of the synthetic rubber of the joint insulation and mainly due to the vacuum pump as used when inserting the cable end into the joint body (in order to eliminate air accumulation). As a result, this extended semi-conductive screen is covered tightly by the stress control cones and cable insulation. Taking into consideration these facts, the test was started with theoretically the most critical defect type 2-size 40 mm. The complete cable was connected to the feeding transformer and energized accordingly to the test procedure presented in Section 5.2.1. The test voltage was slowly increased and PD activity was monitored. In Figure 5.20 PDIV delay time characteristics are presented as a function of the increasing test voltage for the different configuration of defect type 2. PDIV delay time was measured from the moment of setting the required test voltage till the moment of the first PD occurrence-maximum 2 min per voltage step.

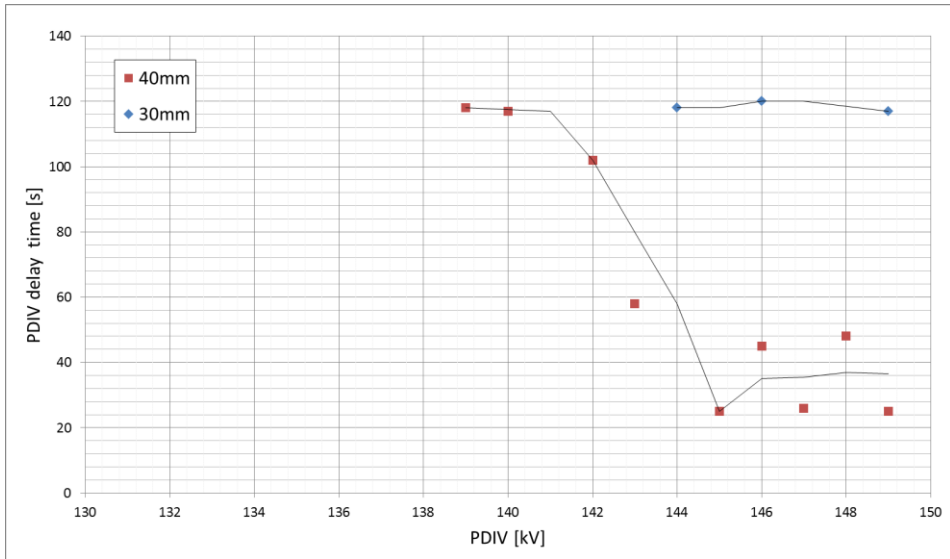


Figure 5.20: PDIV long delay time at different voltage levels. Only two sizes of defect type 2: 30 mm and 40 mm were detectable within 2 minutes of testing time.

Measurements performed at defect type 2 in different sizes confirmed the previous assumptions. Defect type 2 is less critical than defect type 1. We assumed that defect type 2 is more homogeneous and conditions for successive PD occurrence are only at very high test voltage level. The PDIV delay time is also long compared to defect type 1. The lowest PDIV was obtained after 119 seconds at 139 kV_{peak} (40 mm size). It is interesting that the minimum time necessary for successful PD event was in the range of 25 seconds at 145 kV_{peak} and with higher voltage, PDIV delay time varied between 25-40 seconds. For the smaller defect sizes (shorter extension of the semi-conductive screen) the situation was even less critical than in the case of 40 mm. The minimum time necessary to ignite PD was 117 seconds at maximum test voltage level of 1.2xU₀ (150 kV_{peak}). It can be assumed that probably a longer testing time or even higher test voltage level is required to get a shorter delay time for this defect type. For defect type 2 for sizes of 20 mm and 10 mm, no PD was observed up to 1.2xU₀ and 2 min. testing duration per voltage step (even though the test time was extended to 5 min at 1.2xU₀). As a result, for further investigation the defect sizes of 30 mm and 40 mm were only considered.

Minimum PDIV obtained after time:

- 30 mm defect after approx. 119 seconds of testing with 139 kV_{peak}.
- 10 mm defect after approx. 117 seconds of testing with 150 kV_{peak}.

5.5.2 PD magnitude at 50 Hz AC

To check PD behaviour at different voltage levels, for each of the defect's size (30 mm and 40 mm), AC voltage was increased accordingly to the scheme presented in Table 5.5. The results are presented in Figure 5.21.

For PD magnitude at PDIV the following values were measured (for the minimum PDIVs):

1. Defect type 2, size 30 mm- 21 pC at 139 kV_{peak}.
2. Defect type 2, size 40 mm-43 pC at 144 kV_{peak}.

Based on the measurement results, it was shown that the PD amplitude as a function of voltage is twice as much for the size of 40 mm than for the size of 30 mm. Probably, higher PDs might appear at higher test voltage levels, e.g. 1.7xU₀ or higher, however due to the technical limitation it was not possible to check it.

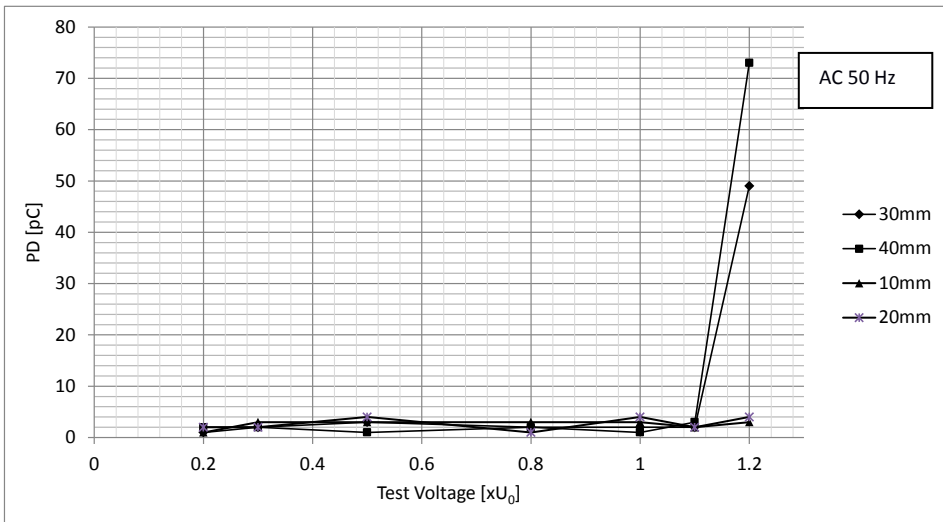


Figure 5.21: PD vs. test voltage for defect type 2 at 50 Hz AC voltage. Note: values presented in the plot are the average PD magnitude obtained during 2 min. measurements.

5.5.3 PRPD patterns at 50 Hz AC

PRPD patterns were monitored through the entire process of testing. The PD phase-resolved patterns for two sizes of defect type 2 were obtained by recording at selected voltage levels for 2 minutes of voltage application. Figure 5.22 shows PRPD patterns observed at PDIV and maximum test voltage level for 2 sizes. It was observed at PDIV for both defect sizes, that the PRPD pattern was asymmetric. The first PD occurs at positive voltage sine wave and later at the highest voltage of 1.2xU₀, the pattern became more symmetric with a characteristic mirrored L-shape form. Based on the results obtained from the measurements on defect type 1 and defect type 2, it can be concluded that PRPD patterns are completely different.

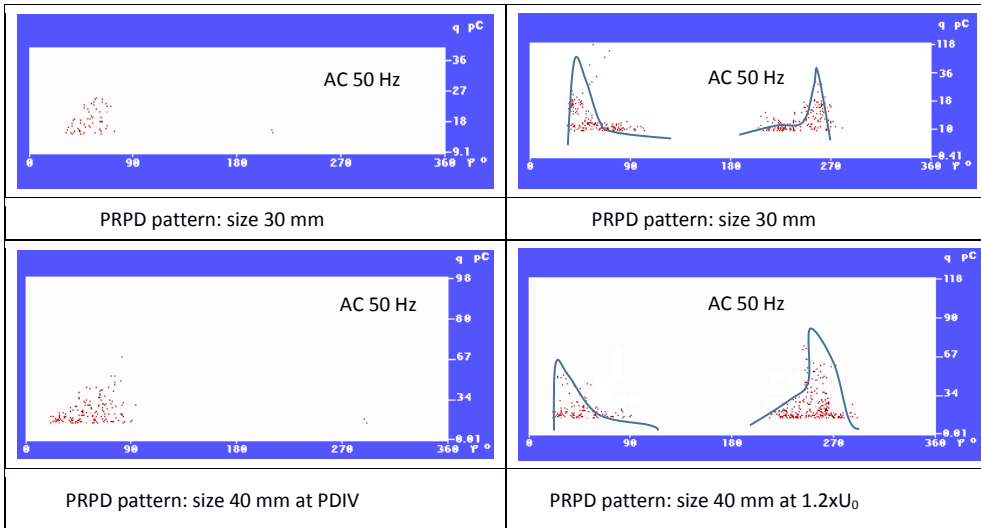


Figure 5.22: PRPD patterns at minimum PDIV on the left side and $1.2xU_0$ for defect 2 at two different sizes on the right side.

5.5.4 PDIV delay time at DAC

Figure 5.23 presents PD delay time in the function of number of DAC excitations. The test procedure was the same as in the case of measurements of defect type 1. The maximum number of DAC excitations was $30xDAC$ per voltage step.

Measurements with DAC voltage confirmed the results of 50 Hz measurements and the PDIV was also lower for defect type 2 in the size of 40 mm than for defect type 2 in the size of 30 mm.

Minimum PDIV (long delay time at 60 Hz DAC) for defect type 2:

- Size 10 mm-no PDIV recorded (even with $50xDAC$ excitations) for $150 kV_{peak}$.
- Size 20 mm-no PDIV recorded (even with $50xDAC$ excitations) for $150 kV_{peak}$.
- Size defect type 2, size 30mm-long delay time related to $28xDAC$ excitations and PDIV at $146 kV_{peak}$.
- Size 40mm-long delay time related $15xDAC$ excitations and PDIV of $141 kV_{peak}$.

Maximum PDIV (short delay time at 60 Hz DAC) for defect type 2:

- Size 10 mm-no PDIV recorded (even with $50xDAC$ excitations).
- Size 20 mm-no PDIV recorded (even with $50xDAC$ excitations).
- Size 30 mm-short delay time related to $27xDAC$ excitations and PDIV of $149 kV_{peak}$.
- Size 40 mm-short delay time related $11xDAC$ excitations and PDIV of $149 kV_{peak}$.

DAC frequencies and PDIV delay time characteristics are presented in Figure 5.

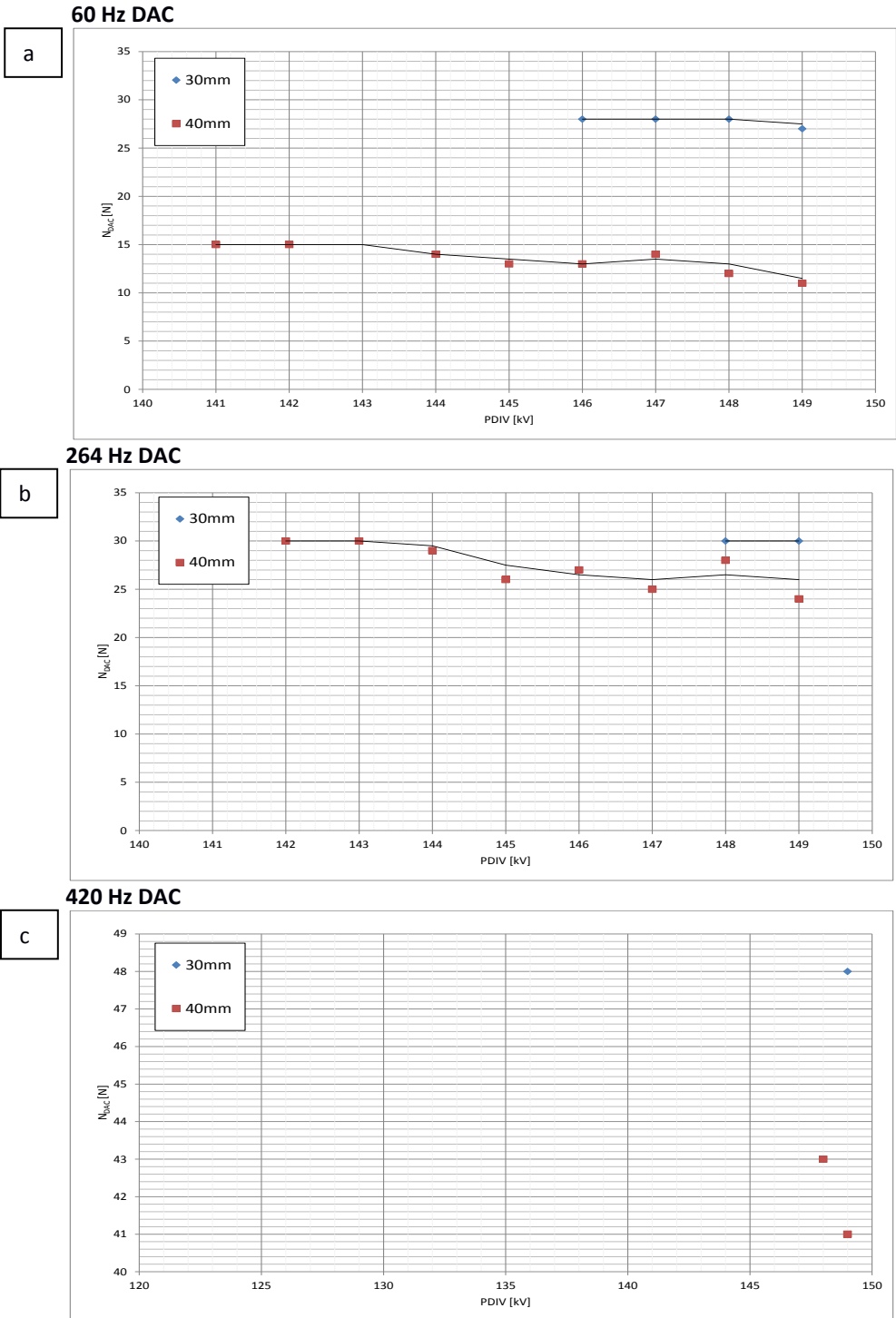


Figure 5.23: PDIV delay time (number of DAC excitations till PD occurrence) at different voltage levels a) 60 Hz, b) 264 Hz, c) 420 Hz.

Based on the PDIV measurements with various DAC frequencies, it can be concluded that for higher test voltage, a larger number of DAC excitations is necessary to obtain first PD activity for defect type 2. It was also observed that for defect type 2 of length of 40 mm with an increasing test voltage, the number of DAC excitations necessary to ignite PD decreases. At 60 Hz the first successive PD occurred after 15xDAC excitations. On the other hand, defect type 2 of size 30 mm had higher PDIV and was visible after 27xDAC excitations.

When the minimum PDIV levels (longest PDIV delay times) are compared between 50 Hz AC and 60 Hz DAC, it is visible that the results are comparable:

- At 50 Hz AC PDIV for defect type 2, size 30 mm was 139 kV_{peak} and for 60 Hz DAC it was 146 kV_{peak}.
- At 50Hz AC PDIV for defect type 2, size 40 mm was 144 kV_{peak} and for 60 Hz DAC it was 141 kV_{peak}.

At higher DAC test voltages, it was observed that a higher number (exceeding 30xDAC) of excitations was necessary to ignite PD but also a much higher test voltage was required. For defect type 2-40 mm at 264 Hz DAC, a minimum PDIV was obtained at 142 kV_{peak} (comparable to 50 Hz AC/60 Hz DAC) but after a double number of excitations in comparison to 60 Hz DAC. At 420 Hz DAC for the same defect the minimum PDIV was obtained after 43xDAC excitations at 147 kV_{peak}. This behaviour confirms that at 264 Hz and 420 Hz DAC, defect type 2, size 40 mm is sensitive to the test voltage frequency change. Interestingly, a relatively small size difference between 40 mm and 30 mm in the case of defect type 2, reflects big differences at PDIV delay time. In particular at 420 Hz DAC frequency at only 147-149 kV_{peak} test voltage level, it was possible to ignite PD activity, however the difference between the minimum PDIV and maximum PDIV was not recordable. It was concluded that possibly at a higher test voltage level the difference between min. and max. PDIV could be more visible, however this was outside the range of our equipment.

5.5.5 PD magnitude at DAC

To check PD behaviour at different voltage levels, for each DAC voltage frequency the comparison for one of the defect’s sizes was done. In this way, the impact of DAC frequency on the PD behaviour could be compared easily. The results of PD level at PDIV are presented in Table 5.7. It has to be mentioned here that adding an extra capacitors to cable can result in lower measured PD amplitude. This lower PD amplitude can be a result of the fact that a part of the PD energy “disappears” in the additional capacitor.

Table 5.7
PD level at minimum PDIV (long delay time) for different DAC frequency and defect sizes.

DAC freq.\size	10mm	20mm	30mm	40mm
60Hz	No PDIV	No PDIV	15pC@146kV	31pC@141kV
264Hz	No PDIV	No PDIV	14pC@148kV	26pC@142kV
420Hz	No PDIV	No PDIV	6pC@149kV	23pC@148kV

It must be noted that PD occurrence at 420 Hz DAC for the defect of 30 mm was almost not visible with low repetitive frequency of PDs during 30xDAC excitations. The average PD

amplitude was in the range of 6 pC with a background noise of 2-3 pC. Therefore, it was concluded that defect type 2 of 30mm size and probably smaller sizes of 10-20 mm at 420 Hz DAC require a much higher voltage level to produce stable PD. However, this assumption could not be confirmed due to technical limitations of the test equipment. PD vs. test voltage plots are presented in Figure 5.24.

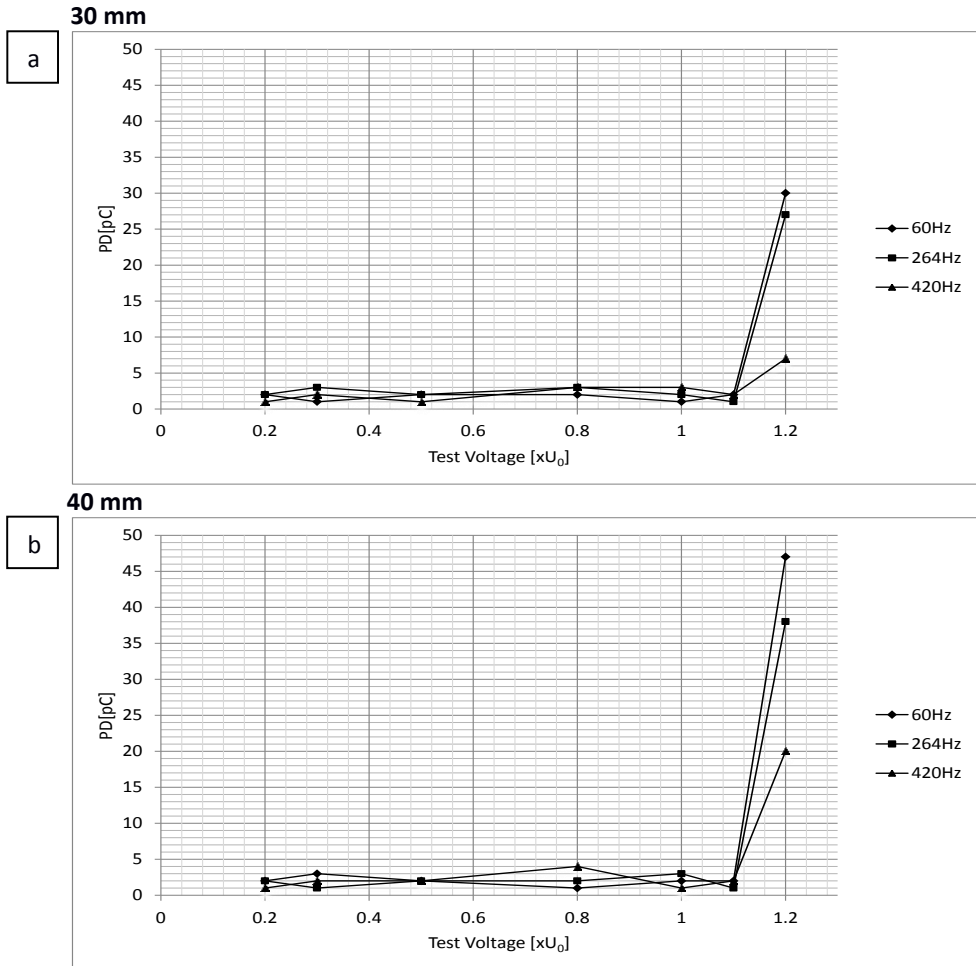


Figure 5.24: PD vs. test voltage for defect type 2 at DAC voltage a) defect size 30 mm. b) defect size 40 mm. Note: values presented in the plot are the average PD magnitude obtained for PD test procedure presented in Table 5.5.

5.5.6 PRPD patterns at DAC

In Table 5.7 the results of PD detection with DAC method are presented for defect type 2 for the size of 30 mm and 40 mm. Due to the fact that the PDIV was recorded at the maximum test voltage level of $1.2xU_0$ the comparison between PRPD pattern and PDIV and a few kilovolts higher maximum test voltage level does not bring any differences at PD

characteristic and phase-resolved PD patterns. At PDIV level PD occurrence is very low and one or two single PD pulses are visible randomly for every 3-5 DAC excitations. For this reason, PRPD patterns were recorded at $1.2xU_0$ and compared for defect sizes of 30 mm and 40 mm at different DAC voltage frequencies (Figure 5.25a and 5.25b).

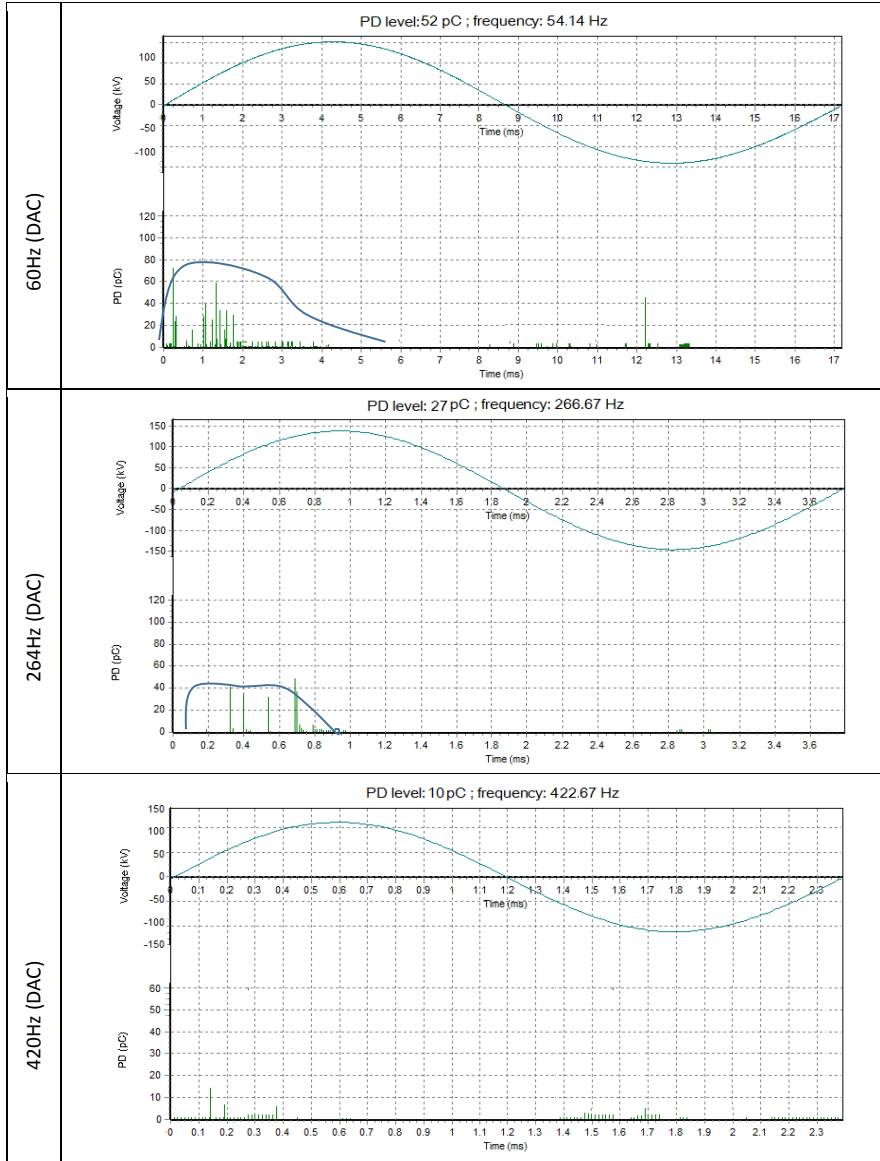


Figure 5.25a: PRPD patterns for defect type 2 (30m) at maximum test voltage level of $1.2xU_0$
 Note: These are random examples (single excitation) from the measuring process of $30x$ DAC excitations.

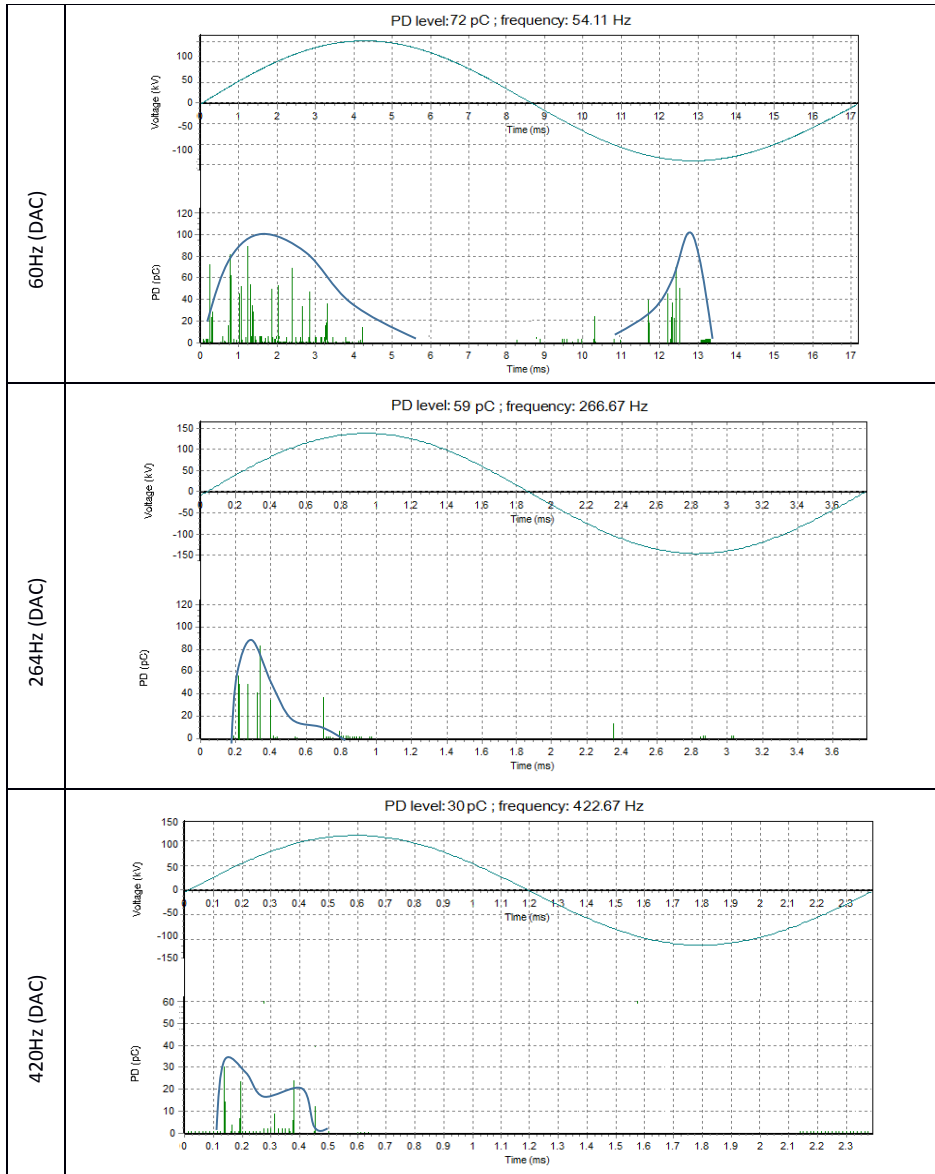


Figure 5.25b: PRPD patterns for defect type 2 (40m) at maximum test voltage level of $1.2xU_0$
 Note: These are random examples (single excitation) from the measuring process of $30x$ DAC excitations.

PD measurements performed on defect type 2 for size 30 mm and 40 mm showed again that at higher DAC voltage frequencies, PD amplitude and PD intensity become smaller. Regarding the PRPD pattern, it can be concluded that at the lower 60 Hz DAC voltage, it is similar to 50 Hz AC voltage. We note that with DAC voltage, only one DAC excitation can be compared to 2 min. of 50Hz measurements. At higher DAC voltage frequencies, the phase resolved pattern becomes asymmetric. This behaviour could be related to the fact that at higher frequencies defect type 2 is strongly dependent on dU/dt . PRPD patters confirm that the PDIV delay time

at a higher frequency of DAC voltage requires more DAC excitations to get the first repetitive PD signal. Based on these results, it can be concluded that defect type 2 of sizes 30 mm and 40 mm are sensitive to test voltage frequency. At higher frequencies the PD signal has a lower amplitude and less PD appear, e.g. at single DAC excitation. For both test voltages: AC 50 Hz and DAC it was however possible to detect PD related to this defect at $1.2xU_0$.

5.6 Investigation: Electrode-bound cavity (Defect type 3): 50 Hz AC vs. DAC

The last artificial defect for the investigation is electrode-bound cavity between cable insulation and outer semi-conductive screen in the area close to the cable joint. This artificial defect is considered as defect type 3 for further discussion. Test procedures for defect type 3 were the same as for defect type 1 and type 2. Due to the fact that defect type 3 was created by permanent damage in the XLPE insulation, this defect was selected as the last one to be investigated.

5.6.1 PDIV delay time at 50 Hz AC

Measurement of PDIV delay time for the electrode-bound cavity was done by slowly increasing the voltage starting from 0 kV to get the PD inception voltage (PDIV). Then PD measurement was applied in steps accordingly to Table 5.5. Initiation of first PD in the cavity was related to the occurrence of a starting electron. The delay of the electron occurrence in a certain type depends on:

- Cavity size (approx.. 1 mm) and regularity of the shape (in defect type 3 it was not regular).
- Test voltage level.
- Test voltage frequency.

The plot of PDIV delay time is presented in Figure 5.26 for defect type 3. It can be directly concluded that at 50 Hz AC, a rather long delay time was observed prior to the first stable PD occurrence. The maximum PDIV delay measuring duration was only 2 min.

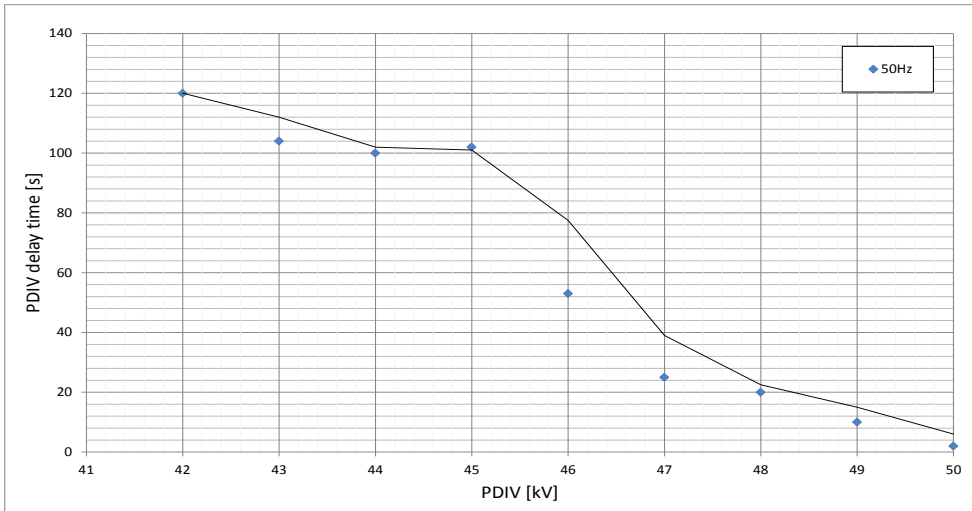


Figure 5.26: PDIV long delay time at different voltage levels.

Based on the measurement results, we conclude, that the minimum PDIV related to the longest PDIV delay time of defect type 3 was 42 kV_{peak}, whereas the minimum PDIV delay time occurs at 50 kV_{peak} which was obtained after 2 seconds. It must be noted that in total 9 measurements were performed to investigate PDIV delay time. After each single voltage increase and measuring duration of 2 minutes, the test voltage was decreased to 0 kV and the cable was grounded for 10 minutes. Figure 5.24 shows the relation between the delay times and the test voltage increase for defect type 3. It is interesting that between minimum PDIV and maximum PDIV there was only 8 kV_{peak} difference. We conclude that defect type 3 is much more sensitive to voltage change than defect type 1 and type 2.

5.6.2 PD magnitude at 50 Hz AC

To check the PD behaviour at different voltage levels, for defect type 3 the voltage was increased accordingly to the scheme presented in Table 5.5. The results are presented in Figure 5.27. For PD magnitude at PDIV, the following values were measured:

1. Defect type 3, size 1 mm-14pC at 42 kV_{peak} (Minimum PDIV).
2. Defect type 3, size 1 mm-16pC at 50 kV_{peak} (Maximum PDIV).

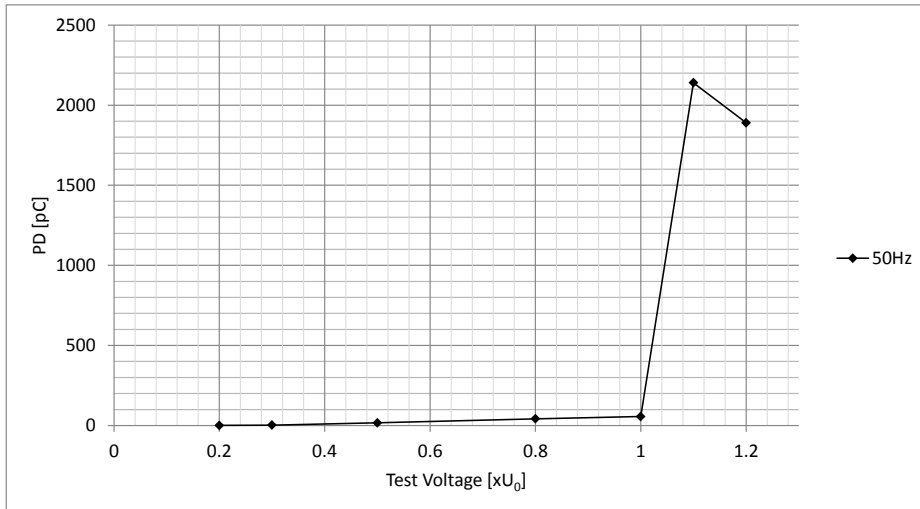


Figure 5.27: PD vs. test voltage for defect type 3 at 50 Hz AC voltage. Note: values presented in the plot are the average PD magnitude obtained during 2 min. measurements.

It is clearly visible that PD magnitude increases rapidly from the nominal voltage of $90 \text{ kV}_{\text{peak}}$ and the amplitude grows up to 2140 pC . At the maximal test voltage level of $1.2xU_0$, the PD magnitude was decreasing slightly to 1800 pC . By comparing the electric field strength inside defect type 3, it can be derived that at the nominal voltage of $90 \text{ kV}_{\text{peak}}$ simulated by Ansoft software, the electric stress is supposed to be around 8 kV/mm . At this voltage level, PD magnitude of 56 pC was measured. At $1.2xU_0$ electric strength inside cavity should be around 13 kV/mm . Comparing these two electric field strengths, it can be concluded that the difference between U_0 and $1.2xU_0$ was approx. 5 kV/mm , however the difference in PD magnitude level was 56 pC to 1800 pC . (approx. 32 times higher). We note that defect type 3 does not represent real spherical cavity and its shape is rather irregular. As a result, it can be assumed that during the voltage increasing a portion of surface charge generated at previous PD event might have a stronger impact on the amount of starting electrons than in the case of a perfectly round cavity. Due to the fact that the cavity surface could easily accumulate a portion of the trapped charges, these charges might be added to injected electrons at the next positive or negative voltage cycle. This behaviour can confirm the rapid increase of PD magnitude between $90 \text{ kV}_{\text{peak}}$ and $150 \text{ kV}_{\text{peak}}$. This assumption can also be confirmed by the fact that the cavity surface has one wall conductive. It leads to a quick re-distribution of the charge which was deposited at the surface by a PD event. Therefore, if the surface of the cavity is not homogenous, more and more charges are trapped with every single PD event. Thus, a breakdown voltage inside the cavity can be reached much faster than in the case of a perfectly spherical void and a cavity in virgin (non-conductive) state. However, these breakdowns in our cavity are more chaotic (occur randomly) due to the fact that the surface irregularity represents different space (capacity) for the trapped electrons. It was discussed in [56, 58, 59, 60] that electrons trapped at the surface of a void did not have any impact on PD repetition rate, however the PD repetition rate increased in time. In the investigation presented in this thesis, it was observed that PD activity produced by defect type 3 showed a higher magnitude for the test voltage (above U_0). Below this level, repetition of PD pulses was low and PD magnitude did not grow significantly with the increasing test voltage and increasing

testing time. (range between $0.2xU_0$ - $1.0xU_0$). After test voltage increases above U_0 , we observed a rapid increase of PD level. We conclude that defect type 3 perhaps could not be visible (detectable) during the so called “soak test” at the network level U_0 .

5.6.3 PRPD patterns at 50 Hz AC

PRPD patterns were monitored through the entire process of testing. PRPD patterns for defect type 3 were obtained at the level of voltage and recorded for 2 minutes. Figure 5.28 shows PRPD patterns which were observed at the minimum PDIV, maximum PDIV, U_0 and $1.2xU_0$ for defect type 3. In this case, the results were presented for three different voltage levels as the PD amplitude and intensity differed a lot for the three test voltage levels.

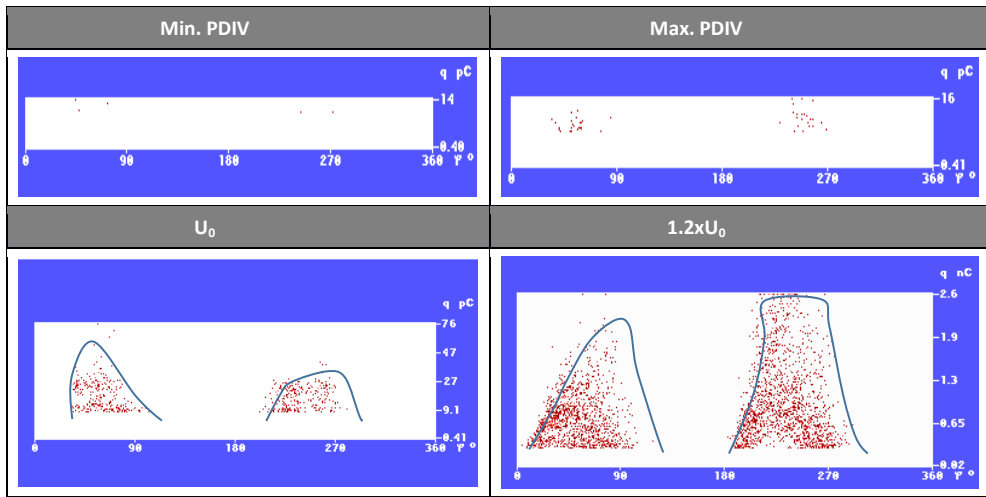


Figure 5.28: PRPD patterns at different test voltage levels of 50 Hz AC.

Based on the PRPD patterns of defect type 3, it can be concluded that there is a difference in the form and characteristics of patterns at U_0 and $1.2xU_0$. The differences are visible through a higher PD occurrence (intensity) and PD pattern shape. At higher voltages the shape is completely different from that at U_0 . It can be observed that the negative half of voltage sine wave generates a higher PD, which creates a sort of pyramid-shape form with the highest PD on the top. At a positive voltage, the sine wave in the shape of a pyramid is also observed but with a much lower magnitude although the PD occurrence (intensity) appears to be higher. It is supposed that the surface charge decay is more intense during the positive voltage cycle in the electrode bound cavity since the charge can recombine or move readily in the copper strip. On the other hand, when a copper strip acts as a cathode in the third half of the voltage cycle, a larger number of PDs will occur in this area near the copper strip. PD pulses amplitude at negative voltage cycles significantly exceeds the PD pulses observed in positive voltage cycles.

5.6.4 PDIV delay time at DAC

In Figure 5.29 the PD delay time as a function of number of DAC excitations is presented. The test procedure was the same as in the case of measurements for defect type 1 and type 2. The maximum number of DAC excitations was 30xDAC per voltage step.

Minimum PDIV (long delay time at 60 Hz DAC):

- For defect type 3, size 1 mm-long delay time relates to 30xDAC excitations and PDIV of 57 kV_{peak}.

Maximum PDIV (short delay time at 60 Hz DAC):

- For defect type 3, size 1 mm-short delay time relates to 1xDAC excitations and PDIV of 69 kV_{peak}.

The DAC frequencies and PDIV delay time characteristics are presented in Figure 5.29.

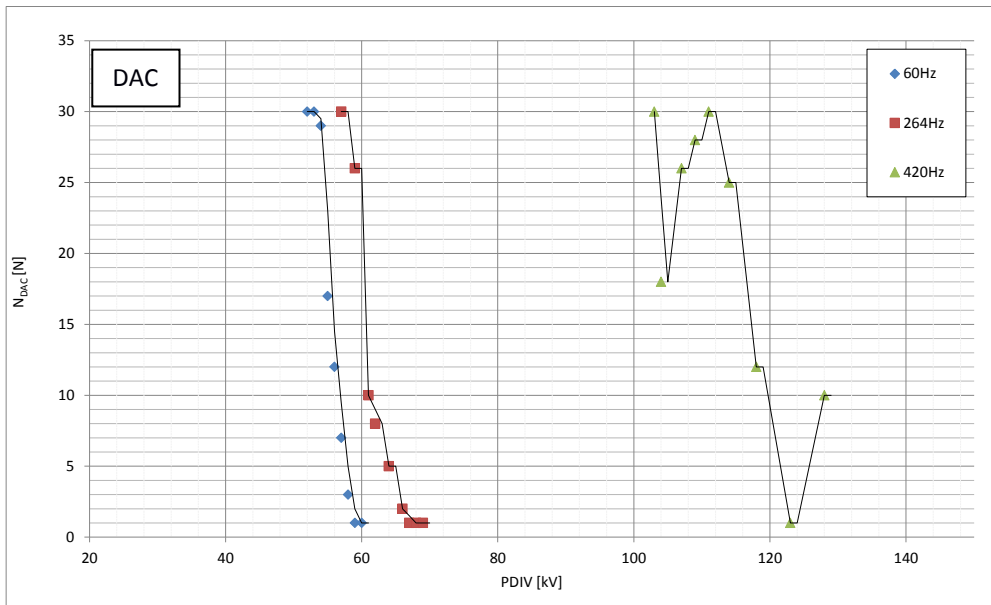


Figure 5.29: PDIV delay time (number of DAC excitations till PD occurrence) at different voltage levels and different DAC frequencies.

It can be concluded that 60 Hz and 264 Hz DAC frequencies show similar behaviour for PDIV delay time records—a decrease in number of DAC excitations with a higher test voltage. At 264 Hz slightly higher values of PDIV level were recorded. A different situation was observed for the 420 Hz DAC frequency. Firstly, the PDIV levels were much higher; secondly the difference between the minimum PDIV and maximum PDIV level was much larger. Moreover, an increasing test voltage level was not always related to the lower number of DAC excitations required to ignite stable repetitive PD signals. Even with a higher test voltage at 420 Hz DAC,

more excitations were necessary to get first PD signals than at lower frequencies. It can be derived that defect type 3 at 420 Hz DAC resulted in unstable PDIV vs. test voltage characteristics between 105 -120 kV_{peak} range and 125-131 kV_{peak}. Similar behaviour was observed for defect type 1 (sizes 10 mm and 15 mm).

5.6.5 PD magnitude at DAC

PD magnitude at different voltage levels is presented in Table 5.8. It has to be mentioned here that adding an extra capacitors to cable can result in lower measured PD amplitude. This lower PD amplitude can be a result of the fact that a part of the PD energy “disappears” in the additional capacitor.

Table 5.8
PD level at minimum PDIV (long delay time) for different DAC frequency and one defect 3 size-1mm.

DAC freq.	PD levels for defect 3 for min. PDIV at different DAC test voltage frequencies Size :1mm
60Hz	20pC at 52kV _{peak}
264Hz	22pC at 57kV _{peak}
420Hz	30pC at 103kV _{peak}

It was shown that defect type 3-electrode bound cavity is sensitive to voltage DAC frequency. At 420 Hz DAC frequency, much lower PD magnitudes were recorded than at 60 Hz and 264 Hz (Figure 5.30).

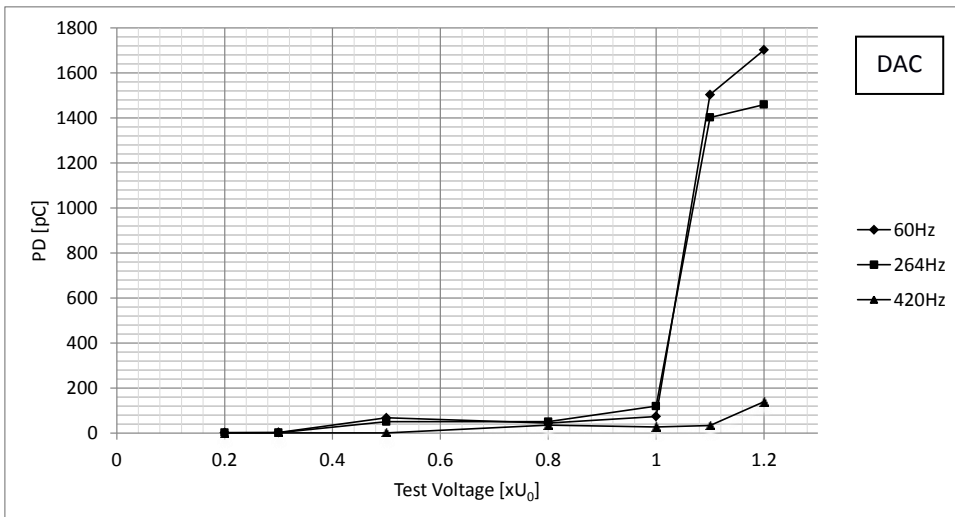


Figure 5.30: PD vs. test voltage for the defect type 3 at DAC voltage.

5.6.6 PRPD patterns at DAC

Based on the results, the following can be concluded: at PDIV level the PRPD pattern was asymmetric (PD in positive half of voltage sine) at 264 Hz and 420 Hz. At 60 Hz a symmetric pattern was observed. At a higher test voltage level, the PD pattern became more symmetric at 60 Hz and 264 Hz, however at 420 Hz it remained asymmetric (Figure 5.31a and 5.31b). At $1.2xU_0$ a slightly higher intensity of PD was recorded at 60 Hz in positive voltage sine but PD magnitude was lower than at positive voltage sine wave. At 264 Hz, a lower PD magnitude was recorded at negative voltage sine. It looks like PDs intensity was much lower at 420 Hz than at 60 Hz and 264 Hz both for the minimum PDIV and the test voltage level of $1.2xU_0$.

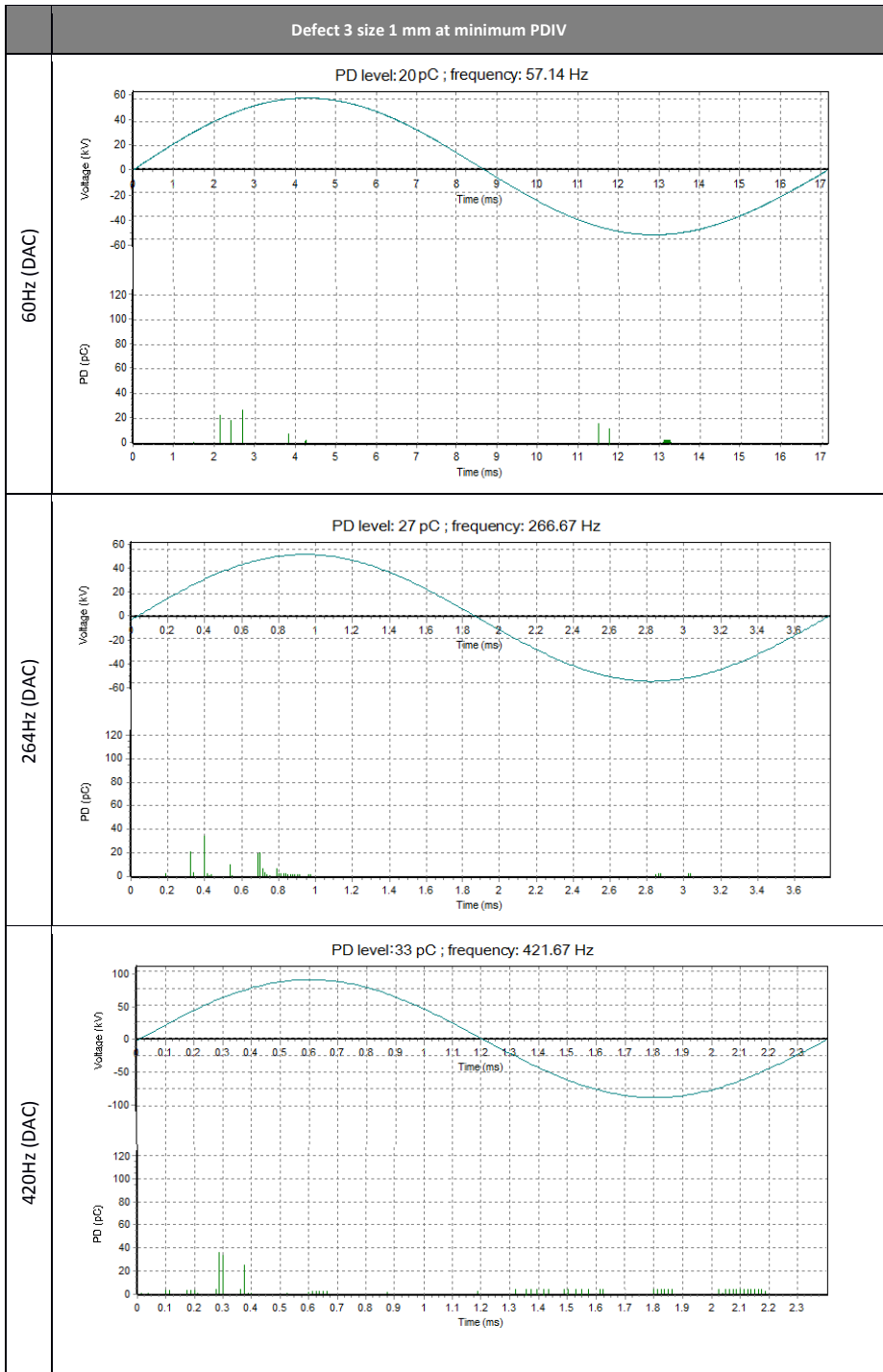


Figure 5.31a: PRPD patterns for defect type 3, size 1mm at minimum PDIV .Note: These are random examples from the measuring process of 30xDAC excitations.

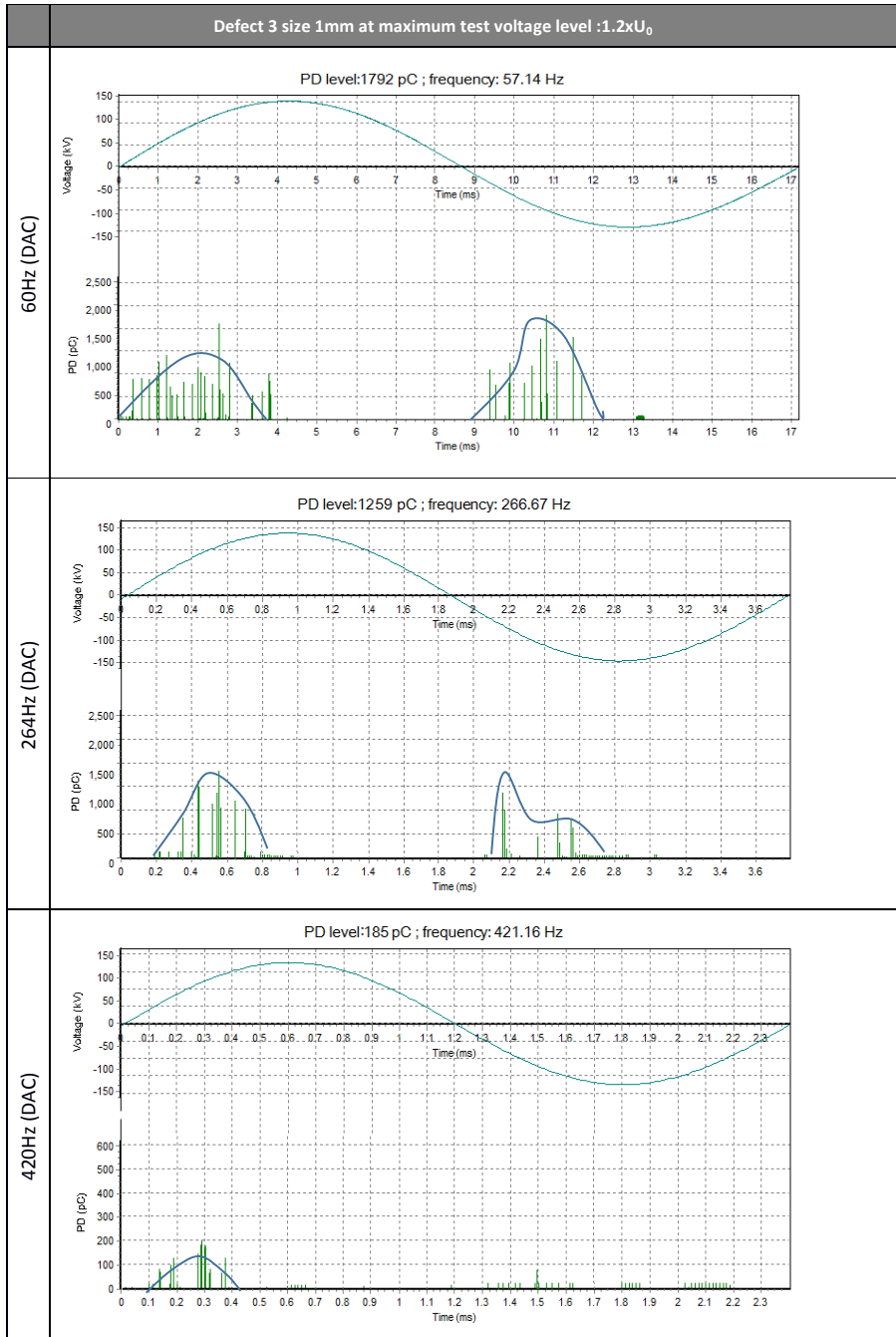


Figure 5.31b: PRPD patterns for defect type 3, size 1 mm at $1.2xU_0$. Note: These are random examples from the measuring process of 30xDAC excitations.

The explanation for lower PD magnitude at higher DAC frequency and lower intensity of PD pulses could be trapped electrons in the shallow structure of our bound cavity. The trapped electrons could add to starting electrons at the next PD event. The trapped electrons

disappear with time [39, 68] and the amount of added electrons decrease for each following positive or negative charging as well. This time after which trapped electrons disappear depends on the test voltage and test frequency. When PD occurs in the cavity, the field in the cavity collapses to the residual value [40] and it changes again. The time necessary to get minimum PDIV is shorter for higher DAC frequency because more electrons are “injected” during unipolar voltage charging in the first stage of DAC excitation. On the other hand, even though the probability of starting electrons is higher for higher DAC frequencies, the minimum PDIV will be close to maximum PDIV. Additionally, according to Figure 5.8, when the test voltage sine is negative, the copper strip acts as a cathode and a higher number of electrons are released (third quarter of voltage sine).

5.7 Conclusions

- Artificial defects created in the test object (joint) could be successfully traced and characterized with PD measurements performed with two different energizing sources: continuous 50 Hz AC and Damped AC (DAC) at frequencies: 60/264/420 Hz using a classical PD detection method according to IEC 60270 implemented in both systems.
- Defect type 1 (Missing outer semi-conductive screen):
 - a. Measurements performed with DAC voltage energizing source at 60Hz and 264Hz PDs on defect type 1, confirmed a similar behaviour of PDIV with a continuous 50 Hz energizing source. The differences were in the range of 1-5 kV. At 420 Hz DAC voltage PDIV was 2x higher than at 60 Hz and 264 Hz.
 - b. Phase-resolved pattern observed with DAC voltage could be compared (shape) to continuous 50 Hz AC. However, the following was observed: at higher frequencies i.e. 264 Hz and 420 Hz, PD pulses were less repetitive and therefore visible but the shape remained the same for all frequencies.
 - c. PD magnitudes as measured were lower for larger defects type 1 only at 264 Hz and 420 Hz. At 60 Hz DAC they followed the same characteristics as for 50 Hz AC continuous voltage source. Therefore, defect type 1 is voltage frequency sensitive and easier detectable at 50 Hz.
 - d. Minimum PDIV for defect type 1 was higher for a larger defect size at 420 Hz than at 60 Hz and 264 Hz (based on 30 DAC excitations).
- Defect type 2 (Extra semi-conductive screen in the joint):
 - a. PD measurements with both energizing sources being 50 Hz continuous AC and 60 Hz DAC confirmed that defect type 2 was less critical than defect type 1 and type 3 if PD level and PDIV was considered as a criterion.
 - b. PDIV levels were comparable with 50 Hz continuous AC and 60 Hz DAC. (Difference 7 kV) and were in the range of 139-146 kV.
 - c. PRPD patterns were comparable with 50 Hz continuous AC and 60 Hz DAC. At higher frequencies of DAC voltages a lower PD amplitude was observed and PD repetition rate decreased as well.

- Defect type 3 (Electrode-bound cavity):
 - a. PD measurements with both energizing sources 50 Hz continuous AC and 60 Hz DAC confirmed that defect type 3 can be successfully detected at continuous AC and DAC voltages, however at 420 Hz DAC voltage PD magnitude was much lower and the repetition rate was very low when compared to lower frequencies of DAC voltage.
 - b. PD measurements with both energizing sources 50 Hz continuous AC and 60 Hz DAC confirmed that a certain time is required to initiate a partial discharge. Assuming constant cavity diameter (shape), PDIV is only test voltage related. At low voltages at 50 Hz continuous AC, a relatively long inception delay time was measured and on the other hand, when we increase the voltage considerably a delay time decreased.
 - c. At DAC voltages 60 Hz 264 Hz PDIV, the delay time characteristics were almost similar and followed the rule: the higher the test voltage, the shorter the delay time to ignite a PD. At 420 Hz DAC test voltage, not only the highest PDIV was observed (2xhigher), but also with higher test voltage, the shortest PDIV delay time was not observed. We observed that at 420 Hz PD characteristics: PD magnitude, PRPD patterns and repetition rate, were very unstable and “unpredictable”.
- Overall we conclude that AC 50 Hz voltage and DAC 60 Hz PD measurements results are almost similar for all defects.
- Due to the fact that it was not possible to energize the test object with the continuous 264 Hz AC and 420 Hz AC voltages we could not directly compare DAC voltage frequencies of 264 Hz and 420 Hz.
- The DAC method showed its capability to detect PD related defects in all tested frequencies, however at higher frequencies it was more difficult. Therefore, we recommend testing the short HV and EHV cables with the test voltage frequency below 400 Hz. This is important especially when testing is accompanied with PD measurements.

6. ON-SITE TESTING AND DIAGNOSIS OF TRANSMISSION CABLES WITH DAC VOLTAGES

In this chapter, the applicability of the DAC voltage method for on-site diagnosis of transmission cables has been evaluated. The described results are derived from a 4-year research and on-site diagnosis on various new and service aged power cables in the voltage range between 50 kV and 220 kV. General goals of the research are described in Figure 6.1. At the beginning of the project, knowledge of on-site PD and dielectric loss diagnosis on transmission cables with DAC method was limited. Testing procedures and data analysis were based on the experimental approach and experience with medium voltage cables.

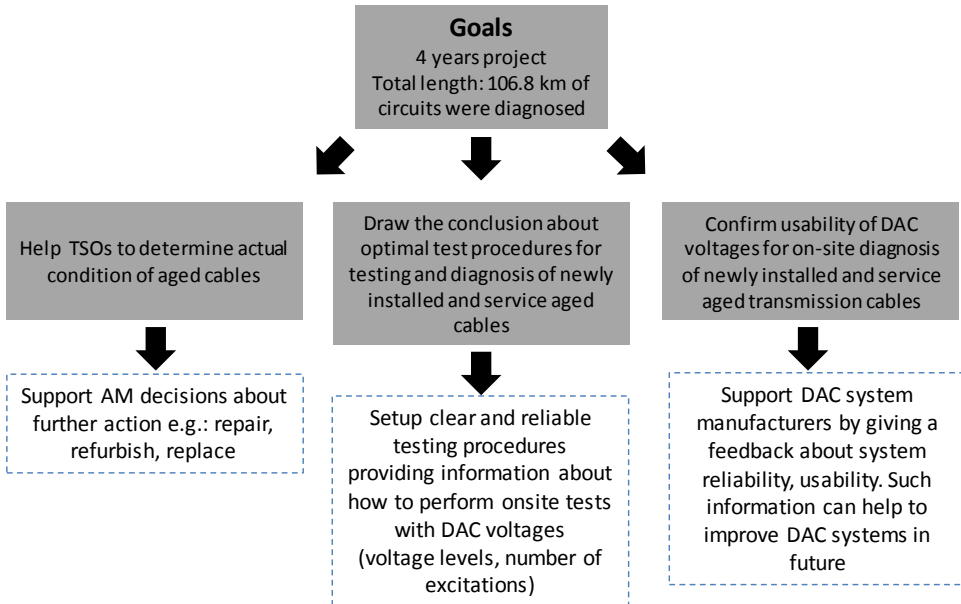


Figure 6.1: General aspects of on-site diagnosis research project performed on service aged transmission cables.

The major purpose of after-laying tests is to demonstrate the correct installation of the cable joints and terminations prior the network energising. Tests are considered successful when there is no breakdown recorded during testing time e.g. 1h at the voltage levels described by standards e.g. IEC 60840. PD and dielectric loss measurements are not actually required by any IEC standards as is in the case of obligatory measurements for after-laying tests. However, these measurements can give additional information about the cable condition [8, 17, 61]. In chapter 5 of this thesis, we have demonstrated that joint installation defects in XLPE HV cables can be successfully detected with DAC voltages and parallel PD measurements at the voltage frequencies between 60 Hz-420 Hz. In chapter 6 we have used the same DAC

method for the on-site measurements of HV and EHV cables. Three different on-site case studies were investigated.

The first case study refers to the after-laying acceptance test on a newly installed 150 kV XLPE cable. PD measurements were performed to find the weak spot that caused a breakdown during a high voltage test performed with a resonant system that was used after cable installation. The second case study concerns acceptance tests on a newly installed 220 kV EHV XLPE cable. PD diagnosis were performed to qualify the workmanship and assess the cable condition. The third case study involved 13 circuits of 50 kV oil-filled cables and 9 circuits of external gas-pressurised 150 kV cables. Measurements were performed as part of condition assessment activates provided by Dutch TSO (Transmission System Operator) and DSO (Distribution System Operator). The main purpose of the measurements was different for each one.

Dutch DSO is an energy network company that provides energy transport and distribution to a large part of The Netherlands. The company has many kilometres of aged and heavy aged 50 kV oil-filled cables in service. Planning of the asset management actions, e.g., cable replacements or cable repairs are based on several aspects: number of failures, age of asset, maintenance intervals, and economic factors [1]. A number of cable failures (excluding third party) can reflect the general cable condition. It was important for DSO to find the actual cable insulation condition for aged cables and to check if there was a direct correlation between the insulation condition and the number of sheathed cable faults resulting in oil leakages. A list of selected cables is presented in Table 6.1.

Dutch TSO has approximately 230 km of 150 kV external gas-pressurised (GP) cables installed in the transmission network in The Netherlands. Many of these cables are 30-40 years old. A low number of failures (a total of 4 failures recorded up to 2008) for such old cables forced TSO to check the oldest cables for PD activity and dielectric loss characteristics at voltages between 0 kV up to $1.3xU_0$. The ageing processes and related defects, e.g. electric treeing could be traced by PD diagnosis. Finding the partial discharge inception voltage, PD characteristics and dielectric loss characteristics may give additional information about the ageing processes. Within the main insulation of the gas-pressurised cables, an electric field is present of maximum 15 kV/mm [4]. This is much higher than the electric field in a 50 kV oil-filled cable. Due to the nitrogen gas-pressurised system that pushes the paper-layers together, normally no cavities (and thus no discharges) can occur within these layers. Under normal conditions, the main insulation can therefore resist this higher field strength. However, due to irregularities of cavities that may exist, this can lead to local field enhancements. As a result, the local breakdown strength can be exceeded and partial discharge may occur and deterioration of the insulation may develop (discussed in Chapter 3). Eventually, this will lead to treeing and breakdown. The breakdown is determined by the local field strength. Since in gas pressurised 150 kV cables, the field strength is rather high, it is assumed that this process can escalate quickly. Based on the data and information available by TSO and in CIGRE publications [2, 3] it was concluded that discharges do not play a dominant role in the ageing process of this type of cable because cavities in the main insulation are rare. However, due to general degradation of the insulation through thermal cycles, an extensive current load in this case, dielectric loss measurements may bring valuable information for TSO.

Table 6.1

Test objects for case study 3 (condition assessment of service aged HV cables). Information given in the last column (age status) were given by DSO and TSO.

Name	insulation	Year of installation	Length [m]	Capacitance per phase [μ F]	Notes: low aged, aged, heavy aged, number of leakages till 2010
Circuit 1	Oil-filled mass impregnated 50 kV	1958	9568	2,8	Strong aged,1
Circuit 2		1968	6780	1,8	Aged,2
Circuit 3		1989	5818	1,5	Aged,2
Circuit 4		1989	2001	1,1	Aged,2
Circuit 5		1989	3297	1,2	Aged,3
Circuit 6		1968	4141	1,3	Low aged,1
Circuit 7		1968	4141	1,3	Low aged,2
Circuit 8		1973	3778	1,2	Aged,3
Circuit 9		1989	1501	0,5	Low aged,2
Circuit 10		1966	4737	1,4	Aged,3
Circuit 11		1970	4716	1,4	Aged,4
Circuit 12		1978	3326	1,3	Aged,3
Circuit 13		1972	3366	1,3	Aged,5
		total length	58054		
Name	Type	Year of installation	Length [m]	Capacitance [μ F]	Notes, number of gas leakages
Circuit 1	External Gas-pressurised 150 kV	1956	6118	1,8	Aged,0
Circuit 2		1987	4884	2,4	Aged,0
Circuit 3		1970	6277	1,6	Aged,0
Circuit 4		1970	6277	1,6	Aged,0
Circuit 5		1978	8410	2.2	Low aged,1
Circuit 6		1978	8500	2.2	Low aged,0
Circuit 7		1976	3600	0,96	Aged,0
Circuit 8		1995	4747	1.4	Low aged,1
Circuit 9		1978	4005	1.1	Low aged,0
		total length	52818		

6.1 Case study 1: Diagnosis of a newly installed 150 kV XLPE cable after breakdown

The first case study is related to a new XLPE 150 kV cable that was installed in Amsterdam. A cable with a length of 4,5 km was installed in metal pipes. These pipes were used as a shield for external gas pressurised HV cables in the past. The decision had been made to replace an old paper-insulated cable with new XLPE three-phase cable system, and use existing pipes to reduce installation costs. As a result 3-phase cable was “pulled in” into pipes without additional digging procedures. This type of cable is called Retrofit Cable and is manufactured by several global HV cable companies. Basic information on the cable type is presented in table 6.2.

Table 6.2
Test object data.

Insulation type:	XLPE, A2XFL2YVF ST2Y
Cable length	approx. 4485 m
Voltage rating:	150 kV
Operation voltage:	$U_0 = 86.7$ kV RMS
Cable capacitance (one phase)	0.92 μ F
Service history	No (new)
Additional info	Breakdown in cable phase L1 during AC resonant voltage withstand test

6.1.1 PD vs. Test voltage characteristics

During the resonant voltage increasing, there was a breakdown recorded in one of the cable phases (L1). Breakdown voltage level was recorded at $0.8 \times U_0 = 72 \text{ kV}_{\text{rms}}$ ($101 \text{ kV}_{\text{peak}}$) where $U_0 = 86.7 \text{ kV}_{\text{RMS}}$. The breakdown location was unknown. In order to find the breakdown source, the pinpointing of the cable fault was performed. Due to the high voltage breakdown level it was not possible to use the arc reflection method. The arc reflection method of fault pre-locating combines the use of a TDR (Time Domain Reflectometer) and a surge generator (thumper). By using an arc reflection filter, a low voltage TDR and a high voltage surge generator can both be connected to the faulted cable and the TDR analysis is performed while thumping. The filter protects the TDR from the high voltage pulses of the surge generator, and it routes the low voltage pulses down the cable. This method utilises the fact that when an arc is created at the fault, its resistance is reduced to a very low value, less than 200Ω , which will reflect radar pulses. The arc location will appear as a downward going reflection on the TDR cable trace. However, the surge generator must create a voltage higher than the breakdown voltage of the cable itself. In the situation when the breakdown voltage is higher than the surge generator, the pinpointing of the fault is not possible. In order to find the location of the breakdown DAC voltage, system 150 kV was used. With DAC voltage, it was possible to slowly increase the test voltage level and at the same time observe PD activity which are pre-breakdown indicators. During increases of DAC voltage at the phase L1, two breakdowns were recorded. The first breakdown occurred in cable phase (L1) at $100 \text{ kV}_{\text{peak}} / 71 \text{ kV}_{\text{rms}} = 0.81 \times U_0$, after the breakdown the cable was grounded for 10 min. and recorded PD data were analysed. After the first breakdown and a waiting period of 10 minutes it was possible to energise the cable again with DAC voltage. The second breakdown occurred in the same cable phase (L1) at $120 \text{ kV}_{\text{peak}} / 85 \text{ kV}_{\text{rms}} = 0.97 \times U_0$ and, at that time, it was a permanent breakdown and energising was not possible any longer. Both breakdowns were followed by PD activity up to 7000 pC. PD vs. test voltage level characteristics are presented in Figure 6.2. The first breakdown occurred at damped resonance voltage, and the second one was recorded during the voltage charging process. The frequency of damped resonance voltage was 60 Hz.

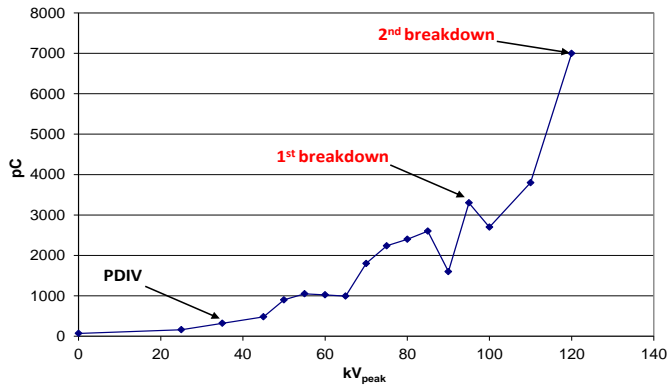


Figure 6.2: PD vs. test voltage characteristics for test performed on cable phase L1.

6.1.2 PRPD patterns analysis

PD measurements were performed at each voltage step until breakdown. After each DAC excitation, the data were recorded and saved for TDR analysis and PRPD (Phase Resolved Partial Discharge) patterns. It can be observed that PRPD patterns are asymmetric at a lower voltage test (up to $0.6xU_0$), while becoming symmetric at higher voltage levels with higher amplitude of PD pulses recorded in 1st quarter of voltage sine (Figure 6.3).

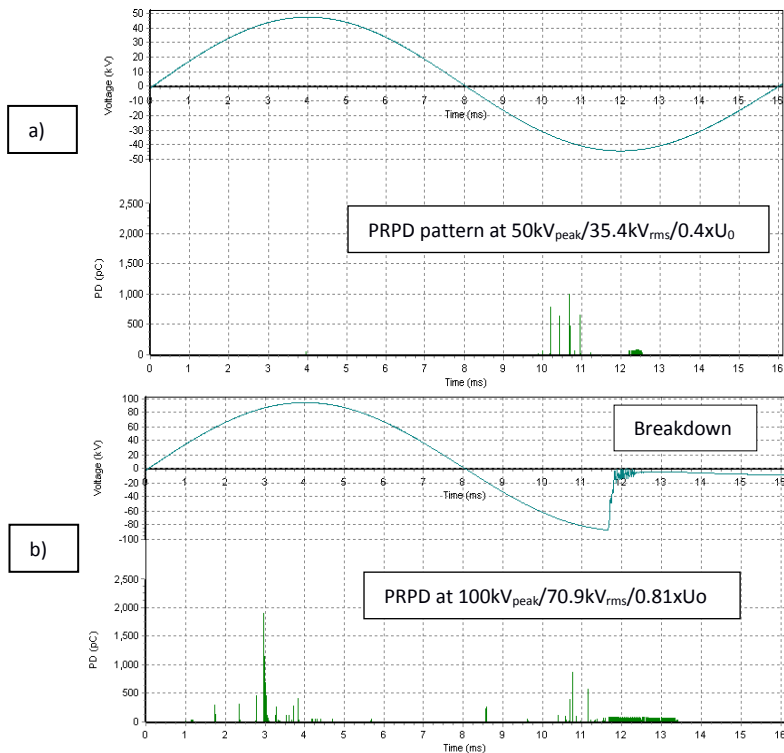


Figure 6.3: PRPD patterns for DAC voltages at a) $0.4xU_0$ b) $0.81xU_0$ 1st breakdown.

6.1.3 TDR traces

Before DAC testing and diagnosis, calibration of the test object and DAC test system was performed. The system was calibrated according to IEC 60270 standard and according to the procedures discussed already in chapter 4. PD detection sensitivity has to be measured which is based on the background noise level. Moreover, PD localisation sensitivity has to be known which is based on the PD pulse attenuation in cable. PD pulses were injected to the test object, and PD pulse velocity and amplitude were measured (Figure 6.4). Calibration pulses from 100 pC up to 100000 pC were injected consecutively. Calibration of a wide range enables measuring from a very low amplitude, e.g., 20 pC up to 100 nC. In this case calibration in the range of 500 pC was the lowest possible value that gave a clear Incident and reflection pulse records.

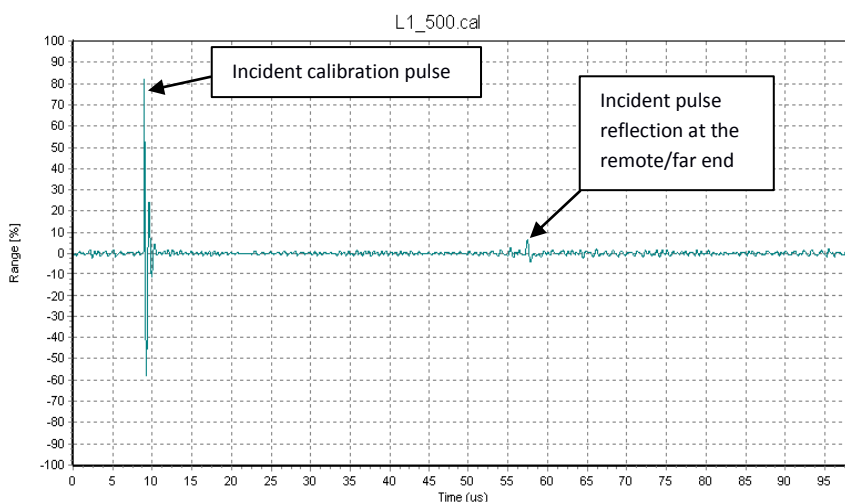


Figure 6.4: Example of calibration of 500 pC pulse. Clear reflection was observed at the remote/far end of cable phase.

It can be concluded from Figure 6.5 that an Incident PD pulse of 500 pC is still visible after reflecting from the far cable end (remote termination). This is direct confirmation that partial discharges in the range of 500 pC could be effectively localised via TDR analysis. The Incident pulse reflection was visible, however, the attenuation of the calibration pulse was rather high. Incident pulse reflection resulting from the far cable end is almost invisible at this range and, therefore TDR analysis is not possible. However it has to be noted that the localisation of the PD pulse from the near-end and far-end is the worst case scenario and can always be compared to the calibration pulse. In the case of the PDs originating e.g. from the middle of the cable, the localisation sensitivity increases as the PD incident pulse reflection has a shorter distance to the measuring system than in the case of PD originating e.g. at the near cable end where PD incident pulse reflection runs 2 x cable length. Pulse attenuation depends on several factors: cable type (construction), insulation (polyethylene or paper), number of joints, and type of joints (in cables with the cross-link joints a cable impedance is not constant at the joint, which gives additional reflection at TDR analysis). TDR traces analysis confirmed PD source in a distance of 2600 meters counted from the near cable end (place of the DAC system connection). Examples of TDR analysis are presented in Figure 6.5 and Appendix D.

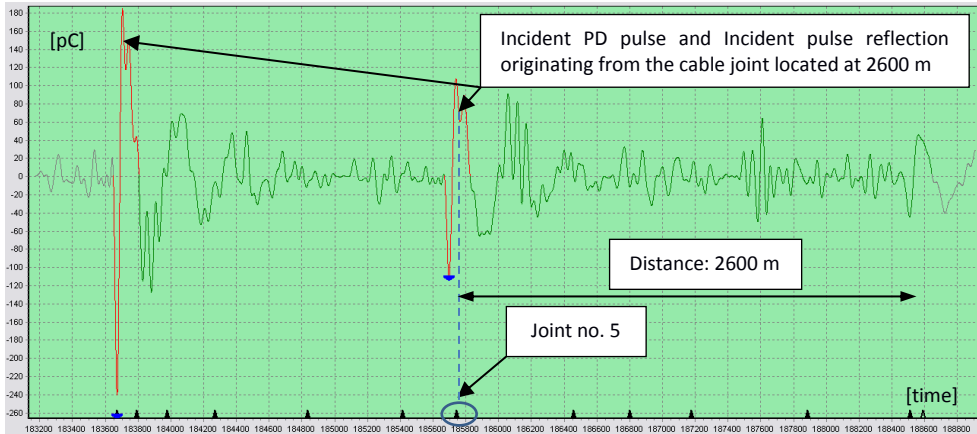


Figure 6.5: Example of TDR analysis of the first recorded PDs (cable phase L1). Partial discharge inception voltage = $0.4xU_0$. PD localised in vicinity of the joints no. 5. Black triangles represent joints positions.

6.1.4 PD mappings

From the TDR analysis, it was concluded that PDs had a source in a faulty joint no. 5. The PD measurements performed on phase L1 indicated the faulty component being already at a relatively low voltage ($0.4xU_0$). At partial discharge inception voltage, PD amplitude was around 250 pC. PD mapping is presented in Figure 6.6. The investigation made after the joint repair eventually confirmed the discharges resulted from the contaminated surface of the XLPE insulation. The joint deflector (electric field steering element) was inserted into contaminated insulation. The contamination that resulted from the peeling process of the semicon screen caused enhanced electric field stress and insulation breakdown. After PD diagnosis the faulty joint was repaired and AC resonant non-monitored withstand test was performed successively. No breakdown during withstand test was recorded.

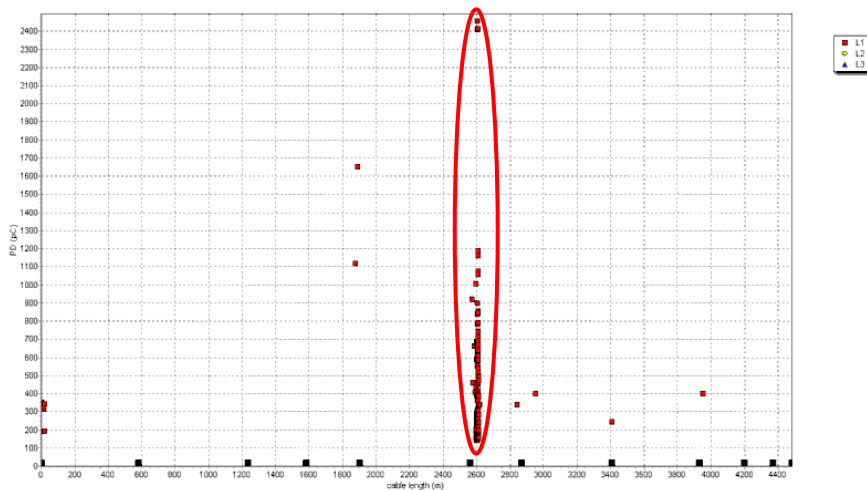


Figure 6.6: PD mapping showing faulty joint no. 5. Red dots represent PDs localised at 2600 m.

6.2 Case study 2: Testing and diagnosis of a newly installed 220 kV XLPE cable

After the installation of 220 kV XLPE cable, PD diagnosis were done. Cable circuit was routed partly underground and partly under sea. A total of 21 joints were installed in a single cable phase (total 63 joints in 3 cable phases). The cable was finished with outdoor type terminations. Cable data are presented in Table 6.3.

Table 6.3
Test object data.

Insulation type:	XLPE 630 mm ²
Cable length	13 300m: 8.9 km land cable, 2.0 km sea cable, 2.4 km land cable
Voltage rating:	220 kV
Operation voltage:	$U_0 = 127$ kV RMS
Cable capacitance (one phase):	2.1 μ F
Service history	No (new)
Additional info	Breakdown in cable phase during DAC test

6.2.1 PD vs. Test voltage characteristics

The agreement on the cable test execution involved PD measurements up to $1.4 \times U_0$, using the DAC voltage monitored withstand test (50 x DAC excitations). Diagnosis was executed separately for each cable phase: L1, L2, L3. During increasing voltage, a breakdown in cable phase L1 occurred. PD activity in the range of 1000-1100 pC was followed by breakdown. External (not localised in cable) PDs were measured in cable phase L2 and L3 consequently. These PDs were related to an external corona effect. The first breakdown occurred in cable phase L1 at $0.4 \times U_0 / 72$ kV_{peak}, after the breakdown the cable was grounded for 10 minutes and recorded PD data were analysed. Another several breakdowns occurred in cable phase L1 at $0.3 \times U_0 / 60$ kV_{peak}, $0.33 \times U_0 / 62$ kV_{peak} and $0.38 \times U_0 / 68,4$ kV_{peak}. PD activity up to 1100 pC was recorded before further breakdowns occurred. Breakdown voltage level was decreasing with an increasing number of excitations applied after the first breakdown. PD vs. voltage level test characteristics are presented in Figure 6.7.

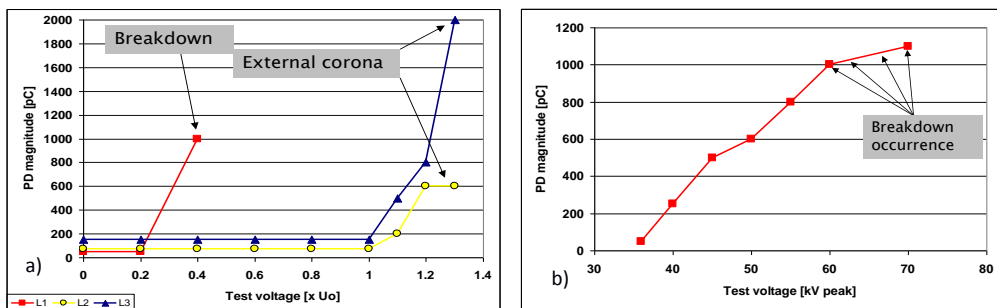


Figure 6.7: a) PD vs. test voltage characteristics for test performed on cable phase L1/L2/L3. b) PD amplitude below the breakdown voltage for cable phase (L1).

6.2.2 PRPD patterns analysis

After each DAC excitation, PD data were recorded and saved for analysis. PRPD patterns were observed during voltage increasing. It can be observed that PD phase-resolved patterns are symmetric at lower voltage tests and at higher voltage levels (Figure 6.8). The highest PDs were recorded on voltage peaks (90^0 and 270^0). Based on the general knowledge of PD characteristics at AC voltages, it can be concluded that these PDs come from the external corona in air (occurrence on the voltage peaks). PRPD patterns observed in cable phase L1 show the breakdown moment. The breakdown occurred on the top of the damped AC voltage in the first period. Voltage level-60 kV peak (Figure 6.8b).

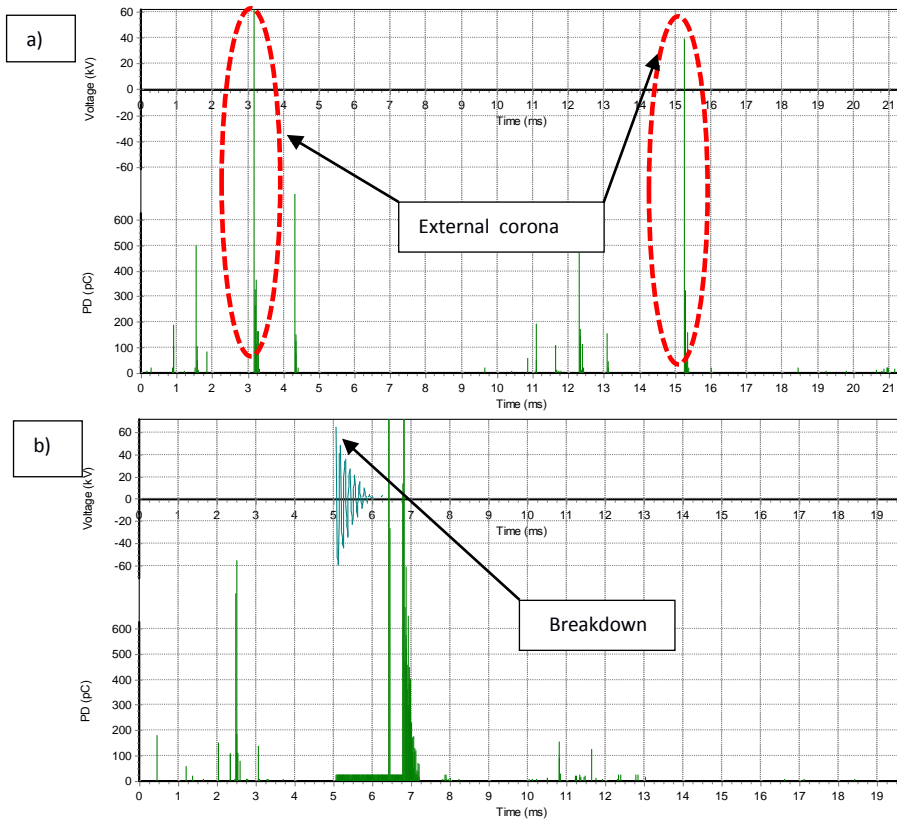


Figure 6.8: PRPD Patterns: a) Cable phase L2 with corona discharges b) Cable phase L1 in the moment of breakdown.

6.2.3 TDR traces

The system was calibrated according to IEC 60270 standard. In the calibration process PD pulses were injected into the test object (cable phase) and readings of the PD pulse velocity and amplitude were made. The calibration was performed with pulses from 100 pC up to

10,000 pC, however, only the highest injected signals of 50 nC and 100 nC were visible, consequently, due to strong signal attenuation in 13 km of XLPE cable. An example of the injected calibration pulses is presented in Figure 6.9. These reflections, as shown during the calibration can also affect the localisation of PD pulses which are estimated during the measurement. Looking closer at the data (Figure 6.10), it can be seen that in the case of PD measured in phase L1, there is also an additional reflection visible. If this reflection is selected, the distance of approximately 11,300 meter is indicated as the PD location. However, from the TDR signal, it can be seen that there is a wider reflection pulse visible. If this pulse is selected, the distance of 8,050 meter is given as the PD source location. This location is close to the joint located at 8,050 m.

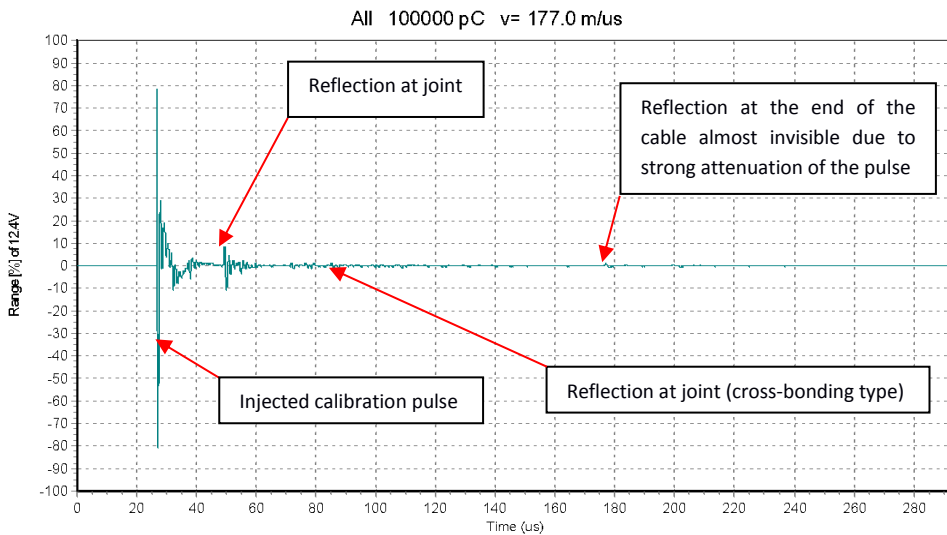


Figure 6.9: Calibration pulse showing the reflections at cross-bonding joints.

This effect can be seen in the TDR screen as shown below in Figure 6.10. Here is an example given for PD pulse, but it can be seen, during the analysis of all PD data, that this behaviour is observed. This shows the importance of connecting all cross-bonding joints in to a straight connection (discussed in chapter 4) without any additional grounding to reduce additional reflection (cable impedance change) and make the analysis simpler.

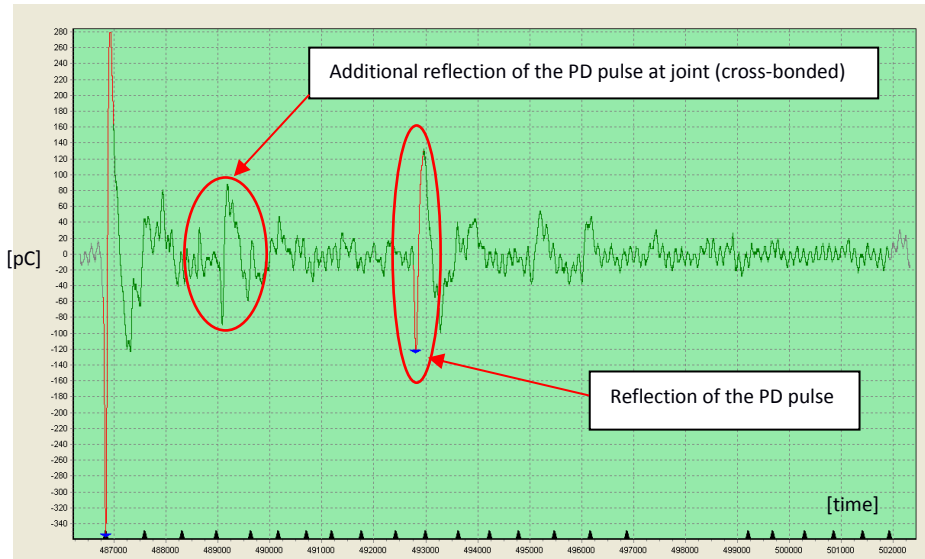


Figure 6.10: TDR screen showing the first detected pulse (original) and the reflected signals.

A full TDR analysis is performed on cable phase L1 in order to localise the breakdown location. A PD amplitude of 1000 pC was recorded in IEC record, and after transferring the signals to the UHF record, localisation process showed TDR traces with clear indication of the incident and incident pulse reflections at 8050 m (Figure 6.10).

This means that, in spite of taking into account additional occurring reflections on cross-bonded joints, the location of the PD occurring at the breakdown location can be found. The locations of PDs from the measurements performed from both sides show the location of the joint located approx. at 8050 m as presented in Figure 6.11. Second measurements were performed two days after the first test. During the second test performed from the far cable end, a breakdown in cable phase L1 also occurred at $0.4 \times U_0$ with PD amplitude approx. 1000 pC. After successful PD localisation, the faulty joint was dug out and inspected.

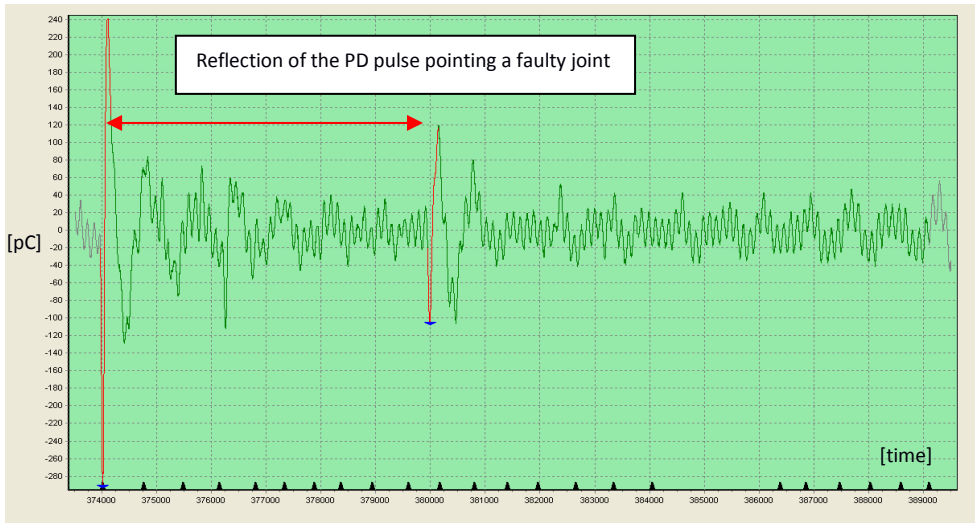


Figure 6.11: Example of TDR analysis of the recorded PD (cable phase L1) at test voltage of 60 kV_{peak}

6.2.4 PD mapping

Based on the obtained results from both cable ends (Figure 6.12), a decision about digging out the joint was taken. The investigation of the faulty joint showed poor workmanship in cable jointing, which resulted in incorrect cable positioning in the joint housing (Figure 6.13). As a result of this wrong positioning, the electric field distribution was distorted and the electric field locally enhanced causing PD activity. The remaining two cable phases: L2 and L3 were tested with DAC voltages up to $1.4 \times U_0$, and no internal PD sources were detected. A monitored voltage withstand test was provided by $50 \times \text{DAC}$ excitations per each cable phase at the maximum test voltage level of $1.4 \times U_0$ according to IEC 62067.

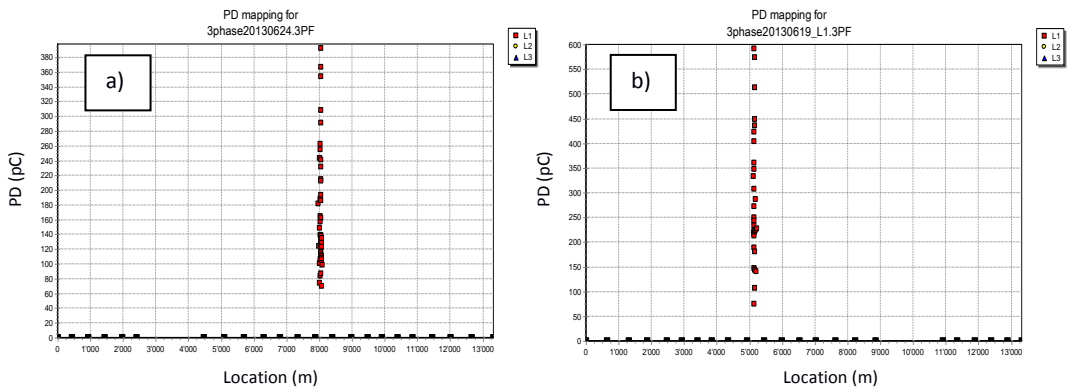


Figure 6.12: PD mappings of 220 kV XLPE cable obtained up to 60kV_{peak}. a) Results obtained from near cable end b) Results obtained from far cable end. Red dots represent PDs. The localisation confirmed the same source of PDs-the so called "mirror effect".

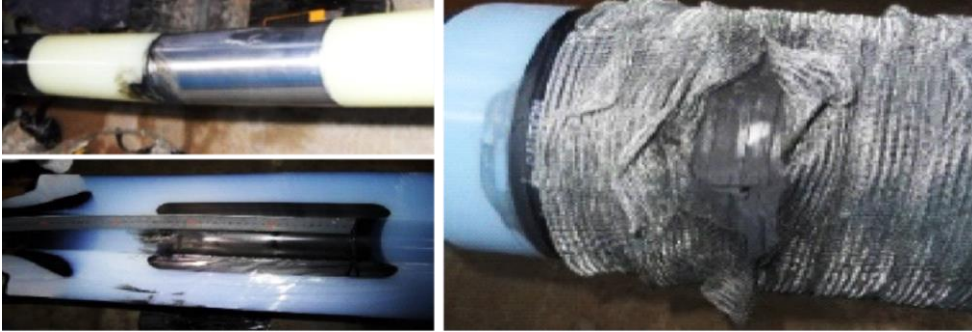


Figure 6.13: Faulty cable joint during inspection. Wrong positioning of joint housing caused a local PD activity and breakdown during DAC testing.

6.2.5 Voltage Withstand Diagnosis

After the repair of the faulty joint, the 220 kV cable was tested again with DAC voltages at $1.4 \times U_0$ ($180 \text{ kV}_{\text{RMS}} / 250 \text{ kV}_{\text{peak}}$). No breakdown was recorded for 50x DAC excitations. The PD level was in the range of 50 pC and no weak spots were localised (Figure 6.14). The cable was accepted for operational condition and put into operation 2 days later.

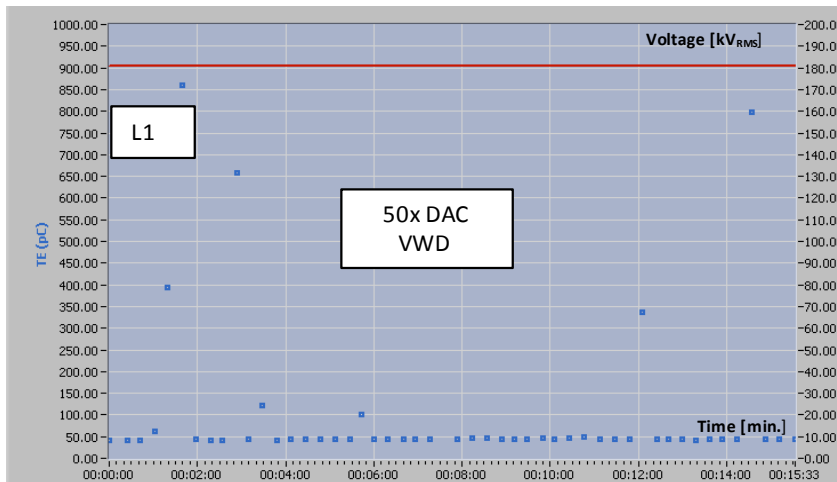


Figure 6.14. Example of VWD results for cable L1. Y-axis represents the average PD level [pC], X-axis represents duration of tests [min.]. Each blue dot represents the average PD detected during single DAC excitation out of 50 excitations.

6.3 Case Study 3: Diagnosis of the service-aged transmission cables.

In The Netherlands, low pressure oil-filled cables were installed between 1957 and 1996. 95% of the total population of this type of cables, were 50 kV rated (DSO and TSO internal data).

The reason for the application of this type of cables (previous 50 kV cables were only mass-impregnated with limited current load) was simple. In the 60's and 70's national industry was fast-growing. A good economic situation in the country and continuously growing demand for the energy produced in domestic plants as well as imported from e.g. Germany, France, forced grid owners to invest in stable and more reliable transmission HV systems. In low pressure oil-filled HV cables, the dielectric liquid (mineral or synthetic oil) goes through the cooling channels and penetrates paper insulation to cool the insulation and keep a constant cable temperature. Dielectric liquids need to have low viscosity. Mineral and synthetic oils were commonly used. The oil pressure for this type of cable is approximately 1 bar. This construction allowed for higher loads to be transferred between substations more reliably at 50 kV range. External gas pressurised cables have a different construction, but conductors are also individually insulated with oil impregnated paper. Each conductor is surrounded by a lead sheath that consists of pure lead. The pure lead has the advantage that it is plastic and, therefore, can change its shape due to its flexibility during thermal expansion when the load changes. When the load of gas-pressured cable is increased, the core of the cable is heated up and the cable changes its volume, which results in the force against external pressure. On the other hand, when the cable load is decreased, the cable temperature decreases as does the volume. Then the external gas (Nitrogen) also acts on insulation, preventing formation of voids in the insulation. Figure 6.15 shows various numbers of installed 50 kV oil-filled cables and 150 kV external gas-pressurised in The Netherlands up to year 2001 (DSO/TSO internal data base).

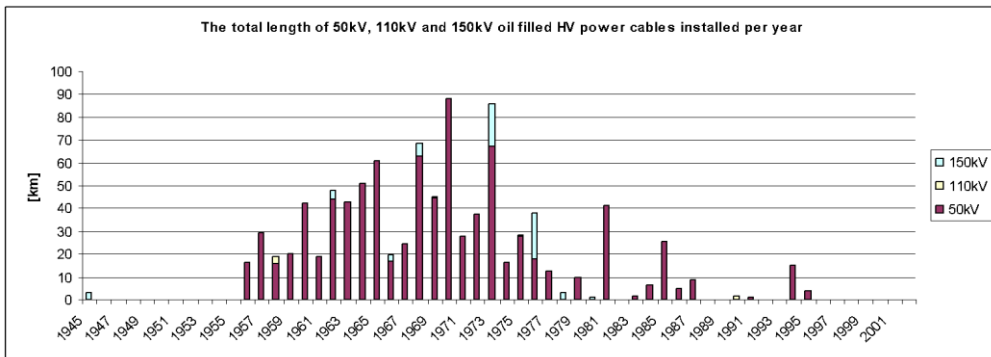


Figure 6.15: The total length of 50kV, 110kV, 150kV oil-filled HV power cables installed in The Netherlands (Data provided by DSO/TSO).

80% of actually service oil-filled cables in The Netherlands are over 40 years old. According to the utility service data, oil-filled systems are in general good condition. Mechanical failures occur in 90% of accessories (joints and termination) and mostly due to third party activities and the environmental factors (discussed in chapter 2). However, some part of the failures are oil leakages, which results in the loss of system integrity. Damages to the external sheaths occur due to digging, and soil topographic changes resulting in the longitudinal forces over the cable. A major problem is, however, the oxidising of the lead sheath. Figure 6.16 presents the number of leakages of 50 kV oil-filled cables per installation year.

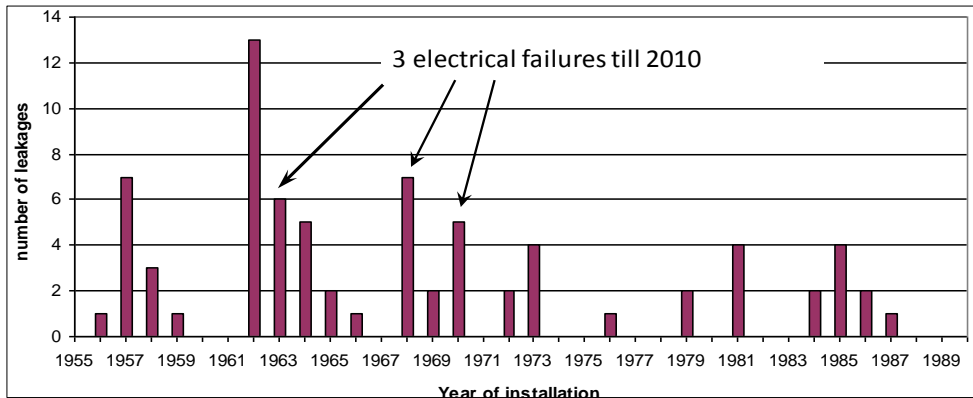


Figure 6.16: Number of leakages by year of installation for 50 kV oil-filled cables in The Netherlands. Only 3 electrical failures were recorded by the year 2010 (Data provided by DSO/TSO).

In aged cable insulation, the ageing symptoms are related to electric trees and thermal instability. Thermal instability happens due to the abnormal operational temperatures resulting in cable electrical breakdowns. Electrical breakdowns in 50 kV cables in The Netherlands appeared because of the extensive electric and thermal ageing processes during their operation. As a consequence of the breakdowns and the increasing number of leakages, the Dutch DSO started an investigation on 50 kV oil-filled cables. Results of this investigation are partly described in this section. Cables selected for the investigation (Table 6.1) had oil leakages due to faulty sheaths in the past.

In the case of external gas-pressurised 150 kV cables, the major problem of the ageing processes is a thermal instability. An increase of the conductor temperature causes decreases in the viscosity of the impregnated material (oil). Charge carriers in the insulation gain higher mobility and the conduction losses will rise. Conduction losses cause an extra source of heat within the insulation. Under normal conditions, a cable has sufficient capability to dissipate this heat. With an elevated temperature it is more difficult, and as a result the loss tangent reflecting dielectric losses also rises [4]. With a mineral oil impregnation, it can occur that at elevated temperatures (above 60°C), oxygen molecules and compounds of a thermal degradation (moisture) of the cellulose paper will react with the impregnated material. This leads to a reduction in dielectric properties (oxidation) and an increase in the overall dielectric losses. This degradation process causes further local temperature shifts. At a certain moment, this process starts to amplify itself, causing a thermal breakdown (discussed in chapter 3). One example of the dielectric behaviour under increasing temperature of paper samples taken out of the 150 kV external gas-pressurised cable after a breakdown is depicted in Figure 6.17. The increased dielectric losses were measured in the cable samples, taken from a different breakdown spot and different cable phases. The measurements were taken at TU Delft laboratory with a Schering bridge device used for dielectric loss measurements on paper samples.

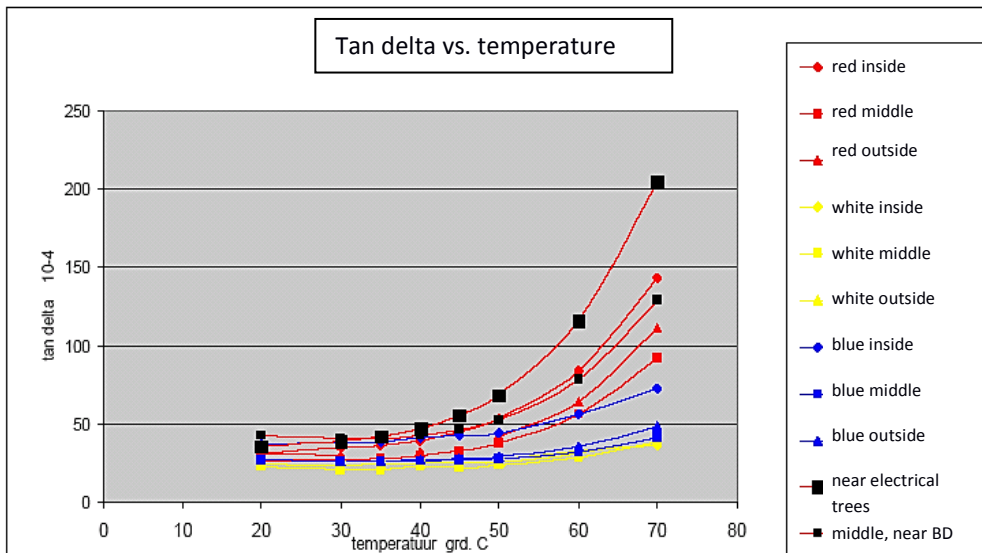


Figure: 6.17: Dielectric loss measurements for the paper samples taken from the faulty cable phase L1 and healthy cable phases L2 and L3. Plot description: red plots represent phase L1, yellow-L2, blue-L3.

The results presented in Figure 6.17 show the increased losses as a function of the paper sample temperature. All the samples taken from the faulty cable phase show higher losses than the healthy phases. Moreover, at a low room temperature of 20°C, samples from the faulty cable phase also reflect higher losses than from healthy cable phases. Based on the results of the Schering bridge measurements, it can be concluded that the increased dielectric losses can be an indicator of the progressive insulation ageing (electric treeing) and upcoming failure. During DAC voltage diagnosis, the temperature of the cable is relatively constant (ground temperature), but the tested voltage can be controlled and the results of the measurements can be directly compared with three cable phases. Moreover, a good reason for using the DAC system is the compact size and high level of test voltage (150 kV_{peak}). The compact size allows the installation of the DAC system in small sub-station buildings close to the cable terminations. This helps to reduce the background noise during PD measurements. However, the major reason for selecting DAC system was an option to conduct PD and dielectric loss in parallel. The parallel PD and dielectric loss diagnosis significantly reduce total diagnosis time. This last feature was especially important due to the weather conditions (fast changing) and limited time available on site for testing activities.

6.3.1 Procedures for onsite diagnosis of service aged cables with DAC

Along with the technical specialists from DSO and TSO, the preliminary test procedures regarding DAC test voltage levels and numbers of DAC excitations were developed after several initial on-site tests on 50 kV cables and 150 kV cables. Univocal test procedures are needed when performing on-site cable diagnosis, due to the following reasons:

- Setting the fingerprint (reference) of the cable insulation-PD and dielectric loss measurements performed for the first time on cables shall be repeated in the same way in each cable phase. Comparison between measurement results shall be possible, e.g., after 10 years at the same voltage levels and number of DAC excitations for a particular cable.
- Evaluation of the cables are based on the comparative basis. On-site PD levels and dielectric loss measurements are not standardised parameters and there are no reference values available.

Other factors, also taken into consideration during DAC testing and diagnosis, are test voltage requirements of the national (NEN 3630 norm) and international IEC standards (IEC 60840) presented in Table 6.4. According to NEN 3630 the acceptance test on newly installed cables shall be performed on 50 kV rated cables ($U_0 = 28 \text{ kV}_{\text{RMS}}$) with $2.5 \times U_0$ for 10 minutes. IEC 60840 requires $2.0 \times U_0$ for 60 minutes. Both tests shall be performed with AC resonance test voltage in the frequency range:

- NEN 3630 range of 25-200 Hz.
- IEC 60840 range of 20-300 Hz.

Neither of these standards were referred to for the DAC voltage application nor the test parameters for the maintenance or the diagnostic test. Only one recommendation is provided in IEC standard: *"For installations which have been in use, lower voltages and/or shorter duration may be used. Values should be negotiated, taking into account the age, environment, history of breakdowns, and the purpose of carrying out the test"* Based on this advice from the IEC standard, service history and experience in MV voltage cable DAC diagnosis, the test voltage range was decreased to the value of $1.7 \times U_0$ for 50 kV cables and $1.3 \times U_0$ for 150 kV cables diagnosis. Due to the fact that the goal of the investigation was the non-destructive assessment of the insulation and not the bulk insulation withstand testing, also the number of DAC excitations at the maximum test voltage level was reduced to $10 \times \text{DAC}$. Only for 3 cables with the lowest number of weak spots, VWD consisting of $50 \times \text{DAC}$ excitations were performed to check the PD behaviour over time at $1.7 \times U_0$. For 150 kV gas-pressurised cables VWD were performed with only $10 \times \text{DAC}$ excitations in order to collect PD data.

Table 6.4

Test voltage levels for acceptance and maintenance/diagnostic tests according to IEC60840 and NEN3630 and tests voltage levels for investigation purpose.

Rated Voltage U [kV]	U ₀	Voltage test after installation (kV _{rms}) new cable Ref.: IEC60840	Voltage test after installation (kV _{rms}) new cable Ref.: NEN3630	Voltage test level used in the investigation for DAC testing and diagnosis (kV _{rms})
45-47 (50)	26 (28)	52	65	50-1.7xU₀
60-69	36	72	90	
110-115	64	128	160	
132-138	76	132	190	
150-161	87	150	217	106-1.3xU₀

For the diagnostic purpose the following procedure was used (Figure 6.18):

- 1) Slow voltage increase. From 0 kV every 0.2xU₀ (ΔV_T)-step up.
- 2) At each voltage step 3xDAC excitations (N_{DAC}) were performed. PDIV, PD levels and PD phase-resolved patterns, dielectric loss values were collected and analysed.
- 3) At U₀ evaluation of PDs is done by means of TDR analysis (Figure 6.18). Information about the indication of weak spots, e.g., in cable joints, or cable parts decision was provided. Based on this information a decision on whether an increase of the test voltage to maximum level and executing short-monitored voltage withstand test or stop the test could be given.
- 4) Execution of the short monitored voltage withstand diagnostic test (VWD): 10xDAC or 50xDAC excitations (only for a few cables).
- 5) De-energising (reducing test voltage to 0 kV).
- 6) Grounding of the cable by use of the external earth-stick.

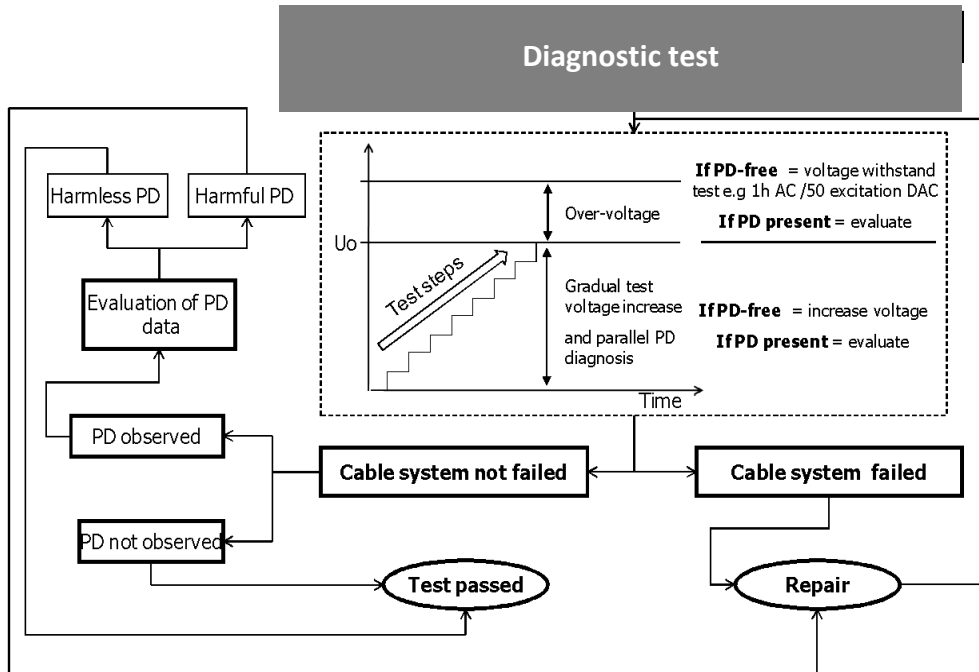


Figure 6.18: Flowchart presenting general procedure and decision process for the diagnostic tests performed with DAC voltages.

In the following sections an example of DAC diagnosis on 50 kV Circuit no. 4 are presented. The historical service data of this circuit, installed in 1989, reported 2 leakages recorded in 1992 and later in 1998. The investigations confirmed mechanical factors (third party) as the source of the sheath damage. After sheath repairs, each time, 5 kV DC test was performed to confirm the sheath continuity. No diagnostic test or measurements were reported during the maintenance and service of this cable. Up till 2007 no failure was recorded in this cable.

6.3.2 PD vs. Test voltage (50 kV Circuit no. 4)

Test voltage was increased every $0.2 \times U_0$ up to $1.0 \times U_0$. The increase in PD level was observed at each step in a tested cable. At the beginning of the test, the PD level was rather low and equal to 75 pC at $0.4 \times U_0$, with a maximum PD level of 250 pC at U_0 . The higher the voltage used, the higher PD amplitude was observed with a stronger concentration in several spots, mainly cable joints. The diagnosis showed that this cable was not PD free below nominal voltage U_0 and PDIV was in the range of $0.8 \times U_0$. Therefore it was concluded that during the cable operational service, PD sources are active, which directly increases the risk of unexpected breakdown and cable failure during operation. After a brief TDR analysis, the decision was made to increase the test voltage. In this situation the maximum test voltage was $70 \text{ kV}_{\text{peak}}$ ($1.7 \times U_0$). Due to the aged status of the cable, the voltage was increased in “small” steps $\Delta V_T = 0.1 \times U_0$. In parallel PD and dielectric loss were recorded (discussed further in this section). Figure 6.19 presents PD characteristics for all three phases.

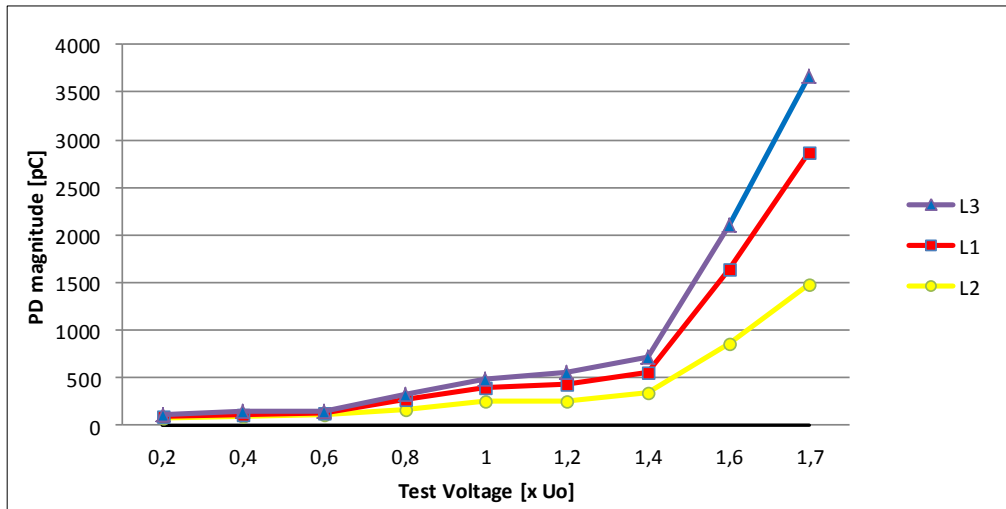


Figure 6.19: PD vs. Test Voltage of Circuit no. 4. Similar PD behaviour is observed. PDIV was similar for all phases but the highest PDs localised in cable joints were in range of 3,5 nC in cable phase L3.

6.3.3 PRPD patterns (50 kV Circuit no. 4)

PRPD patterns were asymmetric at each voltage level up to $1.7 \times U_0$. The observed pattern showed a similar pattern for each cable phase L1, L2, L3. The observed phase-resolved PD patterns were obtained at DAC frequency of 55 Hz. Asymmetric patterns might be a pattern related to the small cavities or an electric treeing (small volume) in impregnated paper insulation. The cavities close to the low voltage side are usually represented by an asymmetric pattern that occurs in the first and third quarter of AC sine voltage cycle [56]. At the beginning, the pattern is asymmetric with much higher PD amplitude observed in the first quarter. At the higher test voltage, an additional number of PDs are released also in a negative third quarter of AC voltage cycle (Figure 6.20).

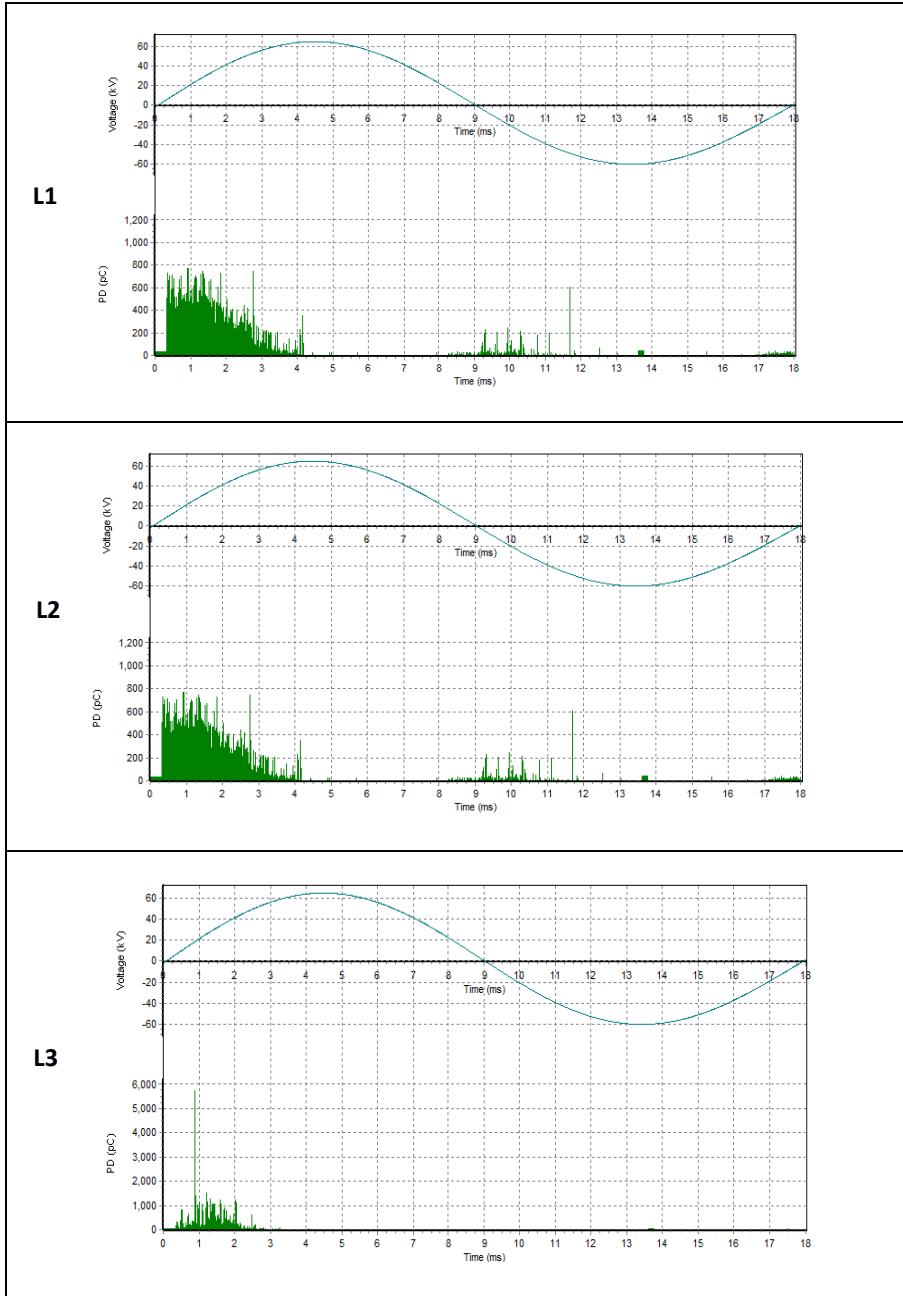


Figure 6.20: PRPD patterns for Circuit no. 4 phase L1 L2 L3 observed at $1.7 \times U_0$. Note: these are patterns taken from a random single DAC excitation.

6.3.4 TDR traces (50 kV Circuit no. 4)

TDR traces for the observed PDs were clear. Low background noise level, in the range of 25 pC, and no other external disturbances, resulted in a relatively easy analysis of PD signals. In Figure 6.21 we can see an example of the reflection resulted from the incident pulse, originating from a distance of 738 m from the near cable end (location of the DAC system connection). The first incident pulse is wide and this means that that pulse was traveling through the cable and was attenuated, however, the amplitude is much higher than the first reflection pulse that was traveling in the cable much longer and was reflected from the cable far end. Amplitude is approximately 900 pC at $1.6xU_0$. The shape and the polarity remains the same for both incident and reflection pulses. Automatic calculation of the distance to PD source indicated cable joint no. 2-counted from the near cable end. Similar clear TDR traces were obtained for other three PD sources at the distance of 250 m, 1360 m and near cable termination (0 m). PD mappings are presented in the next section.

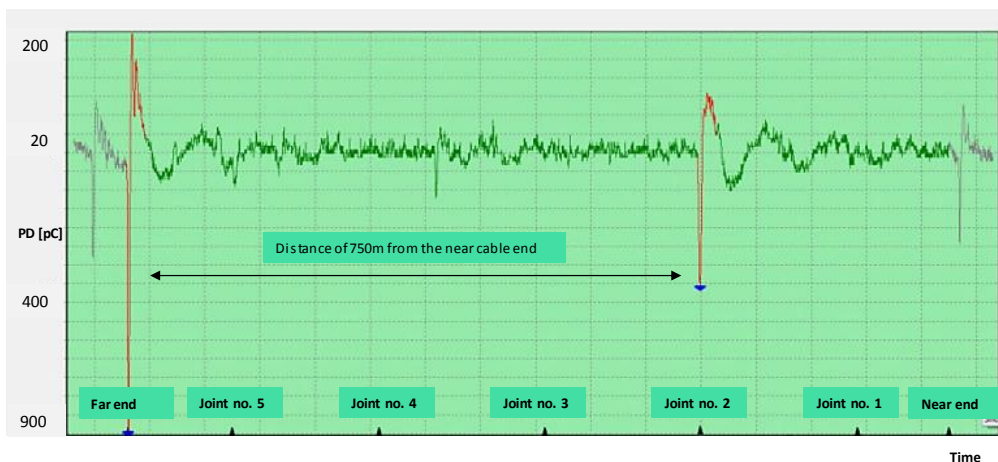


Figure 6.21: Example of TDR traces for PD pulse of 900 pC detected at $1.6xU_0$ in Circuit no. 4.

6.3.5 PD mapping (50 kV Circuit no. 4)

Over-voltage conditions confirmed 4 weak spots which were localised at U_0 (PD concentration at 4 locations). At over-voltage between $1.4xU_0$ and $1.7xU_0$, the PD amplitude was increased rapidly for each cable phase starting from 900 pC up to 1600 pC. PD phase-resolved patterns and TDR analysis showed clearly PDs in the cable termination L1 and cable joint at locations no.: 1, 2, 4, mainly in cable phase L2 and L3. This information was important for the cable owner. Based on the weak spots location and PDIV levels and PD amplitude, a decision about voltage withstand test could be taken to check PD characteristics over time. The withstand test could result in, e.g., a controlled weak spot breakdown or could indicate more weak spots in the cable. In Figure 6.22, a cumulative PD mapping for all cable phases is presented. The mapping was obtained based on the 10xDAC excitations and PD analysis at $1.0xU_0$ and $1.7xU_0$. Analysis of PD mapping indicated the first weak spot located at the cable termination (PDIV= $0.9xU_0$) in cable phase L1 with the maximum amplitude of 90 pC. The second weak spot was localised by increasing PD amplitude (PDIV = $1.0xU_0$) and strong PD intensity in the

location near joint no. 2 at a distance of approx. 750 m (phase L2) in cable phase L2. Furthermore, an increase of PD amplitude was observed with an increasing test voltage level. The TDR analysis resulted in localisation of PD sources in cable phase L2 and L3. The third weak spot was located 240 m from the near cable end close to joint no 1. PDIV was $1.0 \times U_0$, but the maximum PD amplitude was relatively low-650 pC. This weak spot was localised only in cable phase L2.

A fourth weak spot was localised at approx. 1450 m from the near cable end close to cable joint no. 4 with a maximum PD amplitude of 1500 pC and PDIV= $1.3 \times U_0$, and the increasing PD concentration for cable phase L2 and L3 up to $1.7 \times U_0$. Historical data of sheath faults confirmed that localisation of the sheath damage in year 1998 was at a close distance to joint no. 4. However, the first sheath damage recorded in year 1992 was at a distance of approx. 500 m.

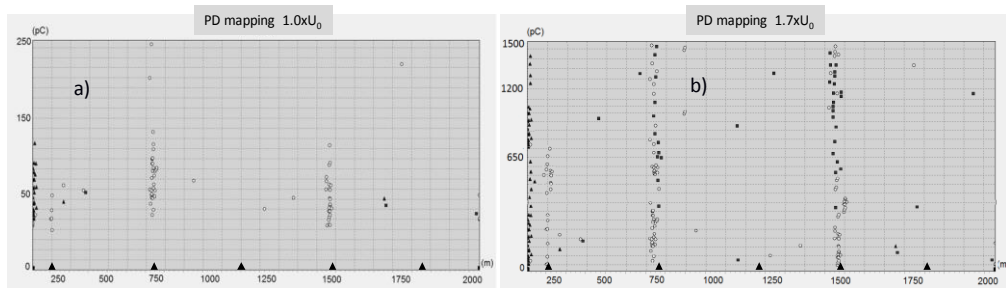


Figure 6.22: PD mappings for 50 kV circuit no. 4 made in the year 2008: a) PD mapping up to U_0 b) PD mapping up to $1.7 \times U_0$. Agenda for PD mapping: large triangles represent cable joints, small triangles cable phase L1, circles cable phase L2 and rectangles cable phase L3.

6.3.6 Dielectric loss (50 kV Circuit no. 4)

Dielectric loss values were measured at 40 kV, 50 kV, 60 kV and 70 kV. One of the methods to measure dielectric losses is the estimation of dielectric loss increment or decrement called: delta $\text{tg}\delta$ ($\Delta\text{tg}\delta$) between two test voltages. To obtain a better impression of the measured values, the values of dielectric loss at $40 \text{ kV}_{\text{peak}}$ up to $70 \text{ kV}_{\text{peak}}$ were plotted in for each measured cable phase (Figure 6.23). In this particular case the dielectric loss values were in the range of 0,30% up to 0,49% (30×10^{-4} and 49×10^{-4}). Dielectric losses for the healthy insulation should not differ between the cable phases as they are covered with the same lead sheath and the same oil is circulating between them. Based on the reference [62], the dielectric loss should not exceed 35×10^{-4} (0,35%) for new insulation at U_0 and 43×10^{-4} (0,43%) at $2.0 \times U_0$ for 50 kV oil-filled mass-impregnated cables (measured with 50 Hz AC bridge method). Additionally, for increased test voltage level starting from $1.0 \times U_0$ up to $2.0 \times U_0$ $\Delta\text{tg}\delta$, it should not increase more than 10×10^{-4} .

Based on the dielectric loss measurements performed on Circuit no. 4 (Figure 6.23) we can conclude the measured values of dielectric loss were low (below IEC reference values) at U_0 and probably higher than the reference value at $2.0 \times U_0$ (maximum test voltage was $1.7 \times U_0$). Calculation of difference of losses between $1.7-1.0 \times U_0$ ($\Delta\text{tg}\delta$) was also exceeded, compared to the IEC reference.

It must be noted that measurements were performed on 20 years old cable with 2 sheath problems reported. Moreover, the measuring method is completely different. Dielectric loss measured with DAC voltage is based on the damping factor of the cable, whereas at 50 Hz AC factory test a Schering Bridge is used.

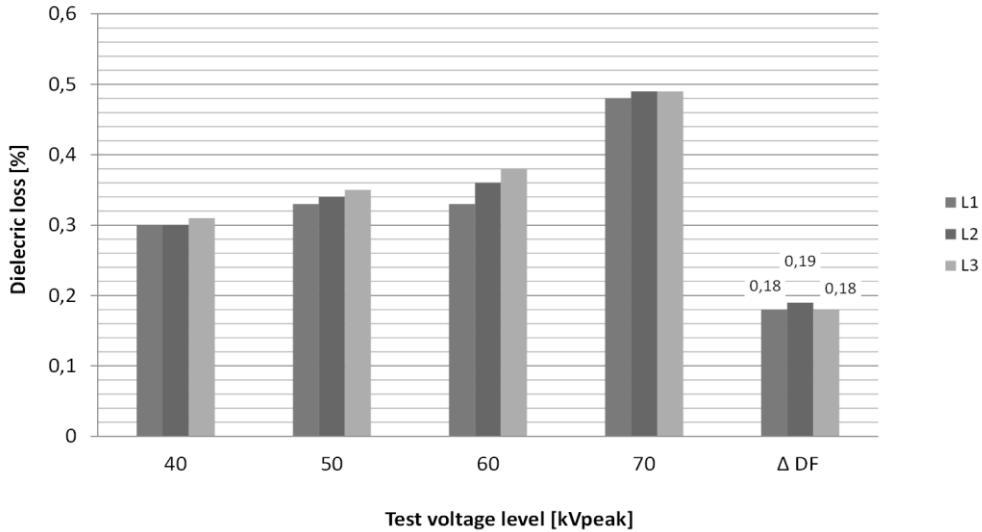


Figure 6.23: Dielectric loss and $\Delta tg\delta$ — measured between 40 kV (U_0) and 70kV ($1.7xU_0$) for Circuit no. 4 with DAC voltages.

6.3.7 Voltage Withstand Diagnosis (50 kV Circuit no. 4)

The main goal of the withstand voltage is the insulation test at over-voltage conditions. Pass/no-pass criterion is based on the breakdown result. Voltage Withstand Diagnosis (VWD) is the same test, but an important aspect is the impact of time for the diagnostic parameters characteristics. With the DAC voltage system withstand test, diagnosis is performed using PD and dielectric loss measurements at the same time for each single DAC excitation. It was interesting for our investigation to check whether a higher number of DAC excitations, e.g., 50 instead of 10 could also result in a higher PD amplitude or more PDs observed and localised in the cable. However, the major question was: can DAC voltage create a breakdown at the test voltage level of $1.7xU_0$ in the weakest spot of aged 50 kV oil-filled cables? Based on the test results of the newly installed HV and EHV XLPE cables (discussed in section 6.1 and 6.2), it was shown that this electric stress level had been high enough to create a breakdown in a faulty pre-moulded 220 kV joint. However, the paper insulation impregnated with oils has the unique ability to “re-heal” itself. This can happen when the carbonised paths of the insulation or burned-out insulation spots are re-filled with the oil that circulates in the cable. A dielectric liquid (oil) “repairs” faulty insulation and decreases PD activity. This is not the case in XLPE cables. As a result, a heavy aged mass-impregnated insulation has a high dielectric breakdown strength even in aged condition [2, 3, 4].

Further in this section it was shown that the breakdown of the insulation did not occur in Circuit no. 4 during withstand testing with 50xDAC. PD amplitude and PD concentration were

increasing within the testing time of 15 minutes (necessary to execute 50xDAC excitations). From the PD observation and TDR analysis, it was concluded that the PD amplitude increment is related to PD sources localised in the position of joint no. 2 and 4. PDs amplitude increment counted at the beginning and the end of the VWD was 100%. Additionally, it can be observed (Figure 6.24) that dielectric loss characteristics are relatively low and stable during 50xDAC excitations. Absolute maximum values equal to 49×10^{-4} (0,49%) were measured.

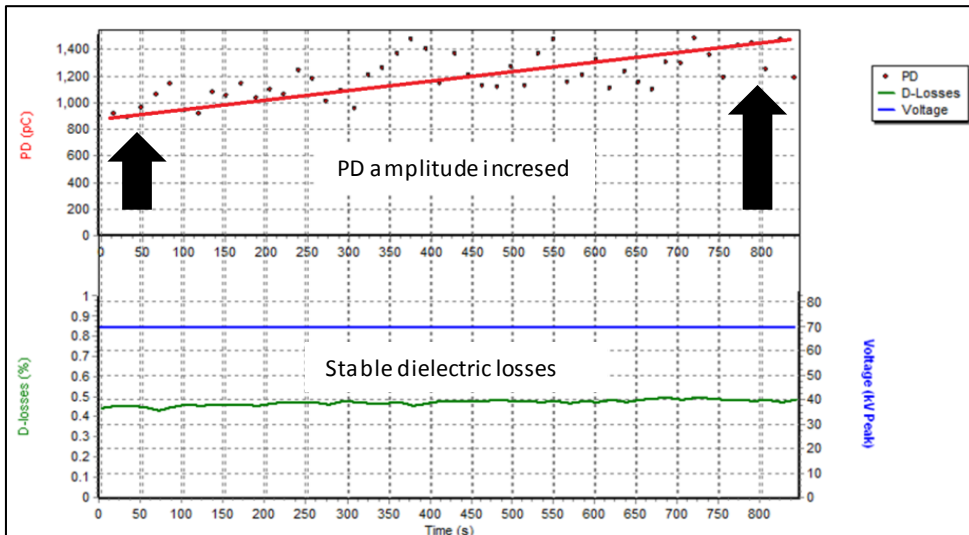


Figure 6.24: Voltage Withstand Diagnosis (VWD) results. Year 2008.

The conclusion derived from the diagnostic test was to repair faulty joints and replace the oil in the termination. After the joint repair and the maintenance of the oil-filled terminations, a decision was taken to repeat the diagnostic test on this particular cable in 2009, 10 months after appropriate repairs. The VWD test results are presented below in Figure 6.25. The diagnostic test performed 10 months after the faulty joint replacement confirmed only one weak spot (joint no. 1) located 250 m from the near cable end. The PD amplitude during voltage withstand test increased after approx. 7th minute rapidly from an average value of 350-300 pC to approximately 600 pC (Figure 6.25).

The dielectric loss measured during voltage withstand test was also lower than in the year 2008. A decrease from 0,49% to 0,38% (at $1.7 \times U_0$) was recorded. Lower dielectric loss absolute values can be explained by two factors:

- Cleaning of the termination and fresh insulation oil in the terminations.
- Faulty joints were removed or repaired (no available information).

As a result almost PD free conditions were obtained.

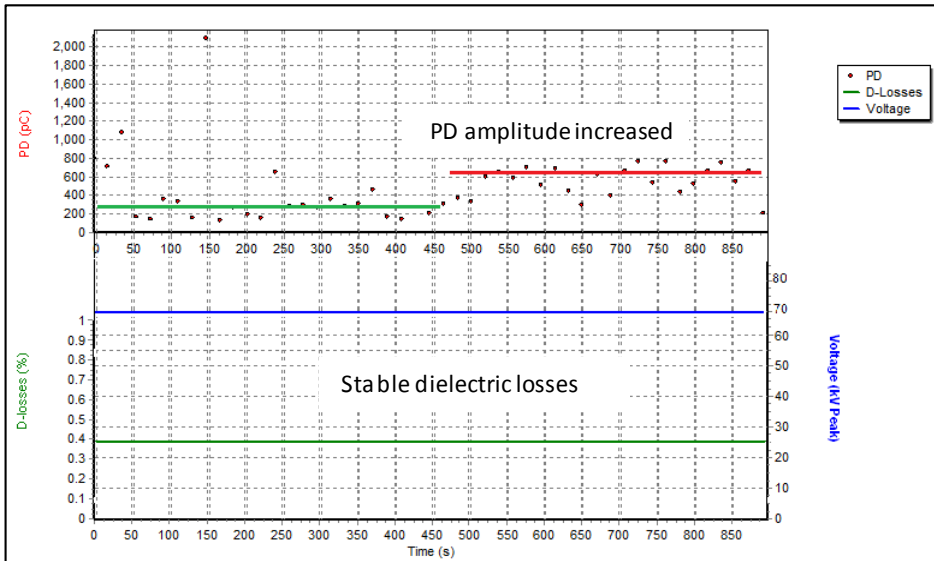


Figure 6.25: Voltage Withstand Diagnosis (VWD) results after repair. Year 2009.

6.4 Overview of the diagnostic results of 13x50 kV oil-filled cables

General

A total of 13 cable circuits had been diagnosed with the DAC system. PD measurements and dielectric loss measurements combined with VWD test provided information about general cable conditions and local weak spots. All of the 50 kV cables investigated in this project were not PD free. The second interesting conclusion was the fact that about 60% of the diagnosed cables represented low dielectric loss compared to, e.g., IEC 60183 reference values. However, more than 60% of the 50 kV cables had a PDIV below U_0 . The third conclusion was: the analysis of the cables installed in 1989 (the youngest cables) showed the lowest PD levels among all the cables and in 3 out of 4 cases, showed the lowest and almost equal dielectric losses for cable populations installed in 1989. The TDR analysis of recorded data showed that the PD localisation had occurred equally in the cable joint and cable insulation (Figure 6.26). The oldest cables represented the highest dielectric losses but not the highest PDs. The observed PDs in the oldest cables always had the strongest PD concentration of localised PDs. No breakdowns were recorded during VWD at the voltage level of $1.7xU_0$ in any of the tested cables. The correlation between the historical sheath damages and weak spots in the insulation was not confirmed in each tested cable. The locations of the damaged lead sheath were in the range of the PD weak spot localisation for 5 of 13 cables. It must be noted that PD localisation accuracy is around 1% of the cable length.

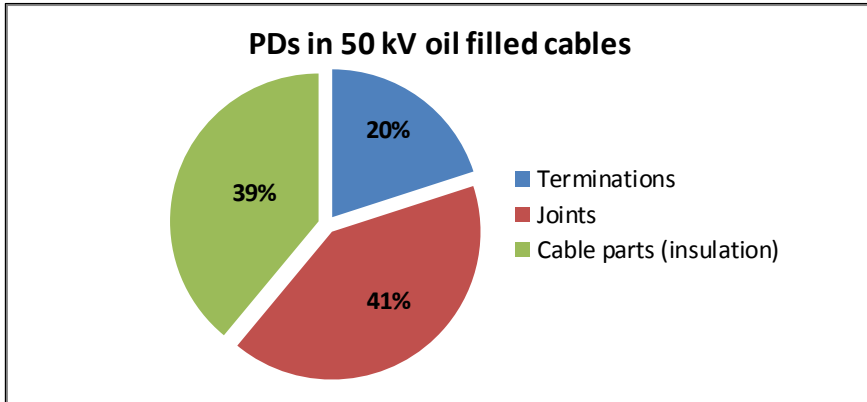


Figure 6.26: Statistics of the PD detection and location in 50 kV oil-filled cables per component. Results based on DAC voltage diagnosis up to maximum test voltage of $1.7 \times U_0$.

PDIV

Partial Discharge Inception Voltage is a very important parameter, as it indicates if the insulation defects remain active at the operational voltage- U_0 , or have become visible above operational conditions. Any cable with a PDIV below U_0 is potentially unreliable as the pre-breakdown conditions take place during operational voltage. Our investigation showed that 61% of total population of diagnosed 50 kV oil-filled cables had a PDIV below U_0 . This situation relates to PDs that were not only detected but also analysed by TDR analysis. In other words, the internal PDs localised in the cable insulation and not, e.g., external PD as corona on the cable terminations. In Figure 6.27, the PDIV analysis is presented.

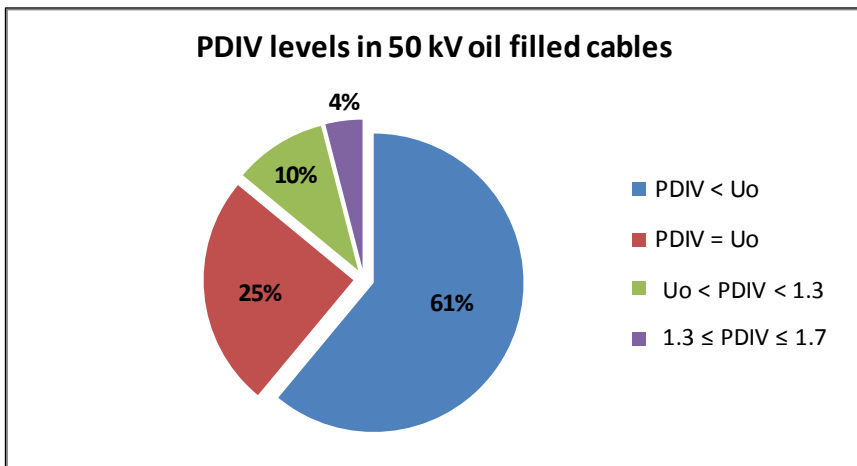


Figure 6.27: Statistics of PDIV of 50 kV oil-filled cables. Results based on DAC voltage diagnosis up to maximum voltage of $1.7 \times U_0$.

PD magnitude

The measurement of PD amplitude was performed at each voltage level, starting from 0 kV with increments of $0.2 \times U_0$ up to $1.7 \times U_0$. The evaluation was done on two test voltage levels:

U_0 and $1.7 \times U_0$ (phase-to-phase voltage). Only localised PD were taken into consideration. Corona PD or external disturbances were filtered out and rejected. The average PD magnitude was calculated based on 3xDAC excitations per voltage level. Four of the cables that were diagnosed were 19 years old at the time of testing in 2008. These cables showed the lowest PD magnitudes in comparison to the total population of cables in this investigation. The oldest cable was 50 years old, however, this was not the cable with the highest recorded PDs but with the highest dielectric losses (shown later in this section). Figure 6.28 presents PD magnitudes for all cables.

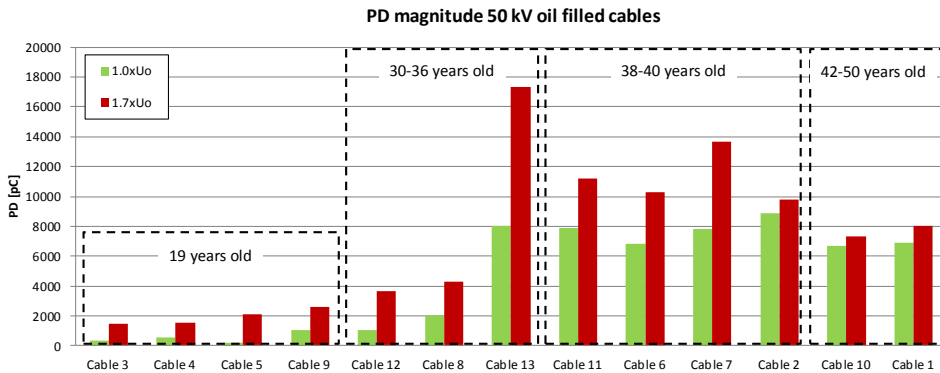


Figure 6.28: The average PD magnitude of 50 kV oil-filled cables measured at two voltage levels.

It can be derived from the analysis presented in Figure 6.28 that for cables that are longer in service, the difference between PD level at $1.0 \times U_0$ and $1.7 \times U_0$ is smaller. The highest PD magnitude was observed in 36 year old circuit no. 13 localised in the cable joint. For cables with an age between 38 and 40 years, the PD magnitude is usually 1/3 lower at $1.0 \times U_0$. The oldest circuits show a very small difference of PD magnitude between two voltage levels: $1.0 \times U_0$ and $1.7 \times U_0$. The analysis of cable sheath faults and PD magnitude showed that circuit no. 13 with the highest PD magnitude had the highest number of sheath problems in the past-total of 5 leakages.

Dielectric loss

The measurements of dielectric loss were taken on 4 levels: $1.0 \times U_0$, $1.2 \times U_0$, $1.5 \times U_0$, $1.7 \times U_0$. At each level the average value was calculated based on 3xDAC excitations. The analysis of the dielectric loss absolute values has shown that the maximum differences between particular cable phases L1, L2, L3 of the same cable (at the same test voltage level) are in the range of 10%. Due to this fact, Figure 6.29 shows the average of 3 phases dielectric loss values as measured for each particular test voltage level. The youngest cables represent the lowest losses of the whole population of 50 kV cables. Only circuit no. 4 has higher losses than older cable No. 12 and 8. An interesting behaviour was observed for the cables in the range <36-42> years old. The loss increase between $1.0 \times U_0$ and $1.7 \times U_0$ doubled for a total of 5 cables No.: 13, 11, 6, 7, and 10. The highest losses were represented by circuit no. 10 (42 years old). General dielectric loss behaviour among the aged cables was confirmed: the older the cable, the higher the losses. We have also concluded that, in spite of the long service life, 60% of the tested population of 50 kV oil-filled cables represented relatively very good integral condition

of insulation. A deviation between measured values for each particular cable phase at one voltage level was not higher than 10%.

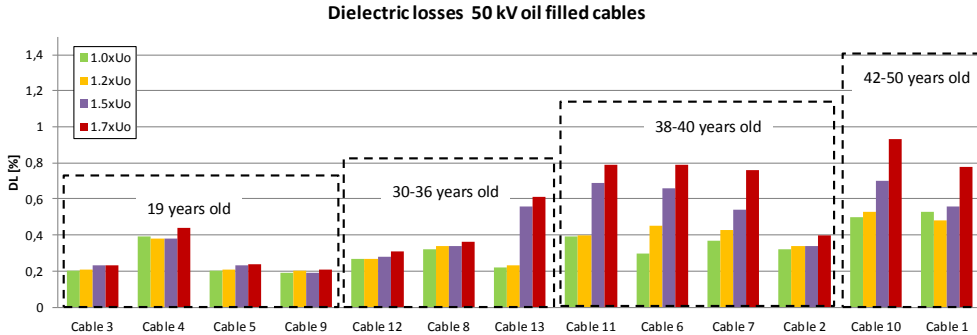


Figure 6.29: The average dielectric loss at four test voltage levels per tested 50 kV oil-filled cable.

6.5 Overview of the diagnostic results of 9x150 kV external gas-pressurised cables

General

Among a total of 9 diagnosed circuits, only 4 out of 9 weak spots were pointed by concentrated PDs. However, concentration of recorded PDs was not strong (less than 6 single PDs per location). Most of the localised PDs were in cable terminations (Figure 6.30). 100% of localised PDs detected in 4 out of 9 circuits had a PDIV above the nominal voltage U_0 and in the remaining 5 circuits no PDs were detected. The PD mappings of the external pressurised cables showed the scattered character of the observed PDs characteristics, rather than concentrated (weak spots) PD characteristics. The highest PD amplitude of 405 pC was observed in Circuit no. 4. Dielectric loss measurements performed at U_0 for all cables were higher than 34×10^{-4} (reference for paper cables in IEC 60183 standard). The lowest losses of Circuit no. 2 installed in 1995 (the youngest diagnosed cable) were 0,34% (34×10^{-4}) at U_0 , and 0,41 (41×10^{-4}) at $1.3 \times U_0$. Likewise 50 kV oil-filled cables, 150 kV gas-pressurised cables show low values of detected PDs and relatively low losses which confirms a good condition of the measured cables. A more detailed analysis is presented later in this section. In general PD behaviour was different for the 150 kV gas-pressurised cables to the 50 kV oil-filled cables. The measurements showed the following relation: the increase of test voltage was not a result of a stronger PD concentration, but in more dispersed PDs over the cable length. Based on the 4 circuits with localised PDs, more detailed information was obtained for each cable, in which PD were localised.

The oldest Circuit no. 1 was 54 years old at the moment of diagnosis in 2010 and showed the lowest PDIV of $1.1 \times U_0$. PDs were localised at a close distance to a cable joint, concentration of PDs was very low-only 3 single PDs. At higher voltages usually scattered PDs were detected and localised in the whole cable length without concentrations, with a maximum PD level of 290 pC.

Circuit no. 3 which was 39 years old at the moment of diagnosis in 2009 has shown PDs in terminations. The inception voltage was $1.3xU_0$ and due to the fact that we were not able to increase the test voltage above this level, it was not possible to give more conclusions about PD characteristics (PD levels and concentrations). At PDIV there were only 4 single PDs localised in the termination of cable phase L1 and 3 single PDs in cable phase L2 and L3. The maximum PD level of the detected PDs was 190 pC.

Circuit no. 4 was 37 years old at the moment of diagnosis in 2007. Based on the PD analysis it was concluded that the condition of this cable was the worst of 9 cables diagnosed with DAC voltages. PDIV was $1.2xU_0$, and relatively high PD were recorded in the cable termination, insulation part (2 weak spots) and at the far end terminations of the cable phase L2. The PDIV PD level was 150-200 pC. After increasing the test voltage up to $1.3xU_0$, the voltage increment between PDIV and $1.3xU_0$ was $12 \text{ kV}_{\text{peak}}$, PD amplitude has increased up to 350-450 pC. The PDs were concentrated in 2 different locations: 360 m and 3200 m counted from the place of the connection of the test system. The concentration of observed PD was 3-6 PDs per location.

Circuit no. 8 was 33 years old. The PDIV level was $1.3xU_0$ with a low PD concentration at the distance of 2300-2400 m. All detected PDs were distributed randomly with the highest amplitude of 200 pC. Maximum 34 PDs were localised in cable phase L2 and L3. Cable phase L1 was PD free.

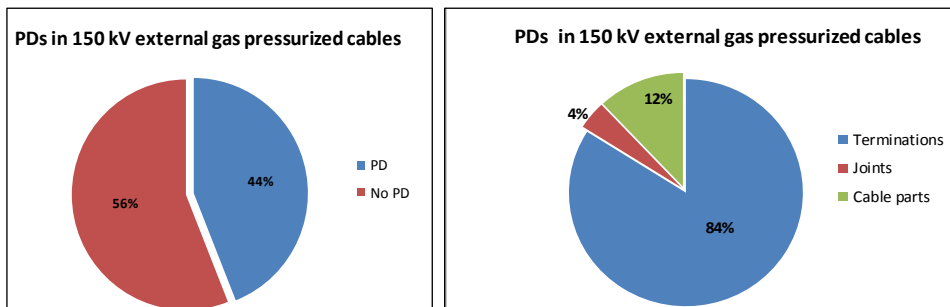


Figure 6.30: a) Statistics of the PD detection in 150 kV gas-pressurized cables. b) PD location in 150 kV gas-pressurized cables per component. Results based on DAC voltage diagnosis up to a maximum test voltage of $1.3xU_0$.

PDIV

All 150 kV gas-pressurized cables were diagnosed up to $1.3xU_0$. PDIV was above U_0 for each tested cable. Only 4 of 9 circuits showed PDs that could be localised through TDR analysis. PDIV levels were as follows:

- 1) Circuit no. 1- $1.1xU_0$.
- 2) Circuit no. 3- $1.3xU_0$.
- 3) Circuit no. 4- $1.2xU_0$.
- 4) Circuit no. 8- $1.3xU_0$.

Due to the relatively high PDIV levels and a small difference between the maximum test voltage, it was difficult to draw more accurate conclusions on PD characteristics, as was in the case of 50 kV oil-filled cables. We expect that, probably, by applying higher test voltages for the DAC diagnosis, more PDs could be detected. On the other hand, the goal of the project was a non-destructive condition assessment of the aged cables, which are very important energy transmission links between major substations in The Netherlands. Therefore, the risk of the potential breakdown had to be minimised by decreasing the maximum test voltage.

PD magnitude

The measurement of PD amplitudes was performed at each voltage level, starting from 0 kV with increments of $0.2xU_0$ up to $1.3xU_0$. The analysis of the obtained data confirmed the highest PD magnitudes for the oldest circuits. The oldest 51 year old circuit represented a lower PD level than the 37 year old circuit. Circuit no. 4 with the highest PDs also showed the strongest concentration of localised PD. The average concentration was 3-6 single PDs per location, whereas the remaining 3 cables represented a concentration of 2-4 single PDs per location. In Figure 6.31 the average PD magnitude is presented as measured for three DAC voltage levels.

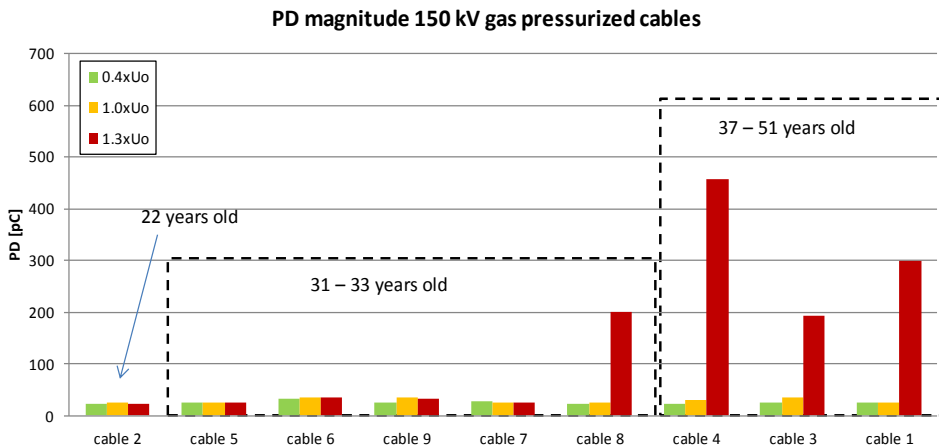


Figure 6.31: The average PD magnitude of 150 kV gas pressurized cables measured at three voltage levels.

Dielectric loss

The measurements of dielectric losses were performed at each voltage increment. For the analysis, the values measured at 3 voltage levels ($0.4xU_0$, $1.0xU_0$ and $1.3xU_0$) were compared with each other, and plotted (Figure 6.32). We conclude that dielectric losses observed in 150 kV external gas-pressurised cables are in the same range for the circuits between 22 and 33 years old. An increase of losses is observed in 3 of the oldest circuits. The 51 year old circuit shows the highest losses. Measurement deviations between particular circuit cable phases at one voltage level were not higher than 10%.

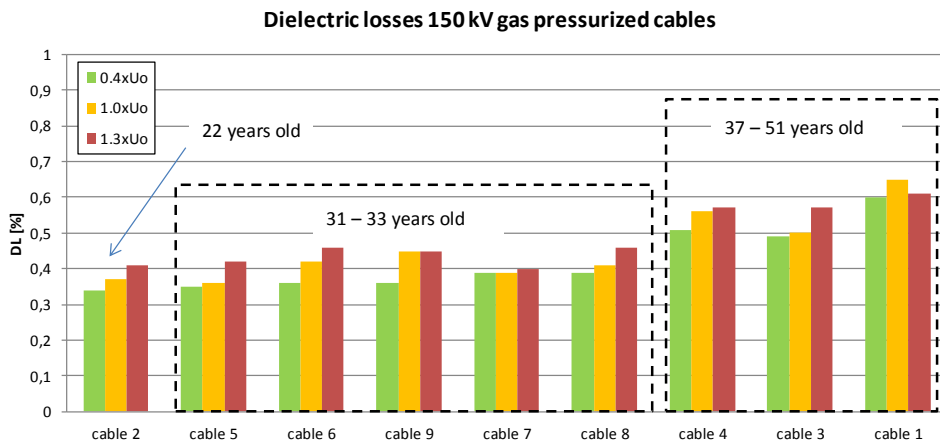


Figure 6.32: The average dielectric loss at three test voltage levels per tested 150 kV gas pressurised cable.

6.6 Conclusions

Application of DAC systems for on-site testing and diagnosis

- DAC voltages in correlation with the PD measurements can be used for after-laying on-site diagnostics and voltage testing for the newly installed HV and EHV power cables due to the following aspects:
 - For the newly installed XLPE cables, PD monitored DAC voltage testing provides information about the presence of PD, the location, and in the event of a harmful defect in the cable insulation or accessories, may finally result in a breakdown in the faulty component of the cable system.
 - TDR analysis performed on the recorded PDs in the time domain resulted in successful recognition and localisation of PDs source in 4.4 km long XLPE cable without the necessity of the over-voltage withstand test (PDIV of this particular defect was well below U_0).
 - On-site after-laying voltage test performed on 13.3 km long 127/220kV XLPE cable resulted in a breakdown in a faulty joint at $0.4xU_0$. The breakdown was followed by PD activity that could be traced with TDR analysis, and resulted in the correct localisation of the faulty component.
 - In both cases: 150 kV and 220 kV XLPE cables after-laying tests, the assumption that the voltage withstand test executed at the maximum test voltage level and performed as, e.g., 50xDAC excitation is not necessary in order to locate faulty components and provide information about the cable condition.
 - The compact size of DAC system and the high output voltage to system weight (approx. 750 kg) ratio makes such a system suitable for any onsite test applications.

- For aged cables with the oil-impregnated paper insulation, DAC voltage, in combination with PD IEC 60270 measurements and dielectric loss measurements, provides a powerful tool for the assessment of an aged cable system condition in the following aspects:
 - Local PD sources detection and localisation, where several related PD parameters can be described: PDIV, PD phase-resolved patterns, PD intensity, PD location. Trending evaluation of the diagnosis parameters is possible by setting a cable reference fingerprint.
 - The evaluation of dielectric loss results in the overall information of insulation condition at the moment of the test being performed (live)-direct results and cable phase comparison are possible.
 - Direct information about cable insulation weak spots (TDR analysis that can be performed during test execution) is available in order to create a weak spot mapping. Based on the obtained results, further testing action (e.g., continuing or ceasing the withstand test) can be taken.
 - Procedures for on-site testing of the aged cables can be adjusted to the actual condition of the cable. A high number of DAC excitations e.g. 50 are not always necessary to provide reliable information of the cable condition.

Evaluation of 50 kV oil-filled cables

- The condition assessment of 50 kV oil-filled cables did not confirm a correlation of PD related weak spot locations with the locations of the historical sheath faults for all cables. The correlation was confirmed in 5 of 13 cables, with an accuracy of 1% of cable length.
- DAC diagnosis showed that 61% of the whole population of tested cables had PDIV below operational conditions U_0 , and an unexpected breakdown in the insulation, or cable joint or termination can occur at any time under operational conditions.
- The highest and most concentrated PD was localised in the oldest cables (37 years and older).
- Dielectric loss measurements of the oldest cables (37 years and older) showed that the absolute values measured at U_0 are 90-100% lower than the values measured at $1.7xU_0$. These results confirmed a worse condition of these cables among other younger cables.
- No breakdown was recorded for any of the diagnosed 50 kV oil-filled cables at a test voltage of $1.7xU_0$.
- TSO activities regarding repairs or the replacement of the aged circuit can be successfully supported with DAC diagnosis. A good example is circuit no. 4. After the repair of the faulty joints and termination maintenance, dielectric losses and PD magnitude decreased significantly.

Evaluation of 150 kV external gas-pressurised cables

- PD and dielectric loss diagnosis confirmed a good insulation condition of 9 cables.
- In each of the diagnosed cables PDIV was below the nominal voltage U_0 . As a result, the risk of unexpected breakdown is much lower than for 50 kV oil-filled cables.
- The highest PD magnitudes and dielectric losses were observed in the oldest cables.
- The weak spots were localised only in 4 of 9 diagnosed cables.
- PD analysis resulted in the conclusion that the cable termination is the weakest part of the aged gas-pressurised cable due to PD presence.
- Cable insulation parts seem to be in a very good condition resulting in a scattered PD localisation (concentration less than 3 PD per location).
- Due to the fact that in all diagnosed cables the PDIV level was relatively high, further on-site testing and diagnosis could be performed at higher voltage levels, e.g., $1.7 \times U_0$ in order to get more accurate PD and dielectric loss characteristics.

7. LIFE TIME ESTIMATION OF SERVICE AGED PAPER-OIL INSULATED CABLES

It was shown in chapter 6 that dielectric loss measurements performed with DAC voltages can be used for condition assessment of aged cables. However, this approach is based on on-site diagnosis at a constant insulation temperature during testing. As it is known, dielectric losses strongly depend on the insulation temperature during operation [63, 64]. The temperature of the insulation may change with the load and soil thermal properties (cables directly buried). The increase of dielectric loss as a function of DAC electrical stress is observed on aged cables (Chapter 6), however, DAC diagnosis are performed with a constant temperature. During operational service of transmission cables, an important aspect is the increase of dielectric loss as a function of temperature (due to current load variations), while at constant electric field stress (Figure 7.1a / Figure 7.1b). As a result, two important aspects are considered in this section:

- What is the relation between changes of dielectric loss as a function of electrical field intensity $\tan \delta=f(E)$ and changes of dielectric loss as a function of temperature at a constant electric field $\tan \delta=f(T)$?
- How to obtain information about permissible future¹⁰ load when the actual insulation degradation and load history are known?

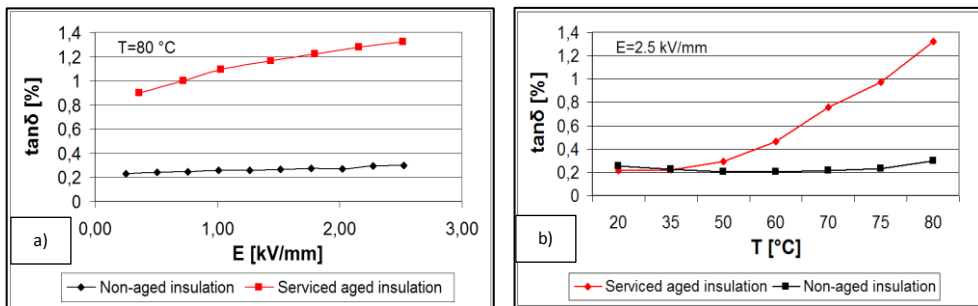


Figure 7.1 Comparison of dielectric loss behaviour for service-aged insulation and non-aged paper-oil insulation at different electric stresses (Figure a) and temperatures (Figure b). Plots present investigations at 50 Hz AC test voltage and dielectric loss ($\tan \delta$) measured with the Schering Bridge on HV cable paper insulation [65].

The second goal of the research presented in this chapter is the development of an asset management decision support tool (model) that can combine both: DAC on-site dielectric loss and diagnostic and operational data as e.g. cable load characteristics, soil properties.

A laboratory investigation on insulation ageing was conducted to understand typical $\tan \delta$ values for the various degradation stages of the paper insulation. As a result of this research, an insulation lifetime consumption model was developed which is based on dielectric loss as

¹⁰ Permissible load - load that allows safe and reliable cable operation in future for an expected period.

measured at different DAC test voltage levels. This model of insulation life consumption is called-ILC. A second insulation life consumption model is based on operational parameters e.g. past cable load history. The second insulation consumption model is called-OLC. The final (third) insulation life consumption model combines the output data of the ILC and OLC models and is used to classify the condition of transmission power cables and to estimate further the remaining life span of these assets, a model that combines all available parameters (operational and diagnostic) is called-total life consumption model-TLC . The general scheme of the three models is presented in Figure 7.2.

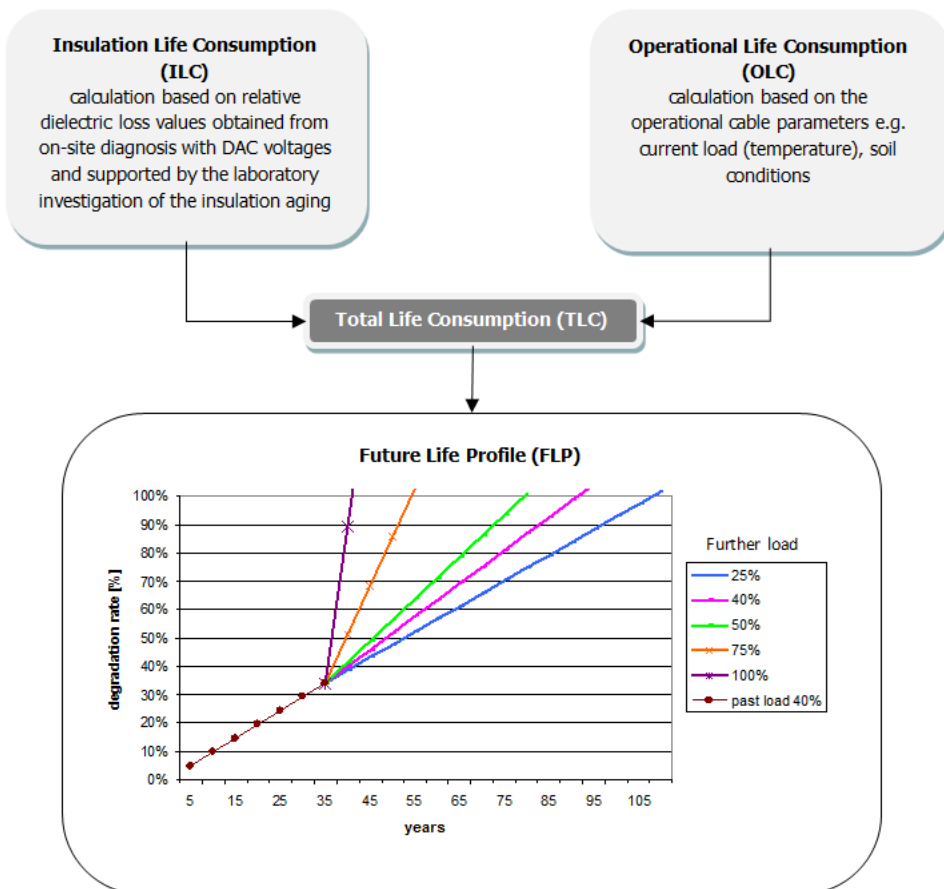


Figure 7.2: Structure of the remaining insulation life time estimation model.

7.1 Laboratory investigation on ageing phenomena of oil-impregnated paper cable insulation

For the purpose of the laboratory investigation two insulation samples were tested in order to develop knowledge of degradation of the insulation and correlated dielectric loss ($\tan \delta$) values:

- First sample-brand new oil-impregnated paper used for 150 kV cable insulation, 0.139 mm thick taken from the cable manufacturer of such cables,
- Second sample-taken from a 30 year old service-aged 150 kV gas-pressurised cable, after the breakdown in one of the cable phases. The sample was taken from a different spot in the vicinity of the breakdown.

In the lab $\tan \delta$ was measured on samples using a 50 Hz AC Schering Bridge (Figure 7.3). The test cell incorporated two flat electrodes, which together enabled controlled simultaneous thermal and electrical stressing of the samples. The electrical stresses (E) applied to paper samples was calculated from the equation [7.1].

$$E = \frac{U_0}{x(\ln \frac{R}{r})} \quad [7.1]$$

Where: x is the distance of the sample from the centre of the conductor (19 mm), R is the radius of the cable insulation (23 mm), and r is the radius of the conductor (10 mm), U_0 is nominal voltage of the cable-(87 kV).

A negligible increase in $\tan \delta$ was observed in the non-aged sample when the electrical stress was increased, contrary to the behaviour of the breakdown sample. Similar behaviour was observed in the dependence of $\tan \delta$ on temperature. This preliminary test gave us an impression about expected $\tan \delta$ values for new and aged insulation (Figure 7.1).

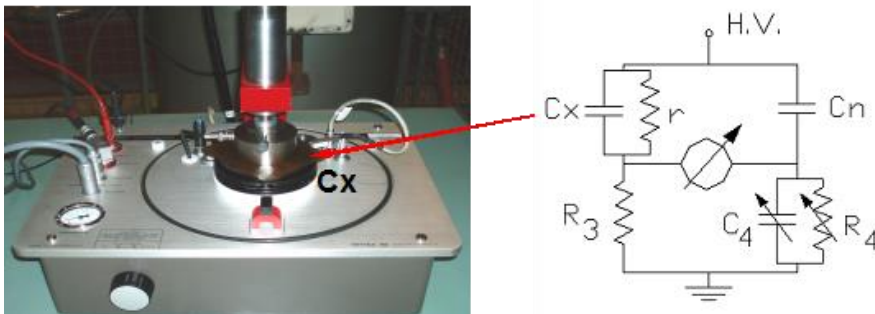


Figure 7.3: Schering Bridge setup with test object between electrodes. C_x -test object capacitance, C_n -standard, loss free capacitor, R_4 C_4 -elements for balance adjustment.

In the test setup, if a balance in the bridge is obtained, the loss tangent can be calculated by using formula [7.2] and values of R_4 and C_4 :

$$\tan \delta = \omega \cdot R_4 \cdot C_4 \quad [7.2]$$

Where: $\omega=2\pi f$, f-power frequency (50 Hz)

Ageing process

A 0.148mm thick insulation sample of a new, non-aged insulation, was subjected to accelerated thermal ageing (thermally controlled chamber). $\tan \delta$ was measured periodically as a function of the applied electrical field (E) and temperature (T). The applied electric field

strength was in the range of 0.7-6.1 kV/mm. This electrical field stress was selected for the insulation sample to simulate electric stress obtained during DAC testing in the voltage range between 0.09-0.84xU₀. In the field, PD and dielectric loss diagnosis are performed at higher voltages e.g. 1.3-1.7xU₀. In this investigation the goal was to find the correlation between dielectric losses and conditions of the cable below U₀ as it is not always possible to perform over-voltage conditions due to safety reasons on the diagnosed aged cables. In Figure 7.4 a schematic approach of tan δ measurements is depicted.

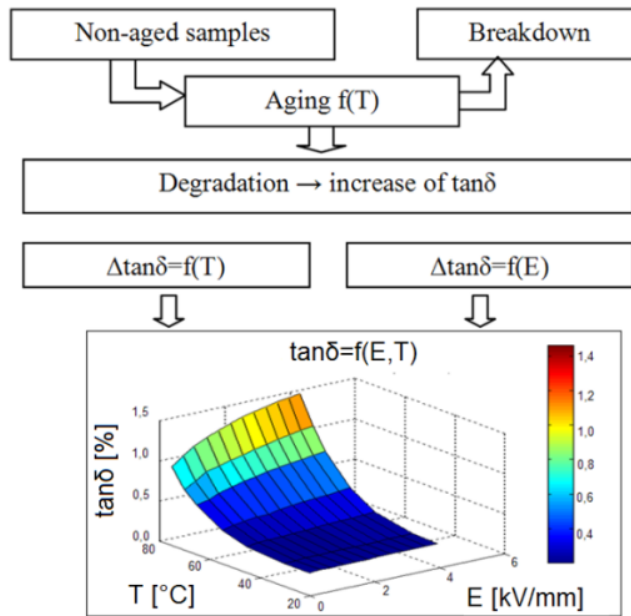


Figure 7.4: Schematic overview of the accelerated ageing and dielectric loss (tan δ) measurements.

The investigation on the insulation ageing took 225 days, and 40 samples were tested. 40 samples represented 40 stages of the life consumption of oil-impregnated paper insulation. The life consumption for these 40 samples was between 1% and 97% of total life consumption [65, 66]. During testing, both electrical and thermal stresses were controlled in the test setup. A temperature of 110°C was chosen based on the calculation of the life consumption that reaches 100%. The time necessary for the accelerated ageing was calculated with the Arrhenius model [68, 69]. The relation between degradation rate of cable insulation (thermal reaction rate) and temperature can be described by Arrhenius law. Arrhenius' equation gives the dependence of the rate constant of a chemical reaction on the absolute temperature, including a pre-exponential factor and other constants of the reaction. In the equation [7.3], the temperature has an exponential influence on the degradation rate k of the insulation.

$$k = Ae^{\left(\frac{-E_a}{RT}\right)} \quad [7.3]$$

Where: A is a constant, E_a is the activation energy of the ageing reaction, R is the universal gas constant (8.31 J K⁻¹mol⁻¹), and T is the absolute temperature.

In The Netherlands, the average yearly ground (soil) temperature T_g at the depth of the buried cable is approximately 10°C [101], T_c is cable temperature, which is given by formula [7.4]:

$$T_c = T_g + (T_{max} - T_g)(I/I_n)^2 \quad [7.4]$$

Where: T_{max} is the maximum permitted cable temperature, I is the load current and I_n is the nominal load current. Knowing the cable temperature for a given load, degradation of the paper insulation can be calculated with the Montsinger law which can be expressed with equation [7.5]. The law of Montsinger describes that at a certain temperature the insulation degradation doubles [68, 69].

$$D_y(T_c) = D_y \cdot 2^{\frac{(T_c-15)}{T_d}} \quad [7.5]$$

Where: $D_y(T_c)$ -is the yearly insulation degradation at cable temperature T_c , D_y is the average yearly thermal insulation degradation at 15°C, given by the cable manufacturer and T_d is the insulation temperature difference to get double insulation degradation. These two last parameters are different for different types of cables (Table 7.1). The fixed value 15 is the average yearly soil temperature in The Netherlands.

Table 7.1
Typical D_y and T_d values for different types of cables [TSO data base].

Cable types	T_d	D_y	T_{max}
External gas-pressure mineral oil cable	13°C	1%	60°C
External gas-pressure synthetic oil cable	21°C	1%	85°C
Paper insulated lead covered (PILC) cable	6,5°C	0,5%	43°C

T_{max} -is the maximum operational temperature for the cable.

For cables impregnated with mineral oil, $D_y(15)$ is equal to 1% (Table 7.2) and T_d is 13°C. A value of 60°C is considered to be the maximum allowable temperature advised by the cable manufacturers. Based on the calculation of the insulation lifetime expectancy at 60°C, the expected service life is 9,1 years. At 15°C, the lifetime expectancy for the mineral oil impregnated insulation is 100 years. In Table 7.2, the results of cable life expectancy calculation for the mineral oil external gas-pressurised cables is shown.

Table 7.2
Cable lifetime and yearly degradation and cable temperature calculated by load , at a constant ground temperature of 10°C.

Conductor temperature [°C]	Load [%]	Yearly degradation [%]	Life [years]
10,5	10	0,78	127
12	20	0,85	117
15	30	0,99	100
18	40	1,17	85
22,5	50	1,49	67
28	60	2	50
34,5	70	2,82	35
42	80	4,2	23
50,5	90	6,6	15
60	100	11	9,1

A temperature of 60°C corresponds to 100% of the nominal load of the cable, and the calculated life expectancy is approximately 10 years. In order to increase the chemical rate and ageing processes of the oil impregnated paper samples, a higher temperature of 110°C was selected. Based on the calculation with formula [7.5], it follows that a temperature of 110°C corresponds to 140% of the nominal load of the cable and the life expectancy at this temperature is approximately 7.5 months. This temperature was chosen for further laboratory research on the insulation ageing.

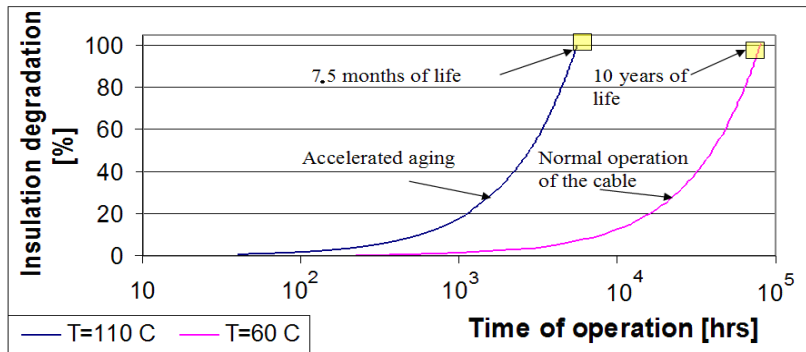


Figure 7.5: Oil-impregnated paper degradation in time at two different operational temperatures [67].

Interpretation of the results

At the first stage of the laboratory investigation, the behaviour of dielectric losses as a function of electrical field intensity for samples at constant temperature was measured. Then, the insulation temperature was increased and measurement was continued. Measurements of dielectric losses as a function of electrical field intensity performed on samples aged for different exposure time are depicted in Figure 7.6.

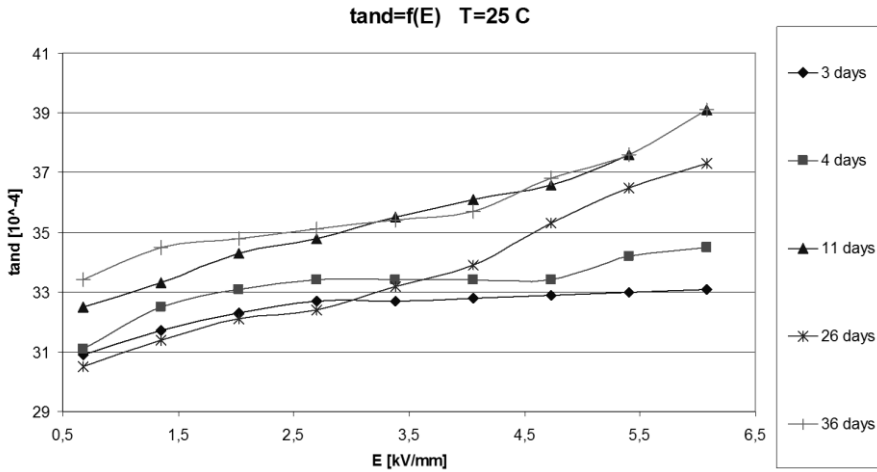


Figure 7.6: Example of dielectric loss behaviour as a function of applied electrical stress for samples subjected to ageing for different periods. Measurements were performed at a constant insulation temperature of 25°C.

It can be concluded from Figure 7.6, that for samples of insulation subjected to ageing for a longer time, the behaviour of dielectric losses is different from samples aged for a shorter time. For samples aged for a longer duration, a stronger dependency between the applied electrical stress and value of dielectric losses can be observed. $\tan \delta$ has higher values for more aged samples—as was expected.

In Figure 7.7, dielectric loss increments between two test voltages $0,09xU_0$ and $0,84xU_0$ at a constant temperature of 25°C are presented. The electric field was gradually increased from 0.7 to 6.1 kV/mm. It can be concluded from Figure 7.7 that $\Delta \tan \delta$ increases non-linearly with ageing time.

$$d \tan \delta (0,09U_0 - 0,84U_0)$$

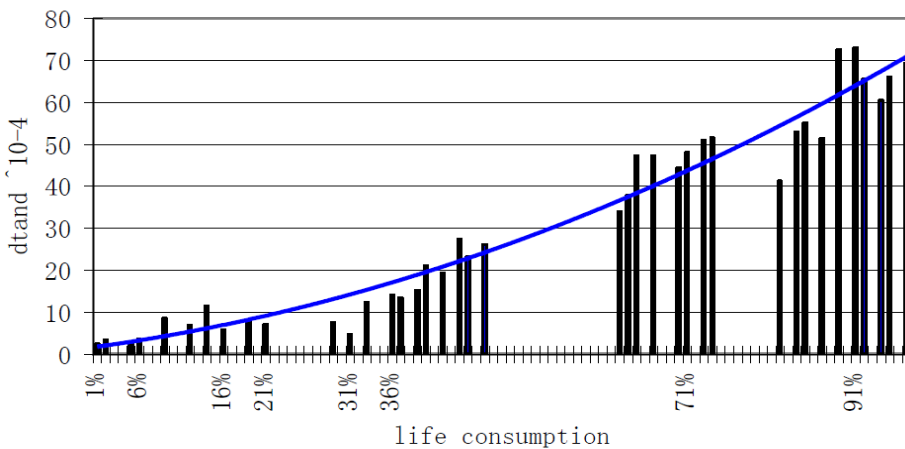


Figure: 7.7: Characteristics of $\Delta \tan \delta$ at 25 °C at two dedicated electric field stresses: 0.7 and 6.1 kV/mm. Values are calculated as voltage value applied on cable: $0.09xU_0$ and $0.84xU_0$.

Tan δ values related to particular ageing periods at constant electric fields were also obtained on the same samples. With increasing ageing (insulation deterioration), tan δ tends to increase more rapidly with increasing temperatures (Figure 7.8). It can be observed that for samples aged for more than 90 days, tan δ increases more rapidly when the temperature exceeds 60°C. For samples characterised by a higher life consumption (longer ageing), this dependency is even stronger.

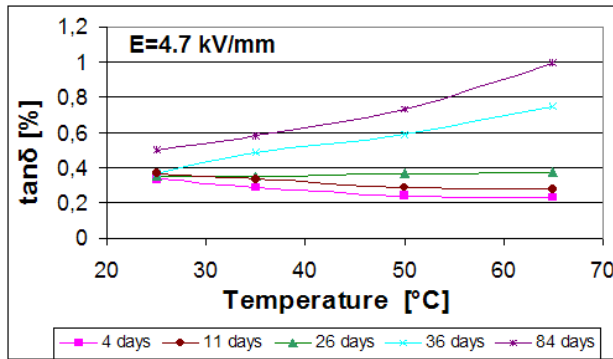


Figure 7.8: Dielectric loss behaviour as a function of temperature at constant electrical field intensity.

Relation between tan δ , percentage life consumption and applied voltage

For 150 kV gas-pressurised cables with mineral oil, a temperature of 60°C, is considered to be the maximum allowable operating temperature and the expected service lifetime (100% life consumption) at this temperature is approximately 10 years. In Figure 7.9, the obtained data were correlated with the particular ageing status (life consumption). It is clear that tan δ increases non-linearly with life consumption at constant electrical stress, and the larger the electric stress, the faster the increase observed.

tand in function of life consumption @ 25C and different applied voltage

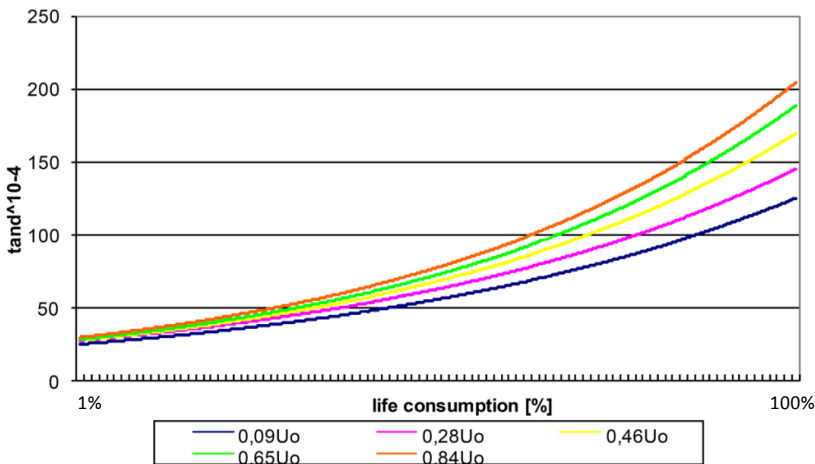


Figure 7.9: Relation between insulation life consumption and measured tan δ values at various voltage levels.

Additionally to show the relation between test voltage and life consumption above $0.84xU_0$, an extrapolation of $\tan \delta$ and applied voltage was carried out. Figure 7.10 shows the obtained extrapolation results for insulation samples representing different life consumption stages. From Figure 7.10, it can be concluded that $\tan \delta$ values are much higher than values measured on-site with the DAC method. Dielectric loss measurements obtained during on-site diagnostic test with DAC method for gas-pressurised cables vary between 0,2% (20×10^{-4}) and 0,6% (60×10^{-4}). More data can be found in chapter 6.

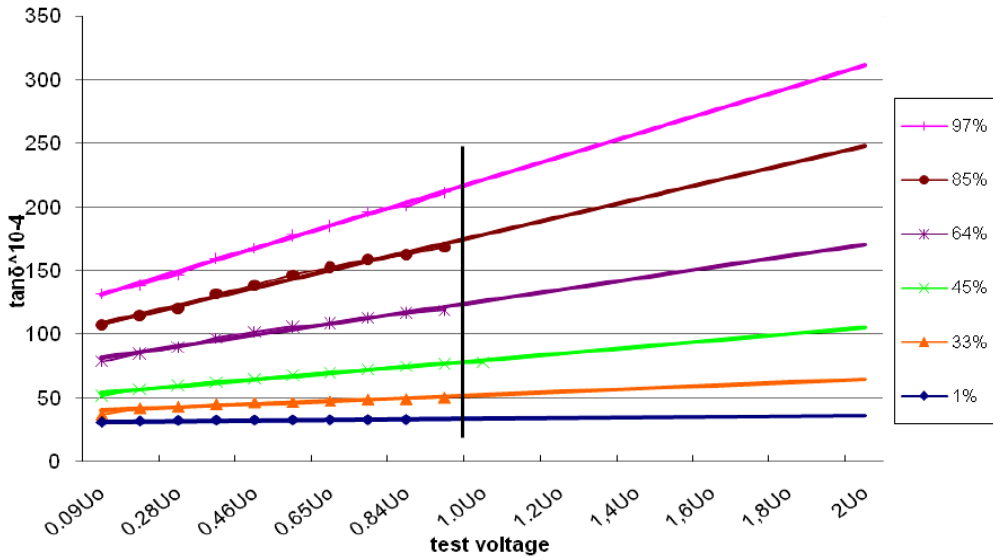


Figure 7.10: $\tan \delta$ as a function of applied test voltage for insulation samples at different life consumptions stages.

If $\Delta \tan \delta$ is divided by $\tan \delta$, the relative $\tan \delta$ value will be obtained. The reason for choosing relative $\tan \delta$ value instead of $\Delta \tan \delta$ is simple. $\tan \delta$ value measured in laboratory conditions are different (smaller) from the real cable $\tan \delta$ values, but for relative $\tan \delta$ value, the measurement value and real cable value are similar (Figure 7.11). The relative $\tan \delta$ values were calculated with the equation [7.6] where U_2 -is the higher test voltage U_1 -is the lower test voltage.

$$\tan \delta_R = \frac{\tan \delta(U_2) - \tan \delta(U_1)}{\tan \delta(U_1)} \quad [7.6]$$

The test voltages for on-site diagnostics performed on service aged external gas-pressurised cables are 40 kV to 150 kV (our research on service aged cables), which corresponds to $0.3xU_0$ to $1.3xU_0$. But relative $\tan \delta$ value measurements with the Schering bridge test voltages are from 0.09 to $0.84xU_0$. For the comparison, the applied voltages are chosen from $0.3xU_0$ to $0.8xU_0$. In Figure 7.11, the pink line indicates the laboratory relative $\tan \delta$ values measured for the following ranges: $0.3xU_0$ and $0.4xU_0$, $0.5xU_0$ to $0.8xU_0$. The life consumption of the measured insulation sample insulation was 47%. We can conclude that values of on-site diagnostic data and the laboratory data are very similar, and the linear relations with voltage

difference are almost the same. Thus, we concluded that also the relative $\tan \delta$ value can be used for the life consumption calculations.

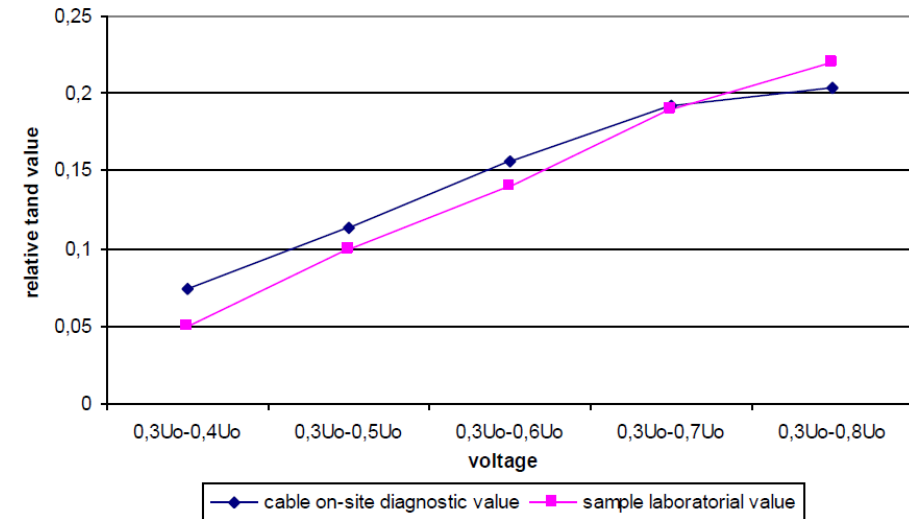


Figure 7.11: On-site DAC and laboratory relative $\tan \delta$ value comparison.

7.2 Insulation life consumption (ILC) calculation

Data obtained through the laboratory experiments were analysed to establish the relation between life consumption and the $\tan \delta$ value at different applied voltages. This relation is needed to build a model for diagnosing life consumption and future life estimation of oil-impregnated paper insulated cable. In order to describe the relation between $\tan \delta$ value at applied test voltage and insulation life consumption, the following aspects were taken into consideration:

- The relative $\tan \delta$ value changes linearly with the voltage difference of U_2 -higher test voltage and the lower test voltage- U_1 .
- The steepness of the linear relation between relative $\tan \delta$ and test voltage changes with the life consumption of the paper insulation.

Based on the above assumptions and the life consumption analysis obtained through the ageing experiments, the fitting formula for calculation of the life consumption can be provided. This formula was created by adjusting the constant values in correlation with measured dielectric loss values with DAC method on service aged gas-pressurised cables at two voltages U_2 and U_1 . Detailed information about formula can be found in Appendix E. The final formula [7.7] used for further calculations of ILC [%] is provided below:

$$ILC[\%] = 10 * \frac{0.09}{U_2 - U_1} * 1.1^{\frac{U_1}{0.09}} * \frac{\tan\delta(U_2) - \tan\delta(U_1)}{\tan\delta(U_1)} * 100\% \quad [7.7]$$

The flow chart which represents particular steps of the ILC calculation is presented in Figure 7.12. It must be noted that in this model, when the ILC is lower than 10%, $\Delta \tan \delta$ has just a very small change so the calculation can't show clear life consumption results under 10%.

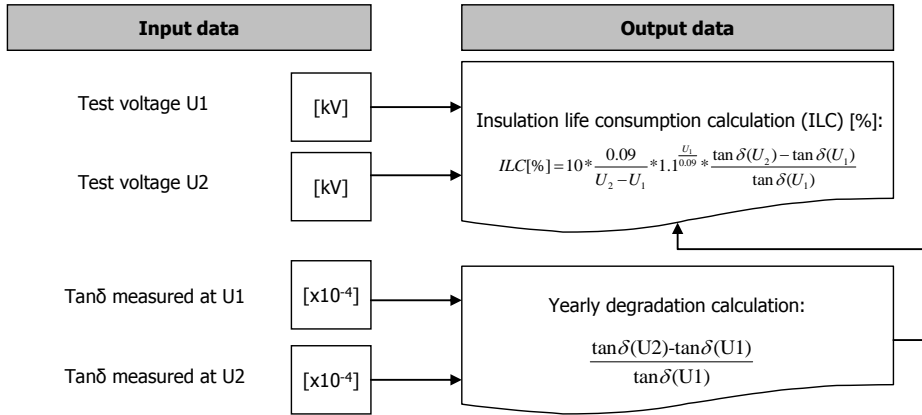


Figure 7.12: Calculation of the Insulation Life Consumption.

7.3 Operational life consumption (OLC) calculation

The OLC model is based on two types of data. The first type of input data is the operational condition of the power cable. This data contains:

- T_{ground} which is the ground temperature in close vicinity of the cable.
- T_{max} is the maximum operational temperature of the cable.
- Load [%] which corresponds to the percentage of the maximum current load.

Using the Arrhenius formula, thermal degradation of the insulation can be obtained. According to Arrhenius law, the degradation rate of the cable insulation increases exponentially with cable temperature. For the oil impregnated paper insulation, the parameters for calculation of the degradation rate depend on cable temperature. In this way by knowing the $T_{conductor}$ parameter, the correlation between Montsinger's and Arrhenius' law can be described by the yearly degradation rate parameter- D_{year} (equation 7.4). Finally, having all the necessary power cable operational parameters, it is possible to calculate the Operational Life Consumption (OLC) according to the flow chart in Figure 7.13.

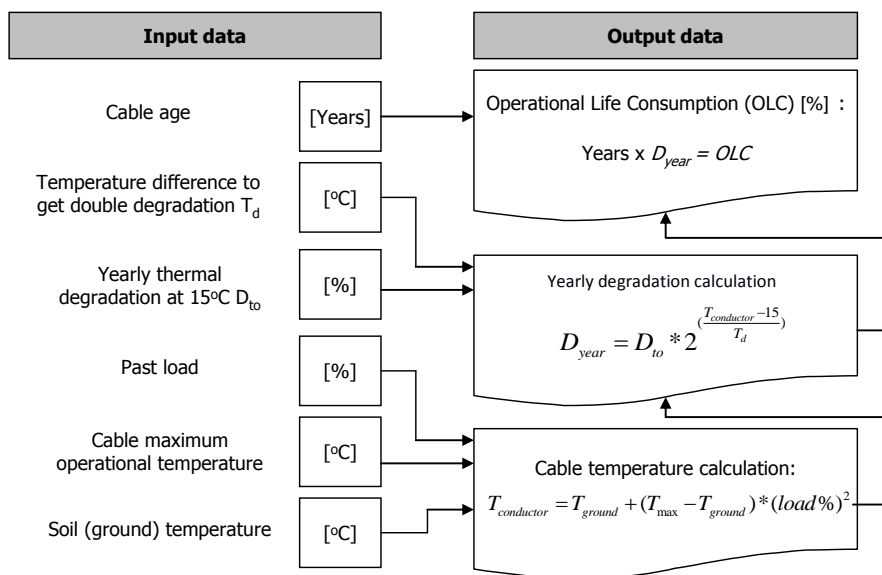


Figure 7.13: Calculation of the Operational Life Consumption.

7.4 Total Life Consumption (TLC) calculation

The total life consumption (TLC) calculation is based on the result of OLC and ILC. Two results of life consumption calculated by different methods are combined together. In further steps, weight parameters are used for better accuracy. The marks L1, L2 and L3 in Figure 7.14 represent three phase cable circuits. For the ILC calculation, three phases are taken into account separately. The ILC results calculated for each cable phase are compared to each other. If the difference in ILC calculation for each particular cable phase is smaller than 3%, a calculated ILC value takes 50% weight and OLC value takes 50% weight. However, if the difference is larger than 3% and smaller than 5%, ILC takes 40% weight and OLC takes 60% weight. In the situation when the difference is larger than 5%, ILC takes 30% weight and OLC takes 70% weight. As a result, the total life consumption value also depends on the difference of ILC value as calculated per each cable phase. These weight assumptions are based on the fact that the dielectric loss diagnostic result may differ and therefore, the condition of the particular cable phases might be different. The 150 kV gas-pressurised cables are constructed as 3 phase systems enclosed in one metal pipe filled with nitrogen gas. In general, such an immune cable system reflects equal losses for each cable phase. When the difference between the measured dielectric losses is relatively high for a particular cable phase, then it could be e.g.: an indicator of the unstable test conditions during on-site diagnosis. A good example is the cable cooling process during on-site diagnostic tests. In this process, the insulation shrinks and oil changes its viscosity. As a result, the dielectric losses also change with decreases in cable temperature. In such a situation, the test results can be less reliable than operational (OLC) data, therefore, the weight factor for ILC is lower than for OLC. A flow chart which presents the TLC calculation is depicted in Figure 7.14 for easier explanation.

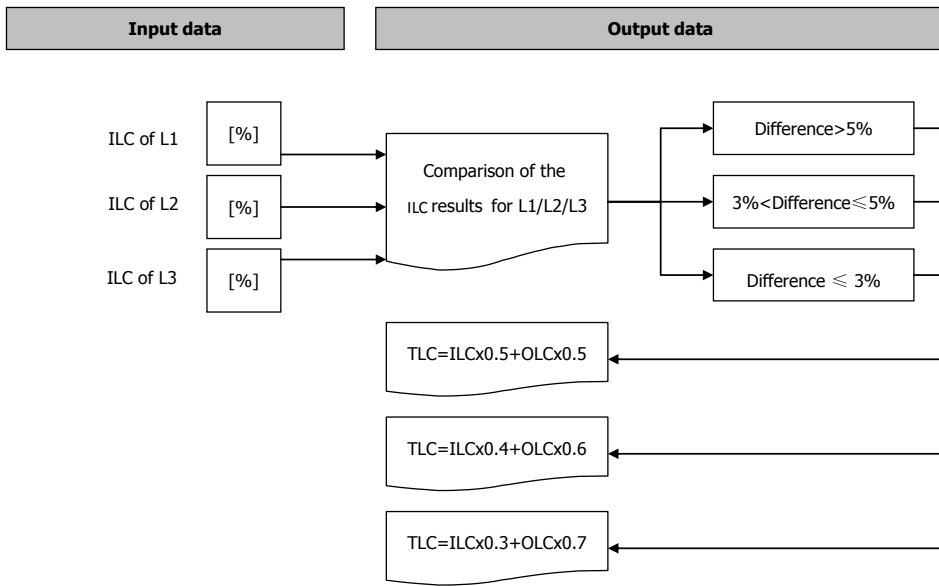


Figure 7.14: Calculation of the Total Life Consumption (TLC) for L1, L2, L3-cable phases.

7.5 Future life profile calculation

The calculation of future life profile (FLP) is based on total life consumption and thermal ageing. Figure 7.15 shows a flow chart referring to calculation of the future life estimation. Calculation of yearly degradation is similar to the life consumption calculation by past load but now the future applied load is taken instead of the past load value. After that, the result of the total life consumption is an input parameter. The output value for the future life estimation is based on the percentage of total life consumption and yearly degradation rate: D_{year} .

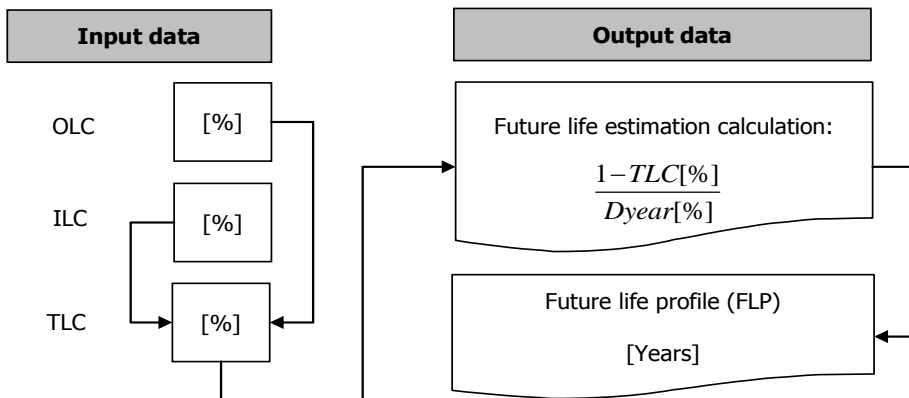


Figure 7.15: Calculation of the Future Life Profile (FLP).

7.6 The further cable lifetime estimation-model application on service aged 150 kV cables.

The scheme of the model presented in Figure 7.16 is based on two different types of input data. In order to verify the applicability and usability of total life consumption (TLC) and future life profile estimation (FLP), practical measurements were performed with the DAC system on two different cable circuits. Operational data has also been analysed to calculate the operational life consumption of both circuits. In the model presented below in Figure 7.16, all steps necessary to estimate further lifetime are shown step-by-step. The blue colour refers to the insulation life consumption calculation and is based on the on-site dielectric loss measurements. The orange colour refers to the operational life consumption which is calculated for the operational cable parameters. The yellow colour represents the future yearly degradation of the insulation. The green colour represents the final further life time estimation. In order to check the model, dielectric loss measurements of two differently aged gas-pressurised circuits were used and analysed according to the procedure as presented in Figure 7.16. The first circuit was marked as moderate condition (condition information provided by TSO) "Circuit A". The second circuit was in good condition (condition information provided by TSO) and marked as "Circuit B".

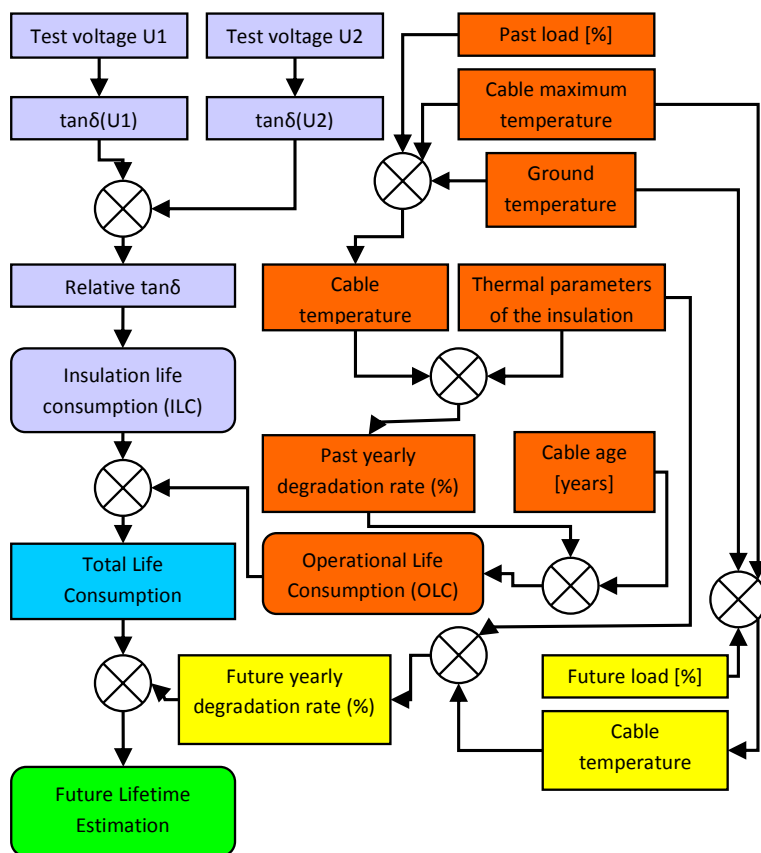


Figure 7.16: Construction of the Further Life time Estimation mode for gas-pressurised HV cables [67].

Circuit A-moderate condition

This circuit is represented by external gas-pressurised 150 kV cable with mineral oil used as the impregnation medium. Measurements on this cable were performed in 2010 with the DAC method as part of the maintenance activities (Figure 7.17). The test voltage was increased from 0 kV up to 130 kV and in particular voltage steps PD and dielectric loss measurements were performed. Circuit A, at the time the measurements were taken, was in service for 35 years with an average current load of 35% of maximum current load. Table 7.3 presents measurement results for both cables.



Figure 7.17: The DAC Diagnosis of the Circuit A.

Circuit B-Good condition

This circuit is also represented by external gas-pressurised 150 kV cable with mineral oil used for impregnation (Figure 7.18). Measurements on this circuit were performed in 2009. The diagnostic test was performed from 0 kV up to 150 kV. Cable 2 was in service for 30 years at the moment of diagnosis. The current load was 40% of maximum current load. Table 7.2 presents test voltage levels for both circuit A and B.



Figure 7.18: The DAC Diagnosis of Circuit B.

During the diagnostic test, the test voltage was increased slowly in small voltage steps of $0.1xU_0$. No breakdown was recorded during testing. In both cable circuits, no PDs have been detected, however, the test voltage was limited to $1.0xU_0$ for circuit A due to agreement with the cable owner and the potential risk of breakdown due to over-voltage. Diagnostic results confirmed the difference in dielectric loss values for circuit A and B and confirmed information given by TSO about general condition of the cable insulation. Circuit A showed much higher values of measured dielectric losses than circuit B (Table 7.3)

Table 7.3
Dielectric loss value [$\times 10^{-4}$] at test voltage steps as measured with DAC voltages.

Test voltage	Tan δ (Circuit A)			Tan δ (Circuit B)		
	L1	L2	L3	L1	L2	L3
$0.3xU_0$	37.71	37.71	31.87	18.15	17.15	17.69
$0.4xU_0$	40.48	40.48	34.22	19.07	17.63	17.47
$0.5xU_0$	42	42	35.97	16.87	16.4	14.81
$0.6xU_0$	43.66	43.66	35.75	18.14	16.61	15.34
$0.7xU_0$	44.96	44.96	37.09	17.61	17.29	16.16
$0.8xU_0$	45.38	45.38	38.36	17.67	17.04	16.69
$0.9xU_0$	48.46	48.46	41.04	18.07	17.29	16.83
$1.0xU_0$	52.72	52.72	65.26	20	19.13	18.56
$1.1xU_0$	No data (over-voltage not possible due to risk of the breakdown)			20.01	19.87	18.74
$1.3xU_0$				20.74	20.27	18.89

ILC calculation

For comparison of the obtained ILC values of both circuits A and B, the $\Delta \tan \delta$ values were used as measured between $0.3xU_0$ and $1.0xU_0$. Additionally, for circuit B, an extra calculation between $0.3xU_0$ and $1.3xU_0$ was performed to check the influence of the higher test voltage levels for ILC calculation quality. Calculation of the ILC indicated insulation life consumption of 100% for each phase of circuit A. Calculation of the ILC for cable circuit B resulted in the following values: 14%-L1, 20%-L2, 9%-L3 (Table 7.4) and confirms the different condition status of these external gas pressurised cables.

Table 7.4:
ILC calculation results for Circuit A and Circuit B.

Phase	ILC calculated between $0.3xU_0$ - $1.0xU_0$			ILC calculated between $0.3xU_0$ - $1.3xU_0$		
	L1	L2	L2	L1	L2	L3
Cable A	100%	100%	100%	No data		
Cable B	14%	20%	9%	15%	22%	8%

OLC calculation

In the second step, the operational life consumption was calculated according to the scheme presented in Figure 7.16. Operational input data were obtained from the TSO database of transmission cable load profiles. The calculation of OLC for the operational cable data is presented in Table 7.5.

Table 7.5
Circuits operational parameters and calculated OLC.

Parameter/object	Circuit A	Circuit B
T_d	13°C	21°C
D_{to}	1%	1%
T_{max}	60°C	85°C
T_{ground} (yearly average)	10°C	10°C
Age	35 years	30 years
Current load profile (average load history)	35%	40%
Calculated $T_{conductor}$	20.5°C	18°C
OLC	37 %	41 %

TLC and future load profile

For circuit A, results of ILC calculation are 100% for all cable phases. Thus, ILC takes 50% weight and OLC takes 50% weight. The OLC value based on thermal ageing is 37%. Thus, the total life consumption (TLC) value is:

$$TLC_{circuit A} = 100 \% * 0.5 + 37%*0.5 = 69\%$$

For Circuit B, the results of ILC calculation are different. The ILC differences between the three phases are larger than 5%. Thus, ILC takes 30% weight and OLC takes 70% weight according to scheme presented in Figure 7.14. The OLC value based on thermal ageing is 41%

and the ILC value is the average value of the three phases, which is 14.3%. Thus, the total life consumption (TLC) value is:

$$TLC_{\text{Circuit B}} = 14\% * 0.3 + 41\% * 0.7 = 32.9\%$$

Finally, the last step is to calculate the future life profile. The assumption of ground temperature and cable maximum temperature are 10⁰C and 60⁰C respectively for circuit A and 10⁰C and 85⁰C for circuit B. The scenario for the further life profiles can be separated into three different (hypothetic) situations:

- The future load remains the same as the past load: circuit A-35% and circuit B-40%-asset management (AM) decision is to maintain the circuit without any changes of the load profile.
- The future load increases to a maximum of 100% of possible load-scenario never possible for important service aged transmission cables.
- The future load decreases to 20%-asset management (AM) decision to maintain the circuit with lower load to keep e.g.: low failure rate and extend service time scenario very often considered by TSOs in case of service aged circuits that do not suffer from any insulation breakdowns and expensive repairs.

Table 7.6 presents the possible future life profiles and FLP calculation for circuits A and B.

Table 7.6
Relation between cable yearly degradation rate and the future load.

Moderate / bad condition-Cable A				Good condition-Cable B			
TLC	Future load [%]	Future degradation rate [%]	Future life profile [years]	TLC	Future load [%]	Future degradation rate [%]	Future life profile [years]
69% (past load 35%)	20	0.85	36.9	32% (past load 40%)	20	0.85	77.4
	25	0.9	34.7		25	0.9	72.9
	30	0.97	32.3		30	0.97	67.7
	35	1.06	29.6		35	1.06	62.1
	40	1.17	26.8		40	1.17	56.2
	50	1.49	21.1		50	1.49	44.2
	75	3.43	9.16		75	3.43	19.2
	100	11.02	2.85		100	11.02	5.99

In Table 7.6, the degradation rate increases with the current load. When the future load expectancy is 20%, the degradation rate per year of cable insulation is 0.85%. In the case of the future load being equal to 100% of the maximum current load, the degradation rate is 11.02% per year. The future life profile decreases (life shortened) with the load. When the future load expectancy is 20%, the future life estimations for circuit A and cable B are respectively: 36.9 years and 77.4 years. When the cable load is increased to 100%, future life estimations (extreme situation) for circuit A and cable B decrease dramatically to 2.85 years and 5.99 years. The future life estimation also depends on the total life consumption of the cable at the time of measuring. When the future loads are the same, the future life

estimation of circuit A is more than double the future life estimation of circuit B. In Figure 7.19 and Figure 7.20, the future load modeling of cable circuit A and circuit B are shown. The first part is a single brown line which shows the past degradation of the cable insulation until the moment of the on-site DAC diagnosis. The second part contains different colour lines which reflect the future life estimations when the future load is different.

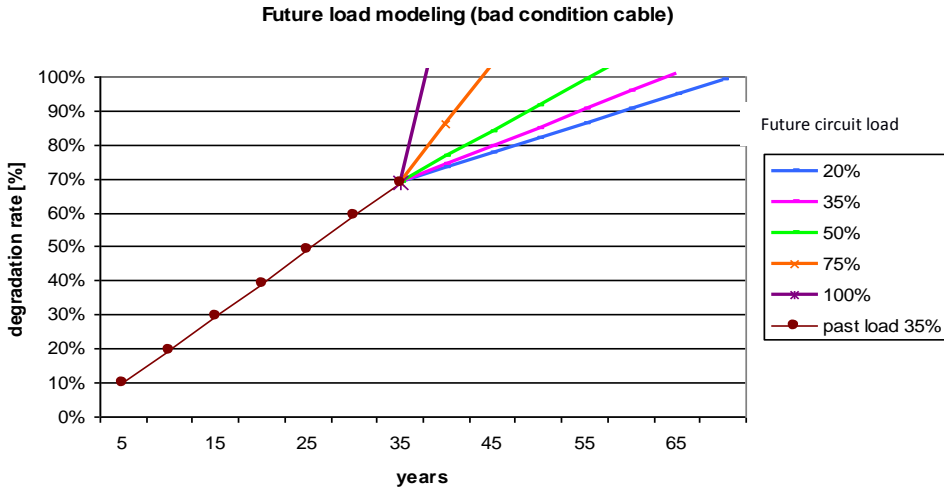


Figure 7.19: Future load profiles and expected life time for circuit A.

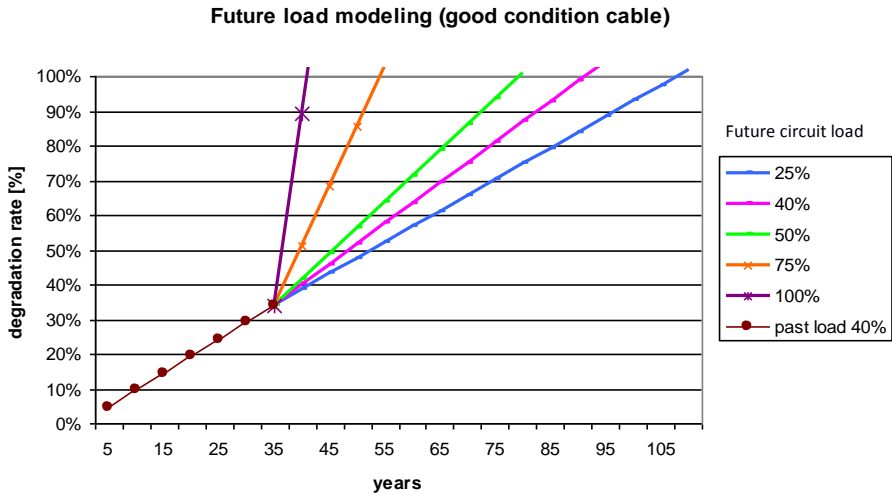


Figure 7.20: Future load profiles and expected life time for circuit B.

7.7 Conclusions

- 1) Diagnosis data (dielectric loss) obtained with DAC voltage testing can be used for condition evaluation of transmission power cables insulation.
- 2) The relation between constant electric field stress and variable temperature of insulating paper in different ageing stages was investigated and results obtained. Investigations show that dielectric losses grow non-linearly with progressive degradation of the insulation.
- 3) There is a correlation between duration of ageing and behaviour of dielectric loss as a function of temperature and electric field stress.
- 4) It can be stated that the combination of the laboratory investigation and on-site DAC dielectric loss measurements can support the AM decision in finding optimal load profile service aged transmission cables. Optimal load profile means the profile, which allows for the relatively safe service period e.g. till cable replacement (end of service).
- 5) Based on the combination of ILC and OLC, TLC can be estimated. This is very important information, when data about permissible future load of the cable is desired in a situation of e.g. a new client that will be linked to the existing network and this client requires high electric power.
- 6) The model of the future permissible load calculation was checked and evaluated on two real HV power cables in different conditions.
- 7) The model presented in this chapter is evaluated on real on-site data. It can be implemented by a TSO as a part of AM decisions about HV cables for assessment of aged cable's life time expectation.
- 8) It could be interesting for AM to implement more cable operational data e.g. failure rate or number of gas leakages per year in our further life time estimation model to get even more accurate estimations.

8. CONCLUSIONS AND FUTURE WORK

Around 300 km of transmission power cable circuits (50 kV, 150 kV and 220 kV) were tested in order to evaluate the condition of cable systems and confirm the DAC method as a powerful diagnostic method. Applying the DAC method in practice showed that it is suitable for PD detection and PD spot localization and as well cable defect identification in whole cable lengths. Moreover, research presented in this thesis resulted in generalization of the DAC method applicability for transmission power cables. Major approach of this research was development of knowledge rules about HV DAC on-site application and this was achieved in two different ways:

- Defect recognition and localization in 150 kV cable in the lab. It was shown that sequences of damped AC resonant voltages are suitable for recognition of different defects in e.g. prefabricated joints. Test results on 3 different defects, simulated in laboratory conditions on a real cable circuit, and comparison with continuous AC 50 Hz showed similar PDIV levels, PD magnitudes and PD characteristics as measured at different voltage test levels.
- Testing and diagnosis performed on-site to collect parameters and to develop general test procedures applicable for onsite conditions. The non-destructive character of DAC voltages is an ideal method for the aged circuits, where risk of possible breakdowns and damages due to testing must be minimized.

Our major conclusions can be summarized as follows:

PD detection and localization in transmission power cables

- The goal of the acceptance test or diagnostic test is to qualify actual power cable condition. Besides, a go/no go HV acceptance non-monitored test performed on the complete cable is not always sufficient to confirm proper workmanship on-site. A way to non-destructively detect installation defects in cable accessories and avoid unexpected breakdowns even after successful non-monitored acceptance test is PD measurement, as PDs are defect symptoms and/or defect initiation spots.
- Installation defects result mostly in local enhancement of the electric field intensity and thus, PD activity.
- Partial discharge parameters are most important symptoms of local defects of cable insulation. As it was shown even for serious joint defects over-voltage (above nominal voltage) conditions are necessary to ignite PD. Over-voltage condition (above U_0) may indicate insulation defects (symptoms) which are not visible during network in-service condition at U_0 .
- DAC test voltage frequency is an important aspect for PD detection. It was shown that at a frequency close to 400 Hz proper PD detection and identification with DAC

voltages is sometimes very difficult. IEC recommendations about test voltage frequency (20-300Hz) for continuous AC voltages are in line with this statement.

Laboratory investigations on dielectric loss measurements:

- In our laboratory aging tests oil-impregnated paper was subjected to accelerated thermal aging at temperatures up to 110⁰C. During the test, different electrical field stresses and temperatures were applied to the samples. The duration of the aging test of 225 days resulted in life consumption in the range from 1% to 100%.
- The investigations of the influences of electrical field intensity and temperature showed that: dielectric loss increases with electrical field intensity even at low temperature much faster for aged insulation than for non-aged insulation. Therefore, on-site diagnostic tests are performed at a stable, relatively low temperature of e.g. 15⁰C, which provides a good proof of the insulation condition.
- Thermally aged paper insulation shows significant increase of dielectric loss after 90 days. The latter is relevant to 30 years of service life, due to which $\tan \delta$ increases rapidly when the temperature of insulation exceeds 28⁰C. Dielectric loss measured with the DAC method gives an indication of the integral condition of insulation. Application of accelerated aging tests on paper insulation confirmed the usability of relative $\tan \delta$ characteristics as measured between two dedicated test voltage stresses for calculating insulation life consumption (ILC).
- Total insulation life consumption (TLC) can be calculated using both cable operational parameters and diagnostic parameters obtained with the DAC method.
- By controlling the power cable load (temperature), the degradation rate can be controlled as well.
- The proposed insulation consumption model was validated on-site on differently aged gas pressurized cables by dielectric loss measurements with the DAC method.
- Periodic dielectric loss measurements on cables in service indicate the increase of insulation degradation and therefore future limits in loading capabilities of particular cable circuits.
- Gas-pressurised 150 kV cables installed in The Netherlands confirmed an in general good condition showing very low PD activity and low dielectric losses.
- Oil-filled 50 kV cables installed in The Netherlands show that for a large number of these cables maintenance actions are necessary to uphold the relatively good condition. PDs and dielectric losses are a good indicator of the local defect in this case. Dielectric loss and PD's periodical tests may help DSO to observe the actual condition of these assets and avoid failures.

Future work and recommendations

1. We recommend that each maintenance and diagnostic test on service aged power cables should include PD and dielectric loss measurements. Also we advise that each acceptance test on newly installed power cables should be performed in monitored mode to increase the effectiveness of defects recognition and providing a so called "PD cable fingerprint".
2. Accelerated thermal aging tests on extruded insulation (XLPE) could be a profitable way to extend the knowledge regarding thermal aging characteristics of e.g. XLPE cables and related dielectric loss characteristics. At this moment still a very limited knowledge exists about dielectric loss behaviour in aging XLPE cable insulation.
3. More installation defects should be investigated with the DAC method to obtain all relevant PRPD patterns and Q vs. V characteristics.
4. Long term evaluation of the impact of the different test voltage frequencies of DAC voltages on the breakdown strength of XLPE insulation could be useful for selection of the optimal duration of acceptance voltage withstand tests in the field.
5. PD localization is more difficult on long cable circuits, due to the PD signal attenuation. Significant improvement of PD measurements with DAC voltages on long (more than 10 km) HV cables will be obtained with additional PD sensors installed on the cable e.g. in the joint cross-bonding boxes. Such sensors should be synchronized, and triggered by the DAC voltage source. The trigger signal can be transferred via cable phase which is not under test (PD measurements are performed phase by phase) and serving as a data link between sensor and DAC system.

APPENDIXES

Appendix A: DAC voltage, test parameters and test circuit parameters according to IEEE400.4 2015.

Table A.1
DAC voltage parameters.

Voltage Parameters	Description
DAC excitation	complete process of charging the test object capacitance C_{TO} with I_{Cmax} to a selected test voltage level V_{DAC} followed by a damped sinusoidal oscillation with circuit resonance frequency f_r and a given damping factor D_f
Damped alternating voltage DAC	starting from a (negative or positive) charging voltage level and having damped sinusoidal oscillation around the zero level. It is characterized by the peak value V_{DAC} , the circuit resonance frequency f_r and the damping factor D_f .
Circuit resonance frequency f_r in [Hz]	equals to reciprocal of the time between two successive peaks of same polarity and it is determined by the C_{TO} and L_c and in most cases the $f_r = 1 / 2\pi\sqrt{L_c \cdot C_{TO}}$.
Damping factor D_f in [%]:	equals to voltage difference between the first and second peak of same polarity, divided by the voltage value of the first peak.
Voltage level V_{DAC} in [kV _{peak}]	this is the actual test voltage level of the DAC voltage which equals to the actual charging voltage as it has to be generated by a DAC system.
Charging time t_c in [s]	equals to the necessary time at given ,e.g. maximum charging current I_{Cmax} to charge the test object capacitance C_{TO} up to selected test voltage level V_{DAC}

Table A.2
DAC test parameters.

Test Parameters	Descriptions
Test voltage level V_T [kV _{peak}]:	this is the selected test voltage level of the DAC voltage 1 st cycle which equals to the actual charging voltage as it has to be generated by a DAC system. For the test purpose this value has to be selected in accordance to valid test recommendations. Depending on the test procedure, the V_T can be selected for on one or even more test levels.
Test voltage steps ΔV_T	applying DAC excitations for an increasing voltage test the steps in the V_T voltage increase have to be defined. The ΔV_T can be defined in [kV _{peak}] or in the unit of U_0 e.g. $0.1U_0$ or $0.2U_0$.
Number of excitations N_{DAC}	these parameter describes the number of DAC excitations that have to at generated at given test voltage level V_T . The total test procedure can consist of different sequences of N_{DAC} e.g. during voltage withstand test $N_{DAC} = 50$ excitations, or during diagnostic test where N_{DAC} can be lower.
Test time in [min]	equals to reciprocal of the total time requested to generate at given test voltage level V_T the selected number of excitations N_{DAC}
DAC voltage withstand test:	series of DAC voltage excitations as applied consecutively to the power cable under test. The duration of the test is determined by a number of DAC excitations which have been applied to the power cable under test at a selected DAC test voltage. The maximum DAC withstand voltage level is determined by the voltage peak values V_{DAC} respectively RMS-values $V_{DAC}/\sqrt{2}$ of the 1 st DAC cycle.

Table A.3
Test circuit parameters.

Test Parameters	Descriptions
Test object capacitance C in [μ F]:	Depends on the cable type, and dimension this value can vary between few nF and several μ F. In the case of a test object with a relative low capacitance of a few nF the total test object capacitance can also be a parallel connection of the test object with some additional HV capacitor. In this case it is of importance that this capacitor is suitable to withstand the maximum test voltage and in the case of monitored tests e.g. PD, dielectric loss measurement it is PD-free and has known dielectric losses.
System inductance L in [H]	Depends on the DAC system type the inductance (one single coil or several coils) of the DAC system can be fixed e.g. 8H or it can be variable in dependence on the test voltages and the test object capacitance.
Maximum test voltage V_{max} in [kVpeak]	The maximum test voltage of the 1 st DAC voltage cycle which equals to the maximum charging voltage as it can be generated by a specific DAC system for the test purpose whereas also the test circuit elements and the test object are designated to be tested.
Maximum charging current I_{Cmax} in [mA]	Depends on the type of system, it can vary between few mA up to hundreds of mA. It has to be considered that in combination with the C_{TO} and with V_{max} this parameter determines the DAC charging time.
Max. switching circuit current I_{Smax} in [A]	Depends on the type of system, it can vary between few A up to several hundreds of A. It has to be considered that parameter in combination with V_{max} determines the maximum test object capacitance C_{TO} .
Switching duration t_s in [μ s]	This is the time which is needed by a DAC system after the maximum test voltage V_{max} is reached after the charging to close the resonance circuit of LC and C_{TO} and to start the damped resonance between LC and C_{TO} .
Quality factor Q_c	$Q_c = (L_c / (C_{TO} \cdot R_2^2))$ whereas R_2 is the equivalent circuit resistance.
The maximum cable capacitance C_{TOmax} which can be tested by a DAC test facility	This can be calculated by $C_{TO} = (I_{Smax} / V_{max})^2 \cdot L_c$. Where V_{max} is the maximum applied test voltage and I_{Smax} is the permissible AC current in the resonance circuit.

Table A.4
DAC test voltages levels (20 Hz...500 Hz) as used for DAC testing
(50 DAC excitations) of newly installed power cables.

Power cable rated voltage U [kV] phase-to-phase	U_0 [kV]	DAC test voltage level V_T [kV _{peak}] phase-to-ground
3	2	6
5	3	8
6	4	12
8	5	14
10	6	17
15	9	26
20	12	34
25	15	43
30	18	51
35	21	60
45-47	26	74
60-69	35	99
110-115	64	181
132-138	77	187
150-161	87	212
220-230	127	254

Appendixes

Table A.5
 DAC test voltages levels (20 Hz...500 Hz) as used for maintenance testing (50 DAC
 excitations) of repaired / refurbished power cables.

Power cable rated voltage U [kV] phase-to-phase	U_0 [kV]	DAC test voltage level V_T [kV _{peak}] phase-to-ground
3	2	5
5	3	6
6	4	10
8	5	11
10	6	14
15	9	21
20	12	28
25	15	35
30	18	41
35	21	48
45-47	26	60
60-69	35	80
110-115	64	145
132-138	77	150
150-161	87	170
220-230	127	204
275-287	159	237
330-345	191	282
380-400	220	293

Appendix B: Laplace transforms for equations [4-10] to [4-13].

We assume that in the moment of switching $t=0$, $i_L(0)$

$$E(s) - R_1 I_L(s) - Ls I_L(s) + L i_L(0) = U_{C0} \quad [B-1]$$

$$-C U_{C0}(0) + C_x s U_{C0}(s) = I_{Cx}(s) \quad [B-2]$$

where: $U_{C0}(0)$ is a voltage on the capacitor (cable) in moment of $t=0$

$$U_{C0}(s) = R_x I_{Rx}(s) \quad [B-3]$$

$$I_L(s) = I_{Cx}(s) + I_{Rx}(s) \quad [B-4]$$

now, we can calculate $I_{Cx}(s)$ from the equation [B-4].

$$I_{Cx}(s) = I_L(s) - I_{Rx}(s) \quad [B-5]$$

from the equation [B-1] we can calculate: $I_L(s)$

$$I_L(s) = [E(s) + L i_L(0) - U_{C0}(s)] \frac{1}{R_1 + sL} \quad [B-6]$$

From the equation [B-3] we can calculate: $I_{Rx}(s)$

$$I_{Rx}(s) = \frac{1}{R_x} U_{C0}(s) \quad [B-7]$$

Equation [B-5] we can express by using two equations [B-6] and [B-7]:

$$I_{Cx}(s) = \frac{E(s)}{R_1 + sL} + \frac{L}{R_1 + sL} i_L(0) - \frac{U_{C0}(s)}{R_1 + sL} - \frac{1}{R_x} U_{C0}(s) \quad [B-8]$$

$$I_{Cx}(s) = \frac{E(s)}{R_1 + sL} + \frac{L}{R_1 + sL} i_L(0) - \left(\frac{1}{R_x} + \frac{1}{R_1 + sL} \right) U_{C0}(s) \quad [B-9]$$

equation [B-9] can be used in the equation [B-2] and now it will result in the following form [B-10]:

$$C_x s U_{C0}(s) - C U_{C0}(0) = \frac{E(s)}{R_1 + sL} + \frac{L}{R_1 + sL} i_L(0) - \left(\frac{1}{R_x} + \frac{1}{R_1 + sL} \right) U_{C0}(s) \quad [B-10]$$

from equation [B-10] now $U_{C0}(s)$ can be expressed by the following derivation [B-11]:

$$U_{C0}(s) \left(C_x s + \frac{1}{R_x} + \frac{1}{R_1 + sL} \right) = \frac{E(s)}{R_1 + sL} + \frac{L}{R_1 + sL} i_L(0) + C U_{C0}(0) \quad [B-11]$$

$$U_{C0}(s) \frac{R_x R_1 C_x s + R_x L C_x s^2 + R_1 + sL + R_x}{R_x (R_1 + sL)} = \frac{E(s)}{R_1 + sL} + \frac{L}{R_1 + sL} i_L(0) + C U_{C0}(0) \quad [B-12]$$

$$U_{C0}(s) \frac{R_x LC_x s^2 + (L + R_x R_1 C_x) s + R_1 + R_x}{R_x (R_1 + sL)} = \frac{E(s)}{R_1 + sL} + \frac{L}{R_1 + sL} i_L(0) + C U_{C0}(0) \quad [B-13]$$

We can express temporarily numerator : $R_x LC_x s^2 + (L + R_x R_1 C_x) s + R_1 + R_x = M$ so now equation [B-10] will result in the following form [B-14]:

$$U_{C0}(s) = \frac{R_x (R_1 + sL)}{(R_1 + sL)M} E(s) + \frac{L(R_1 + sL)R_x}{(R_1 + sL)M} i_L(0) + \frac{C R_x (R_1 + sL)}{M} U_{C0}(0) \quad [B-14]$$

$$U_{C0}(s) = \frac{R_x}{M} E(s) + \frac{L R_x}{M} i_L(0) + \frac{R_1 R_x C_x + R_x C_x s L}{M} U_{C0} \quad [B-15]$$

If we assume that $E(s) = 0$ and before the switching process $i_L = const$ than:

$$i_L(0) = \frac{U_{C0}(0)}{R_x} \text{ and } i_{Cx}(0) = 0$$

$$U_{C0}(s) = \frac{L R_x}{M} \frac{U_{C0}(0)}{R_x} + \frac{R_1 R_x C_x + R_x LC_x s}{M} U_{C0}(0) \quad [B-16]$$

voltage can be expressed by following form [B-17]:

$$U_{C0}(s) = \frac{R_x LC_x s + R_1 R_x C_x + L}{R_x LC_x s^2 + (L + R_1 R_x C_x) s + R_1 + R_x} U_{C0}(0) \quad [B-17]$$

Dividing numerator and denominator by $R_x LC_x$ we get another form:

$$U_{C0}(s) = \frac{s + \frac{R_1}{L} + \frac{1}{R_x C_x}}{s^2 + \left(\frac{R_1}{L} + \frac{1}{R_x C_x}\right) s + \frac{R_1 + R_x}{R_x LC_x}} U_{C0}(0) \quad [B-18]$$

Equation [B-18] in Laplace form express output voltage in the moment $t=0$.

To solve this equation we shall solve second degree equation with two unknowns and therefore Δ need to be calculated:

$$\Delta = \alpha^2 - 4\beta = \left(\frac{R_1}{L} + \frac{1}{R_x C_x}\right)^2 - 4 \frac{R_1 + R_x}{R_x LC_x} \quad [B-19]$$

The solution are two variables:

$$s_1 = -\alpha - j\sqrt{\omega_0^2 - \beta^2} = -\alpha - j\omega_1 \quad [B-20]$$

$$s_2 = -\alpha + j\sqrt{\omega_0^2 - \beta^2} = -\alpha + j\omega_1 \quad [B-21]$$

$$\alpha = \frac{1}{2} \left(\frac{R_1}{L} + \frac{1}{R_x C_x}\right) \quad [B-22]$$

By introducing [B-23]

$$\frac{s+2\alpha}{(s+s_1)(s+s_2)} = \frac{A}{s+s_1} + \frac{B}{s+s_2} \quad [\text{B-23}]$$

$$A = \frac{2\alpha-s_1}{s_2-s_1} \quad \text{and} \quad B = \frac{2\alpha-s_2}{s_2-s_1}$$

Equation [B-18] we can express by using A and B:

$$U_{C0}(s) = \left(\frac{A}{s+s_1} + \frac{B}{s+s_2} \right) U_{C0}(0) \quad [\text{B-24}]$$

And in time domain:

$$U_{C0}(t) = (Ae^{-s_1t} + Be^{-s_2t})U_{C0}(0) \quad [\text{B-25}]$$

$$U_{C0}(t) = \left[\left(\frac{1}{2} - j \frac{3\alpha}{2\omega_1} \right) e^{-\alpha t} e^{-j\omega_1 t} + \left(\frac{1}{2} + j \frac{3\alpha}{2\omega_1} \right) e^{-\alpha t} e^{-j\omega_1 t} \right] U_{C0}(0) \quad [\text{B-26}]$$

$$U_{C0}(t) = U_{C0}(0) \left[\left(\frac{1}{2} e^{-j\omega_1 t} \right) - j \frac{3\alpha}{2\omega_1} e^{-j\omega_1 t} + \frac{1}{2} e^{j\omega_1 t} + j \frac{3\alpha}{2\omega_1} e^{-j\omega_1 t} \right] e^{-\alpha t} \quad [\text{B-27}]$$

and as a shorter form by using $\cos(\omega_1 t)$ and $\sin(\omega_1 t)$

$$U_{C0}(t) = U_{C0}(0) \left[\cos \omega_1 t - \frac{3\alpha}{\omega_1} \sin \omega_1 t \right] e^{-\alpha t} \quad [\text{B-28}]$$

$$U_{C0}(t) = U_{C0}(0) \sqrt{1 + \left(\frac{3\alpha}{\omega_1} \right)^2} \left[\frac{1}{1 + \left(\frac{3\alpha}{\omega_1} \right)^2} \cos \omega_1 t - \frac{\frac{3\alpha}{\omega_1}}{1 + \left(\frac{3\alpha}{\omega_1} \right)^2} \sin \omega_1 t \right] e^{-\alpha t}$$

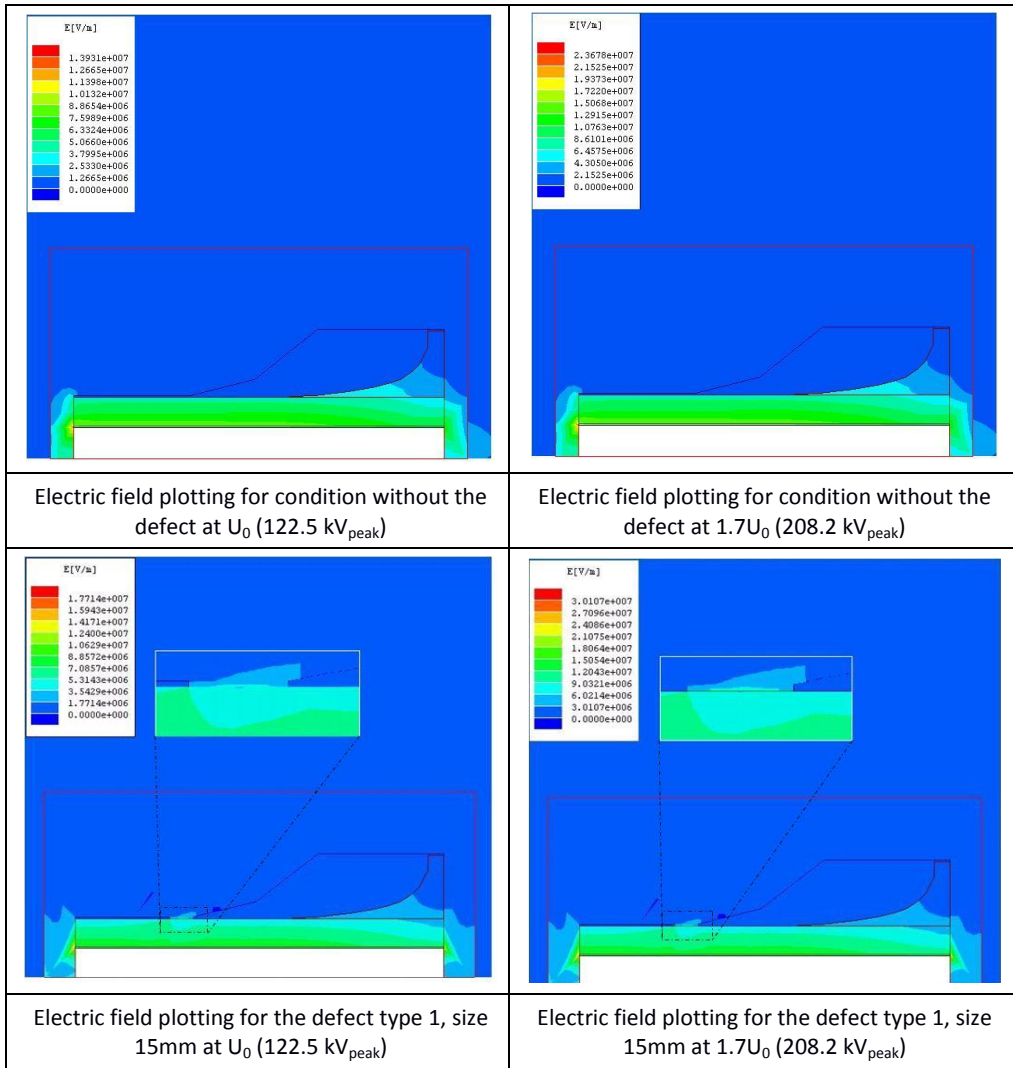
$$U_{C0}(t) = U_{C0}(0) \sqrt{1 + \left(\frac{3\alpha}{\omega_1} \right)^2} [\cos \theta \cos \omega_1 t - \sin \theta \sin \omega_1 t] e^{-\alpha t} \quad [\text{B-29}]$$

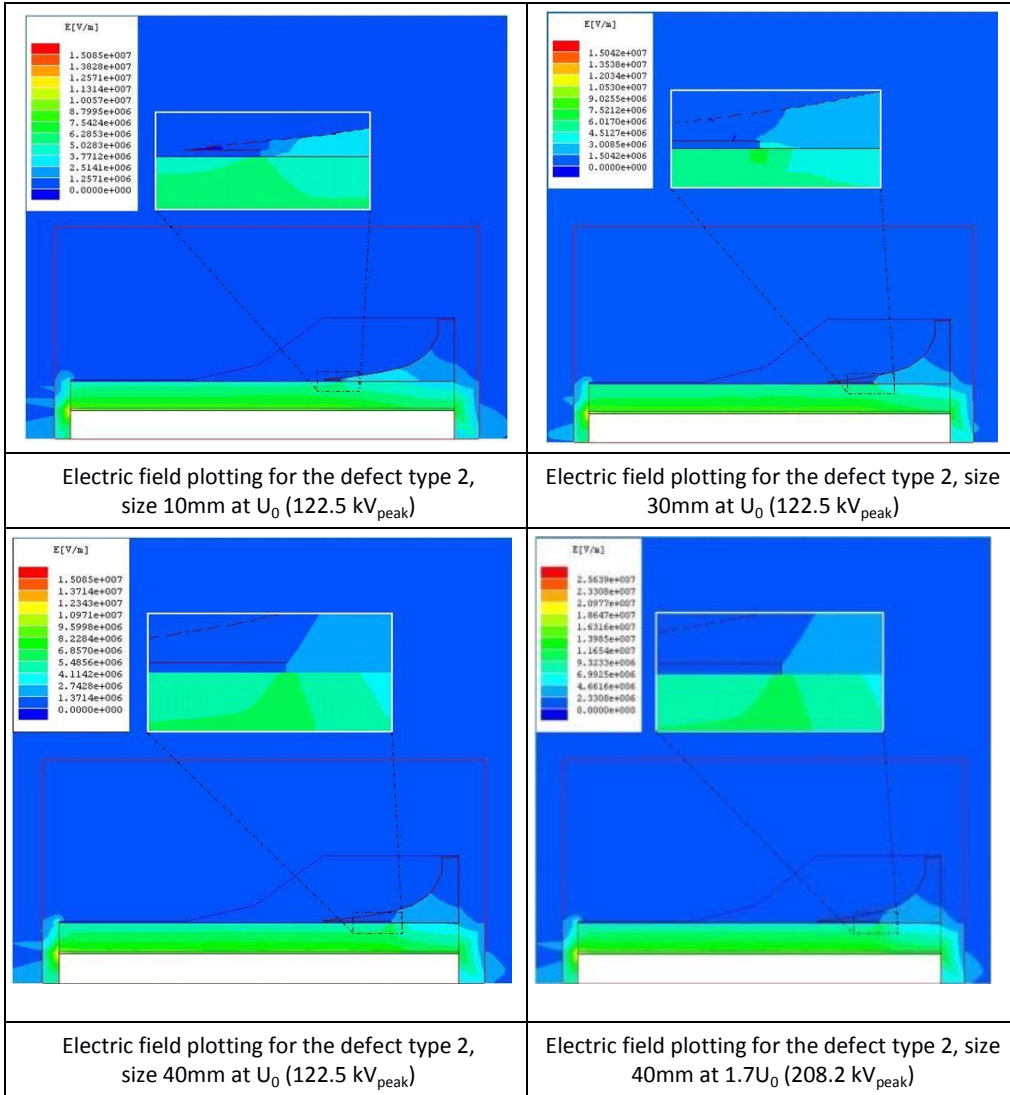
$$\cos \theta = \frac{1}{\sqrt{1 + \left(\frac{3\alpha}{\omega_1} \right)^2}} \quad [\text{B-30}]$$

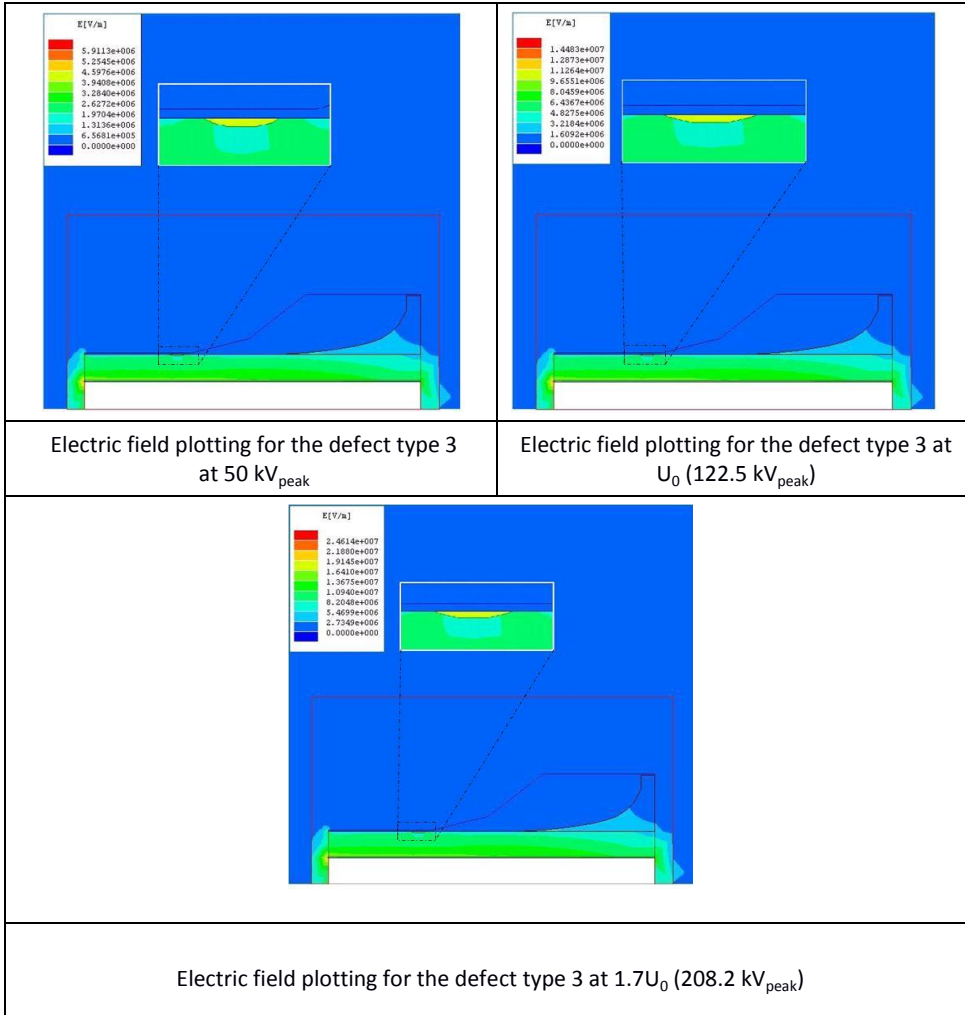
$$U_{C0}(t) = U_{C0}(0) \sqrt{1 + \left(\frac{3\alpha}{\omega_1} \right)^2} e^{-\alpha t} \cos(\omega_1 t + \theta) \quad [\text{B-31}]$$

Due to the fact that in practice $\sqrt{1 + \left(\frac{3\alpha}{\omega_1} \right)^2} \approx 1$

Appendix C: Field Plotting Simulation Ansoft 9.0 software for the defects 1,2,3 (screen shots).







Electric field plotting for the defect type 3 at 50 kV_{peak}

Electric field plotting for the defect type 3 at U₀ (122.5 kV_{peak})

Electric field plotting for the defect type 3 at 1.7U₀ (208.2 kV_{peak})

Appendix D: TDR traces at different DAC test voltages for cable phase L1 (Case study 1).



Appendix E: Insulation life consumption (ILC) experimental formula [7.7].

The electrical field intensity during laboratory measurements were as follows: 0.7 kV/mm, 1.4 kV/mm, 2.0 kV/mm, 2.7 kV/mm, 3.4 kV/mm, 4.0 kV/mm, 4.7 kV/mm, 5.4 kV/mm, 6.1 kV/mm, 6.7 kV/mm. Taking into account the thickness of the aged samples and the thickness of the insulation layers taken out of the cable, the electrical field intensity can be expressed by the cable test voltage (factor x multiplied by U_0). The values are depicted in Table E.1

Table E.1
Electrical field intensity related to test voltage $x \cdot U_0$.

E [kV/mm]	Factor x value
0,7	0,09
1,4	0,18
2,0	0,28
2,7	0,37
3,4	0,46
4,0	0,56
4,7	0,65
5,4	0,74
6,1	0,84
6,7	0,93

Steps for the formula fitting:

1. Measurements of dielectric loss at different voltage stresses showed, that life consumption can be roughly correlated by linear regression with the relative $\tan \delta$ value within the voltage range applied. The correlation between life consumption and relative $\tan \delta$ at certain voltages is depicted below as $y=mx+q$.

- a) For $\tan \delta_R$ between the voltages of $0,18xU_0$ and $0,28xU_0$, the relation is: $y=8,22x+0,13$, as presented in Figure E1. (in the Table E.2 factor 12 is taken into account-rounded up for better fitting with other voltages used).

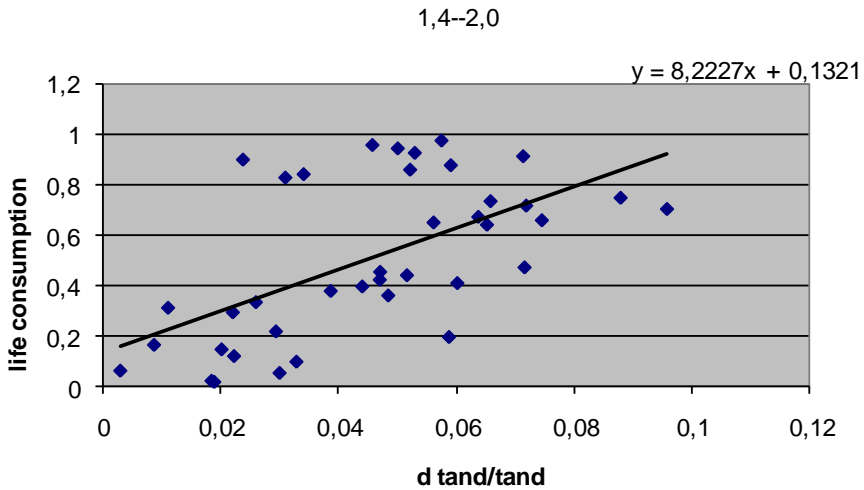


Figure E1: Life consumption vs. $\Delta \tan \delta$. Electric field intensity: 1.4-2.0 [kV/mm].

- b) For $\tan \delta_R$ between voltages $0,18xU_0$ and $0,37xU_0$ the relation is $y=5,13x-0,0033$, as presented in Figure E2. In the Table E.2 factor 6 is taken into account.

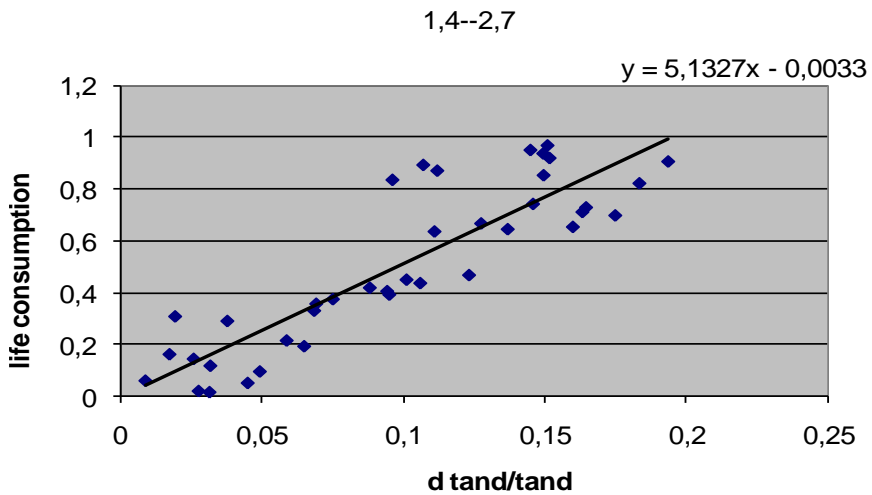


Figure E2: Life consumption vs. $\Delta \tan \delta$ Electric field intensity: 1.4-2.7 [kV/mm].

- c) For $\tan \delta_R$ between voltages $0,18xU_0$ and $0,46 xU_0$ the relation is $y=3,76x-0,0195$, as presented in Figure E3. In Table E.2 factor 4 is taken into account.

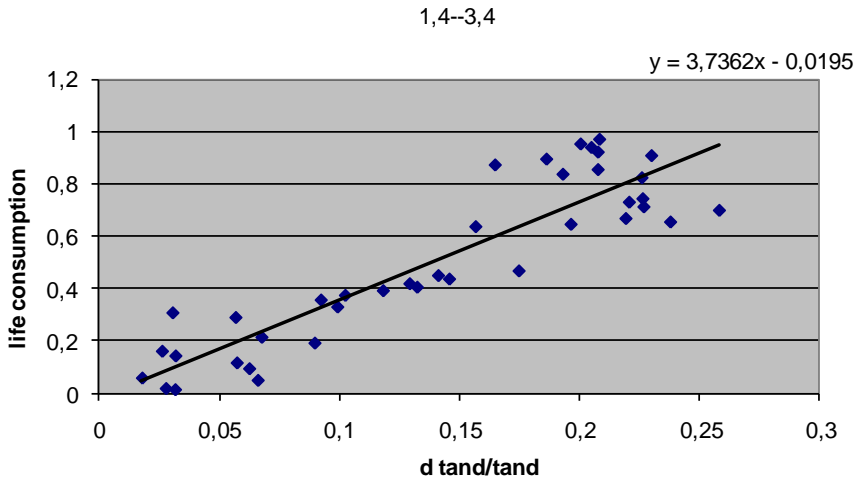


Figure E3: Life consumption vs. $\Delta \tan \delta$. Electric field intensity: 1.4-3.4 [kV/mm].

- d) For $\tan \delta_R$ between voltages $0,18xU_0$ and $0,54xU_0$ the relation is $y=2,78x+0,0041$, as presented in Figure E4. In Table E.2 factor 3 is taken into account.

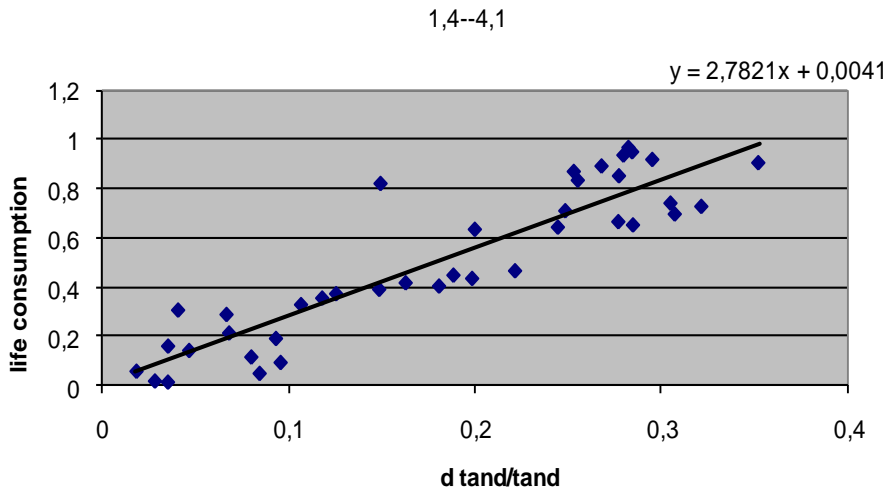


Figure E4: Life consumption vs. $\Delta \tan \delta$. Electric field intensity: 1.4-4.1 [kV/mm].

- e) For $\tan \delta_R$ between voltages $0,18xU_0$ and $0,65xU_0$, the relation is $y=2,13x - 0,0601$, as presented in Figure E5. In Table E.2 factor 2 is taken into account.

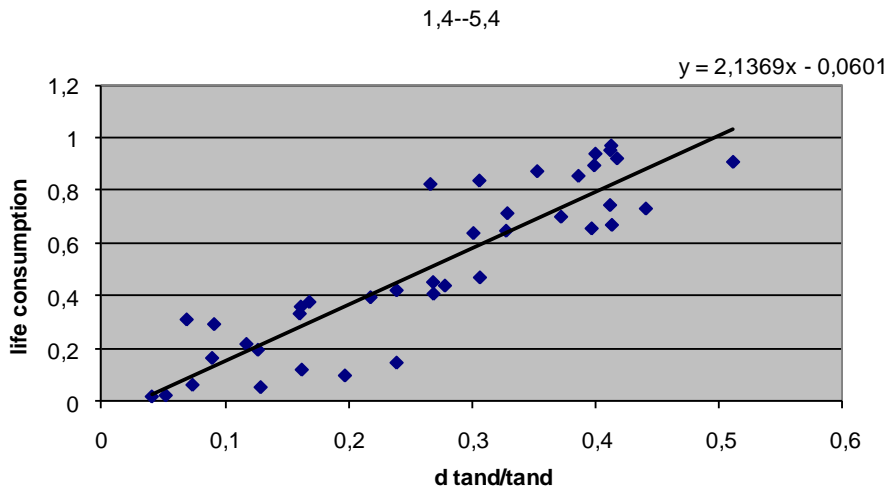


Figure E5: Life consumption vs. $\Delta \tan \delta$. Electric field intensity: 1.4-5.4 [kV/mm].

- f) For $\tan \delta_R$ between voltages $0,18xU_0$ and $0,74xU_0$, the relation is $y=1,89x - 0,074$, as presented in figure E6. In Table E.2 factor 1,8 is taken into account.

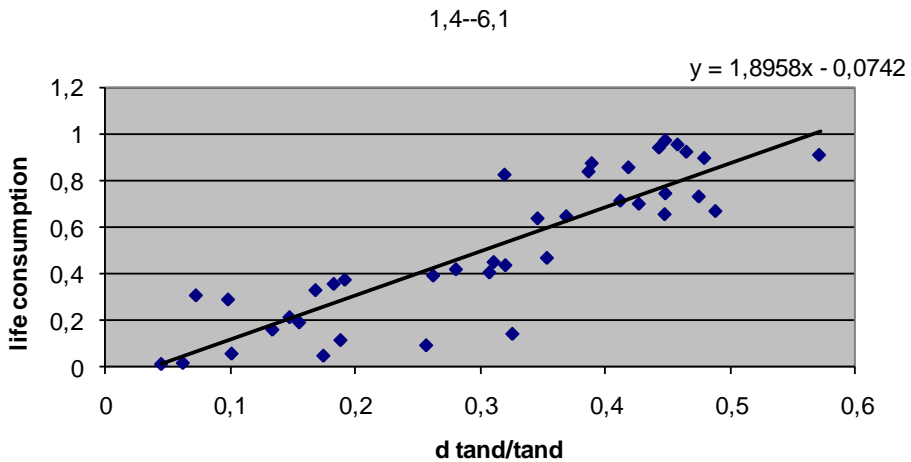


Figure E6: Life consumption vs. $\Delta \tan \delta$. Electric field intensity: 1.4-6.1 [kV/mm].

- g) For $\tan \delta_R$ between voltages $0,18xU_0$ and $0,84xU_0$, the relation is $y=1,89x - 0,074$, as presented in Figure E6. In Table E.2 factor 1,5 is taken into account.

Further relations at different electric field intensities were investigated in the same way. Summarizing, the formulas giving the correlation between relative $\tan \delta$ and life consumption are as presented in table E.2.

Table E.2
Relation between life consumption and relative $\tan \delta$ at two dedicated test voltages.

Lower voltage	Higher voltage	Relation between life consumption and relative $\tan \delta$
0.18 U ₀	0.28 U ₀	Life consumption $\approx 12 \cdot \text{relative } \tan \delta$
0.18 U ₀	0.37 U ₀	Life consumption $\approx 6 \cdot \text{relative } \tan \delta$
0.18 U ₀	0.46 U ₀	Life consumption $\approx 4 \cdot \text{relative } \tan \delta$
0.18 U ₀	0.56 U ₀	Life consumption $\approx 3 \cdot \text{relative } \tan \delta$
0.18 U ₀	0.65 U ₀	Life consumption $\approx 2 \cdot \text{relative } \tan \delta$
0.18 U ₀	0.74 U ₀	Life consumption $\approx 1.8 \cdot \text{relative } \tan \delta$
0.18 U ₀	0.84 U ₀	Life consumption $\approx 1.5 \cdot \text{relative } \tan \delta$

Life consumption slopes m result from the linear regression approximations for $\tan \delta_r$ at each voltage interval (Figures E1-E6) and these values are shown in the 3rd column of table E.2. From the Table E.2, it can be seen that factor m depends on the voltage difference. Now a parameter “ $a=m_0/n$ ” is derived, that will be the slope divided by the number n of incremental voltage steps and is related to the slope m_0 at the lower voltage $0,18 \times U_0$. To better fit all intervals we rounded up the m -value of the first regression from 8,22 to 12. This is described by equation E-1 as follows:

$$a = 12 * \frac{0.09}{U_2 - U_1} \quad [E-1]$$

As a result:

$$\text{Life consumption} = 12 * \frac{0.09}{U_2 - U_1} * \text{relative } \tan \delta \quad [E-2]$$

Introducing [E-1] makes the relation [E-2] applicable for all intervals.

It must be noted that the data is analysed in the same way when the lower voltage is increased according to values in Table E.3. Then the other values of “ a ” parameters are obtained. This is summarized in Table E.3.

Table E.3
Relation between life consumption and lower voltage (U1).

Lower voltage	Relation between life consumption and relative tan δ
0.18xU ₀	life consumption=12* $\frac{0.09}{U_2 - U_1}$ *relative tan δ
0.28xU ₀	life consumption=13* $\frac{0.09}{U_2 - U_1}$ *relative tan δ
0.37xU ₀	life consumption=15* $\frac{0.09}{U_2 - U_1}$ *relative tan δ
0.46xU ₀	life consumption=16* $\frac{0.09}{U_2 - U_1}$ *relative tan δ

It can be seen that the value of “a” parameter depends not only on the voltage difference, but also on the lower value of voltage. This leads to the introduction of the formula E-3 for description of “b” parameter, which becomes:

$$b = 10 * \frac{0.09}{U_2 - U_1} * 1.1^{\frac{U_1}{0.09}} \quad [E-3]$$

Factor 1.1 comes from dividing 13/12, 15/13, 16/15 and so on (it gives value close to 1.1). From the values, it can be seen that it depends on the lower voltage (U1) and the voltage step (voltage difference-the smallest voltage step is 0,09xU₀). When b is substituted for a in E-2, then empirical equation [7.7] results.

LIST

Abbreviations

AC	Alternating Current
AM	Asser Management
CBM	Condition Based Maintenance
CIGRE	Conseil International des Grands Reseaux Electriques (International Council on Large Electric Systems)
TF	Task Force (CIGRE)
WG	Working Group (CIGRE)
DAC	Damped AC (Alternating Current)
PD	Partial Discharge
HF	High Frequency
VHF	Very High Frequency
VLF	Very Low Frequency
HV	High voltage (Transmission level)
IEC	International Electrotechnical Commission
LV	Low Voltage
MV	Medium Voltage
XLPE	Cross-linked polyethylene
SCFF	Self Contained Fluid Filled Cables e.g. oil-filled cables
GP	Gas-pressurised Cables
HPFF	High Pressure Fluid Filled Cables
TDR	Time Domain Reflectometry
HTS	High Temperature Superconductive Cables
TSO	Transmission System Operator
DC	Direct Current
PDIV	Partial Discharge Inception Voltage
PILC	Paper Lead Insulated Cable
DGA	Dissolved Gas Analysis
OWTS	Oscillating Wave Test System
Tan δ	Tangent delta (dielectric loss)
VWD	Voltage Withstand Diagnosis
ILC	Insulation Life Consumption
OLC	Operational Life Consumption
TLC	Total Life Consumption
ARC	Reflection Method for cable fault localization
DL	Dielectric Loss
Long delay of PDIV	(Minimum PDIV)-situation where the test voltage is low enough not to ignite PD directly but high enough so that after a certain time, the first successive PD event will be recorded (without changing the voltage magnitude).
Short delay of PDIV	(Maximum PDIV) situation where the test voltage is high enough to ignite PD event directly almost without any detectable delay.
FEA	Finite Element Analysis

PRPD pattern	Phase Resolved Partial Discharge Pattern
PDEV	Partial discharge extinction voltage
PDIV	Partial discharge inception voltage
PI	Insulation Polarization Index

List of symbols:

V_T	Test voltage level of the DAC voltage of the 1 st cycle which equals to the actual charging voltage as it has to be generated by a DAC system
R_1	DAC system losses in Ω
R_2	Test object losses in Ω
L	Inductance in H (Henry)
C	Capacitance in F (Farads)
X_L, X_C	Inductive and capacitive inductance
β	Attenuation factor (damping factor) of DAC voltage
R_M	Resistive divider of DAC system
C_M	Quadrupole of DAC system
C_{HV}	HV coupling capacitor of DAC system
C_{LV}	Measuring capacitor of the quadrupole unit of DAC system
N_{DAC}	Number of DAC excitations
U	Power cable rms rated voltage, phase-to-phase
U_0	Nominal rms operating voltage, phase-to-ground
ΔV_T	DAC voltage test step
t_{ch}	Charging time necessary to charge the tested cable to the required voltage be DC voltage source
i_{load}	Charging current of DC voltage source in DAC system
I_{load}	Charging current of DC source
q	Charge displacement expressed by calibrated readings of apparent charge value in [pC]
τ_{cd}	Charge decay time [s]
τ_{cavity}	Time constants related to charge re-distribution on the cavity surface (shape dependent)
$\tau_{material}$	Time constants related to charge re-distribution in the surrounding insulation material
ϵ_r	Dielectric constant of the insulation [F/m]
Δt	Time difference (between incident and reflected pulse)
Δt_{cal}	Propagation time of twice the cable system length

List of units

m	meter (unit of the length)
C	Coulomb
eV	electronvolt
F	Farad
H	Henry
Hz	Hertz
s	second
S	Siemens
V	Volt
Ω	Ohm

REFERENCES

1. B. Quak, "Information Strategy for Decision Support in Maintaining High Voltage Infrastructures", PhD thesis, ISBN 978-90-8559-334-8, Delft University of Technology, Netherlands 2005
2. "Statistics of AC Underground Cables in Power Networks", CIGRE Working Group B1.07, Technical Brochure 338, ISBN 978-2-85873-026-1, December 2007
3. "Update of Service Experience of HV Underground and Submarine Cables System", CIGRE Working Group B1.10, Technical Brochure 379, ISBN 978-2-85873-066-7, April 2009
4. E. Peschke, R. von Olshausen, "Cable Systems for High and Extra-High Voltage", ISBN 3-89578-118-5. Pirelli Kabel und Systeme GmbH, Berlin 1999
5. "Rodzaje kabli SN/WN zainstalowane w latach 2010-2015 w grupie PGE Dystrybucja", dokument wewnętrzny 2016/Internal statistics about installed MV/HV cables in PGE Group in years 2010-2015 (PGE TSO internal document)
6. E. Zaccone, "High voltage underground and subsea cable technology options for future transmission in Europe", Europacable High Voltage Systems Group, E-Highway 2050, WP3 workshop proceedings, April 15th, Brussels 2014
7. E. Pultrum, S.A.M. Verhoeven, "Testing of Extruded Cables: Experience in Type Testing, PQ Testing and Test After Installation. What do we learn from it?", KEMA High Voltage Laboratory, Netherlands, CIGRE Working Group B1.104, Session papers and proceedings, Paris 2004
8. E. Gulski, P. Cichecki, F. Wester, J.J. Smit, "On-site Testing and PD Diagnosis of High Voltage Power Cables", IEEE Transactions on Dielectrics and Electrical Insulation Vol. 15, No. 6, pages 1691-1700, December 2008
9. "Remaining Life Management of Existing AC Underground Lines", CIGRE Working Group B1.09, Technical Brochures 358, ISBN: 978-2-85873-046-9, October 2008
10. "Maintenance for HV Cables and Accessories", CIGRE WG B1.04, Technical Brochures 279, August 2005
11. TenneT (TSO) internal data base of HV Cables, used in 2009 not published (internal conversation with TSO representatives)
12. Gulski, E, Jongen, R, Parciak, J, Rakowska, A. "Effective on-site testing and non-destructive diagnosis of new installed and service aged (E) HV power cables up to 230 kV" Jicable-Versailles 21-25 June, 2015

13. Aucourt, C., Boone, W., Kalkner, W., Naybour, R.D. Ombello, F. "Recommendations for a New After Laying Test Method for High Voltage Extruded Cable Systems." CIGRE Session Papers and Proceedings 21-105, Study Committee B1 (was 21), 16 August 1990
14. IEEE 400.4 2015 Guide for Field-Testing of Shielded Power Cable Systems Rated 5 kV and Above with Damped Alternating Current Voltage (DAC)
15. Ulrich Herrmann, Andreas Kluge, Ronald Plath, IPH Berlin "After-installation Testing of HV/EHV Cable Systems-Procedures and Experiences", Jicable 2007
16. D. Pepper, Grundlagenuntersuchung zum Teilentladungsverhalten in kunststoffisolierten Mittelspannungskabeln bei Prüfspannungen mit variabler Frequenz, PhD thesis, Technical University of Berlin, 2003
17. Gulski, E., Cichecki, P., Smit, J.J., de Vries, F., Pellis, J., van Houwelingen, D., Wester, F., Bodega, R. Hermans, T.J.W. H. "Condition assessment of transmission power cables", 8th International Conference on Insulated Power Cables. Deschamps, L. (ed.). Versailles, France: Jicable'11, p. 1-1 1 p. 2011
18. F.H. Kreuger-"Industrial high voltage" Part: 1,2,3. Delft University Press, ISBN 90-6275-562-3 Delft 1992
19. John H. Cooper, Power Delivery Consultants, Inc. "Field Measurement of Transmission Cable Dissipation Factor" Workshop proceedings 2000, Alexandria, Virginia, 13 14 September 2000
20. Cichecki, P., Jongen, R. A., Gulski, E. Smit, J.J. "Statistical approach in power cables diagnostic data analysis", IEEE Transactions on Dielectrics and Electrical Insulation. 15, 6, p. 1559-1569 11 p. 2008
21. Gulski, E., Cichecki, P., Wester, F. J., Smit, J.J., Bodega, R., Hermans, T.J. W.H., Seitz, P.P., Quak, B., de Vries, F. "On-site testing and PD diagnosis of high voltage power cables" , IEEE Transactions on Dielectrics and Electrical Insulation. 15, 6, p. 1691-1700 10 p. 2008
22. E-Highway 2050, WP3 workshop April 15th, 2014 Brussels "High voltage underground and subsea cable technology options for future transmission in Europe"
23. Accessories for HV Cables With Extruded Insulation CIGRE Working Group 21.06 (B1 now) TB 177, 2001
24. N.H. Malik, A.A. Al-Arainy. M.I. Qureshi and F.R. Pazheri, "Calculation of Electric Field Distribution at High Voltage Cable Terminations", Journal of Energy Technologies and Policy www.iiste.org ISSN 2224-3232 (Paper) ISSN 2225-0573 (Online) Vol.1, No.2, 2011

25. Nebojsa B. Raicevic, Slavoljub R. Aleksic, and Sasa S. Ilic "New EEM/BEM Hybrid Method for Electric Field Calculation in Cable Joints", World Academy of Science, Engineering and Technology 79, 2011
26. J.Densley, R.Bartnikas, B.S.Bernstein. "Multi-stress ageing of extruded insulation system for transmission cables". IEEE Electrical insulation magazine, Vol. 9. No. 1. pp 15-17, January/February 1993
27. Doble Engineering Company-76th Annual, International Doble Client Conference proceedings
28. Service Aged Insulation Guidelines on Managing the Aging Process, CIGRE Working Group D1.11 Service Aged Materials (Task Force D1.11.01), 2003
29. Petri Hyvönen, "Prediction of Insulation Degradation of Distribution Power Cables Based on Chemical Analysis and Electrical Measurements", Doctoral Dissertation, Helsinki University of Technology Faculty of Electronics, Communications and Automation Department of Electrical Engineering, SBN 978-951-22-9403-9, 2008
30. J. Unsworth, F. Mitchell. "Degradation of electrical insulating paper monitored with high performance liquid chromatography". IEEE Transactions on electrical insulation. Vol.I 25, No. 4, August 1990. p 737
31. L.A. Dissado, J.C. Fothergill, "Electrical Degradation and Breakdown in Polymers" ISBN 0-86341-196-7, IEEE Materials and Devices Series 9, Peter Peregrinus Ltd., London, U.K., 1992
32. Insulating liquids-Determination of the breakdown voltage at power frequency — Test method, IEC 60156 (1995-1997)
33. Ageing of cellulose in mineral-oil insulated transformers. CIGRE brochure 323, TF D1.01.10 October 2007. P51
34. Jean-Pierre Crine, Consultant, St-Bruno (Canada), also with Ecole Polytechnique de Montréal (Canada), "A Molecular Approach to the electrical aging of XLPE cables", Jicable 2007
35. Larbi Boukezzi, Ahmed Boubakeur, Christian Laurent, and Mouhamed Lallouani, "Observations on Structural Changes under Thermal Ageing of Cross-linked Polyethylene Used As Power Cables Insulation", Iranian Polymer Journal 17 (8), 2008, p.611-624

36. A.Harlin, M.G.Danikas, P.Hyvönen. Polyolefin insulation degradation in electrical field below critical inception voltages. Journal of electrical engineering. Vol. 56, No. 5-6. 2005. pp 135-140
37. Losif Lingvay, Cristina Stancu, Andrei Cucos, Carmen Lingvey, INC DIE ICPE-CA, Bucharest. "Degradation of Power Cables Polyethylene Insulation Due to Thermal Cycling" 17th Energy Engineering Conference Felix Spa, 2-4 June 2011
38. R.C.A.M. Koevoets, KEMA, The Netherlands, "A New After Laying Dielectric Test For Underground HV Extruded Cables", Conference Record of the 1990 IEEE International Symposium on Electrical Insulation, Toronto, Canada, June 3-6, 1990
39. Auclair, H., Boone, W., Papadopoulos, M.S., "Development of a new after laying test method for High Voltage power cable systems", CIGRE Paper 21-06, Paris, 1988
40. A. Aucourt, W. Boone, W. Kalkner, R.D. Naybour, F. Ombello, Task Force 21.09/02. "Recommendations for a new after laying test method for High Voltage extruded cable systems, CIGRE Session 26th August-1st September 1990, Paris
41. Aucourt, C., Louis, M. "After Laying Test of Accessories of Synthetic Insulated Cables with Oscillating Wave." 6th ISH, Paper No. 47.05, New Orleans, U.S.A. August, 1989
42. P.P. Seitz, B. Quak, E. Gulski, J.J. Smit, P. Cichecki, F. de Vries, F.Petzold, Novel Method for On-site Testing and Diagnosis of Transmission Cables up to 250kV, Proceedings Jicable '07. 7th Intern. Conf. Insulated Power Cables, Versailles, France, Paper 16, 2007
43. Frank J. Wester, "Condition Assessment of Power Cable using Partial Discharge Diagnosis at Damped AC Voltages" Ph.D. dissertation, Delft Univ. Tech., Delft, The Netherlands, 2004
44. S.A.A. Houtepen, "Dielectric Loss Estimation Using Damped AC Voltages" 1st June 2010, TU Delft Master Thesis
45. R. Jongen, P.P. Seitz, B. Quak, F. de Vries, P. Cichecki, New Generation of On-site Testing Technology for Transmission Power Cables, paper A.8.3, 8th Jicable 2011
46. R. Plath, 'Oscillating Voltages' als Prüfspannung zur Vor-Ort-Prüfung und TE-Messung kunststoffisolierter Kabel, Book ISBN 3-89574-023-3, Verlag Dr. Köster, Berlin, Germany, 1994
47. E. Gulski. P. Cichecki, E.R.S. Groot, J.J. Smit, F. de Vries, J. Slangen, Slangen. E.R.S.Groot, J. Pellis, D. van Houwelingen, T.J.W.H. Hermans, B. Wegbrands and L. Lamballais, "Condition Assessment of Service Aged HV Power Cables", CIGRE, Paper D1-206, 2008

48. E. Lemke, E. Gulski, W. Hauschild, R. Malewski, P. Mohaupt, M. Muhr, J. Rickmann, T. Strehl, F.J. Wester: Practical aspects of the detection of partial discharges in power cables. CIGRE WG D1.33.TF 05, Technical Brochure 297, ELECTRA No. 232, pp. 63-70, 2006
49. S. Meijer, E. Gulski, P.D. Agoris, P.P. Seitz, T.J.W.H. Hermans, L. Lamballais, 2006, "Non-Conventional On-Site Partial Discharge Diagnostics of Transmission Power Cable Accessories", Proceedings of the 16th Conference of the Electric Power Supply Industry
50. F.H. Kreuger, Industrial High Voltage, volume 1,2,3., Delft University Press 1992
51. E. Gulski, F.J. Wester, J.J. Smit, P.N. Seitz, M. Turner, Advanced partial discharge diagnostic of MV power cable system using oscillating wave test system. In: IEEE electrical insulation magazine, Year: 16, 2, 2000, p. 17-25. ISSN: 0883-7554
52. E. Pultrum, E.F. Steennis, M.J.M. Van Riet, Test after laying, diagnostic testing using partial discharge testing at site, CIGRE Session, paper 15/2/33-12, 1996
53. IEC 60270 High-voltage test techniques-Partial discharge measurements, International Standard, 2000
54. Guide For Partial Discharge Measurements in Compliance to IEC 60270-Working Group D1.33, Task Force 05, CIGRE 2008
55. IEC 885-3: Test methods for partial discharges measurements on lengths of extruded power cable, 1988
56. A. Krivda "Automated Recognition of Partial Discharges", IEEE Trans. on Dielectrics and Electrical Insulation, Vol. 2, No. 5, pp. 796-821, October 1995
57. I.J. Tigchelaar, EPS.07.A.186 "Propagation of partial discharge pulses through cross-bonded high-voltage cable systems" University of Eindhoven, master thesis, January 2007
58. P. H. F. Morshuis, "Partial Discharge Mechanisms" Ph.D. dissertation, Delft Univ. Technology, Delft, The Netherlands, 1993
59. R. Bodega, A. Cavanelli, P.H.F. Morshuis and F.J. Wester, "The effect of voltage frequency on partial discharge activity, Conference on Electrical Insulation and Dielectric Phenomena". pp 685-689
60. Riccardo Bodega, Peter H.F. Morshuis, Massimo Lazzaroni, and Frank J. Wester, "PD Recurrence in Cavities at Different Energizing Methods" IEEE Transaction on instrumentation and measurements, Vol. 53, No. 2, April 2004
61. Guidelines for partial discharge detection using conventional (IEC 60270) and unconventional methods, CIGRE WG D1.37 662, August 2016

62. IEC 60183:2015 "Guidance for the selection of high voltage A.C cable systems"
63. J. Densley, "Ageing Mechanism and Diagnostics for Power Cables-An Overview" IEEE Electrical Insulation Magazine, Vol. 17 no. 1 pp14-21, Jan/Feb 2001
64. J.G. Head, P.S. Gale, D.J. Skipper and A.W. Stannet. "Ageing of Oil-filled Cable insulation", CIGRE paper 15-08, 1982
65. H. Jin, E. Gulski, L.A. Chmura, "Application of dielectric loss measurements for life consumption and future life estimation modelling of oil-impregnated insulation in HV power cables" M.Sc. Thesis, TU Delft, 06 2010
66. H. Jin, Lukasz Chmura, Piotr Cichecki, Edward Gulski, Johan J. Smit. "Application of dielectric loss measurements for life consumption and future life estimation modelling of oil-impregnated paper insulation in HV power cables" CMD conference paper 2010
67. Chmura, L., Huifei Jin, Cichecki, P., Smit, J.J., Gulski, E., Vries, F. "Use of dissipation factor for life consumption assessment and future life modelling of oil-filled high-voltage power cables"-Electrical Insulation Magazine, January/February 2012, ISSN: 0883-7554
68. Montsinger, V.M. Transactions American Institute of Electrical Engineers no. 49, 1930, pp. 776-792
69. Dakin, T. W. Transactions American Institute of Electrical Engineers no. 67, 1948, pp. 113-122

LIST OF PUBLICATIONS

Author:

1. Cichecki, P., Gulski, E., Smit, J.J. de Vries, F. "Integral condition assessment by dielectric response diagnosis of service aged external gas pressure HV power cables", Electrical Insulation, 2008. ISEI 2008. Conference Record of the 2008 IEEE International Symposium on Piscataway: IEEE Society, p. 11-14 4 p. 2008
2. Cichecki, P., Gulski, E., Smit, J.J., Jongen, R. A. Petzold, F. "Interpretation of MV power cables PD diagnostic data using statistical analysis", Conference record of the 2008 IEEE international symposium on electrical insulation, 2008. ISEI 2008. Piscataway: IEEE Society, p. 15-195 p. 2008
3. Cichecki, P., Onderwater, L.P.A., Gulski, E., Smit, J.J., Seitz, P.P. de Vries, F. "On-site application of dielectric response diagnosis on service aged oil-impregnated HV power cables", Proceedings of 2008 International conference on condition monitoring and diagnosis CMD 2008. Piscataway: IEEE Society, p. 1136-1140 5 p. 2008
4. Cichecki, P., Gulski, E., Smit, J.J. Onderwater, L.P.A. "On-site diagnostics of HV power cables using dielectric losses and recovery voltage measurements", Proceedings 2008 4th IEEE Benelux young researchers symposium. Encica, L., Gysen, B. L. J., Jansen, J.W. Krop, D.C.J. (eds.). Eindhoven: IEEE Society, p. 1-5 5 p. 2008
5. Cichecki, P., Gulski, E., Smit, J.J., Jongen, R.A., Petzold, F. "Statistical analysis of large amount of power cables diagnostic data", Proceedings of 2008 International conference on condition monitoring and diagnosis CMD 2008. Piscataway: IEEE Society, p. 1288-1292 5 p. 2008
6. Cichecki, P., Jongen, R. A., Gulski, E., Smit, J.J. "Statistical approach in power cables diagnostic data analysis", IEEE Transactions on Dielectrics and Electrical Insulation. 15, 6, p. 1559-1569 11 p. 2008
7. Cichecki, P., Gulski, E., Smit, J.J., Jongen, R.A., Hermans, T., Bodega, R. de Vries, F. "Comparison of PD measurement results by means of different energizing and detection methods", Proceedings of the 16th international symposium on high voltage engineering. Nixon, K.J., Reynders, J. P. (eds.). Johannesburg: South African Institute of Electrical Engineers, Innes House, p. 1029-1033 5 p. 2009
8. Cichecki, P., Gulski, E., Smit, J.J., Hermans, T., Bodega, R. Seitz, P.N. "Conventional and unconventional partial discharges detection in power cables using different AC voltages", Proceedings IEEE Electrical Insulation Conference, 2009. EIC 2009. Piscataway: IEEE Society, p. 5-9 5 p. 2009

9. Cichecki, P., Gulski, E., Smit, J.J., van Nes, P.V.M., Ejigu, A.G., de Vries, F. "Dielectric losses diagnosis of serviced aged oil impregnated paper insulation of HV power cables", Proceedings IEEE Electrical Insulation Conference, 2009. EIC 2009. Piscataway: IEEE Society, p. 216-219 4 p. 2009
10. Cichecki, P., Gulski, E., Smit, J.J., de Vries, F. "Measurements of dielectric losses on paper-oil insulation samples of serviced aged HV power cables", Proceedings of the 16th international symposium on high voltage engineering. Nixon, K. J. Reynders, J. P. (eds.). Johannesburg: South African Institute of Electrical Engineers, Innes House, p. 197-200 4 p. 2009
11. Cichecki, P., Gulski, E., Smit, J.J., de Vries, F., Hermans, T.J.W.H. Seitz, P.P. "On-site testing and diagnosis of transmission power cables", Proceedings of the 16th international symposium on high voltage engineering. Nixon, K.J. Reynders, J.P. (eds.). Johannesburg: South African Institute of Electrical Engineers, Innes House, p. 976-979 4 p. 2009
12. Cichecki, P., Gulski, E., Smit, J.J., Seitz, P.P., de Vries, F. "One-site testing and diagnosis of HV transmission cables using PD and dielectric losses diagnosis", Proceedings of the 11th Insucon International Electrical Insulation Conference. Birmingham: IET Centre, p. 184-189 6 p. 2009
13. Cichecki, P., Gulski, E., Smit, J.J., Seitz, P.P., Bodega, R. Hermans, T. "PD sensitivity estimation for unconventional detection of discharging defects at ac voltage", Proceedings of the 11th Insucon International Electrical Insulation Conference. Birmingham: IET Centre, p. 49-55 7 p. 2009
14. Cichecki, P., Gulski, E., Smit, J.J., Jongen, R.A. "Statistical analysis of transmission power cables condition data", Proceedings of the 16th international symposium on high voltage engineering. Nixon, K.J. Reynders, J.P. (eds.). Johannesburg: South African Institute of Electrical Engineers, Innes House, p. 851-856 6 p. 2009
15. Cichecki, P., Ayan, J.S., Gulski, E., Smit, J.J., Chmura, L. A. "Investigation of PD occurrence and detectability in high voltage power cable accessories", International Conference on High Voltage Engineering of Application. New Orleans: IEEE Society, p. 264-267 4 p. 2010
16. Cichecki, P., Gulski, E., Smit, J.J., Chmura, L.A., Jongen, R. "On-site diagnosis of XLPE transmission power cables with damped AC technique", IEEE International Symposium of Electrical Insulation. Bomben, S. G. (ed.). San Diego: IEEE Society, p. 1-5 5 p. 2010

Co-author:

1. Meijer, S., Cichecki, P., Agoris, P., Smit, J.J., Lopez-Roldan, J. "UHF partial discharge diagnostics for condition assessment of power transformers", Proceedings of the

- 16th conference of the electric power supply industry. Gurgaon, India: CEPSI, p. 1-4
4 p. 2006
2. Gulski, E., Cichecki, P., Smit, J.J., Seitz, P.P., Quak, B., Petzold, F., de Vries, F. "Advanced diagnosis of high voltage power cables", Proceedings of the 15th International Conference on High Voltage Engineering. Mladen Iglic Maks Babuder, J. K. (ed.). Ljubljana: University of Ljubljana, p. 1-6 6 p. 2007
 3. Meijer, S., Gulski, E., Agoris, P., Cichecki, P. "Partial Discharges Diagnosis in Power Transformers", Proceedings of Cigre International Conference Transformator 2007. Andrzej Pazda (ed.). Poznań: PTPIREE, p. 41-49 9 p. 2007
 4. Agoris, P., Cichecki, P., Meijer, S., Gulski, E., Smit, J.J. "Analysis of artificial defects in Transformer Insulation using the UHF technique", Proceedings of the 15th International Conference on High Voltage Engineering. Mladen Iglic Maks Babuder, J. K. (ed.). Ljubljana: University of Ljubljana, p. 1-4 4 p. 2007
 5. Agoris, P., Cichecki, P., Meijer, S., Smit, J.J. "Building a Transformer Defects Database for UHF Partial Discharge Diagnostics", Proceedings of 2007 IEEE Lausanne PowerTech. Hans-Björn Püttgen (ed.). Lausanne: Ecole Polytechnique Federale, p. 1-6 6 p. 2007
 6. Gulski, E., Smit, J.J., Cichecki, P., Petzold, F., Seitz, P.P., Quak, B., de Vries, F. "Insulation Diagnosis of High Voltage Power Cables", Proceedings of 7th International Conference on Insulated Power Cables (Jicable '07). Lucien Deschamps (ed.). Paris: SEE, p. 802-807 6 p. 2007
 7. Gulski, E., Meijer, S., Cichecki, P., Smit, J.J., Seitz, P.P., Petzold, F., de Vries, F. "Insulation Diagnosis of High Voltage Power Cables", proceedings of the 2007 IEEE International Conference on Solid Dielectrics. University of Southampton (ed.). New York: IEEE Society, p. 721-724 4 p. 2007
 8. Gulski, E., Smit, J.J., Cichecki, P., Petzold, F., Seitz, P. P., Quak, B., de Vries, F. "Novel Method for On-site Testing and Diagnosis of Transmission Cables up to 250 kV", Proceedings of 7th International Conference on Insulated Power Cables (Jicable '07). Lucien Deschamps (ed.). Paris: SEE, p. 841-846 6 p. 2007
 9. Meijer, S., Cichecki, P., Agoris, P., Smit, J.J. "UHF Sensors for Partial Discharge Diagnostics of Power Transformers", Proceedings of the 1st International Conference on Electrical Engineering and Informatics. Dr. Suwarno (ed.). Bandung: Institut Teknologi Bandung, p. 769-772 4 p. 2007
 10. Gulski, E., Cichecki, P., Smit, J.J., Seitz, P.P., Quak, B., de Vries, F. "On-site condition monitoring of HV power cables up to 150 kV", Proceedings of 2008 International conference on condition monitoring and diagnosis CMD 2008. Piscataway: IEEE Society, p. 1199-1202 4 p. 2008

11. Gulski, E., Cichecki, P., Wester, F.J., Smit, J.J., Bodega, R., Hermans, T.J.W.H., Seitz, P.P., Quak, B., de Vries, F. "On-site testing and PD diagnosis of high voltage power cables", IEEE Transactions on Dielectrics and Electrical Insulation. 15, 6, p. 1691-1700 10 p. 2008
12. Meijer, S., Jongen, R.A., Cichecki, P., Seitz, P.P., Bodega, R., Hermans, T.J.W.H. "Sensitivity analysis of RF measurements to detect PD in power cable accessories", Proceedings of 2008 International conference on condition monitoring and diagnosis CMD 2008. Piscataway: IEEE Society, p. 1074-1077 4 p. 2008
13. Gulski, E., Cichecki, P., Smit, J.J., de Vries, F., Bodega, R., Hermans, T., Seitz, P.P. "Dielectric loss diagnosis of serviced aged HV power cables", Proceedings of Cigre SCD1-coloquium 2009. Gockenbach, E. (ed.). Budapest: Cigré, p. 1-8 8 p. 2009
14. Gulski, E., Sinambela, E. J., Cichecki, P., Smit, J.J. "Optimal partial discharge diagnosis of medium voltage power cables", Proceedings of the 16th international symposium on high voltage engineering. Nixon, K.J. Reynders, J. P. (eds.). Johannesburg: South African Institute of Electrical Engineers, Innes House, p. 1046-1051 6 p. 2009
15. Gulski, E., Cichecki, P., Chojnowski, P., Parciak, J., Rakowska, A., Siodla, K., Duniec, J. Jongen, R.A." Nowoczesne metody badania i diagnostyki kabli wysokiego napięcia w miejscu ich zainstalowania", Proceedings VII Konferencja naukowo-techniczna elektroenergetyczne linie kablowe. Poznań Polskie Towarzystwo Przesyłu i Rozdziału Energii Elektrycznej, p. 83-92 10 p. 2009
16. Jin, H., Chmura, L.A., Cichecki, P., Gulski, E., Smit, J.J. "Application of dielectric loss measurements for life consumption and future life estimation modeling of oil-impregnated paper insulation in HV power cables", International Conference on Condition Monitoring and Diagnosis 2010. Tokyo, Japan, p. 273-276 4 p. 2010
17. Chmura, L.A., Cichecki, P., Gulski, E., Smit, J.J., de Vries, F. "Life time estimation of serviced aged oil-paper insulated HV power cables based on the dielectric loss measurements", IEEE International Symposium of Electrical Insulation. Bomben, S.G. (ed.). San Diego: IEEE Society, p. 1-4 4 p. 2010
18. Chmura, L.A., Cichecki, P., Gulski, E., Smit, J.J. "On-site testing and diagnosis of new and serviced aged HV power cables-evaluation based on diagnostic parameters", International Conference on High Voltage Engineering of Application. New Orleans: IEEE Society, p. 140-143 4 p. 2010
19. Gulski, E., Cichecki, P., Jiankang, Z., Rong, X., Jongen, R., Seitz, P.P., Porsche, A. Huang, L. "Practical aspects of on-site testing diagnosis of transmission power cables in China", Proceedings 2010 International Conference on Condition Monitoring and Diagnosis. Paris, France: Cigré, p. 675-678 4 p. 2010

20. Smit, J.J., Cichecki, P., Gulski, E., de Vries, F., Pellis, J. Wester, F.J. "Condition assessment of transmission power cables", 8th International Conference on Insulated Power Cables (Jicable'11). Deschamps, L., Awad, R. et al. (eds.). Versailles, Frankrijk: Jicable'11, p. 1-1 1 p. 2011
21. Gulski, E., Cichecki, P., Smit, J.J., de Vries, F., Pellis, J., van Houwelingen, D., Wester, F., Bodega, R., Hermans, T.J.W. H. "Condition assessment of transmission power cables", 8th International Conference on Insulated Power Cables. Deschamps, L. (ed.). Versailles, France: Jicable'11, p. 1-1 1 p. 2011
22. Smit, J.J., Gulski, E., Cichecki, P., Rakowska, A., Siodla, K., Pots, L.D. "Implementation of modern methods of on-site testing and diagnosis of HV power cables", 8th International Conference on Insulated Power Cables (Jicable'11). Deschamps, L., Awad, R. et al. (eds.). Versailles, Frankrijk: Jicable'11, p. 1-1 1 p. 2011
23. Smit, J.J., Gulski, E., de Vries, F., Cichecki, P. "Modern methods of installation and diagnostic testing of distribution", 8th International Conference on Insulated Power Cables (Jicable'11). Deschamps, L., Awad, R. et al. (eds.). Versailles, France: Jicable'11, p. 1-1 1 p. 2011
24. Chmura, L.A., Jin, H., Cichecki, P., Smit, J.J., Gulski, E., de Vries, F. "Use of dissipation factor for life consumption assessment and future life modeling of oil-filled high-voltage power cables", IEEE Electrical Insulation Magazine. 28, 1, p. 27-37 11 p. 2012
25. Jongen, R., Quak, B., Cichecki, P., Gulski, E., de Vries, F." On-site testing and diagnosis of long medium voltage cables", Proceedings of 2012 IEEE International Conference on Condition Monitoring and Diagnosis. Suwarno (ed.). Piscataway, NJ, USA: IEEE Society, p. 659-662 4 p. 2012
26. Gulski, E., Rakowska, A., Siodla, K., Jongen, R., Minassian, R., Cichecki, P., Parciak, J. Smit, J.J. "On-site testing and diagnosis of transmission power cables up to 230 kV using damped AC voltages", IEEE Electrical Insulation Magazine. 30, 3, p. 27-38 12 p. 2014

ACKNOWLEDGMENT

During the years of my research in The Netherlands and until the moment of finishing this thesis many people inspired and helped me. Especially I would like to thank the following people:

- My promotor prof. dr. J.J. Smit, first of all for giving me the opportunity to join his department, secondly for many fruitful discussions. I would like to thank for his patience and all contributions to my thesis. Moreover, I am grateful for our long, valuable Skype conversation during which he shared his knowledge, wisdom and stimulated me to fulfil this task.
- Prof. dr. hab. Ir. E. Gulski, for “introducing” me into the world of power cable diagnosis. In particular, I would like to thank for sharing his onsite experience and knowledge, which helped me during HV and EHV cable testing and diagnosis.
- For many interesting and funny discussion at “tea time” I would like to thank employees and staff of the Delft University of Technology High Voltage Lab. In this respect I would like to mention: Ing. P.V.M. van Nes, Ad van der Graaf, Bertus Naagen and Wim Termorshuizen. I am thankful to them for helping me in designing and constructing the test set-ups used in this research and trying to teach me Dutch language.
- Furthermore, I would like to thank the employees of Alliander DSO, Tennet TSO and Stedin, especially: Frank de Vries, Cor de Jong, Frank Wester, Jos Slangen, Dik van Houwelingen, Jan Pellis who were involved in this research.
- Living and working in Delft is not only a study time. Therefore, many thanks to my former colleagues from the department of High Voltage Technology and Management (Dept. Electrical Sustainable Energy). Thank you guys for providing a friendly, stimulating work conditions but also many “after-work” activities. Special thanks to: Roy Zuijderduin, Łukasz Chmura, Barry Lennon, Tomasz Kołtunowicz, Thomas Andritsch, Dhiradj Djairam.
- Employees of Prysmian Cables and Systems, especially employees with whom I travelled around the world, when I was testing HV cables. In particular my warm thanks go to Riccardo Bodega, Theo Hermans and William Bontje.
- It was great pleasure to meet Ed and Nicolet Prent, Hans Hoogstraaten, T. Hoogendoorn, Tom Rutjes, Melissa Duyzer from KMT services-thank you all for warm and peaceful working environment after I finished my work at TU Delft.
- My parents who are always supporting me in each moment of my life.
- Finally, special thanks to my wife Edyta for her encouragement and support during the last years. I have to also mention my children, who always helped me to look at the problems at a different perspective.

CURRICULUM VITAE

Piotr Cichecki was born on April 15, 1982 in Garwolin (Poland). He started his studies at Warsaw University of Technology in 2001 where he graduated in 2006 with master degree in Electrical Engineering. In the same year he joined the High Voltage Technology and Management section at TU Delft University as PhD student. In this group he started his research on on-site diagnosis with DAC systems of which this thesis resulted.



Photo: Piotr in the TU Delft HV Lab with a DAC system.